Glycerolipid homeostasis in *Candida albicans*, its role in virulence, and the potential for lipotoxicity as an anti-biofilm therapeutic

Jack Davis

School of Natural Sciences
University of Kent

August 2025.

Declaration of Authorship

No part of this thesis has been submitted in support of an application for any degree or other qualification at the University of Kent, or any other University or Institution of learning.

Jack Davis

August 2025.

Abstract

Candida albicans is highly adaptable to changes in a given environment, a trait that allows it to colonise and thrive in several niches of the human body as a commensal yeast. An opportunistic pathogen, *Candida albicans* takes advantage of changes in circumstance to drive pathogenicity and cause infection. A better understanding of how metabolic processes influence the fitness, stress response mechanisms and virulence traits of *Candida albicans* is an important step in better understanding its interactions with the host, what drives certain pathogenic traits, and thus be able to implement successful treatment regimens. In this work we explored the role that glycerolipid metabolism, or the sequestration and mobilisation of excess fatty acids within lipid droplets, play in *Candida albicans* virulence traits. We discovered that disruption of the DAG acetyltransferases *DGA2* and *LRO1* limited hyphal induction, increased sensitivity to cell wall and azole stresses, increased β-glucan exposure leading to more pronounced innate immune responses and an overall reduction in virulence. We also observed a filamentation and polarity defect when disrupting putative triacylglycerol lipase *TGL2*, coupled with a significant reduction in virulence. Lastly, we explored the potential for induction of lipotoxicity as an anti-biofilm measure, and determined the monounsaturated fatty acid palmitoleic acid as an efficacious prophylactic to prevent *C. albicans* biofilms. Overall, this work contributes to the understanding of glycerolipid storage in *Candida albicans* and uncovers a role for appropriate regulation of glycerolipid metabolism in virulence.

Acknowledgements

I would firstly like to thank Kent Cancer Trust, who part-funded this project; if not for them, and their support in a time when things were looking bleak, this PhD never would have had a second chance and I would not be submitting a thesis at all.

I want to thank members of my lab and the KFG at large, past and present, for their friendship over the years and for making Kent such a welcoming place for such a long time. In particular, Dr Patrick Rockenfeller, for showing me the microbiology ropes during my masters and then being so welcoming in hosting me during my PhD.

I want to thank "Le Bois", who have been there for me for many years despite us all being scattered to the four winds. Special mention to the members of the Creine Mill Lane gang, who got me through a rocky start and showed me the power of friendship (and hydraulic arms), and to Phil, who put up with me squatting in his flat for the first few months of writing and who was my first friend in Kent some 12 years ago. And to LD, I owe my first foray into TC, a secret that will be taken to the grave. A special thank you to my wonderful partner Phoebe, who for the last 2 and a half years has put up with me and my shenanigans; she always knew how to perk me up when writing a thesis seemed an insurmountable task, and it is her that has kept me going through thick and thin.

To my family, I owe so much; to my mum, whose faith in me and support throughout my PhD journey has meant everything, and to my dad, who was and continues to be the biggest supporter of my scientific career.

And of course, Professor Campbell Gourlay, who has been my supervisor, mentor and friend for the past several years. I am sure he is sick of the sight of me by now and this submission has certainly been a long time coming, but I can thank Campbell for many of the opportunities that have come my way, and I will be forever grateful of his support.

Jack Davis, August 2025.

Abbreviations

AmpB	amphotericin B
ATP	adenosine triphosphate
C. albicans	*Candida albicans*
cAMP	cyclic adenosine monophosphate
CDP-DAG	cytidine diphosphate diacylglycerol
C. elegans	*Caenorrhabditis elegans*
CFU	colony forming unit
CL	cardiolipin
CLR	C-lectin-type receptor
CMP	cytidine monophosphate
CO_2	carbon dioxide
CSLM	confocal scanning laser microscopy
CTP	cytidine triphosphate
CWI	cell wall integrity
DAG	diacylglycerol
DBS	donor bovine serum
DHAP	dihydroxyacetone phosphate
DMSO	dimethyl sulfoxide
DNA	deoxyribonucleic acid

ECM	extracellular matrix
ER	endoplasmic reticulum
EtOH	Ethanol
FA-CoA	fatty acid-Coenzyme A
FBS	foetal bovine serum
FFA	free fatty acid
G3P	glycerol-3-phosphate
GAP	GTPase activating protein
GDP	guanosine diphosphate
GEF	guanosine exchange factor
GO	gene ontology
GPCR	G protein coupled receptor
GPI	glycerophosphatidylinositol
GTP	guanosine triphosphate
H_2O	water
HSGs	hyphal-specific genes
HPTLC	high-performance thin-layer chromatography
IMM	inner mitochondrial membrane
ITAM	immunoreceptor tyrosine-based activation motif
KO	Knock out
LRR	leucine rich repeat
MAPK	mitogen-activated protein kinase
MDP	muramyl dipeptide
MIC	minimum inhibitory concentration
MQ	milliQ

mRNA	messenger ribonucleic acid
NLRs	nod-like receptors
OD	optical density
OPC	oropharyngeal candidiasis
PA	phosphatidic acid
PAK	p21-activated kinase
PAMP	pathogen-associated molecular pattern
PBS	phosphate-buffered saline
PC	phosphatidylcholine
PCR	polymerase chain reaction
PDME	phosphatidyldiethanolamine
PDMS	polydimethylsiloxane
PE	phosphatidylethanolamine
PEMT	phosphatidylethanolamine methyltransferase
PI	phosphatidylinositol
PKA	protein kinase A
PMME	phosphatidylmonomethylethanolamine
POA	Palmitoleic acid
PRR	pattern recognition receptor
PS	phosphatidylserine
RA	Ras association
RNA	ribonucleic acid
ROS	reactive oxygen species
rpm	revolutions per minute
RPMI-1640	Roswell Park Memorial Institute 1640

RVVC	recurrent vulvovaginal candidiasis
S. cerevisiae	Saccharomyces cerevisiae
SAP	secreted aspartyl protease
SE	sterol ester
SOD	superoxide dismutase
SYK	spleen tyrosine kinase
TAG	triacylglycerol
TLR	toll-like receptor
UAS_{INO}	inositol-sensitive upstream activating sequence
VVC	vulvovaginal candidiasis
XTT	sodium 3´-[1- (phenylaminocarbonyl)- 3,4- tetrazolium]-bis (4-methoxy6-nitro) benzene sulfonic acid hydrate
YPD	yeast extract peptone dextrose

Contents

Chapter 1

Introduction and background

1.1 *Candida albicans*: commensal yeast and opportunistic pathogen

Candida albicans (*C. albicans)* is a commensal yeast of the family *Saccharomycetaceae*, a member of the CTG clade of *Candida* spp, referring to its translation of the codon CTG as serine [1]. Approximately 50% of individuals are colonised by *C. albicans* as a normal component of their microbiota [2]. *C. albicans*, owing to a remarkable adaptability, is able to survive in several niches within the human body, most prominently oral [3], gastrointestinal [4] and vulvovaginal tracts [5]. There are examples of *C. albicans* undergoing significant adaptations to thrive within their niche. For example, cells within the mammalian gut have a transcriptomic profile that prepares them for gut commensality, including upregulation of genes associated with utilisation of fatty acids as an energy source to compensate for glucose deplete conditions of the GI tract [6]. *C. albicans* exists on the spectrum of commensal and pathogen; some studies suggest that residence of *C. albicans* within the vulvovaginal tract is owing to a mutualistic relationship with the host, whereby *C. albicans* colonisation reduces colonisation of *Escherichia coli*, and as such, mitigates the risk of bacterial urinary tract infections [7, 8, 9].

C. albicans is an opportunist, and as such, can take advantage of environmental changes to gain a foothold within its niche. The majority of *C. albicans* infections in otherwise healthy individuals are superficial; a prominent example of this would be pseudomembranous candidiasis (or oral thrush), which presents as *C. albicans* plaques on the mouth and tongue [10]. Immunocompromised patients are more

likely to experience oral thrush [11], but there is also an increased prevalence in individuals taking antibiotics [12, 13] as bacterial competition is eliminated and *C. albicans* is able to establish a stronger foothold.

T-cell deficiency is linked to more chronic disease states, such as chronic mucocutaneous candidiasis (CMC), which presents as chronic infection of skin, genital and oral mucosa [14].

Vulvovaginal candidiasis (VVC) presents as an infection of the genital mucosa in women, and is very common; over 50% of women will have at least 1 episode of VVC in their lifetime [15, 16]. Women with truncated dectin-1 receptors, responsible for β-1,3-glucan detection and incitation of an immune response to *C. albicans*, exhibit higher rates of recurrent vulvovaginal candidiasis (RVVC) [17, 18].

As well as superficial infection, *C. albicans* has the potential to cause much more severe infection, given the opportunity. Host epithelia as well as other immune cells typically elicit a prompt immune response to colonising and invading *C. albicans* [19] that keeps the yeast in balance, but in immunocompromised and vulnerable individuals such as cancer patients, HIV patients, and the elderly [20] there is a much higher risk of more severe infection. *C. albicans*' pathogenicity is underpinned by the ability to switch from a commensal, yeast-like morphology to a filamentous, hyphal morphology [21]. Epithelial colonisation and hypha-driven penetration can lead to a translocation of *C. albicans* into the circulatory system, and systemic infection with mortality rates upwards of 40% [22, 20, 23]. Candidaemia, or bloodstream infection often resulting from invasive candidiasis, is

one of the more common bloodstream infections [24], and in the US alone, sees approximately 25,000 cases a year with at least 25% mortality [25].

1.2 *C. albicans* virulence traits

C. albicans can attribute its success as a human pathogen to several factors. First and foremost is its morphological plasticity, balancing commensalism as in yeast form and changes in the immediate environment to drive a switch to filamentous growth [21]. This morphological plasticity also facilitates the development of robust *C. albicans* biofilms on biotic and abiotic surfaces [26]. There are other reported *C. albicans* cell morphologies driven by exposure to the environment that lead to increased survival in host niches. For example, GUT cells have a distinct transcriptomic profile following passage through the mammalian gut that predisposes them to existence in the digestive tract, including better utilisation of fatty acids as a carbon source [6].

Able to survive in several host niches, *C. albicans* also displays a remarkable adaptability to the environment, and this includes the capacity for development of antifungal tolerance and resistance; with a highly plastic genome, chromosomal aneuploidy often accompanies resistant strains [27, 28]. *C. albicans* can also attribute its adaptability and capacity for existence in multiple host niches to robust stress response mechanisms. For example, *C. albicans* is highly tolerant to oxidative stresses when compared to other similar yeasts [29], expressing GPI-anchored Sod proteins for rapid detoxification of the environment [30]. *C. albicans* also persists at a variety of environmental pHs, with pH sensing Rim101 contributing to

pH adaptation morphological switches mediated by pH [31, 32]. Alongside this environmental adaptability comes methods through which *C. albicans* modulates immune responses; through both transcriptional and post-translational mechanisms, *C. albicans* shields its β-glucan cell wall behind a thick mannan layer, limiting recognition by immune cells [33, 34, 35]. All of this, and more, contributes to *C. albicans*' success as an opportunistic fungal pathogen.

1.2.1 *C. albicans* morphogenesis and signalling

1.2.1.1 Ras-cAMP-PKA signalling

One pathway involved in the control of the yeast-to-hypha transition is the Ras-cAMP-PKA pathway (Fig. 1.1). Ras signalling is highly conserved throughout fungi and higher eukaryotes [36, 37, 21]. There are two Ras coding genes in *C. albicans*; *RAS1* and *RAS2* code for the small GTPases Ras1 and Ras2, respectively. Ras2 largely diverges in function from what is understood about Ras2 functionality in *S. cerevisiae*, whose two Ras proteins ScRas1p and ScRas2p are redundant and share considerable sequence homology with *C. albicans*' Ras1 [38]. Deletions of *RAS1* render *C. albicans* unable to form hyphae in response to stimuli [39]. Activation of the small GTPase Ras1 is contingent on a switch from a guanosine diphosphate (GDP)-bound state to a guanosine triphosphate (GTP)-bound state, under the control of guanine exchange factors (GEFs) [40] (Cdc25 in *C. albicans*) [41]. Activated Ras1 associates with the adenylyl cyclase Cyr1 to promote synthesis of the second messenger cyclic adenosine monophosphate (cAMP) [21, 37,

41, 42].

At the centre of Ras signalling, Cyr1 is considered an environmental sensor, with multiple domains besides a Ras association (RA) domain [42] capable of catalysing cAMP production. In response to certain sugars and amino acids, the G-protein coupled receptor (GPCR) Gpr1 activates G protein Gpa2, which then binds to the Gα domain of Cyr1 [44, 45, 46, 47]; deleting *GPR1* or *GPA2* causes filamentation defects, though only on solid medium [45]. Cyr1 is capable of activation in response to elevated temperature; the heat shock protein (Hsp) Hsp90 is thought to regulate Cyr1 [48] with co-chaperone Sgt1 [49], binding to Cyr1's leucine-rich region (LRR). In response to elevated temperature (37°C), Hsp90 disassociates from Cyr1 and derepresses cAMP production; indeed, a *hsp90* null mutant exhibits greatly increased transcript levels of hyphal specific gene *HWP1* [48]. The LRR region of Cyr1 has also been observed to interact with bacterial peptidoglycan fragments such as muramyl dipeptide (MDP) to promote cAMP production [50, 51]. Linked to this, is *C. albicans*' strong filamentous behaviour in response to serum; serum's bacterial peptidoglycan content has been posited as the trigger [51], while others suggest that serum's D-glucose content and basic pH trigger filamentation [39, 52]. Lastly, CO_2 has been established as a prominent yeast-to-hypha trigger in a Ras1 independent but Cyr1 dependent manner; mutants without Ras1 are still able to filament on solid medium in response to elevated CO_2, but mutants without Cyr1 are not [53]; it has also been shown through truncation of Cyr1 that

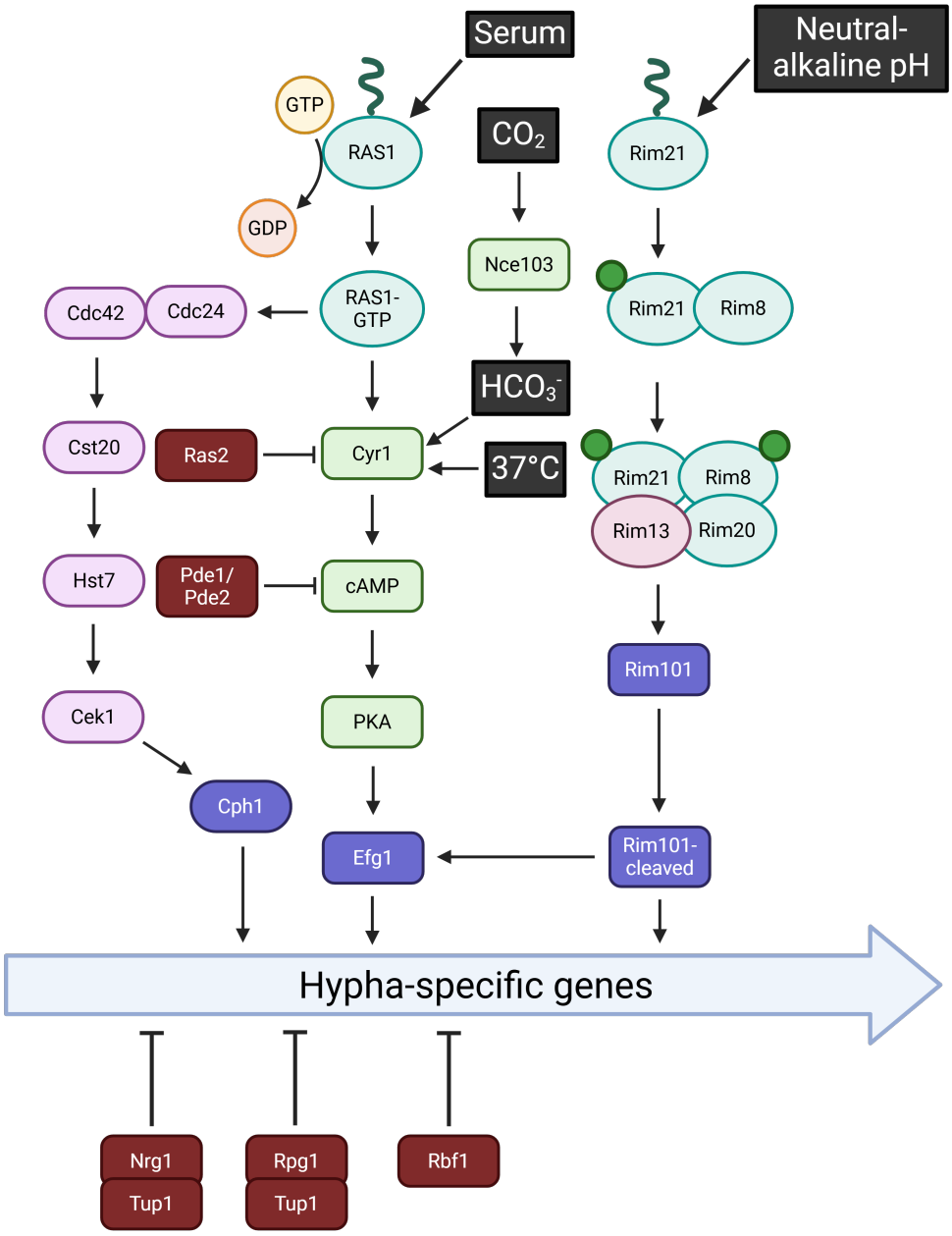

FIGURE 1.1: ***C. albicans* filamentation: Ras signalling, pH sensing and crosstalk with MAPK**

Schematic highlighting some pathways contributing to *C. albicans*' filamentation. The Ras1-GTPase is activated in response to serum, associates with Cyr1. Elevated CO_2 raises intracellular HCO_3^-, and elevated temperature triggers a derepression of Hsp90 from Cyr1. Each of these cues triggers Cyr1 production of cAMP, leading to PKA activation and expression of HSGs. Ras1 activation also activates Cdc24 and, in turn, Cdc42, which triggers a Cek1-MAPK response and activation of HSGs. A neutral to alkaline pH, sensed by Rim21, leads to phosphorylation of Rim21 and Rim8, formation of a complex with Rim13 and Rim20, and C-terminal cleavage of Rim101. This cleavage activates Rim101, which activates HSGs. Modified from Sudbery 2011 [43], created in https://BioRender.com.

only the catalytic domain is necessary for this effect. *C. albicans* maintains intracellular CO_2 as bicarbonate (HCO_3^-), driven by the carbonic anhydrase Nce103, [53] and bicarbonate directly interfaces with the catalytic domain of Cyr1 to drive cAMP production. This mechanism is also potentially a colony-wide signalling mechanism; CO_2 buildup within a colony microenvironment is sufficient to drive CO_2-dependent Cyr1 activation [54]. CO_2 is of physiological interest with regard to filamentation and virulence of *C. albicans* owing to the elevated CO_2 present in niches of the human body [55, 56]. pH has also been linked to the regulation of the cAMP-PKA pathway, with some groups suggesting that a more acidic pH causes bicarbonate ions to exist as their conjugate carbonic acid and thus prevent interaction with Cyr1 [57].

Elevated intracellular cAMP causes the activation of protein kinase A (PKA). PKA is a heterotetramer comprised of two regulatory subunits (both encoded by *BCY1*) [58] and two catalytic subunits (encoded by *TPK1* or *TPK2*) [37, 59, 60]. Deletion of *TPK2*, but not *TPK1*, renders *C. albicans* avirulent in an oropharyngeal candidiasis model [61]. cAMP causes a derepression of PKA by binding to Bcy1 and causing a conformational change that dissociates it from PKAs catalytic subunits, allowing PKA to phosphorylate downstream effectors and transcription factors, including transcription factors Efg1 [37, 21, 62]. Efg1 has been heavily implicated in the hyphal induction and expression of hyphae-specific genes (HSGs), as well as in its own regulation; Efg1 has been shown to bind the *EFG1* promoter and cause a downregulation [63], suggesting that Efg1 itself is important for hyphal induction but not sustained filamentous growth. Deletion of *EFG1*, and as

such inhibition of filamentation, renders *C. albicans* avirulent [64]. cAMP levels are negatively regulated via hydrolysis by the phosphodiesterases Pde1 and Pde2 [65, 66], though Pde1 has a relatively low affinity for cAMP in comparison to Pde2 and has more specific roles in mitigating cAMP signalling in response to glucose acquisition [66].

1.2.1.2 Ras1 crosstalk with Cek1 MAPK signalling

Ras signalling has been demonstrated to induce filamentation in a cAMP-PKA independent manner. Using a constitutively active Ras1 mutant, Ras1 G13V, a link was discovered between Ras1 and the mitogen-activated protein kinase (MAPK) Cek1 signalling pathway [67] (Fig. 1.1. GTP-bound Ras1 is thought to activate GEF Cdc24, in turn activating Cdc42 [68, 69]. Among other roles within the cell, Cdc42 has been attributed to activating the p21-activated kinase (PAK) Cst20 of the Cek1 pathway and activating the cascade [70, 71]. Reducing Cdc24 or Cdc42 transcript levels does impact filamentation; cells are still capable of induction of HSGs, but incapable of maintaining the induction required for continued and typical filamentous growth [69]. Cek1, the MAPK of this pathway, activates transcription factor Cph1, known to induce transcription of HSGs [72]. Without Cph1, cells are unable to filament on solid medium, but are still capable of serum-induced filamentation, likely as a result of Ras-cAMP-PKA induction.

1.2.1.3 Rim101 induction of *C. albicans* filamentation

Independent of Ras1 or PKA activation, *C. albicans* filamentation can be induced through the sensing of a more alkaline pH through processing of Rim101 [21, 32, 31]. pH sensor Rim21 [73] is phosphorylated in neutral-alkaline pH [74] and associates with β-arrestin-like protein Rim8 [74, 73], and endocytosed in an ESCRT-dependent manner. Rim8 phosphorylation promotes formation of a complex containing recruiting protein Rim20 [74] and calpain-like proteolytic protein Rim13 [75]. This complex allows for the recruitment of, and C-terminal cleavage of, Rim101 [32, 74, 76, 75]. Intact Rim101 is inactive, and Rim13-mediated cleavage of the C-terminus from Rim101 triggers its activation [21, 75, 74]. Genetic knockdown of any one of these proteins prevents alkaline-induced filamentation. When Rim101 is cleaved and active, it triggers transcription of hyphal-specific genes [77], and also transcriptionally represses Rim8 as part of a negative feedback mechanism [74].

1.2.1.4 Negative regulation of filamentous growth

The global transcriptional regulator associated with repression of *C. albicans* filamentation is Tup1 [78], whose inhibition is mediated by DNA binding proteins Rfg1 and Nrg1 [79, 80]. *TUP1*, *NRG1* and *RFG1* knockout is sufficient to drive filamentation, typical hypha-inducing conditions or otherwise [78, 79, 81, 80]. Nrg1 expression has been shown to be downregulated in the presence of serum, and

thus has been postulated that as Nrg1 expression drops, Tup1-Nrg1 mediated repression of HSGs is lost [81]. Further work suggests that *NRG1* transcription is repressed largely by Brg1 [82], a transcriptional regulator largely associated with induction of filamentation [82, 83].

1.2.2 Biofilms

C. albicans' virulence and persistence within a human host can be largely attributed to its ability to develop and maintain robust biofilms on biotic and abiotic surfaces [84, 85, 86, 87]. A biofilm can be described as a microbial colonization of a surface, with an extracellular matrix (ECM) coating [88]. The risk to life posed by fungal and bacterial biofilm development notwithstanding, biofilm growth and associated complications are thought to cost upwards of $400 billion to global healthcare sectors, with perhaps 10% of that value the result of fungal biofilms [88, 89]. Difficulties associated with biofilm development can be numerous. *C. albicans* was determined one of the primary colonisers and biggest contributors of biomass on voice prostheses in total laryngectomy patients [55], triggering recurrent device failures and necessitating frequent replacement of the device, at both cost to the NHS and to patient wellbeing. *C. albicans* biofilms prove difficult to treat, owing to an inherent drug resistance promoted by the protective ECM [90, 91]; it is thought that the ECM causes sequestration of antifungal drugs, acting as an impermeable barrier that protects the cells.

Second and more concerning regarding biofilm formation is the significant infection risk they pose; difficult to treat with regular antifungal and antibiotic regimen

[90, 91, 92, 93], a single species or polymicrobial biofilm presents a resilient source of pathogenic fungal and bacterial species [94, 95, 87] that can contribute to infection. During the COVID-19 pandemic, there was a considerable increase in ventilator-associated pneumonia and non-viral respiratory infections, owing to the prevalence of biofilm formation on ventilator tubing [96, 97, 98, 99]. In many of these instances, whilst the microbe responsible was not necessarily a *Candida* spp. , the presence of *C. albicans* isolates from many of the patients still alludes to a role for the fungi in the establishment of the infection. Some research suggests that *C. albicans* biofilms, being robust as they are, may act as a platform or protective scaffold for other microbes to better establish themselves [55, 56]. Indeed, there is some evidence to suggest that the protective ECM produced by *C. albicans* benefits other microbes; studies have determined *Staphylococcus aureus* biofilms grown in concert with *C. albicans* are more tolerant to vancomycin as a result of *C. albicans*' ECM secretion [93].

1.2.2.1 Biofilm growth cycle

The development of a *C. albicans* biofilm follows 4 universal stages, whether on a biotic or an abiotic surface (Fig. 1.2).

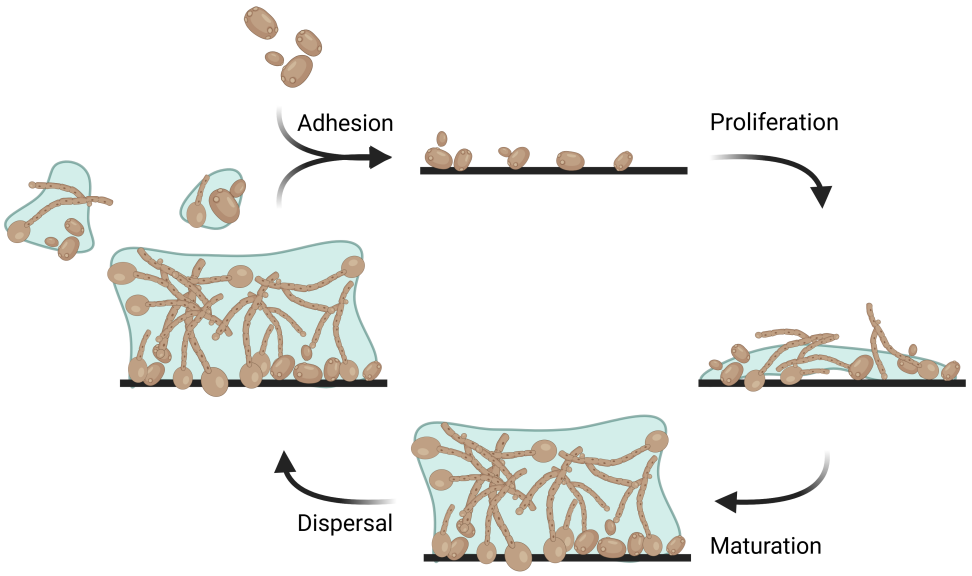

FIGURE 1.2: ***C. albicans* biofilm formation**
C. albicans biofilm formation follows four stages of growth. **Adhesion** to a biotic or an abiotic surface, mediated by expression of adhesins. **Proliferation**, where *C. albicans* rapidly colonises the surface through division and drives expression of hypha-specific genes. **Maturation** is the generation of a complex and robust colony enclosed within a protective extracellular matrix. **Dispersal** is a shedding of yeast and hyphal cells from the mature biofilm, capable of colonising a surface and beginning a separate biofilm, or of causing infection. Reproduced from Alim 2018 [100], Created in https://BioRender.com.

Surface colonization: Predominantly yeast-form *C. albicans* attaches to a surface [88, 101, 102]. This early cell-surface or cell-cell interaction is dependent on expression of adhesins, with early colonization reliant on members of the agglutinin-like sequence (Als) family of proteins [102, 103]. Als1, Als2 and Als4 have been implicated in contributing to early biofilm development [104, 105]. The Als proteins are glycerophosphatidylinositol (GPI)-anchored, and whilst the method by which they promote adhesion to an abiotic surface is not fully understood, an *als1/als3* Δ/Δ mutant displays reduced adhesion capacity in vitro [106].

Proliferation: Following establishment on a surface, cells undergo a drastic shift toward rapid proliferation and establishment of themselves upon the surface. In *C. albicans*, this process is accompanied a yeast-to-hyphal switching of some cells

through an interplay of pathways previously mentioned [21, 41, 54, 88]. As fungal biomass grows, CO_2 generated by the developing biofilm drives further filamentation [54].

Maturation: This marks the establishment of a robust biofilm, accompanied by excretion of ECM that lends the biofilm additional structure and protection [90, 91]. *C. albicans* ECM is comprised largely of mannan and β-glucan polysaccharides [90, 107], extracellular proteins, neutral lipids [107], and DNA [107, 108]. There is heterogeneity within the biofilm population, a mixture of yeast and hyphal cells all housed within the ECM [26].

Dispersal: The final stage of the biofilm cycle, and perhaps the start of a new cycle, dispersal refers to the shedding of cells from the mature biofilm; these shed cells are then capable of establishing further biofilms or potentially causing infection [94]. Whilst the process of biofilm dispersal is the lesser understood aspect of the cycle, it has been observed that cells shed from biofilms, or "persister cells" are more virulent in a murine model compared to typical planktonic *C. albicans* [94].

1.2.2.2 Regulation of biofilm development

Given the degree of intricacy involved in *C. albicans* biofilm development, it stands to reason that transcriptional control of these processes is complex. Early studies determined a core of 6 transcription regulators that coordinated expression of over 1000 genes for biofilm formation [109, 110, 111]. These 6 core transcription factors, *EFG1*, *BCR1*, *BRG1*,*ROB1*,*TEC1* and *Ndt80* display a considerable degree

of overlap in the genes they interacted with, highlighting clusters of biofilm related genes that are regulated by multiple transcription factors [110]; these transcription factors were also shown to regulate expression of one another, and autoregulate. Further work added 3 more transcription factors to this biofilm regulatory core: *GAL4*, *FLO8* and *RFX2* [104]. While there are upward of 30 transcription factors that positively or negatively regulate genes associated with different stages of biofilm formation, deletion of any one of these 9 core transcription factors greatly alters *C. albicans* biofilm formation in vitro and in vivo [110, 104]. Each core transcriptional regulator contributes to temporal control of genes necessary for biofilm development; *EFG1* and *TEC1* have been implicated in early biofilm proliferation, driving the yeast-to-hypha transition and expression of HSGs [63, 88, 110]; *BCR1* is important for expression of key adhesins that promote initial surface colonization including Als1, Als3 and Hwp1 [111, 105, 112].

1.2.3 Fungal Cell Wall

Whilst not a virulence trait in and of itself, the *C. albicans* cell wall is subject to immune recognition, and the mechanisms through which *C. albicans* mitigates this recognition (discussed under Immune Evasion below) contribute to *C. albicans*' virulence and success within the host. An overview of *C. albicans*' cell wall structure can be seen in Fig. 1.3. The cell wall is largely comprised of different polysaccharides and glycoproteins forming an "inner" skeletal layer and an outer mannoprotein brush layer, the composition and generation of which is outlined below. GPI-anchored proteins covalently linked to β-1,3-glucans and chitin by

β-1,6-glucan linkers can be post-translationally mannosylated, and these complex mannan oligosaccharides form the outer layer of the cell wall [113].

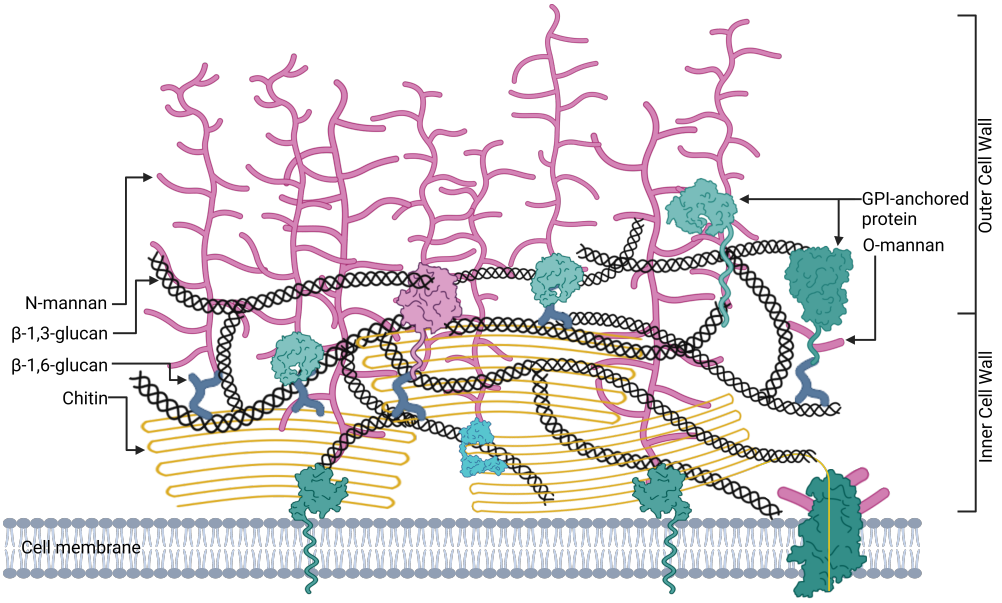

FIGURE 1.3: ***C. albicans* cell wall structure**
C. albicans inner cell wall is a structural, "skeletal" layer built of chitin microfibrils (yellow) and β-1,3-glucan helices (black). Within the inner layer are GPI-anchored proteins (teal), bound to chitin and β-1,3-glucan by β-1,6-glucan linkers (dark blue). GPI-anchored proteins can be mannosylated, and these mannan residues form the fibrillar structure making up the bulk of the outer cell wall. Reproduced from Lenardon 2020 [113], Created in https://BioRender.com using schematic resources generated by Lenardon *et al.*

1.2.3.1 Inner cell wall

The inner cell wall, or skeletal layer, acts to tether to the membrane, provide rigidity and support. The skeletal, inner layer of the *C. albicans* cell wall is composed of the oligosaccharides chitin and β1,3-glucan (β1,3G) and β-1,6-glucans (β1,6G). Chitin is a polymer built up of N-acetylglucosamine (GlcNAc) monomers [114, 115]. Chitin has been referred to as fungal "armour" [116], owing to its importance in lending protection and stability to fungi, offering a counter to the turgor

pressures of the cell [117]. Chitin also plays a role in septation fidelity at the end of the yeast cell cycle [118, 119].

Chitin synthesis in *C. albicans* is controlled through the action of 4 chitin synthase gene families: *CHS1*, *CHS2*, *CHS3* and *CHS8* [114, 117, 120, 121], responsible for the polymerization of GlcNAc residues. Studies have credited Chs3p with synthesizing the majority of total chitin during both yeast and hyphal growth [118]. Whilst all chitin synthases contribute to chitin synthesis, Chs1 has a low basal expression in both yeast and hyphal growth, and Chs2 and Chs3 are more highly expressed and upregulated during hyphal growth [117, 118].

Transcriptional control of chitin synthesis has been seen to predispose cells to increased resistance to echinocandins, an antifungal drug that targets β-glucan synthesis [121, 120]; cells stressed with either chitin binding agent calcofluor white (CFW) or treated with Ca^{2+} show increased chitin content owing to calcineurin, Mkc1 and Cek1 driven activation of "cell salvage" mechanisms [117]. A pre-treatment with either CFW or Ca^{2+} has proven to increase resistance to echinocandin treatment in vitro [120] and in vivo [121].

β-glucans make up the most abundant component of the fungal cell wall [122, 123] and as such lend considerable structure and rigidity to *C. albicans*. The synthesis of β-1,3-glucans is predominantly orchestrated by the *FKS* family of genes [124, 125, 126, 127, 122]. The protein Fks1 is responsible for the majority of glucan synthesis [128], with some functional redundancies in Fks2 and Fks3 [129]. Fks1 forms a β-glucan synthase complex; a transmembrane complex that coordinates generation of oligomeric chains of β-glucan, using UDP-glucose as a sugar donor [122, 113]. *FKS1* is essential, and gene knockouts are inviable. As such, it is the

target of the echinocandin class of antifungal [124, 127]. *C. albicans* treated with the echinocandin caspofungin exhibits severely diminished β-glucan content in its fungal cell wall, though typically with an accompanying increase in chitin content to compensate [130], likely through activation of cell wall salvage mechanisms described above [117].

1.2.3.2 Outer cell wall

The outer layer of the fungal cell of the fungal cell wall is comprised predominantly of mannan sugars attached to cell-wall associated proteins [131, 132]. It plays a multi-faceted role in the regulation of *C. albicans*' interaction with non-self entities, virulence, and immune evasion, as well as protection of the inner cell wall from damage [131]

.

O-linked mannosylation is the post-translational attachment of mannose sugars to serine/threonine residues on nascent proteins [131, 132, 133, 134, 135]. The process begins in the rough endoplasmic reticulum (rER), whereby dolichylphosphate-mannose (Dol-P-man) donates sugar residues through the action of the *PMT* family of mannosyltransferases, *PMT1*, *PMT2*, *PMT4*, *PMT5* and *PMT6* [134, 135]; the first α-mannose is attached to a nascent protein via ester bond to a serine or threonine. Homozygous null deletion of *PMT1* and *PMT4* causes an overall reduction in mannan content of the outer cell wall[134, 135], a *PMT4* deletion impacts virulence in a murine model, and *PMT2* is an essential gene, with a deletion proving lethal [134]. Stephan Prill proposed an environment specific role for the

various *PMT* family genes, as *pmt4* Δ/Δ led to a filamentation defect in normal air but was comparable to wild type in hypoxic conditions [134].

Following initiation of O-mannosylation in the rER, modifications are elaborated on in the Golgi complex, whereby the α1,2-mannosyltransferases Mnt1 and Mnt2 add further mannose residues, generating linear chains of up to 5 mannose residues [133, 136, 137]. Other members of the *MNT* family of genes have functions unaffiliated with O-mannosylation, but instead with phosphomannan elaboration of N-linked mannan, to be elaborated on further later [138]. *MNT1* and *MNT2* deletions both have truncating effects on O-mannan chains in the fungal cell wall [133, 139], a sensitivity to cell wall perturbing agents and limited biofilm development [133, 134, 135, 140]. O-mannan largely fills a role facilitating interactions with the host, and deletions of genes associated with appropriate assembly of O-mannan chains typically lead to attenuated virulence [133, 134]. It has been hypothesized that this could, in part, be due to the proteins known to be post-translationally mannosylated, including the adhesin Als1, Kre9 and Pir2 [134].

N-linked mannosylation is the attachment and elaboration of complex mannan-containing oligosaccharides to asparagine residues of proteins [131, 132, 141], and oligosaccharides are typically more complicated and branched than O-linked mannan. Again, beginning within the rER, N-mannosylation depends upon the establishment of a glycan core. Dolichol pyrophosphate acts as a lipid carrier upon which the initial core of 3 glucose residues, 9 mannose residues and 2 N-acetylglucosamine residues ($Glc_3Man_9GlcNAc_2$) is assembled through the action of several genes from

the *ALG* family [131, 132, 142]. Following transfer to an asparagine residue of a nascent protein through the action of the OST complex [143] the core is further modified, through the action of the glycosidases Rot2, Mns1, and Cwh41, to remove the 3 glucose residues and a mannose residue to yield a complete core ($Man_8GlcNAc_2$) [142]; null mutations of *ROT2*, *MNS1* or *CWH41* exhibit attenuated virulence, highlighting the necessity for appropriate glycan core formation for downstream N-mannan elaboration. This process is highly conserved throughout eukaryotes, but downstream of core assembly N-mannosylation in *C. albicans* diverges from what is known about human N-mannosylation.

In the Golgi complex, asparagine-linked glycan cores can be further elaborated upon in several ways, beginning with the establishment of a α1,6 mannose backbone; Och1 is responsible for the attachment of the first α1,6 mannose residue, and homozygous null deletions of *OCH1* display no α1,6 mannose backbone, a sensitivity to cell wall perturbing agents and constitutive activation of the cell wall integrity (CWI) signaling pathway, as well as an attenuated virulence independent of fungal burden [144]. This deletion also typically displays increased chitin and glucan content in the inner cell wall following activation of the cell salvage pathway [131, 144]. Elongation of the α1,6 mannose backbone is coordinated by mannan polymerase complexes I and II (M-Pol-I, M-Pol-II); in *S. cerevisiae*, M-Pol-I is a heterodimeric complex between Mnn9 and Van1, responsible for the addition of up to 7 α1,6 mannose residues to the initial residue [132]. M-Pol-II, in *S. cerevisiae*, is a multimeric protein complex of Mnn9-11, Anp1 and Hoc1 [132]. There

is evidence to suggest Mnn9 fulfills a similar function in *C. albicans*, and an *MNN9* deletion in *C. albicans* leads to 50% reduced mannan, morphogenic defects and a sensitivity to osmotic stress [145], suggesting that whilst the complexes themselves have not been further elaborated on in *C. albicans*, Mnn9 functionality at least is likely conserved.

Following elongation of the α1,6 mannose backbone, N-mannans may be further elaborated upon through the addition of α1,2 mannose residues to create branches through the action of mannosyltransferases Mnn2, Mnn4 and Mnn5 [138, 141], with Mnn1 adding an α1,3-mannose residue as a means of capping α1,2 chains [146]. With the generation of these α1,2 chains, the outer cell wall takes on a fibrillar, brush-like appearance that is diminished upon deletion of *MNT2*, *MNT4* and *MNT5* [131].

N-mannans can be further modified through the addition of β-mannan chains through a phosphodiester linkage [138, 147]. Indeed, O-mannans can also be modified in a similar fashion [132]. These β-mannan chains, or phosphomannans, have been implicated in masking of β-1,3-glucans, and disruption of phosphomannan attachment and elongation to both O and N-linked mannan reduces virulence[132, 138, 147], although a previous study found that disruption of β-mannan chain development on N-glycans had no impact on immune recognition [148].

1.2.4 Immune evasion

Another way in which *C. albicans* establishes itself as a successful opportunistic fungal pathogen is its capacity for avoidance of host immune responses. Human innate immune systems employ several strategies for detection and clearance of pathogenic fungi, primarily stemming from expression of various pattern recognition receptors (PRRs) on the immune cell surface [149, 150, 151, 152, 153, 154, 155, 156]. PRRs are categorised further based on their structure and downstream intracellular impacts following ligand binding, into toll-like receptors (TLRs), Nod-like receptors (NLRs) and C-type lectin receptors (CLRs) [149]. These receptors are responsible for the detection of a vast array of pathogen-associated molecular patterns (PAMPs) that, following recognition and binding, trigger a host of downstream effects from cytokine and chemokine release to phagocytosis [149, 157].

CLR	PAMP	Expressed by
Dectin-1	β-Glucan	Macrophages, dendritic cells, monocytes, neutrophils
Dectin-2	α-Mannose, low affinity	Dendritic cells, macrophages
Mannose Receptor	GlcNAc	Macrophages, dendritic cells
Collectins	Mannose, fucose, GlcNAc	N/A- secreted, soluble
DC-SIGN	Mannin	Dendritic cells
MGL	GalNAc	Dendritic cells, macrophages
Langerin	Mannose, fucose, GlcNAc, mannin	Langerhans cells

TABLE 1.1: A summary of CLRs, their associated PAMPs and the cells that express them. Table adapted from Hollmig *et al*, 2009 [157]

CLRs typically recognise carbohydrate structures; a list of CLRs and their respective PAMPs can be found in table 1.1. Comprised largely of carbohydrate, the *C. albicans* cell wall is a prime target for CLR detection. As an example, the CLR dectin-1, expressed on the surface of dendritic cells, macrophages and neutrophils, recognises and binds β-glucans [149, 152, 157, 33, 158]. This recognition and ligand binding leads to a tyrosine kinase-mediated phosphorylation of an immunoreceptor tyrosine-based activation motif (ITAM) in the receptor's cytosolic tail [152, 157] which leads to recruitment of the spleen tyrosine kinase (SYK), its activation, and activation of downstream targets [152, 154]. Disruption of dectin-1 ligand binding has been shown to lead to a reduced phagocytic uptake of *Aspergillus fumigatus* and increased fungal burden [159]. The cytosolic ITAM domain is also important for phagocytic uptake; a study determined that disrupting the ITAM sequence eliminated dectin-1-mediated phagocytic uptake, despite the receptor recognising and binding its ligand [152].

Dectin-1 ligand binding, ITAM phosphorylation and SYK activation promotes phagosome formation and phagocytosis through signal transducer Card9 [149, 152, 160]. Genetic manipulation of Card9 has been shown to reduce phagocytic uptake of *C. albicans*. The importance of this particular response and signal transduction in combating fungal pathogens is underpinned by a study that identified a family predisposed to recurrent fungal infections; the family had lost children to fungal infections during adolescence. Studies into the family determined that those who were subject to chronic fungal infections had point mutations in the *CARD9* gene

that led to a protein truncation, and as a hindered innate immune response [155].

60% of *C. albicans*' cell wall is composed of β-glucan [157]. One of the strategies that *C. albicans* has developed as a means of evading immune detection is a "masking", or hiding of this particular PAMP by modulating the composition and thickness of the outer mannan layer of the cell wall [35, 34, 161]. It has been shown in several instances that genetic manipulation of *C. albicans*' ability to remodel its cell wall, in particular the mannan layer, increases its recognition by and subsequent engulfment by macrophages [132, 138, 147].

PRR ligand binding also leads to chemokine and cytokine production, as well as a phospholipase C (PLC) and NADPH-oxidase mediated generation of reactive oxygen species (ROS) [154, 30], both within the immediate area and within developing phagosomes [30] in a mechanism referred to as an oxidative burst. This rapid toxification of the immediate environment is an effective response able to kill many microorganisms. Through increased expression of intracellular and GPI-anchored superoxide dismutase (Sod) proteins, as well as catalases, *C. albicans* proves itself incredibly resilient to this particular attack; Sod4, Sod5 and Sod6 are able to convert O_2^- free radicals to H_2O_2, which is subsequently converted to oxygen and water [30, 162, 163]. *sod4* and *sod5* gene disruption in *C. albicans* leads to a hypersensitivity to macrophage oxidative bursts [30].

Another facet of the innate immune system that *C. albicans* contends with is the complement system. Complement proteins are circulating zymogens that act to enhance detection and clearance of pathogens. Complement cascades can be broken up into classical, alternative and lectin pathways [164, 165]. Briefly, each complement cascade converges on production of complement protein C3, the cleavage of which generates C3a and C3b; C3a is a pro-inflammatory anaphylatoxin that, as well as triggering responses in macrophages and other immune cells, can also cause vasodilation and alter blood vessel permeability to allow for more rapid flooding of immune cells to a site of infection [166]. Complement C3b, however, serves a few roles- it is an opsonin, and can therefore decorate the surface of a pathogen in order to facilitate opsonophagocytosis [167]. C3b also forms a part of the alternative pathway's C3 convertase, and can therefore spark a cascade of further C3 cleavage [164]. C3b also forms a part of the C5 convertase complex that results in the formation of membrane attack complexes for pathogen killing by forming pores in lipid bilayers [168].

Candida spp have mechanisms to combat and mitigate complement activation. A prominent example of this is production of secreted aspartyl proteases (SAPs), capable of complement protein cleavage and turnover [169, 170, 171, 172], though some evidence suggests that instead of allowing for immune evasion, Sap proteins instead modulate and trigger proinflammatory responses leading to host damage [170]. Further examples of *C. albicans* modulating the complement cascade pertain to a demonstrated proclivity for recruitment of the complement regulatory factor factor H. Factor H is responsible for inactivating C3b to temper the immune

response. Pra1, a protein responsible for zinc sequestration from the extracellular environment [173], also has demonstrable factor H binding capabilities that, when secreted, recruit factor H and promote rapid inactivation of complement C3b [174, 175, 176]. Similarly, a recent study determined that an adaptation to oestrogen exposure causes an upregulation and surface localisation of protein Gpd2. Gpd2 displays a high binding affinity for Factor H, and these cells displayed greater levels of factor H recruitment to the cell surface and a drastic reduction in phagocytic uptake, suggesting a rapid turnover of C3 and C3b and a prevention of opsonophagocytosis [5].

Failing avoidance and following phagocytosis, *C. albicans* displays a resilience in its ability to survive and escape prior to lysosomal degradation, and a shift to hyphal growth in an effort to escape. There is evidence to suggest that *C. albicans* is capable of regulating the pH within a phagosome to a more basic pH to stimulate hyphal formation [177]. This process involves an upregulation of amino acid transport and arginine catabolism by the urea amydolyases Dur1p and Dur2p, yielding ammonia to raise the pH of the surrounding environment [177]. Further research into this mechanism posits that, given that another byproduct of this reaction is CO_2, that the yeast-to-hyphal switch triggered within the phagosome is, in part, owing to both the basic pH and CO_2 mediated activation of adenylate cyclase cAMP production and PKA signalling [177, 178]. However, it is not just filamentation that allows *C. albicans* to escape from inside macrophages; studies have determined that expression of the toxin candidalysin plays an important

role in macrophage membrane lysis, and hence, escape. *ece1* Δ/Δ cells, unable to produce and secrete candidalysin, show a greatly hindered ability to escape macrophages once phagocytosed, regardless of their ability to form hyphae [179].

1.3 Lipid droplet metabolism

Lipid droplets are transient organelles found in organisms from single-celled eukaryotes to mammals [180, 181]. They comprise a core of non-polar, "neutral" lipids encapsulated by a protein-studded phospholipid monolayer [42, 181, 182, 183]. The make-up of the neutral lipid core varies from organism to organism; within yeast, typically neutral lipid cores triacylglycerols (TAG) and sterol esters (SE) in roughly equal measure [180, 182], where TAG forms a central core and SE form "shells" [184, 185]. The role of lipid droplets within the cell is largely concerned with storage of these neutral lipids as a mechanism to mitigate lipotoxicity; storage of TAGs and SEs provides cells with resources for membrane building and energy upon growth resumption [180, 186, 187].

Lipid droplet formation occurs within the ER [188, 189, 190]. As neutral lipids build up within the bilayer, the start of a neutral lipid core begins to form as a lens; further growth of this lens causes gradual bulging of the bilayer into the cytosol as a nascent lipid droplet develops [180, 191] (Fig. 1.4. This process is reliant on the protein Fld1, believed to localise to and define subdomains in the

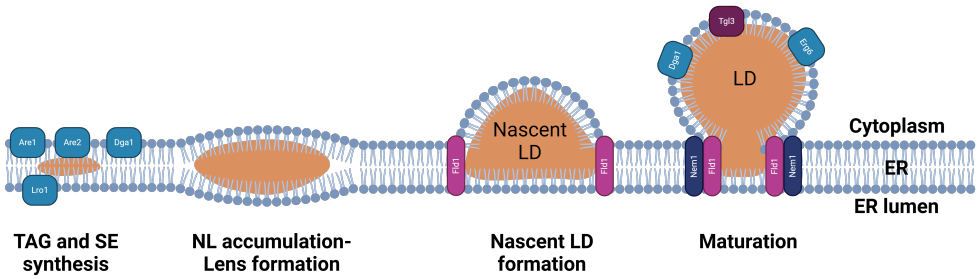

FIGURE 1.4: **Lipid droplet formation**
DAG acyltransferases Dga1 and Lro1 Drive TAG biosynthesis and deposition within cytosol-facing endoplasmic reticulum phospholipid bilayer, whilst Are1 and Are2 generate and deposit sterol esters. As neutral lipid content in the domain builds, membranes begin to curve and form lenses. Proteins such as Fld1 facilitate further curvature and the formation of nascent LDs. Curvature is dependent on enrichment of curvature-imposing phospholipid classes. Mature LDs comprise a neutral lipid core surrounded by a protein-studded phospholipid monolayer, largely remaining associated with the endoplasmic reticulum. Created in https://BioRender.com.

ER for LD bud emergence [183]. It has been suggested that this process is also dependent on demixing of the plasma membrane at sites of LD growth; an alteration of PL composition that supports membrane curvature, likely through enrichment of PL species whose presence, owing to their structure, imparts curvature on a membrane such as PA, PE and LPC [191] (Fig. 1.5).

As LDs continue to mature, neutral lipid biosynthetic enzymes translocate from the ER membrane to the LD monolayer to continue neutral lipid deposition within the developing core [192]. Lipid droplets remain associated with the ER membrane upon reaching maturity [190].

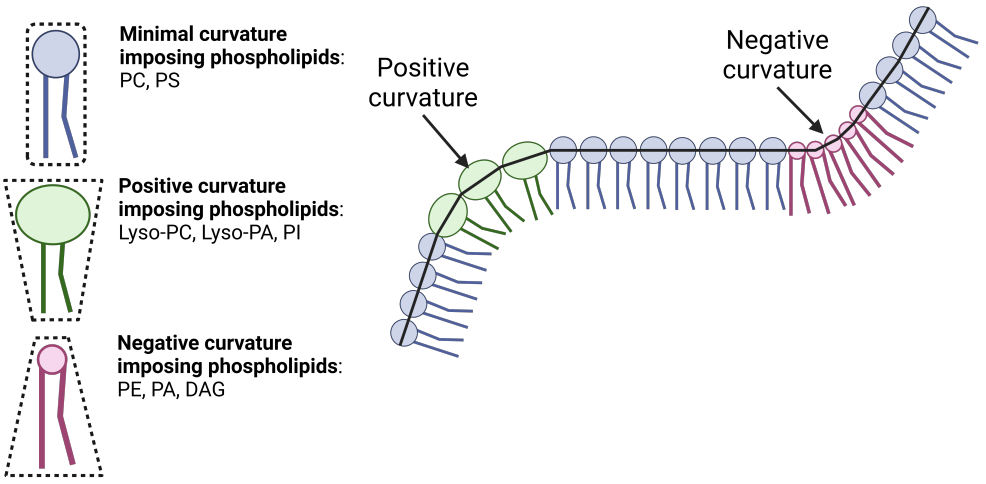

FIGURE 1.5: **Phospholipid structure imparts different curvatures to membrane**
Phospholipids with a more "cylindrical" shape impart little to no curvature on a membrane. Positive and negative curvature is imposed by "conical" or "inverse conical" phospholipids, where either the head group is significantly smaller than normal (DAG, with no phosphate/ choline/; PA, whose headgroup comprises glycerol and phosphate) or the head group is larger relative to the fatty acid tails (Lyso-PC with only one fatty acid moiety; PI, with a large phosphate-inositol headgroup).Created in https://BioRender.com.

1.3.1 Triacylglycerol storage

Triacylglycerol comprises a glycerol backbone with 3 fatty acid moieties [193, 194, 195, 187]. Generation of the molecule TAG, first and foremost, acts to mitigate lipotoxic effects imposed on a cell by accumulation of too much free fatty acid (FFA) [180]. Given the importance of FFAs in membrane biosynthesis and as an energy source, it is beneficial to the cell to store lipids for use during times of growth. TAG is an ideal molecule for this owing to its non-polar nature; it is possible to densely pack the molecule without an inherent charge disrupting surrounding hydrophilic regions, with the added benefit of a much higher energy to mass ratio when compared to carbohydrate energy sources [194]. What follows outlines the assimilation of endogenous and exogenous fatty acids and glycolytic

products into lipid droplets as triacylglycerols.

1.3.1.1 Phosphatidic Acid production

Phosphatidic acid (PA) is a molecule that sits at the crossroads between phospholipid and neutral lipid biosynthesis. It comprises a phosphate head group and a glycerol backbone with two fatty acid moieties attached [196]. PA is synthesised downstream of glycolytic processes within the cell (Fig. 1.6); in *S. cerevisiae*, Dihydroxyacetone phosphate (DHAP) can be metabolised into lyso-PA in both NADPH-dependent and independent means [197, 198, 199]. With DHAP as a substrate, proteins Gpt2 and Sct1 catalyse an acylation to generate 1-acyl-DHAP, and a subsequent NADPH-dependent reduction of 1-acyl-DHAP by protein Ayr1 yields lyso-PA [198, 199]. DHAP can also be converted into glycerol-3-phosphate (G3P) by triose phosphate isomerase Tpi1 [200]. G3P is another substrate for Gpt2 and Sct1 [199], and its NADPH independent conversion to lyso-PA relies instead on fatty acid-CoA (FA-CoA) molecules as fatty acid-donors. FA-CoA can either be derived from acetyl-CoA or through the processing of exogenous fatty acids [201, 202]. This mechanism allows for the assimilation of exogenous fatty acids from the environment, such as growth media or otherwise, for downstream use.

Whether derived from DHAP or G3P, lyso-PA is then donated a second fatty acid moiety in a reaction catalysed by partially redundant proteins Slc1 and Slc4, again with FA-CoA as a donor [203].

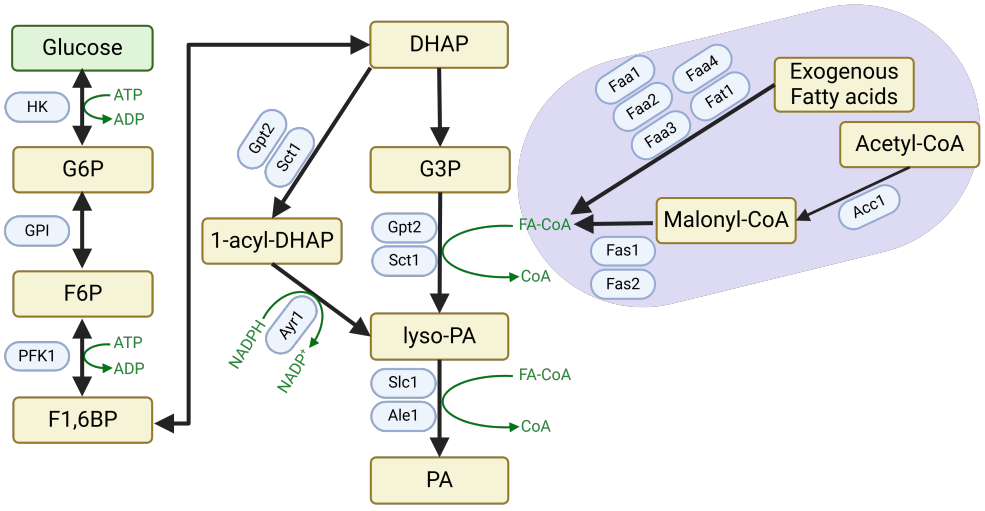

FIGURE 1.6: **Biosynthesis of phosphatidic acid from glycolysis derived metabolites**
Yeast generates phosphatidic acid species in manners both dependent and independent of NADPH. Donation of fatty acid groups from FA-CoA is a mechanism by which exogenous fatty acids can be assimilated, used or stored for downstream processes. Whether G3P or DHAP is the substrate, both are catalysed by redundant proteins Gpt2 and Sct1 to yield lyso-PA. A second reaction donates a second fatty acid chain, catalysed by Slc1 and Ale1. Reproduced from Khondker 2022 [204]. Created in https://BioRender.com.

Phosphatidic acid fulfils multiple functions within the cell. Other than being an important lipid precursor in both neutral lipid and phospholipid metabolism, it has also been determined that PA exerts a degree of transcriptional control over genes associated with glycerophospholipid biosynthesis [205, 197, 206]. The "Henry regulatory circuit", named for the lab whose work discovered it [205], describes PA flux on ER and nuclear membranes and how this impacts phospholipid regulation (Fig.1.7). Several phospholipid biosynthesis genes, including *CHO1*, *INO1* and *PSD1*, contain a repeated inositol-sensitive upstream activating sequence (UAS_{INO}) promoter sequence that is transcriptionally activated by Ino2 and Ino4 [207, 208]. During stationary phase and in nutrient scarcity, the transcriptional repressor Opi1 binds Ino2 and represses transcriptional activation,

essentially switching off de novo phospholipid biosynthesis [205, 209, 210]. During growth resumption and exponential phase, however, Opi1 is instead sequestered on the ER membrane by the protein Scs2 in a PA-dependent interaction [211, 212]; this leads to a derepression of Ino2/Ino4 and thus increased expression of de novo phospholipid biosynthetic processes.

PA is utilised in both the de novo generation of PL species [213], and the generation of diacylglycerol (DAG) species [196, 214]. In humans, control of this commitment to DAG synthesis is controlled by the protein lipin [215]. The *S. cerevisiae* homolog, Pah1, fulfils a similar role, exhibiting phosphatidate phosphatase activity [214, 196] and in doing so, coordinating storage of excess fatty acids as neutral lipids [214]. Indeed, disruption of *PAH1* in *S. cerevisiae* causes aberrant phenotypes associated with misregulation of lipid regulation, including altered phospholipid profiles in both log and stationary phase, hindered lipid storage and vacuolar defects, and protection against lipotoxicity [214, 216, 196]. The transcriptional and post-translational control of Pah1 is outlined in Fig.1.8.

Pah1 is a heavily regulated protein; its expression is transcriptionally controlled by nutritional availability [217], and following expression, Pah1 maintains a cytosolic localization [216]. It is a typically unstable protein, but for phosphorylation by several protein kinases, including PKA [218], PKC [219], and Pho85-Pho80 [220]; an overview of its phosphorylation sites and the kinases associated with their phosphorylation has been outlined in table 1.2 [204].

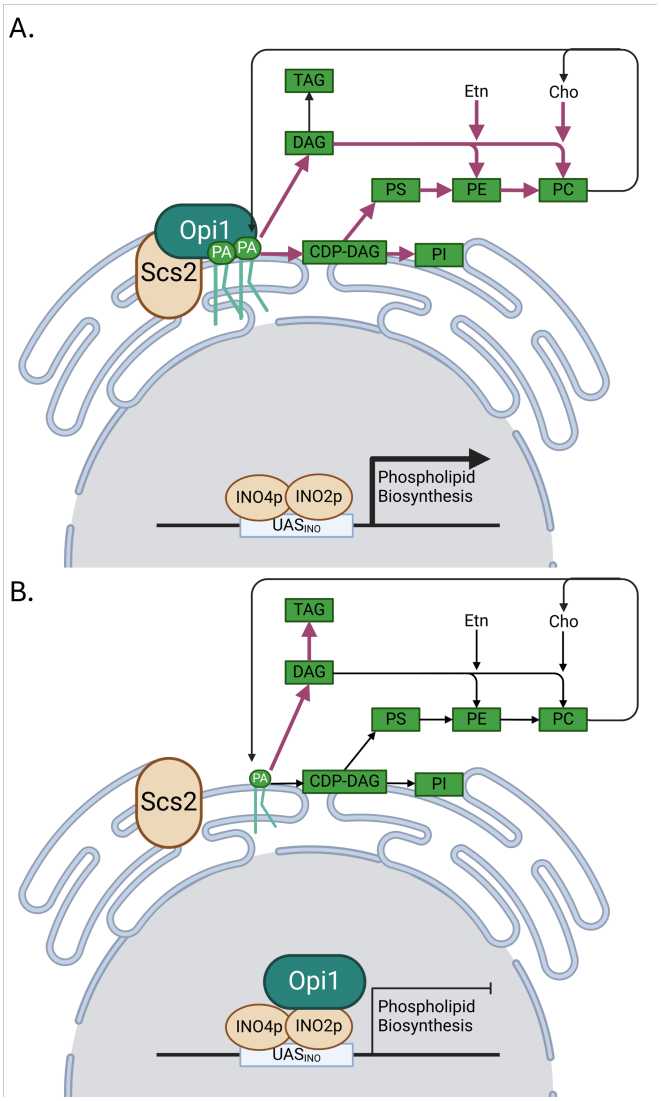

FIGURE 1.7: **Henry regulatory circuit controlling de novo phospholipid metabolism**

(A) Exponential phase, an increased abundance of PA leads to sequestration of the transcriptional repressor Opi1 and increased transcription of genes associated with de novo phospholipid biosynthesis. **(B)** During stationary phase, as PA levels reduce, Opi1 translocates to the nucleus and represses transcriptional activation of UAS_{INO}-controlled phospholipid biosynthesis genes. Created in https://BioRender.com.

There is a considerable degree of crosstalk between kinases in the regulation of the phosphorylation state of Pah1, and a degree of redundancy and overlap in the phosphorylation of particular residues. For example, Yck1, or casein kinase I,

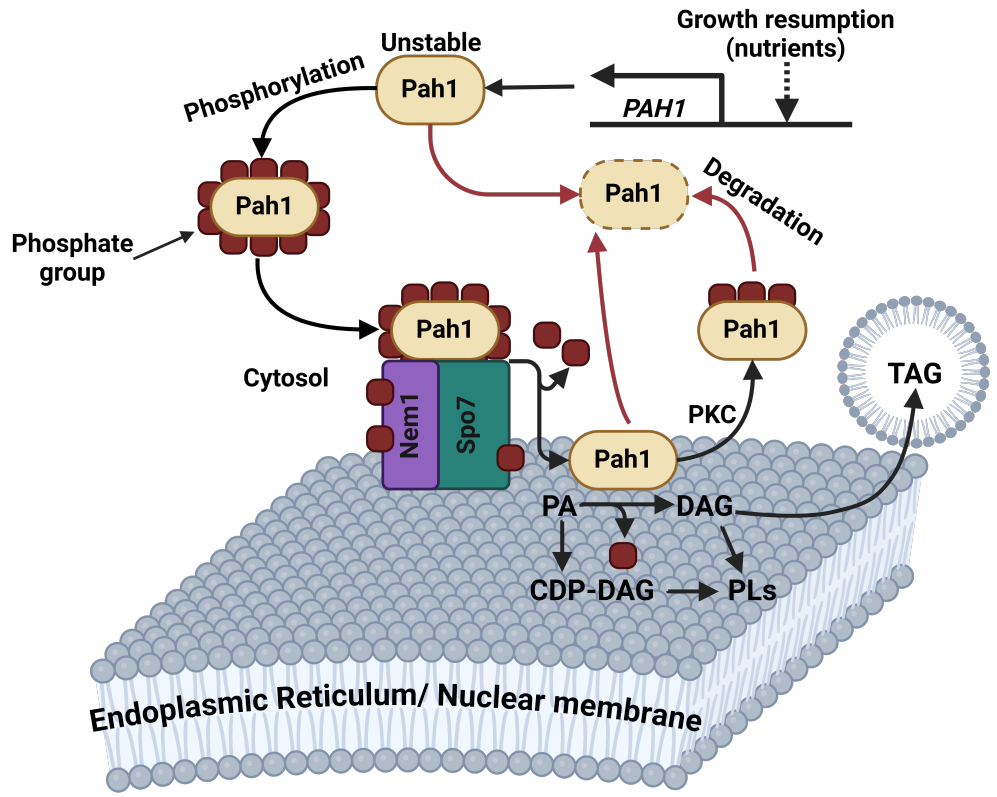

FIGURE 1.8: **Regulation of phosphatidate phosphatase Pah1 relies on phosphorylation by several kinases and dephosphorylation by the Nem1-Spo7 complex**

In *S. cerevisiae*, *PAH1* is differentially expressed according to nutritional availability within cells. The protein Pah1 is stabilised through phosphorylation by kinases such as PKA, Pho85-80 and casein kinase I, and there is considerable overlap in post-translational control by multiple pathways. Stable Pah1 is recruited to ER or nuclear membranes by the Nem1-Spo7 complex, whereby it translocates onto the membrane and is dephosphorylated by Nem1. Dephosphorylation allows for scooting across the membrane and dephosphorylation of PA species to yield DAG. Pah1 is inactivated and targeted for proteasomal degradation via phosphorylation by PKC. Red arrows denote mechanisms of Pah1 degradation. Created in https://BioRender.com.

maintains a constitutive activation and hence has the capacity to phosphorylate Pah1 when other kinases may be inactive [221]. Phosphorylation of Pah1 does not activate the protein, but instead stabilises it and limits turnover within the cytosol[217, 216, 204]. Its activity is contingent on its recruitment to the ER or nuclear membrane by the Nem1-Spo7 complex [204, 222]. The Nem1-Spo7 complex is comprised of catalytic subunit Nem1 and regulatory subunit Spo7 [204,

PKA	PKC	Casein kinase I	Casein kinase II	Cdc28-cyclin B	Pho85-80
S10					
		S114			S114
					S110
			T170		
			S250		
			S313		
		S445			
		S551			
S677	S677	S677			
		S602		S602	S602
S788	S788				
S774		S774			
S773	S773				
	S769				
		S748			
				S744	S744
				T723	T723
			S818		
			S814		

TABLE 1.2: A summary of phosphorylation sites that regulate the stability of the phosphatidate phosphatase Pah1 within the cytosol in *S. cerevisiae*

223], both of which are also subject to considerable kinase-mediated regulation [224, 225, 226]. The importance of the Nem1-Spo7 complex in the recruitment of and functional control of Pah1 has been heavily studied in *S. cerevisiae*, and mutational studies have underpinned the necessity for correct localization of these proteins to facilitate Pah1 activation. Spo7 has a chain of leucine-leucine-isoleucine residues that are critical for appropriate interaction with Nem1, and disruption of this sequence phenocopies a *pah1* deletion [227]. Indeed, disruption of Nem1 or Spo7 expression is sufficient to phenocopy a *pah1* deletion and greatly perturb

phosphatidate phosphatase activity [227, 228], and alteration of the tail region of Spo7 negatively impacts the protein's ability to bind Pah1 [228].

The Nem1-Spo7 complex is responsible for dephosphorylation of Pah1 [204, 227, 228], and this dephosphorylation is at least partially stimulated by increased abundance of PA species [229]. Once Pah1 has appropriately translocated or "hopped" onto the ER or nuclear membrane, a membrane association mediated by the protein's amphipathic helix region [222]. Once dephosphorylated by Nem1 and membrane bound, Pah1 "scoots" across the membrane and facilitates the conversion of PA to DAG, its phosphatase activity driving the PA dephosphorylation [196, 224, 229]. Following DAG generation, active Pah1 continues to "scoot" across the ER membrane to search for further PA molecules. The structure of fatty acid moieties on PA molecules are unimportant for Pah1 activity; the primary prerequisite is the presence of the phosphate head group [229]. Active, membrane-bound Pah1 is subject to negative regulation through phosphorylation by PKC [219]; this phosphorylation results in dissociation from the ER or nuclear membrane, a return to the cytosol and subsequent proteasomal degradation to control the abundance of Pah1 and PA [219, 204].

1.3.1.2 Diacylglycerol

As previously described, dephosphorylation of PA yields diacylglycerol. DAG molecules comprise a glycerol headgroup with two fatty acid moieties attached at any two of three available positions, with sn-1,2 isoforms being the most common

in yeast [230]. Within yeast, this conversion marks a commitment toward lipid storage that accompanies late-log/stationary phases of growth [231, 230]. DAG exhibits a high degree of fluidity and mobility within membranes; it is capable of transbilayer movement without the assistance of flippases [232]. Low levels of DAG are present throughout all stages of growth, owing to the impact that it has on membrane curvature; due to its conical shape and absence of phospholipid head, whilst still being amphipathic and existing within plasma membranes, DAG imposes a net negative curvature to plasma membranes [230, 233]. Regulation of localised pools of diacylglycerol is instrumental in SNARE-mediated vacuolar fusion [233]; deletion of *PAH1*, mitigating one of the cell's mechanisms for DAG regulation has been shown to cause vacuolar fragmentation or reduced vacuolar fusion, and that without the activity of Pah1, the protein Sec18p is unable to appropriately bind SNARE complexes to initiate vacuolar fusion [234]. A study in the yeast *Yarrowia lipolytica* also determined that DAG translocation from the inner to outer leaflet of developing peroxisomes applies a curvature that promotes recruitment of proteins necessary for membrane fission and the final stages of peroxisomal biogenesis [235]. Work has also shown that, during growth resumption, pools of DAG hitherto associated with vacuolar membranes localise to bud-sites before identifiable emergence of a bud, likely fuelling glycerophospholipid biosynthetic processes during bud development [231].

There is a degree of debate as to other roles for DAG within yeast; accumulation of DAG has been linked to Rim101-dependent commitment to programmed cell death [236], and there is also evidence to suggest that DAG takes part in signalling processes; phosphorylation of Pkc1 has been shown to be dependent on

DAG and PS [225]; the role that DAG plays as a secondary messenger in yeast cell signalling has yet to be fully elucidated. There has been considerably more research on the additional roles, aside from typical lipid metabolism, of DAG in mammalian cells. Specifically, comprehensive studies have determined the necessity for DAG in appropriate PKC activation [237], recruitment of PKC and the ras GEF rasGRP1 to plasma membranes in T-cells [238] and that without appropriate DAG levels to support these processes, T-cells fall into a state of anergy (an inability to appropriately elicit a response in the presence of an antigen) [238, 237, 239, 240]. Recently, mammalian PKC C1 domain structures were resolved to determine interactions with DAG as a secondary messenger, with the eventual aim of determining whether drugs can be designed to mimic this functionality and potentially treat Alzheimer's and cancers [241]. In the nematode *Caenorhabditis elegans*, DAG levels also control synaptic transmission. Elevation of DAG triggers accumulation of UNC13, a protein that primes vesicles for neurotransmitter release and as such facilitates neurotransmission [242, 243]. There is evidence to suggest that DAG fulfils a similar, if more complex and involved role, in mammals, coordinating PKC-dependent and independent synaptic transmission [244].

1.3.1.3 Triacylglycerol generation

Whilst PA and DAG themselves form constituent components of signalling pathways and sit as a pillar of phospholipid biosynthesis (offering both transcriptional

control and building blocks to fuel the biosynthetic processes), one of the primary fates of DAG following its production is a final chemical reaction to generate the non-polar, or neutral lipid, TAG. TAG generation from DAG is an acylation reaction that is predominantly orchestrated by one of two acyltransferases, diacylglycerol:acyl-CoA acyltransferase (Dga1p in *S. cerevisiae*) [193, 245, 246] and LCAT-related open reading frame (Lro1p in yeast) [247, 248, 249], so named owing to its homology to human LCAT (lethicin: cholesterol acyltransferase). Dga1 shows a preference for palmitoyl-CoAs, oleoyl CoAs and other fatty acid-CoAs as a substrate and source of fatty acid moiety [187]. In *S. cerevisiae*, Dga1's catalytic domain sits within the cytosol [248]. Dga1 is said to be more pronounced during the stationary phase, and is ER/LD bound [250]. Lro1, however, showing a preference for DAG acylation using phospholipids such as PC PE as a fatty acid donor, is an ER-bound transmembrane protein with a catalytic domain that sits within the ER lumen. In *S. cerevisiae*, deleting *DGA1* or *LRO1* cause marked drops in TAG synthesis, with a *dga2/lro1* Δ/Δ almost completely nullifiying neutral lipid storage [193, 250]

As DAG is funnelled into neutral lipid storage, both Dga1 and Lro1 catalyse the acylation and deposition of TAG within the hydrophobic leaflet of the cytosolic facing ER phospholipid bilayer [180].

1.3.2 Sterol ester storage

Sterols are polycyclic lipid molecules typically composed of 4 carbon rings, an alcohol and an acyl tail [251]. They fulfil an array of functions within the membrane:

control of plasma membrane permeability and dynamics [251, 252], protection of mitochondrial DNA [253, 254] and adaptation to stresses [255, 256]. Ergosterol, or the "fungal hormone", is the primary sterol present in yeast [253]. Cells with deficiencies in ergosterol typically exhibit slow growth and growth defects, and increased sensitivity to stress [254].

1.3.2.1 Ergosterol biosynthesis

In yeast, while cells can maintain other sterol classes, by far the most abundant sterol is ergosterol [253, 257]. Its maturation takes place predominantly in the ER, by a cascade of reactions controlled by the *ERG* family of genes (Fig. 1.9). In brief, the sterol precursor squalene undergoes reactions to generate the cyclic sterol lanosterol, which is further matured via oxidation, reduction and methylation reactions to zymosterol, fecosterol, episterol and eventually ergosterol [258, 259, 260, 261, 253]. Erg11 is responsible for initiating the cascade from lanosterol down to ergosterol [258, 262], and is the target for the azole class antifungal fluconazole; inhibition of Erg11 inhibits ergosterol biosynthesis [258]; overexpression of Erg11 is often the cause of fluconazole resistance [263], and several studies have highlighted the presence of mutations to Erg11 in clinical isolates that render them fluconazole resistant [50, 264, 265].

In *S. cerevisiae*, transcriptional control of ergosterol biosynthesis is coordinated by zinc cluster transcription factor paralogs Upc2 and Ecm22, with a displayed capacity for the binding and activation of the *ERG2* promoter, with overexpression of *UPC2* increasing *ERG2* transcription [267]. Studies investigating *C. albicans*

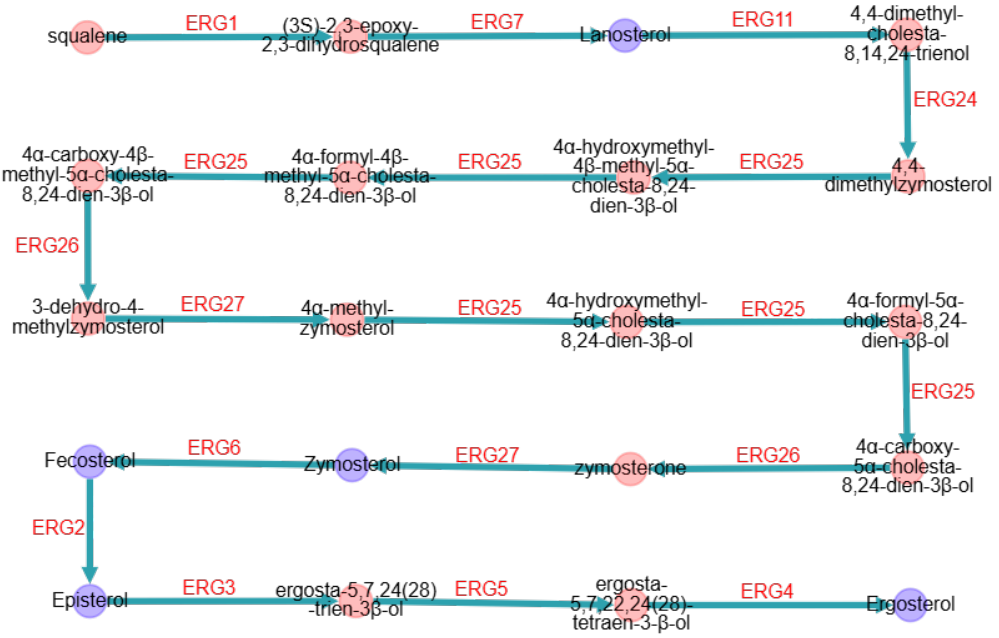

FIGURE 1.9: **Ergosterol biosynthethetic process from the precursor squalene**

Ergosterol biosynthesis takes place within the ER through a cascade reaction conducted by the Erg family. Erg1 (squalene monooxygenase) and Erg7 (2,3-oxidosqualene-lanosterol cyclase) generate lanosterol from squalene. Erg11 (cytochrome P450 lanosterol 14a-demethylase), the target of the drug fluconazole, begins conversion of lanosterol to zymosterol. Several downstream reactions are catalyzed by Erg25 (methylsterol monooxygenase). Conversion of zymosterol to fecosterol, espisterol, and lastly ergosterol is catalyzed by Erg2 (C-8 sterol isomerase), Erg3 (C-5 sterol desaturase), Erg5 (C-22 sterol desaturase) and Erg4 (C-24 sterol reductase), respectively. Figure generated using Pathway Collages [266]

clinical isolates displaying resistance to azole class antifungals identified an gain-of-function A643T mutation to Upc2 that caused overexpression of *ERG11* [268], and site directed mutagenesis to generate the same mutation in lab strains and fluconazole-susceptible clinical isolates led to heightened expression of Erg family elements, restored ergosterol biosynthesis and fluconazole resistance [269]. It is believed that Upc2 is negatively regulated by elevated sterol concentrations; it has a ligand binding domain with ergosterol specificity, and Upc2 is sequestered in the cytoplasm when sterol concentrations are high, and translocates to the nucleus

upon sterol depletion [270]. Mutations that alter the ligand binding domain such that ergosterol cannot bind triggers constitutive activation of Upc2 [271].

1.3.2.2 Esterification of sterols

Sterol esters form the second neutral lipid component of the lipid droplet core [180]. Their synthesis stems from the attachment of a fatty acid moiety to a sterol through an ester bond, rendering the lipid neutral [272]. This process is coordinated largely by two enzymes in *S. cerevisiae*; acyl-CoA: sterol acyltransferases 1 and 2 (Are1 and Are2) [273, 272, 274]. Whilst both are involved in esterification of sterols, Are1 has been shown to preferentially esterify ergosterol precursors such as lanosterol, whilst Are2 esterifies predominantly ergosterol [275]. Expression is increased as cells approach stationary phase, when need for further sterol production is reduced [276]. In *C. albicans*, so far only one acyl-CoA:sterol acyltransferase has been identified, CaAre2 [277], though little research has investigated whether CaAre2 is responsible for all sterol acyltransferase activity in *C. albicans*. In *S. cerevisiae*, for example, Are1 and Are2 fulfil a minor role in acyl-CoA: DAG acyltransferase activity, as demonstrated by the necessity for a quadruple knockout to eliminate TAG generation in the yeast [272, 274, 278, 181]. Similar to the generation of TAG components of lipid droplets, sterol esterification takes place on the ER membrane, with neutral lipids building up within the cytosol-side ER leaflet [275].

1.3.3 Neutral lipid mobilization

Lipid droplets accumulate as nutritional availability drops and yeast cells approach stationary phase. Upon growth resumption, however, lipid droplets act as an effective resource for precursor molecules affiliated with building plasma membrane; TAG can be mobilised to DAG, and SEs can be converted back into ergosterol.

TAG catabolism has not yet been characterized in *C. albicans*. In model yeast *S. cerevisiae*, TAG mobilization is coordinated predominantly by members of the triacylglycerol lipase (Tgl) family, [279, 280] with some moonlighting TAG lipase activity displayed by Ayr1 [281]. Tgl3 was the first identified member of the Tgl family capable of TAG lipolysis in *S. cerevisae*, localizing to the LD monolayer [282, 279], with Tgl3 Δ displaying increased TAG, a reduced rate of TAG lipoylsis and a sensitivity to the fatty acid inhibitor cerulenin, owing to an overreliance on synthesis and assimilation of fatty acids from sources besides those stored [279]. A *tgl4* knockdown exhibits a similar response, whilst a *tgl5* knockdown does not; a tgl4/tgl5 Δ/Δ, however, shows a greater accumulation of TAG than tgl4 Δ alone, suggesting that Tgl5 plays a minor role in TAG lipolysis. Tgl4 is actively regulated by Cdc28; it is phosphorylated on residues T675 and S890, and its phosphorylation coincides with lipolytic activity [283]. Mutating T675 and S890 to alanine residues prevents phosphorylation and phenocopies a *tgl4* knockdown and reduces TAG mobilization. Curiously, this link to cdc28 highlights a role of TAG mobilization in cell cycle progression; deleting *tgl3* in conjunction with prevention of Tgl4 phosphorylation showed a delayed bud emergence upon resumption from growth, whilst a synchronised treatment with cerulenin prevented bud emergence

completely [283] and highlighting the importance of TAG lipolysis for membrane development. Curiously, genetic knockdown of any combination of *TGL3, TL4* and *TGL5* does not alter expression of the other in compensation [284].

SE is mobilized through lipolysis also, through the action of Tgl1, Yeh1 and Yeh2 [285, 286], where genetic knockdown of any combination of the 3 reduces SE catabolism, suggesting a degree of functional redundancy, and knocking down two whilst overexpressing the third more than sufficiently restores SE lipolysis [285]. Curiously, Yeh2 maintains a plasma membrane localization rather than LD localization [285]. Inability to lipolyse SE to sterols also causes a reduction in SE biosynthesis, though without an alteration to *ARE1* or *ARE2* transcript levels, with researchers suggesting the presence of a feedback loop [287].

1.3.4 Role of lipid droplets within the cell

1.3.4.1 Storage of phospholipid and sterol precursors

The first and most notable role of lipid droplets is the previously discussed control of lipid storage to allow for resumption of growth not dependent on exogenous sources for phospholipid and sterol precursors [279, 280, 213]. This storage benefits the cell through accumulation of resources whilst also mitigating their lipotoxic effects; dense packing of TAG, and their non-polar nature, make them an extremely effective storage molecule [194]. TAG lipolysis and further processing allow for de novo generation of phospholipids for plasma membrane biogenesis, further detailed

in a latter section.

1.3.4.2 Cell cycle and bud development

As previously discussed, there are multiple connections between LD homeostasis and cell cycle progression. Pah1 is phosphorylated and regulated in part by Cdc28 [216, 288], so too is the TAG lipase Tgl4 [283], with Tgl4 disruption impacting upon bud formation. Control of phospholipid/TAG intermediate DAG is also tethered to bud formation and polarized growth [231].

1.3.4.3 β-oxidation

Owing to its dense packing, TAG also constitutes a good source of energy when appropriately metabolised [194]. There are several means through which LDs and their constituent components can be used for energy. Firstly, through the process of β-oxidation [289, 290]. In yeast, β-oxidation is the catabolism of fatty acids within peroxisomes- yeast grown on fatty acids as a carbon source are capable of growth through peroxisomal turnover of fatty acids [291]. Lipid droplet-peroxisome contact sites have been observed in yeast [289], with peroxisomes forming close to ER-LD contact sites [292], and pexopodia stretching into the neutral lipid core [289].

1.3.4.4 Lipophagy

LDs can be subject to a specialized autophagy known as lipophagy [293, 294, 295]. In eukarya, there are 3 distinct methods of lipophagy [293], though in yeast, LDs are solely autophagised by microlipophagy [293, 295] in response to nitrogen starvation, ER stress and glucose reduction. Microlipophagy, in brief, is the engulfment of LDs within the yeast and the gradual lipolysis to yield constituent components [294].

1.3.4.5 Stress response

It is well noted that in response to several stresses, including cell wall stress, peroxide stress and exposure to excessive concentrations of fatty acids, *S. cerevisiae* accumulates lipid droplets [296, 297, 298]. Following cofilin stabilization and considerable cell wall stress, with a constitutively active cell wall integrity (CWI) pathway, yeast cells display a drastic accumulation of smaller lipid droplets alongside other aberrant phenotypes; deletion of *DGA1* or *LRO1* in this instance is sufficient to switch off constitutive Slt2 phosphorylation, suggesting a link between TAG homeostasis and CWI siganlling [296]. Some studies have proposed that LDs act as a "ROS sink", or as preferential targets for reactive oxygen species (ROS) to mitigate damage to membranes [299].

LDs, TAG and SE have been implicated in long-term survival through autophagy. Autophagy is contingent on a steady supply of FFAs, and deletion of *DGA1*, *LRO1*, *ARE1* and *ARE2* has been shown to remove a starved cell's capacity to form autophagosomal compartments for organelle turnover in *S. cerevisiae* [300].

The LD proteome also highlights a role in adaptation to antifungal stresses [301, 302], as several members of the Erg family exhibit LD localization in yeast [253, 301, 302], suggesting a mechanism by which SE may be rapidly by hydrolysed and restructured to compensate for azole or allylamine inhibition of sterol processing.

1.4 Phospholipid metabolism

Control of glycerophospholipid metabolism is of great importance within the cell, owing to their ubiquity and the myriad functions they fulfil. In yeast, de novo phospholipid biosynthesis is contingent on cytidine diphosphate diacylglycerol (CDP-DAG) [303, 213]. CDP-DAG is a phospholipid precursor synthesized in a reaction with phosphatidic acid using cytidine triphosphate (CTP) as a donor, yielding CDP-DAG and inorganic phosphate as a product [304, 305]. CDP-DAG synthesis is under the control of two separate CDP-DAG synthases, endoplasmic reticulum-bound Cds1 [305, 306] and inner mitochondrial membrane (IMM)-bound Tam41 [306, 307, 304]. The PA necessary for CDP-DAG biosynthesis can be acquired through multiple avenues. Firstly, through phosphorylation of DAG by Dgk1 [308], which in turn can be acquired either through catabolism of the neutral lipid TAG, stored within lipid droplets [279, 280], or from pools of DAG maintained within the cell [231]. Or secondly, as described above, through conversion of G3P and free fatty acids or DHAP to PA. CDP-DAG species are a precursor for several phospholipids. Through the action of the phosphatidylinositol (PI) synthase, Pis1, a serine residue is exchanged with cytidine monophosphate (CMP) on CDP-DAG to yield PI [309, 310]. PI plays an important role within cells; phosphorylation

of PI by Pik1p and Stt4p generates secondary messenger PI-4-phosphate (PI4P) and further phosphorylation to generate PI4,5-bisphosphate (PI4,5BP) [311], with links to signal transduction in pathways including MAPK CWI signalling [312, 313, 314].

CDP-DAG is also used to generate phosphatidylglycerol (PG) and cardiolipin (CL) within mitochondria. PG biosynthesis is a two-step process, whereby an intermediate, phosphatidylglycerol phosphate (PGP) is formed following a reaction catalyzed by Pgs1 [315] with CDP-DAG and (G3P). PGP phosphatase Gep4 catalyzes dephosphorylation of PGP to yield PG [316]. PG is a relatively low abundance PL, important primarily in the synthesis of CL, a mitochondrial inner membrane (MIM) PL class that is vital for mitochondrial function [317]. The above are the only described pathways for PI, PG and as such CL generation in yeast, with CDP-DAG as the lynchpin; as such, disruption of genes associated with CDP-DAG synthesis are lethal [305].

A third branch of CDP-DAG dependent de novo phospholipid biosynthesis concerns the generation of phospholipids, phosphatidylserine (PS), phosphatidylethanolamine (PE) and phosphatidylcholine (PC). Through the action of PS synthase Cho1, a serine molecule is exchanged for CMP on CDP-DAG, and the resultant molecule, two fatty acyl tails conjoined to a serine-phosphate-glycerol head group, comprise PS [303, 213, 318].

PS can be decarboxylated by Psd1 and Psd2 to yield PE [303, 213, 319, 320]. In *C. albicans*, the phosphatidylserine decarboxylases Psd1 and Psd2 are redundant

proteins, with the majority of decarboxylase activity fulfilled by Psd2 [321]. Aside from being an intermediate in the production of PC, PE is also an important component of GPI-anchors and therefore is important in cell wall assembly [322].

De novo PC biosynthesis is the result of phosphatidylethanolamine methyltransferase (PEMT) activity. Cho2 (or alias, Pem1) catalyzes the first step to yield the intermediate molecule phosphatidylmonoethanolamine (PMME), and Opi3 (or alias, Pem2) catalyzes an additional two methylation steps, yielding phosphatidyldiethanolamine (PDME) and PC, respectively [323, 324]. PC is the most abundant PL species in yeast, comprising approximately 40% of the plasma membrane's phospholipid bilayer [325]. As such, biosynthesis of PC is a critical process in cellular structure and function.

A second pathway, the Kennedy pathway, exists to generate PE and PC species in a CDP-DAG independent manner. In yeast, DAG is converted to either PE or PC through phosphotransferase activity to attach an ethanolamine or a choline molecule. In *S. cerevisiae*, the terminal steps for PC biosynthesis and PE biosynthesis are under the control of choline phosphotransferase Cpt1 [326, 327] and ethanolamine phosphotransferase Ept1 [327], respectively. In *C. albicans*, however, it has been shown that Ept1 exhibits dual function, catalyzing PE and PC biosynthesis; an *EPT1* overexpression in *C. albicans* causes increases to both PE and PC species [328] as well as hypervirulence in a murine model.

Acquisition of choline and ethanolamine is essential in yeast for Kennedy PL biosynthesis, and is a bottleneck for membrane biogenesis. Typically, ethanolamine

and choline have to come from environmental sources- media, or the host [329, 321])- as such, yeast relies predominantly on CDP-DAG PL biosynthesis.

Disrupting *CHO1*, and as such CDP-DAG biosynthesis of PS, leads to an ethanolamine and choline auxotrophy in yeast [213, 303, 321] as cells have to rely on the Kennedy pathway for PE and PC biosynthesis. A *cho1* mutant in *C. albicans* typically has no detectable PS species, with a partial restoration to 37% PS compared to the wild type following reintegration of one *CHO1* allele. A *cho1* null mutant cannot grow in choline and ethanolamine deplete conditions, and is still relatively slower growing when supplemented with ethanolamine and choline [303]. Similarly, *psd1* and *psd2* null mutants that prevent decarboxylation of PS to PE have reduced PE, a buildup of PS, and a double KO is also auxotrophic for ethanolamine and choline [303].

Deleting *CHO1* or both *PSD1* and *PSD2* renders *C. albicans* avirulent in a *Caenorhabditis elegans* (*C. elegans*) [330] and murine model [303]. Davis *et al* posited that this reduction in virulence is owing to cells not being able to acquire sufficient ethanolamine to support sufficient Kennedy synthesis of PE; when ectopically expressing an *Arabidopsis thaliana* serine decarboxylase, allowing for serine conversion to ethanolamine, virulence in a murine model is restored [321]. Curiously, disrupting *PEM1* and *PEM2* in tandem, whilst causing a choline auxotrophy, does not render *C. albicans* avirulent; this is likely indicative that *C. albicans* is capable of scavenging enough choline from the host to support Kennedy synthesis of PC [328]. In fact, *pem1/2* Δ/Δ was determined to be hypervirulent; this, in tandem with the finding that overexpressing *EPT1* and increasing

Kennedy-derived PE and PC caused hypervirulence, suggests a role for increased PE in the virulence of *C. albicans* [328] that is potentially owing to increased PL availability for membrane development [320].

1.5 Lipid metabolism as an antifungal target

Current antifungals largely fall into one of four categories. Echinocandins, such as caspofungin, function through the inhibition of β-1,3-glucan synthase Fks1 [125, 127].

The other three antifungal classes all concern themselves with perturbation of lipid metabolism, hinging on the importance of ergosterol for membrane homeostasis and trafficking [251, 252, 254]. Ergosterol makes a promising antifungal target not only because of its importance to fungal viability, but to its unique presence as a fungal sterol; its targeting, therefore, does not impact upon mammalian sterols. Azole class antifungals target and inhibit Erg11, responsible for the commitment of the cascade that converts lanosterol to ergosterol [268]. Allylamines target the squalene monooxygenase Erg1, necessary for the initial step for lanosterol biosynthesis from squalene [331] and, as such, again, inhibit ergosterol biosynthesis. Polyenes such as amphotericin B (ampB) and nystatin act by binding ergosterol within the plasma membrane, increasing membrane porosity and inducing cell death. However, owing to poor solubility, typically high concentrations of AmpB had to be used in a clinical setting, in which it exhibited nonspecific, albeit lower affinity for human cholesterol [332]. More recent advancements have reduced the

toxicity of ampB through liposomal delivery, overcoming issues of solubility and allowing for efficacious treatment at lower dosages [333].

Glycerolipid metabolism makes for an interesting antifungal target owing to its interplay with many of the adaptation processes that make *C. albicans* a successful fungal pathogen. Recent studies have identified a competitive inhibitor of *C. albicans* phosphatidylserine synthase Cho1 [334], a promising discovery: Cho1 is fungal specific, is conserved in many fungal pathogens, and is vital for CDP-DAG biosynthesis of PS, PE and PC [213, 303]. Disruption of this demonstrably causes a reliance for Kennedy biosynthesis of PC and PE, and limitations on exogenous choline and ethanolamine availability render *C. albicans* avirulent [321].

1.6 Aims of this study

C. albicans poses a significant threat to at-risk and immunocompromised individuals, and with increased usage of medical devices comes an increased risk of medical device-related infection. The aims of this study were twofold. Whilst glycerolipid metabolism has been well characterized in the model yeast *S. cerevisiae* [180], current understanding of these processes, lipid droplet regulation, and their role in the pathogenic yeast *C. albicans* is lacking. This work sought to bridge the gap, with a focus on TAG storage and catabolism, and the roles these processes play in the virulence of *C. albicans*; a better understanding of how the opportunist utilises scavenged and stored lipids may prove insightful when developing further treatment regimens for *C. albicans* infection. Secondly, this work sought to determine the efficacy of lipotoxicity as an anti-fouling strategy to prevent biofilm formation

on medical devices. I focus on *C. albicans* biofilm formation on silicone, using the mono-unsaturated fatty acid palmitoleic acid as both a wash and a coating to determine whether dietary fatty acids could supplement antifungal treatment to mitigate risk of biofilm growth on medical devices.

Chapter 2

Materials and Methods

2.1 Strains and growth conditions

TABLE 2.1: *C. albicans* strains used in this study

Strain	Background	Genotype	Source
SC5314	SC5314	Wild Type	[335]
Smp2 Δ	SC5314	SMP2/smp2::smp2 HIS1::FRT/HIS1::FRT	This study
Lro1 Δ/Δ	SC5314	lro1::lro1/lro1::lro1 HIS1::FRT/HIS1::FRT	This study
Are2 Δ/Δ	SC5314	are2::are2/are2::are2 HIS1::FRT/HIS1::FRT	This study
Tgl1 Δ/Δ	SC5314	tgl1::tgl1/tgl1::tgl1 HIS1::FRT/HIS1::FRT	This study
Tgl2 Δ/Δ	SC5314	tgl2::tgl2/tgl2::tgl2 HIS1::FRT/HIS1::FRT	This study
Psd1 Δ/Δ	SC5314	psd1::psd1/psd1::psd1 HIS1::FRT/HIS1::FRT	This study
Cho1 Δ/Δ	SC5314	cho1::cho1/cho1::cho1 HIS1::FRT/HIS1::FRT	This study
SN250	SN152	his1/his1, leu2::C.d.HIS1/leu2::C.m.LEU2, arg4Δ/arg4Δ	[336]
Dga2 Δ/Δ	SN250	DGA2::stop/DGA2::stop, Neut5L::FRT	This study
Lro1 Δ/Δ	SN250	*lro1*::C.d.HIS1/ *lro1*::C.m.LEU2	[336]
Dga2/Lro1 Δ/Δ	SN250 Lro1 Δ/Δ	DGA2::stop/DGA2::stop, Neut5L::FRT	This study

2.1.1 yeast growth conditions

Candida albicans strains were maintained on Yeast extract peptone plates with glucose (YPD) (1% yeast extract, Gibco; 2% peptone, Gibco; 2% glucose, Fisher Scientific; 2% oxoid agar, thermofisher). Unless stated otherwise, for assays strains were inoculated into YPD media (without agar) and shaken at 30°C, 180rpm overnight.

TABLE 2.3: Other strains used in this study

Organism	Strain	Genotype/description	Source
Murine macrophage	J774A.1	Immortalised murine macrophage cell line	[337]
E. coli	DH5α	Plasmid expression cell line	[338]
	pV1524	DH5α expressing plasmid pV1524, for recyclable Cas9 expression	[339]
	pADH99	DH5α expressing plasmid pADH99, for Cas9 expression in Hernday CRISPR system	[340]
	pADH110	DH5α expressing plasmid pADH110, for generation of Fragment A of the Hernday CRISPR sequence	[340]
	pADH147	DH5α expressing plasmid pADH147, for generation of gRNA specific Fragment B of the Hernday CRISPR system	[340]

2.1.2 Bacterial growth conditions

Bacterial strains were struck onto on luria broth (LB) agar plates (1% tryptone, Gibco; 0.5% yeast extract, Gibco; 1% NaCl, Fisher Scientific, 2% oxoid agar) and grown overnight at 37°C with the inclusion of 100μg/mL ampicillin (sigma aldrich). Liquid cultures were made in LB media (without agar) with 100μg/mL ampicillin and grown overnight at 37°C.

2.1.2.1 Isolation of plasmid DNA from bacteria

Plasmids were isolated from bacteria using a miniprep plasmid DNA isolation kit (Qiagen). Concentration of eluted DNA was confirmed using a SPECTROstar-Nano plate reader.

2.1.3 Maintenance of macrophages

J774A.1 cells were maintained at 37%C, 5% CO_2, adhered to the bottom of T75 culture flasks in Dulbecco's modified eagle medium- complete containing 10% FBS and pen/strep (Gibco, hereby referred to as DMEM).

J774A.1 cells were split at a confluency of approximately 90%. In brief, media was removed from 90% confluent cells, and 12mL fresh DMEM added gently to the flask. J774A.1 cells were scraped from the bottom of their T75 culture flask using a cell scraper to resuspend and cell suspensions were diluted as required for maintenance or assay into appropriate receptacle.

2.2 Strain generation using CRISPR Cas9

2.2.1 Fink approach- Stop codon insertion

TABLE 2.5: Primers used in Fink CRISPR Cas9 gene editing

Primer	**Sequence**
DGA2_guide1_fwd	ATTTGGTAGCCTTCTCTGTATGTTCG
DGA2_guide1_rev	AAAACGAACATACAGAGAAGGCTACC
DGA2_rep1_fwd	TATTTTTCCATATTTGCTTGCAATGACAGACACATCTG ACCTTAAATAAGAATTCGAACA
DGA2_repair_rev	ACTTCCTTAGAAGTAGAGAGCCCTGTAGCCTTCTCTGT ATGTTCGAATTCTTATTTAAGG
DGA2_check_fwd	CCACACTGTTCGCTCAAGTT
DGA2_check_rev	CAAATCCGTACCACCAAATA
DGA2_check_rev	CAAATCCGTACCACCAAATA
pv1524_sequencing	GGCATAGCTGAAACTTCGGCCC

Mutants were generated through the implementation of a stop codon and restriction site at the start of the open reading frame, as described by Evans *et al* [339]. Briefly, designed guide RNAs were ligated into linearized expression vector pV1524 containing Ca-Cas9 (Cas9 machinery codon optimized for *Candida albicans*), and co-transformed into *C. albicans* alongside repair templates designed for insertion of a stop codon sequence and EcoR1 restriction site. Colonies capable of growing on 200μg/mL nourseothricin (NAT, Jen Bioscience) were screened with colony PCR and restriction digest. Successful clones were grown on YP-maltose (2%)to remove integrated CRISPR machinery from the NEUT5L locus.

2.2.2 Hernday approach- Cas9 mediated ORF excision

Table 2.6: Primers used in Hernday CRISPR Cas9 gene editing

Primer	Sequence
AHO1096	GACGGCACGGCCACGCGTTTAAACCGCC
AHO1098	CAAATAAATAGTTTACGCAAG
AHO1236	TAAAGCTGCCACAAGAGGTATTTC
AHO1238	TGTATTTTGTTTTAAAATTTTAGTGACTGTTTC
AHO1097	CCCGCCAGGCGCTGGGGTTTAAACACCG
SMP2 gRNA del	CGTAAACTATTTTTAATTTGACAAACTAGCAACACCAG GGGTTTTAGAGCTAGAAATAGC
DGA2 gRNA del	CGTAAACTATTTTTAATTTGCATTAACGGAAGCGACGC AGGTTTTAGAGCTAGAAATAGC
LRO1 gRNA del	CGTAAACTATTTTTAATTTGGAAGCATTTGTTGATATT AGGTTTTAGAGCTAGAAATAGC
ARE2 gRNA del	CGTAAACTATTTTTAATTTGATTGCCAAACTACAACAA GAGTTTTAGAGCTAGAAATAGC
TGL1 gRNA del	CGTAAACTATTTTTAATTTGTCCCCAGCAACAACACCG CAGTTTTAGAGCTAGAAATAGC
TGL2 gRNA del	CGTAAACTATTTTTAATTTGACAATTTCGACTCCACAC CAGTTTTAGAGCTAGAAATAGC

Continued on next page

Table 2.6 – continued from previous page

Primer	Sequence
TGL99 gRNA del	CGTAAACTATTTTTAATTTGTTGGATGATTTAAATTTT GGGTTTTAGAGCTAGAAATAGC
PSD1 gRNA del	CGTAAACTATTTTTAATTTGACATACAAAGACGAACAC GAGTTTTAGAGCTAGAAATAGC
CHO1 gRNA del	CGTAAACTATTTTTAATTTGTGTTCTGAATCCAATAGC AAGTTTTAGAGCTAGAAATAGC
SMP2 repair fwd	GCTTTCCTATTTCTGTACAACACTTTTTTCTTTCTTTTT TCCCCTATTTTAAGCATTATACCCAAGAGATCGTACGC TGCAGGTCGACAGTGG
SMP2 repair rev	GAGAACCTAATGCGCCTCTTTCTTTTTTTTTACAATTTT TGGACAATAAAAACAGACACATTCATTCATTCTCCACT GTCGACCTGCAGCGTACG
DGA2 repair fwd	CACACTCGAATATATTTATTTATTTTTCCATATTTGCTT GCACCATCCATACTTCTGGCGGTATTTCCAGAGC
DGA2 repair rev	AGTCTTGGCTTCTATTTGCTCTGGAAATACCGCCAGAA GTATGGATGGTGCAAGC
LRO1 repair fwd	CCCCCCTTTATCATATTAGTTTTCATACATTTTTTCAAT TTAAACTTCAAACCCACGTACGCTGCAGGTCGACAGTA GACCAAAAGGAGAGG

Continued on next page

Table 2.6 – continued from previous page

Primer	Sequence
LRO1 repair rev	CCAATCATATGTATTACATACTAAACATTAATTACTCT TCCTTTCTTCCTTTCCTCTCCTTTTGGTCTACTGTCGAC CTGCAGCGTACGTGG
ARE2 repair fwd	TTCAGCAATTCGTCTAAAAAATCACCTTTCTTCATTAG TGAACAGGATTTTTTTCAGAAAAGCGATCCGTACGCTG CAGGTCGACAGTGG
ARE2 repair rev	TGAGGTAGCTATAATGGGAGCCCTTAACTTTTTGGGTG TACAACAACTCACCCAACAACCACCCTTCCCACTGTCG ACCTGCAGCGTACG
TGL1 repair fwd	CACCTTTACTACATACTTTCTACAAGAGCTGAATAATA CAACAAACCTTCAAATACTATACGACACGTACGCTGCA GGTCGACAGTGG
TGL1 repair rev	CTATACGACACGTACGCTGCAGGTCGACAGTGGAGAAT GGTAATATATGTATGTAAGTAGTATGATATCGAGAGAG ACAAAAAGCGATTGCAAATG
TGL2 repair fwd	CATTAACAGTTACGAAAATGAACAAAAGGTATCACACC AAGAACAGCTTCACCATCCATACTTCTGGCGGTATTAA GACG

Continued on next page

Table 2.6 – continued from previous page

Primer	Sequence
TGL2 repair rev	CACCATCCATACTTCTGGCGGTATTAAGACGATACCCG CCATATGAGCTGGAAAAATAATAAAGCTATGGGTTTCC ATGTTTCATGCC
PSD1 repair fwd	CTCCATCGTTTAGTTTATTTTATTTCGTTACTCCTTTGT TTGACTGAATTAGGAAATTGAAACGTACGCTGCAGGTC GACAGTGGAGGAAGC
PSD1 repair rev	CGTACGCTGCAGGTCGACAGTGGAGGAAGCTCAGCGTA ATGGTTAACTTTTACATGACGTAATGGGGCCAACATTA TCCAGAATATC
CHO1 repair fwd	CTTCCTCCTCACATTCAGCTCTTCTTCCACTTTTCTTAC TCCACACATACACACCTATTCCGTACGCTGCAGGTCGA CAGTGG
CHO1 repair rev	TCTTACTCCACACATACACACCTATTCCGTACGCTGCA GGTCGACAGTGGAGATGATTCTAAAATAGAATCCTTTT CTC
SMP2 check fwd	TGAGACCAGCAATCGCTCCTGA
SMP2 check rev	GGGTACCCCTGTTGCTAATCATGCA
DGA2 check fwd	ACCTTGGTTTTGTTGGCTCATTTCC

Continued on next page

Table 2.6 – continued from previous page

Primer	Sequence
DGA2 check rev	ACCGCCATATCAACGAGGTGATCC
LRO1 check fwd	GGGGCCAACTTTTCAAATTCGGCA
LRO1 check rev	TTCCCCTCGCACTACTGCCCTT
ARE2 check fwd	TGGGGTCGAGAACCTTTCCACT
ARE2 check rev	TGGAACGCCATTCTTATGACACT
TGL1 check fwd	TGGCACAGCCCGTTCTTGATTG
TGL1 check rev	TCTGAATCAGCTTCCAGGTCGCT
TGL2 check fwd	GTTCGAGCCTCTCCCTGGTCGT
TGL2 check rev	ACATCGTGATCCCCTTGGGGCT
PSD1 check fwd	TCACGTGGAGCTGGATTTGCGT
PSD1 check rev	ACAAAGGCGGATCAGCATTCAC
CHO1 check fwd	ACGAATGTCCATCACTGGGCGC
CHO1 check rev	GTTAGCTGAACGTCCTGTGGACT

Genes of interest were deleted using the Hernday method for CRISPR Cas9 gene editing, optimised for *C. albicans*. PAM sites (NGG sequences) were selected within the open reading frame of the targeted gene; an appropriate PAM site was chosen using Benchlings CRISPR tool, generating on-target scores [341] and off-target scores [342], to determine optimal targets for cleavage whilst mitigating off-target effects. guide RNA oligos (table

2.6) were generated with specificity to the chosen PAM site, as well as sequence homology upstream of the gRNA scaffold on plasmid pADH147 (table 2.3). Repair template primers (table 2.6), approximately 90 bp in length, were designed such that the forward primer had at least 50 bp sequence homology to the region immediately upstream of the ORF to be disrupted, included a targettable "addtag" sequence to allow for reintegration, as well as some sequence homology to the area downstream of the ORF. The opposite was done for the reverse primer, with at least 50 bp sequence homology to the region immediately downstream of the ORF. PCR amplification using HIFI polymerase (PCRBio) generated repair templates with sequence homology upstream and downstream of the ORF of interest.

"Fragment A", a universal fragment comprising the second portion of a nourseothricin (NAT) resistance marker and the promoter sequence pSNR52 was amplified from plasmid pADH110 (table 2.3) with the universal primers AHO1096 and AHO1098 (table 2.6)using phusion hi fidelity polymerase (Thermofisher). "Fragment B", a fragment containing a target-specific gRNA sequence and sequence homology to the region downstream of the *C. albicans HIS1* locus, was generated using primers "X gRNA del", where X is the gene of interest, and universal primer AHO1097. Fragments A and B were stitched together to generate fragment C with primers AHO1236 and AHO1238 (table 2.6) using phusion polymerase.

Prior to conducting a *C. albicans* lithium acetate transformation (described below), plasmid pADH99 (table 2.3) was linearized using FastDigest MssI (thermofisher), and the restriction enzyme heat inactivated at 80°C for 20 min. Linearized pADH99 contained a sequence homologous to the region upstream of *C. albicans*' *HIS1* locus, as well as the *C. albicans* codon optimised Cas9 under an *ENO1* promoter, a maltose-inducible FLP recombinase, and the first half of the NAT resistance marker. The construct and

generated fragments were designed such that, upon transformation and appropriate insertion into the *HIS1* locus, cells would have an intact NAT resistance marker, Cas9 machinery and gRNA targeting sequences, flanked by FRT sites to allow for maltose induced removal of the inserts from the locus.

Following transformation, cells were plated onto YPD agar plates containing 200μg/mL NAT and allowed to grow for 2-3 days at 30°C. Colonies were patched onto fresh YPD-NAT plates and screened for appropriately sized fragments using colony PCR to determine successful ORF deletion from both alleles. Successful transformants were grown on YP-maltose agar to promote removal of Cas9 machinery from the *HIS1* locus.

2.3 Chemical transformation of *C. albicans*

C. albicans was grown overnight as described above, and then inoculated into fresh YPD liquid media to an OD_{600} of 0.2 (allowing 5mL cell suspension per transformation), and grown at 30°C for 4-6 hours, reaching an OD_{600} below 1. Cells were then washed twice with sterile milliQ water, then resuspended at $1/100^{th}$ of the original cell culture volume. Cells to be transformed were then added to the following mixture: Where PLATE is

PLATE	1000μL
C. albicans cell suspension	50μL
Transforming DNA	$\tilde{2}$0μL
Salmon sperm DNA	10μL

comprised of PEG3350 (43.75% w/v), lithium acetate (25mM, pH 7) and 1x TE (10mM Tris pH 7.4, 1mM EDTA pH 8). Transformation suspension was left overnight at 30°C without shaking. The following day, cells were subject to a 15 min heat shock at 44°C,

then spun down at 4000 rpm for 2 min and washed in 1mL YPD. Following a further spin down at 4000 rpm for 2 min, cells were resuspended in 2 mL YPD and allowed to recover at 30°C shaking at 180 rpm for 5 hr prior to being plated on YPD agar plates containing 200 μg/mL NAT.

2.4 Chemical transformation of *E. coli*

2.4.1 Preparation of competent cells

10mL LB media was inoculated with DH5α and grown overnight at 37°C. 15μL of overnight culture was added to 28mL LB media, and grown to just below an OD_{600} of 0.5 (approximately 4.5h growth). As cells approached OD_{600} of 0.5, 3.75mL of pre-warmed 15% glycerol was slowly added to the swirling flask. Cells were immediately chilled on ice for 10 min, and then pelleted at 4000 rpm for 10 min in a 4°C centrifuge. Cells were gently resuspended in equal volumes ice cold $MgCl_2$ solution and 15% glycerol. Cells were then pelleted at 4°C for 8 min at 3800 rpm. Cells were then gently resuspended in 6.25mL ice cold T-salt solution (0.075M $CaCl_2$, 0.006M $MgCl_2$, 15% glycerol) and incubated on ice for 20 min with occasional gentle swirling. Cells were then pelleted at 4°C for 6 min at 3600 rpm. Cells were resuspended in 1.25mL ice cold T-salt solution, aliquoted into pre-cooled sterile 1.7mL eppendorf tubes, and then frozen at -70°C prior to use.

2.4.2 *Competent cell transformation*

Frozen competent cells were thawed on ice for 20 min. 1μL plasmid DNA was added to 20μL competent cells and gently mixed. This mixture was incubated on ice for 30 min, and then heat shocked at 42°C for 45 seconds before returning to the ice for 2 min. 1mL LB media was added to the mixture and cells were allowed a recovery period of 45 min at 37°C. Cells were then plated on LB agar plates containing 100μ/mL ampicillin and incubated at 37°C overnight to allow colony growth of successful transformants.

2.5 Growth Assays

Strains were grown overnight in YPD medium, and inoculated into fresh medium to an OD_{600} of 0.1 in chosen medium (either YPD or RPMI-1640) with the inclusion of any drug or chemical treatments to be assayed, in 96-well plates (sarstedt, 100uL volume per well.) Assays were conducted over 24-48h in a BMG LabTech SPECTROstarNano plate reader, running a script of alternating orbital shaking.

For POA studies, cells were inoculated into RPMI-1640 to an OD_600 of 0.1, with and without a POA dilution series from 1mM down to 0.03mM. For POA and fluconazole combination treatments, several dilution series were created with a fixed starting POA concentration of 400μM and fluconazole concentrations from 0.5-4μg/mL. Combinations were serially diluted and inoculated with OD_{600} 0.1 *C. albicans* and analysed as above. Area under the curve analysis was conducted as a proxy for inhibition, and data fit to a logistic growth curve model.

2.6 Filamentation assay

Yeast strains were grown overnight in YPD medium, washed and diluted to an OD_{600} of 0.025 in DMEM containing 10% FBS. 250μL cell suspension was added to the well of an 8-well ibidi ibi-treat μ-slide, and incubated at 37°C, either in normal air or in a 5% CO_2 incubator, for 90'. Samples were stained with calcofluor and imaged as described above using the Zeiss LSM 880, though imaging was conducted using the Airyfast detector. Cells were scored on the presence or absence of a developing germ tube, as well as how many germ tubes could be seen per mother cell. For mother cells with developing and identifiable germ tubes, the length of the actively growing tube (determined by the presence of an unmasked tip) was measured manually in imageJ- 750 hyphae were measured per condition over 3 biological replicates to assess mean hyphal length.

2.7 Filamentation on spider agar

Spider medium was prepared (0.1% beef extract, 0.2% yeast extract, 0.5% peptone, 1% D-mannitol, 0.2% dibasic potassium phosphate (K_2HPO_4), 2% agar) and sterilized through autoclaving, plates poured and cooled. Cells from an overnight culture were diluted such that approximately 250 cells were plated onto spider medium plates. Cells were incubated at 37°C for 6 days. Colonies were imaged using a Leica MZFLIII dissecting scope and (Light source).

2.8 Western blotting detection of p-MKC1

Yeast cells from an overnight culture were either inoculated to an OD_600 of 0.1 and grown to log phase over a 4h incubation at 30°C, 180RPM, or harvested after 24h growth. $5x10^7$ Cells were resuspended in a lysis buffer (0.1M NaOH, 2% SDS, 2%β-mercaptoethanol, 0.05M EDTA) and heated at 90°C for 10'. 5μL 4M acetic acid was added to samples, followed by an additional 10' incubation at 90°C. Samples were then mixed 1:1 with a 2x sample loading buffer (0.125M Tris-HCl pH 6.8, 20% glycerol, 4% SDS, 2% β-mercaptoethanol, 0.02% (w/v) bromophenol blue). Samples were centrifuged to clear lysate prior to gel loading.

Samples were run on a Nupage 4-12% Bis-Tris polyacrylamide gel with Nupage MOPS SDS running buffer at 180Volts and transferred to PVDF membrane via semi-dry transfer on an Invitrogen power blotter station. Membranes were blocked for 1h in a skimmed milk solution (5% skimmed milk in 0.1 PBS-Tween). Membranes were then probed in a skimmed milk solution including 1:1000 P-p44/42 MAPK (T202/Y204) antibody (Cell signalling technology) at 4°C overnight, subject to a total 30' washes in PBS-T at room temperature, followed by a 30' incubation in a skimmed milk solution containing 1:4000 anti-rabbit HRP-linked antibody (Cell signalling technology. Membranes were then washed for a total 45 min in PBS-T. Membranes were then incubated at room temperature in the dark for 1 min in fresh ECL solution (1.25mM luminol, FLUKA; 198μM p-coumaric acid, Sigma; 100mM tris-HCl, pH 8.5; 94mM H_2O_2). Blots were then immediately imaged in a Syngene G box. Tubulin was probed as a loading control (1:2500, alpha-tubulin raised in mouse, Thermofisher) with an anti-mouse HRP-lnked secondary antibody (1:5000, Thermofisher) following the same methods described above.

2.8.1 Densitometry analysis of western blots

For semi-quantification of relative protein levels between samples, a densitometry approach was employed using Imagej. Images were loaded into imagej, converted to 8-bit and the lookup table (LUT) inverted. A region of interest (ROI) was drawn around bands, lanes assigned, and densitometry plots generated. % intensity of each sample was compared to that of the control condition to generate a relative intensity; these values were divided by that of the relative intensities of corresponding loading control bands to generate adjusted relative intensity values.

2.9 Lipid extraction and quantification using high-performance thin-layer chromatography

Yeast strains were inoculated into YPD from an overnight to an OD_600 of 0.1, and at 24h 80 OD units per strain were pelleted. Total lipid extraction was achieved in a chloroform/ methanol 2:1 (v/v) as described in Folch et al. Briefly, the addition of acid washed glass beads, chloroform/methanol and internal standard before a 40' bead bash and and phase separation through centrifugation. The aqueous upper phase was removed and replaced with an artificial upper phase consisting of methanol/H_2O and chloroform (48:47:3 v/v). The samples were then vortexed and subject to an another centrifugation. The organic lower phase was collected in full, evaporated under nitrogen stream, and then dissolved in 1mL chloroform/methanol (2:1).

Neutral lipid resolution was conducted on HPTLC siluca gel 60 plates, 20 x 10 cm (Merck, 1.05641.001). 20μL sample was sprayed onto the plate with a CAMAG automatic TLC sampler (ATS4). Resolution was performed in a CAMAG automatic

developing chamber (ADC2) with an n-hexane, n-heptane, diethylether, acetic acid (63:18.5:18.5:1 v/v) mobile phase.

Plates were derivatized using a 0.01% primuline solution, applied uniformly by a CAMAG derivatizer, and heated for 40°C for 2 minutes with a CAMAG TLC plate heater 3.

Resolved and derivatized neutral lipid bands were visualized with a CAMAG TLC visualizer 2 and analyzed using the software VisionCATS. Chromatograms were derived from the HPTLC bands and quantified through polynomial regression of standard curves included on plates. Included neutral lipid standard was a solution containing equal parts oleic acid (Sigma 01008), diacylglycerol (16:0-18:1, 8008150),cholesteryl-oleate (700269P), cholesteryl formate (S448532), triolein (870110O) and ergosterol (Thermofisher, 117810050) all at a final concentration of 500μg/mL in Heptane/Isopropanol (1:1 v/v). Standards were sprayed onto the plate in ranges from 1-30μL (or 0.5-15μg).

Samples were normalized to the quantity of internal standard present; in brief, the expected final concentration of cholesteryl formate (the internal standard added prior to extraction) was 250μg/mL. Interpolation from cholesteryl formate standard curve attained from chromatograms was used to determine the actual concentration and quantity in μ/g of internal standard and as such % efficiency of lipid extraction, allowing for normalization of data.

2.10 Transcriptomic analysis

2.10.1 RNA isolation from *Candida albicans*

Strains were grown to log phase and subjected to prerequisite conditions required for the assay (namely, 90' 16μg/mL fluconazole treatment in RPMI and a xμg/mL congo red treatment, both at 37°C. RNA was then isolated using a RiboPure^{tm} yeast RNA purification kit (Thermofisher Scientific, AM1926), snap frozen and stored at -80° prior to downstream use.

2.10.2 RNA sequencing analysis

All analysis was conducted using Galaxy. Raw data was first checked for quality using FastQC version using default settings, trimmed using TrimGalore version to ensure removal of adapter sequences and low quality ends of phred score ¡20, followed by an additional round of FastQC to ensure successful removal. Downstream of this any read shorter than 40bp was omitted from further analysis. Data was aligned to a the *Candida albicans* reference sequence (A22_Chromosomes_29.fasta.fai) using HISAT2; input parameters were as default other than denoting the library preparation as unstranded with paired ends. Output aligned read BAM files were run through HTSeq-Count to denote overlapping of reads with features in GFF file C_albicans_SC5314_current_features.gff. Reads aligning to more than one gene, overlapping, were discarded; only reads aligning to a single gene were included. Deseq2 was used to conduct pairwise comparisons between given conditions, generating a list of genes differentially expressed between datasets. Extractions and sequencing were completed in at least a biological duplicate.

In downstream processing, a cutoff of adjusted p-value ≤ 0.05 was applied. Venn diagrams were generated using Venny 2.1 [343], comparing overlap of differentially expressed genes (DEGs) from each condition (with cutoffs at a fold-change of 1.5x). Gene ontology and GOSlim was conducted on Candidagenome.org for lists of differentially upregulated and downregulated genes; a p-value of 0.1 was applied to Gene ontology terms. KEGG enrichment overrepresentation analysis was conducted using KOBAS [344], and relevant KEGG pathways were mapped using KEGG color mapper, mapping fold-changes in differentially expressed genes to the genes in the pathway with a heatmap scale denoting fold-change.

2.11 Flow cytometry

2.11.1 Cell Wall profiling with flow cytometry

Cells from an overnight culture were inoculated to an OD_600 of 0.1 and grown to log phase over a 4h incubation at 30°C, 180RPM. Cells were washed in PBS and fixed with a 4% paraformaldehyde (PFA) solution on ice for 30' before washing three times in PBS. mannans were stained using a Concanavalin A-FITC conjugate to a final concentration of 50μg/mL on ice for 30' in PBS, before being washed twice and resuspended in PBS. chitin was stained using a wheat-germ agglutinin-FITC conjugate to a final concentration of 50μg/mL in PBS, before being washed twice and resuspended in PBS.

For β-1,3-glucan probing, $2x10^6$ cells were blocked on ice with PBS + 2% BSA for 30'. Cells were then washed in PBS +2% BSA, and treated with PBS +2% BSA containing 3μg/mL FC-dectin-1 on ice for 60 minutes. Cells were then washed 3 times with PBS, before treating with a 1:200 anti-mouse secondary antibody conjugated to FITC on ice

in PBS + 2% BSA for 30'. Cells were then washed three times and resuspended in PBS. Cells were run through a BD accuri C6 plus flow cytometer, excited with a 488nm laser and gated for singlets prior to analysis. 20,000 cells were recorded per biological repeat and median fluorescence intensity used as a readout for signal compared to an unstained control.

2.11.2 Assessment of viability with flow cytometry

To assay effects of POA on viability cultured overnight as described above, and diluted to an OD_{600} of 1 in PBS. Following a 90' incubation at 37°C, 5% CO_2 with and without 1mM palmitoleic acid, cells were washed and resuspended in PBS and stained with 2μg/mL propidium iodide for 5 min.

Cells were run through a BD accuri C6 plus flow cytometer, excited with a 488nm laser and gated for singlets prior to analysis. 20,000 cells were recorded per biological repeat. A LP 635 filter was applied and fluorescence intensity recorded for each cell. Unstained and heat-killed controls were included to allow for accurate gating and downstream analysis.

2.12 Chronological lifespan assay

Cells from an overnight culture were inoculated to an OD_{600} of 0.1 in 25mL YPD, in a 150mL conical flask. Flasks were incubated at 30°C for a total of 7 days. On days 0, 1, 3, 5 and 7, the necrotic populations of strains were assessed through flow cytometry.

At least 1x10^6 cells were washed once in PBS, then resuspended in a PBS solution containing 2μg/mL propidium iodide.

Propidium iodide staining was assessed as described above in "Assessment of viability with flow cytometry". Unstained and heat-killed controls were included to allow for accurate gating and downstream analysis.

2.12.1 Transmission electron microscopy

Sample preparation and transmission electron microscopy was kindly carried out by Dr Louise Walker of the Aberdeen Fungal Group. Cells were grown for 4h, and 1mL cell suspension was pelleted an pressure-frozen using a Leica EM AFS2 automatic frreeze substitution system and EM FSP freeze substitution processor (Leica microsystems). Dehydration of samples was carried out in an anhydrous acetone solution containing 1% osmium tetroxide (OsO_4) for 10h. Dehydrated samples were warmed to -30°C over 8h in the acetone/OsO_4 solution, and then to 20°C over the course of 3h in acetone. Samples were embedded in increasing concentrations of Spurr's epoxy resin over 24h. Sections were cut using a 45° Diatome diamond knife in a Leica UC6 ultramicrotome. 100nm sections were adhered to a 300nm copper mesh grid. Samples were stained with uranyl acetate and lead citrate at 20°C in an automated staining machine (Leica AC20 EM). Images were captured on a JEOL 1400 Plus transmission electron microscope (Jeol UK) running at 80 kV, with an AMT ActiveVu XR16M camera (Deben UK). Thickness measurements were taken manually in ImageJ, with 5 measurements across the cell, 10 cells per condition, for a total 50 measurements.

2.13 Fluorescence Microscopy

Imaging was conducted on either an Olympus IX81 inverted widefield microscope with a coolLED pE4000 illumination system and an Andor Zyla 4.2 PLUS sCMOS camera, or on a Zeiss LSM 880 Confocal system. Unless stated otherwise, samples were resuspended in PBS and applied to a glass microscope slide with a 0.13mm thickness coverslip.

Neutral lipid staining was achieved with 10μM BODIPY 493/503 (Thermofisher), excited with a 488nm laser and captured with a GFP bandpass filter.

Chitin staining for the purpose of visualization was acheived with a drop of Calcofluor white solution (Sigma), excited with a 405nm laser and captured within a DAPI bandpass filter.

2.14 Biofilm assays

For biofilm growth on medical plastics, silicone sheets were cut into 1cm x 1cm squares, rinsed with EtOH, and fastened into a specialized 24-well plate lid fitted with clips (Academic Centre for Dentistry Amsterdam, AAA-model)- this setup allows for suspension of leaflets within a 24-well plate. Silicone leaflets were incubated in 50% donor bovine serume (DBS, Gibco), 30 min at 30°C, then rinsed twice in a second plate with sterile PBS. Yeast cells from an overnight culture were washed and resuspended in PBS to an OD_{600} of 1. 1mL cell suspension was added to the wells of 24-well plates (greiner), and silicone leaflets were submerged in cell suspension and incubated at 37°C, 5% CO_2 for 90' to allow cell attachment. Silicone leaflets were then washed twice in PBS, followed by submersion in 1mL RPMI-1640 in a fresh 24-well plate, and incubated for 24 hours. For attachment phase treatments, 50mM stock POA was diluted in the PBS cell suspensions

during the 90' attachment. For maturation phase treatments, POA was diluted in RPMI.

For high-throughput screening of biofilm formation, biofilms were grown on in the bottom of 96-well plates. As above, wells were treated with 100μL 50% DBS for 30' at 30°C, gently washed twice with PBS to remove excess DBS. Yeast cells were washed and resuspended to an OD_600 of 0.1, with 100μ being added to each well. Plates were treated as described above; 90' attachment phase, two PBS washes, addition of equal volume RPMI-1640, and a 24 hour maturation phase.

2.14.1 Quantification of biofilms

Biofilm size and metabolic activity were determined in one of three ways:

96-well biofilm size was assessed through crystal violet staining. Matured biofilms were washed twice with PBS, and then incubated for 15' at ambient temperature with 0.1% w/v crystal violet solution solubilised in 100% EtOH. Biofilms were subsequently washed 4 times with ddH_2O, and then allowed to dry at ambient temperature for 24h.

100 μL 30% acetic acid was added to crystal violet stained biofilms and incubated at ambient temperature for 15' to solubilise bound crystal violet. Plates were subsequently spun down at 4000 RPM for 5'. 90μL supernatant from each well was transferred to a fresh 96-well plate, and analysed in a SPECTROstarNano plate reader, reading an absorbance of 595nm to assess degree of crystal violet staining.

24-well silicone leaflet biofilms were assessed using an XTT (sodium 3´- [1 - (phenylaminocarbonyl) - 3,4- tetrazolium]-bis (4-methoxy6-nitro) benzene sulfonic acid hydrate) assay (roche). Silicone leaflets were washed twice with PBS. an XTT- electron coupling reagent mixture was prepared with 1μ PMS (N-methyl dibenzopyrazine methyl

sulfate) electron couple reagent for every 50 μL 1mg/mL XTT reagent, then diluted 5-fold with PBS to a final XTT concentration of 196.08μg/mL and 0.4% v/v PMS. 1mL XTT- electron coupling reagent solution was added to the wells of a fresh 24-well plate, and silicone leaflet biofilms submerged for 2h at 37°C. XTT assays are colorimetric assays assessing cell viability; level of reduction of XTT reagent was assessed in a plate reader at absorbance 492nm.

2.15 Biofilm thickness determination

Biofilms were grown in ibidi μ-slides for imaging. Briefly, cells grown overnight as described above were seeded to OD_600 0.1 in RPMI-1640, and 200μL added to the well of a chamber slide. Biofilms were allowed to grow for 24-48h prior to staining with 10μM BODIPY 493/503 and calcofluor white. Biofilms were imaged with a Zeiss LSM 880 Confocal system, using an Airyscan detector. BODIPY was imaged using a 488nm argon laser with a 495-550 bandpass filter, and calcofluor was imaged with a 405nm laser with a 420-480nm bandpass filter, and subject to airyscan image processing prior to downstream analysis.

2.15.1 Assessment of biofilm thickness from scanning confocal microscopy

Airyscan processed images were subject to a maximum intensity orthogonal projection in Zen Blue (Zeiss). Multichannel images were split, and the 420-480nm channel (for calcofluor stained cell walls), was used as an approximation for biofilm thickness from

base to brush layer. Briefly, a percentile threshold was applied to images and 200 thickness measurements were taken across 2 biological replicates for each condition.

2.16 POA absorption into silicone

POA-treated silicone squares were created courtesy of Professor Simon Holder and his students, Lyon Bowen and Morgan White. Briefly, PDMS was synthesised through a 10:1 ratio of Sylgard-184 base to Sylgard-184 curing agent. The mixture was mixed at 3000 rpm for 3', then cured on a hotplate at 150° for 10'. Cured PDMS was cut into 2x2cm for further processing.

For absorption of POA into the PDMS, 2x2cm PDMS squares were weighed and placed into glass vials. 0%, 2% and 5% w/w POA was added to each vial relative to the mass of the silicone square, and solubilised in 600μL dichloromethane (DCM). Vials were agitated for 30', flipping silicone squares after 15' to allow for uniform absorption of POA. Squares were then removed from their respective POA-DCM solutions, and excess DCM allowed to evaporate off in a fume hood for 30'. PDMS squares were then quality control checked using infrared spectroscopy prior to use.

2.17 Phagocytosis assays

J77A.1 cells that had reached a 90% confluency were resuspended in fresh DMEM as described previously. Cells were counted in a haemocytometer and the cell suspension adjusted to 1x10^5 cells/mL. 100,000 cells were seeded into the well of a 24-well plate and incubated overnight under usual J77A.1 conditions. Meanwhile, desired yeast strains were inoculated into YPD and allowed to grow overnight as previously described. The

following day, yeast strains were inoculated to OD_600 0.1 and allowed to grow for 4h. Media was removed from the macrophages, and they were activated with 1ml serum-free DMEM media with .015% (v/v) PMA for no longer than 1h. meanwhile, yeast cells were washed in PBS, counted with a haemocytometer and adjusted to $5x10^5$ cells/mL in fresh, serum-free DMEM. PMA-containing media on macrophages was replaced with 1mL yeast cell suspension; 5 yeast cells for every 1 macrophage seeded. Cells were incubated at 37C, 5% CO2 for 1h. Cells were washed twice with PBS, fixed with 4% PFA for 10', then washed twice more with PBS. External yeast cells were stained with 50μg/mL ConA-FITC for 30', and washed twice more prior to imaging.

2.18 Galleria Mellonella infection assay

Overnight cultures of yeast strains were prepared as described. The following day, cells were washed with PBS and diluted to $2.5x10^7$ cells/mL in PBS. Galleria mellonella larvae (livefoods ltd) were selected based on sizes similar to one another. Galleria were injected using (needle type) with 10μ cell suspension to a total inoculum of 250,000 cells; injections were made into the last left proleg and galleria checked for trauma immediately after injection. Alongside those infected with *Candida albicans*, a PBS control and trauma control were also included. For each condition, 20 galleria were injected, completing the assay in biological duplicate to a total of 40 infected larvae. Over the course of 7 days, galleria were scored on whether living or dead as well as their melanization state.

2.19 Statistical analysis

All statistical analysis for the paper was conducted within GraphPad Prism. Unless stated otherwise, statistical significance was determined with an ordinary one-way ANOVA and Tukey's test for multiple comparisons, with where * denotes $p \leq 0.05$, **= $p \leq 0.01$, ***= $p \leq 0.005$, ****= $p \leq 0.001$. HPTLC data was analyzed with a 2-way ANOVA of grouped data, and a Dunnet's multiple comparisons test. Growth curve data was analyzed by fitting datasets to nonlinear regression curves for determination of doubling time, carrying capacity, and comparing these parameters to determine statistical significance between curves. Galleria mellonella survival data was fitted to a Kaplan meier survival plot, and significance between two curves determined with log-rank (Mantel-Cox) tests.

Chapter 3

CRISPR Cas9 generation and phenotyping of a glycerophospholipid knockout library in *C. albicans*

3.1 INTRODUCTION

C. albicans is a commensal fungal pathogen capable of transitioning between yeast and filamentous forms, a property critical for its virulence and pathogenicity [43, 83, 345]. This morphological plasticity is tightly regulated by a network of metabolic and signalling pathways- several transcription factors, regulated by the Ras-PKA-cAMP pathway, control the yeast-to-hyphal switch [83, 36].

C. albicans' morphological plasticity relies on considerable control of cell wall structure and integrity [303] and regulation of phospholipids and intracellular glycerolipids for plasma membrane integrity and signalling [225, 241]. The phospholipid phosphatidylcholine (PC) makes up the bulk of plasma membrane phospholipids in yeast, with biosynthesis controlled by two mechanisms; de novo biosynthesis with CDP-DAG as a precursor [303, 213] and Kennedy biosynthesis, relying on intracellular and extracellular sources of choline for PC biosynthesis [321, 328]. Tight regulation of diacylglycerols (DAG) and funnelling of DAG into phospholipid biosynthesis has been highlighted as critical for typical membrane proliferation in the yeast *S. cerevisiae* [231]. As such, the fidelity of glycerolipid metabolic control likely plays a role in morphological plasticity of the yeast *C. albicans*, though as of yet the relationship between glycerolipid metabolism and filamentation has not been fully explored.

In *S. cerevisiae*, and indeed in all higher eukaryotes, excess lipids (and indeed the source of fatty acids for future membrane biogenesis) are stored in lipid droplets as discussed in 5. Briefly, lipid droplets comprise a core of neutral lipids (TAGs and SEs) wrapped

in a protein-studded phospholipid monolayer [346, 347]. These transient organelles support regulation of autophagy [186], act as a source of energy through peroxisomal β-oxidation [348] and fuel CDP-DAG dependent phospholipid biosynthesis through the activity of triacylglycerol lipases *TGL*s [303, 213, 349, 350]. In *S. cerevisae*, the *TGL* family have a diverse range of functions, including sterol ester catabolism and triacylglycerol catabolism, but the *TGL* family has yet to be characterized in *C. albicans*.

This work sought to better understand the function of lipid droplets and the metabolic control they provide on the morphological plasticity and virulence of *C. albicans*. I used CRISPR Cas9 to generate null mutants for several components of glycerolipid metabolic pathways, including the putative triacylglyceride lipase *TGL2*, sterol esterase *TGL1*, DAG: acyltransferase *LRO1*, Acyl-CoA:steroltransferase *ARE2*, PS synthase *CHO1* and putative phosphatidate phosphatase *SMP2*. I determined changes to the lipidome through high-performance thin layer chromatography (HPTLC) analysis and assessed the impact of gene deletions on lipid droplet number and the ability to filament. A *TGL2* homozygous null mutation led to increased intracellular TAG and lipid droplets, an inability to filament on spider medium and abnormal cell morphology when grown in hyphal-inducing conditions. *tgl2* Δ/Δ cells also displayed a reduced virulence in a *Galleria mellonella* (*G. mellonella*) model. Our findings suggest a role for the TAG lipase Tgl2 in the breakdown of TAG as a mechanism for cellular adaptation and morphological plasticity.

3.2 RESULTS

3.2.1 Generation of homozygous null gene deletions using CRISPR Cas9

Following determination of gene targets, I sought to generate homozygous null deletions to determine the impact of different glycerolipid and glycerophospholipid deficiencies on various virulence and fitness traits of *C. albicans*. The approach I employed for the generation of this particular library was a *C. albicans*-optimised CRISPR Cas9 system developed in the Hernday lab [340] (Fig. 3.1, 3.2 and A.2-A.4).

This strategy employed 3 separate plasmids: one containing one half of a nourseothricin (NAT) resistance marker and Cas9 expression machinery, a second "universal" plasmid containing the second half of the NAT resistance marker and pSNR52 promoter, and a third with a gRNA scaffold. Amplification of universal "fragment A" from pADH110 (Fig. 3.1, 3.2A). Unique "fragment B" was amplified from pADH147 using a target-specific oligonucleotide sequence (Fig. 3.1, 3.2A), designed such it would target a protospacer adjacent motif (PAM) site found relatively early in the open reading frame (ORF) of a gene of interest. gRNA primers and PAM sites were selected to balance on target [341] and off target [342] scores to mitigate off-target effects whilst ensuring transformation efficiency. Amplification of fragment B included an upstream sequence to allow for overlap with fragment A, such that a stitch PCR could be performed to stitch fragment A to fragment B to generate "fragment C" (Fig. 3.1, 3.2B).

3 components were co-transformed into *C. albicans*: linearized and digested pADH99, inclusive of Cas9 and NAT resistance marker part 1 of 2, hence referred to as "fragment

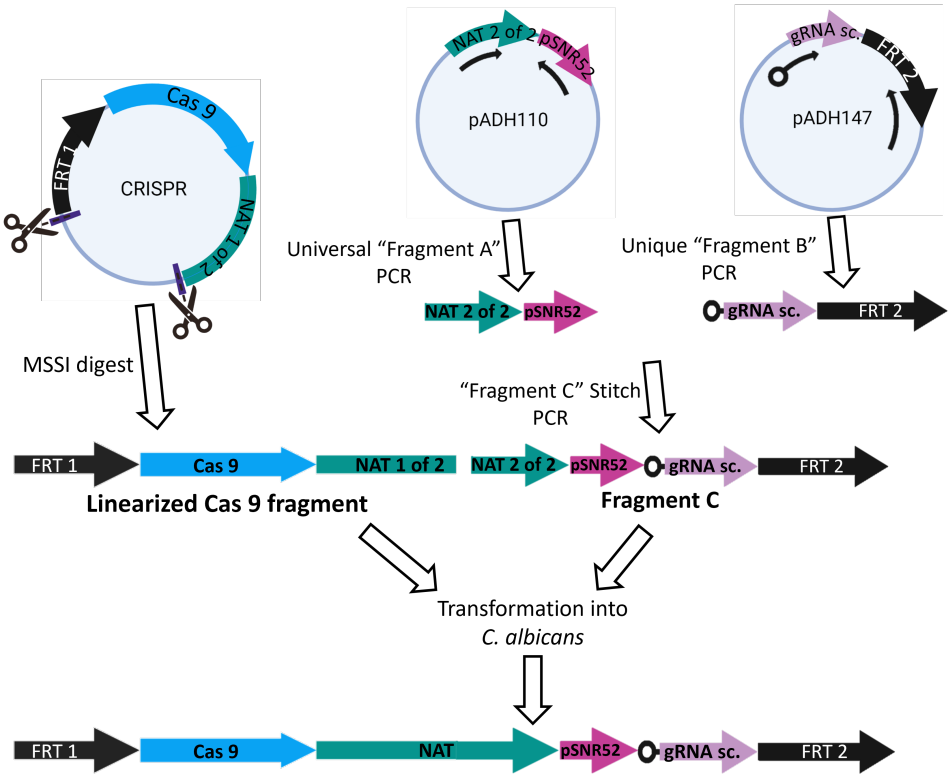

FIGURE 3.1: **Hernday CRISPR Cas9**
Schematic outlining Hernday CRISPR strategy. "Fragment Cas9", containing Cas9 promoter and coding sequence, FRT recombinase and FRT site, as well as half of a Nourseothricin (NAT) resistance marker, is attained through digestion of "CRISPR" plasmid pADH99. Universal fragment A, containing the second half of the NAT resistance marker and promoter pSNR152, is amplified from pADH110. "Unique" fragment B, containing an overlap with fragment A as well as the second FRT site and a unique gRNA scaffold specific to targeting ORF of interest, is amplified from pADH147. A stitch PCR to combine fragment A with fragment B yields a unique fragment C, containing half of a NAT resistance marker, an intact gRNA scaffold and FRT site 2 of 2.
Transforming fragment C, as well as fragment Cas9, into *C. albicans* allowed for insertion of fragments into the *HIS1* locus. Correct orientation of the two fragments generated an intact NAT resistance marker, as well as Cas9 coding sequence and gRNA scaffold to target expressed Cas9 to the ORF of interest. When co-transformed with a designed repair template, Cas9-generated double-strand breaks are repaired through homology-directed repair to yield the desired mutation. Cas9 machinery and resistance marker can be recycled by growing on maltose to promote maltose-dependent induction of FLP recombinase.

Cas9"; fragment C, inclusive of NAT resistance marker part 2 of 2 promoter and gRNA targeting scaffold; and a repair template amplified from genomic DNA (Fig. 3.2B). Repair templates were designed such that products had at least 60 base pairs (bp) sequence

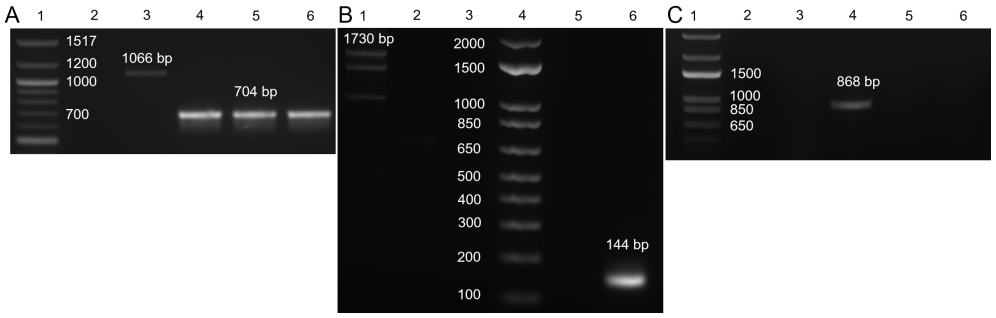

FIGURE 3.2: **Representative confirmation of PCR products and clones generated with Hernday CRISPR Cas9**
(A-C) Electrophoresis confirmation of PCR products. Samples were run on a 1% agarose gel containing ethidium bromide and imaged.
(A) A gel displaying a fragment A amplification band and the fragment B amplifications for 3 unique constructs. Samples loaded: **lane 1**, 100bp DNA ladder; **lane 2**, empty; **lane 3**, fragment A (1066 bp); **lane 4**, *SMP2* fragment B (704 bp); **lane 5**, *DGA2* fragment B (704 bp); **lane 6**, *LRO1* fragment B (704 bp).
(B) A gel containing *LRO1* "Fragment C" product of fusion PCR (fusing fragment A and *LRO1* fragment B) and repair template amplified from genomic DNA. Samples loaded: **lane 1**, fragment C, *LRO1* (1730 bp); **lane 2**, empty; **lane 3**, empty; **lane 4**, 1kb plus DNA ladder; **lane 5**, empty; **lane 6**, *LRO1* repair template.
(C) A gel displaying PCR product from colony PCR to check for successful ORF removal. Samples loaded: **lane 1**, 1kb plus DNA ladder; **lane 2**, *LRO1* colony PCR 1 (no amplification); **lane 3**, *LRO1* colony PCR 2 (no amplification); **lane 4**, *LRO1* colony PCR 3 (868 bp, successful clone); **lane 5**, empty; **lane 6**, empty.

homology upstream of the target ORF, at least 60 bp downstream of the target ORF, but with removal of the ORF itself and replacement with a targetable sequence. The constructs generated and used depend on the HIS-FLP system. As such, upon transformation and correct arrangement, fragments Cas9 and C integrate into the *HIS1* locus, forming a complete NAT resistance marker and functional Cas9 machinery inclusive of a targeting sequence specific to the ORF marked for removal (Fig. 3.1). Inclusion of the repair template allowed for homology-directed repair (HDR) following cleavage of the ORF.

Following confirmation of the mutants through colony PCR (Fig. 3.2C), successful transformants were patched onto agar plates using maltose as a carbon source instead of

glucose to induce the maltose-inducible FLP recombinase to excise CRISPR machinery. Table 3.1 outlines the mutants generated as a part of this study in the manner described above. *SMP2*, the putative phosphatidate phosphatase orthologous to *S. cerevisiae*'s *PAH1* was discovered to be heterozygous null, but was included in the study to determine whether deletion of one copy was sufficient to hinder functionality.

TABLE 3.1: A summary of null mutants generated using Hernday CRISPR Cas9

Target gene	Function	Homozygous or Heterzygous null
SMP2	Phosphatidic acid phosphatase	Heterozygous
LRO1	DAG acyltransferase	Homozygous
ARE2	Acyl-CoA steroltransferase	Homozygous
TGL1	Sterol esterase	Homozygous
TGL2	Triglyceride lipase	Homozygous
PSD1	Phosphatidylserine decarboxylase	Homozygous
CHO1	Phosphatidylserine synthase	Homozygous

3.2.2 HPTLC lipid profiling and neutral lipid staining of neutral lipid storage, mobilization, and de novo phospholipid biosynthesis mutants

The generated CRISPR mutants can be grouped into broad categories: *SMP2*, *LRO1* and *ARE2*, whose *S. cerevisae* orthologues feed free fatty acids and sterols into storage as TAGs and SEs; *TGL1* and *TGL2*, whose *S. cerevisiae* orthologues orchestrate breakdown of TAGs and SEs back into DAG and sterols; and *PSD1* and *CHO1*, whose activity generates phospholipid species for membrane proliferation. I sought to first determine the impact that our various CRISPR mutants had on the lipidome of *C. albicans*. Total lipids were extracted from comparable amounts of stationary phase cells and resolved

through high-performance thin-layer chromatography (HPTLC) (Fig. 3.3,3.4, B.2,B.3).

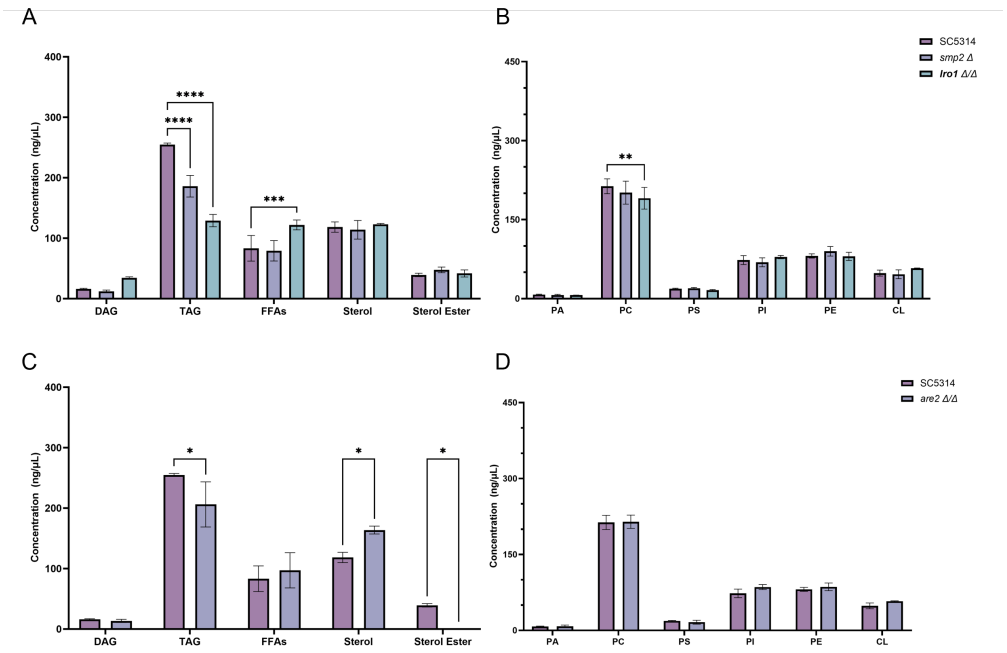

FIGURE 3.3: **HPTLC analysis of neutral lipids and phospholipids** **(A-D)** HPTLC lipid profiling of wild type, *smp2* Δ and *lro1* Δ/Δ **(A-B)** and *are2* Δ/Δ **(C-D)** at stationary phase. Lipids were harvested from stationary phase cells, resolved and compared to neutral lipid (A,C) and phospholipid (B,D) standards. **(A,C)** Neutral lipids diacylglycerol (DAG), triacylglycerol (TAG), sterol esters (SE), sterols and free fatty acids (FFAs) were analysed as described above, all stained with primuline and compared to standards. **(B,D)** Resolved phosphatidylcholine (PC), phosphatidic acid (PA), phosphatidylinositol (PI) and cardiolipin (CL) were stained with primuline to allow for quantification; phosphatidylethanolamine (PE) and phosphatidylserine (PS) require additional staining detection with ninhydrin. Lipids were quantified as described in methods. Data represents 3 biological replicates. Significance was determined with a 2-way ANOVA and Dunnett's multiple comparisons test, where * = $P < 0.05$, ** = $P < 0.01$, *** = $P < 0.001$, and **** = $P < 0.0001$

I first looked at deletions of the DAG acyltransferase *LRO1* and the phosphatidate phosphatase *SMP2*. In *S. cerevisiae*, ScLro1 catalyses the terminal reaction of DAG to TAG biosynthesis, and ScPah1 (Smp2 ortholog), catalyses DAG biosynthesis from PA- as such, both are responsible for glycerolipid biosynthesis. *lro1* Δ/Δ displayed a more than 50% reduction in intracellular TAG when compared to that of the wild type,

as well as an accompanying increase in free fatty acids (FFAs) (Fig. 3.3A). The *lro1* Δ/Δ mutant also displayed significantly reduced phosphatidylcholine (Fig. 3.3B). The heterozygous null *smp2* Δ displayed a 25% reduction in intracellular TAG (Fig. 3.3A), though this proved to be the only significant change in the *smp2* Δ lipidome.

Looking at the Acetyl-CoA: steroltransferase *are2* Δ/Δ mutant, there was a minor decrease in TAG. More notably, there was an increase in intracellular sterol compared to the wild-type, and loss of detectable sterol ester (Fig. 3.3C). Disruption of sterol storage did not have a notable change in phospholipid content, however (Fig. 3.3D).

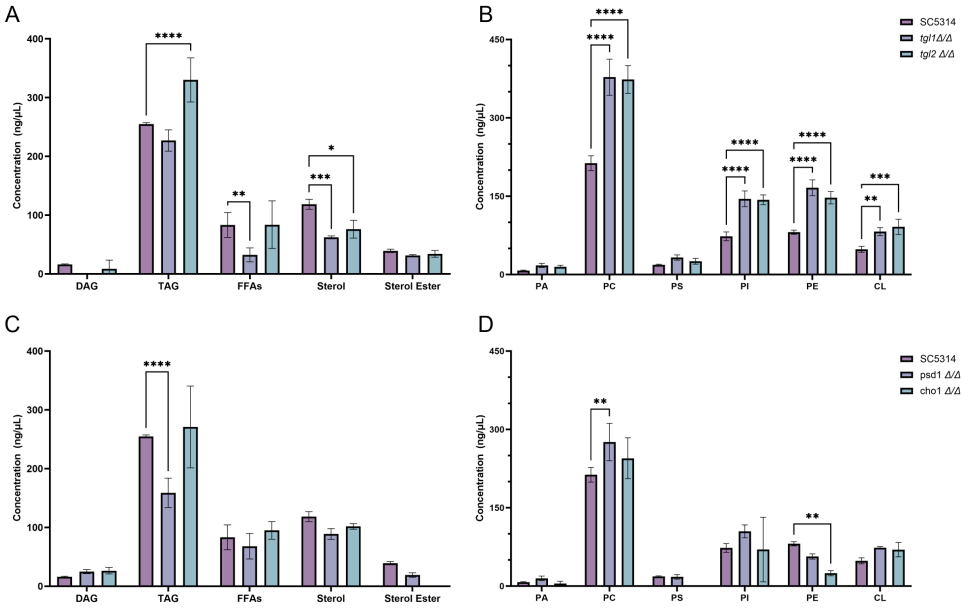

FIGURE 3.4: **HPTLC analysis of neutral lipids and phospholipids** **(A-D)** HPTLC lipid profiling of wild type, *tgl1* Δ/Δ and *tgl2* Δ/Δ **(A-B)**, *psd1* Δ/Δ and *cho1* Δ/Δ **(C-D)** at stationary phase. Lipids were harvested from stationary phase cells, resolved and compared to neutral lipid (A,C) and phospholipid (B,D) standards. **(A,C)** Neutral lipids diacylglycerol (DAG), triacylglycerol (TAG), sterol esters (SE), sterols and free fatty acids (FFAs) were were analysed as described above, all stained with primuline and compared to standards. **(B,D)** Resolved phosphatidylcholine (PC), phosphatidic acid (PA), phosphatidylinositol (PI) and cardiolipin (CL) were stained with primuline to allow for quantification; phosphatidylethanolamine (PE) and phosphatidylserine (PS) require additional staining detection with ninhydrin. Lipids were quantified as described in methods. Data represents 3 biological replicates. Significance was determined with a 2-way ANOVA and Dunnett's multiple comparisons test, where * = $P < 0.05$, ** = $P < 0.01$, *** = $P < 0.001$, and **** = $P < 0.0001$

Looking at the neutral lipid profile of *tgl1* Δ/Δ, whose *S. cerevisiae* orthologue exhibits sterol esterase activity, there was a reduction in intracellular FFAs compared to that of the wild type, as well as a 50% reduction in sterol content (Fig. 3.4A). There was also a significant increase in PC, PI, PE and CL in *tgl1* Δ/Δ compared to wild type levels. *tgl2* Δ/Δ, whose *S. cerevisiae* orthologue is a TAG lipase, revealed significantly increased intracellular TAG and sterols (Fig. 3.4A). Like the *tgl1* Δ/Δ, *tgl2* Δ/Δ also displayed elevated PC, PI, PE and CL compared to the wild type (Fig. 3.4B).

Lastly, I analyzed the effect of deleting phosphatidylserine synthase (Cho1) and phosphatidylserine decarboxylase (Psd1) on the lipidome (Fig. 3.4C-D). *psd1* Δ/Δ, responsible for conversion of PS to PE displayed a reduced TAG content compared to the wild type (Fig. 3.4C), and surprisingly, an elevated PC concentration (Fig. 3.4D). Cho1 is responsible for the initiation of de novo phospholipid biosynthesis through the generation of PS from cytidine diphosphate-diacylglycerol (CDP-DAG). The *cho1* Δ/Δ showed no changes in neutral lipid profile, other than a lack lack of detectable SE (Fig. 3.4C) but a significant reduction in intracellular PE (Fig. 3.4D).

I sought next to determine the impact, if any, of the described gene deletions on lipid droplet formation. Using BODIPY 493/503 neutral lipid stain, I was able to observe lipid droplets in stationary phase cells (Fig. 3.5).

Of those imaged, there were no significant differences in lipid droplet number in the *smp2* Δ (Fig. 3.5B, *lro1* Δ/Δ (Fig. **??**C) and *tgl1* Δ/Δ (Fig. **??**D) mutants when compared to the wild type(Fig. 3.5A, G), though lipid droplets in the *tgl1* Δ/Δ mutant appeared larger than wild lipid droplets (Fig. 3.5D). There was a significant increase in lipid droplet number in the *tgl2* Δ/Δ (Fig. **??**E) mutant compared to the wild type (Fig. 3.5G), in line with expectations owing to elevated TAG (Fig. 3.4A). *Cho1* Δ/Δ

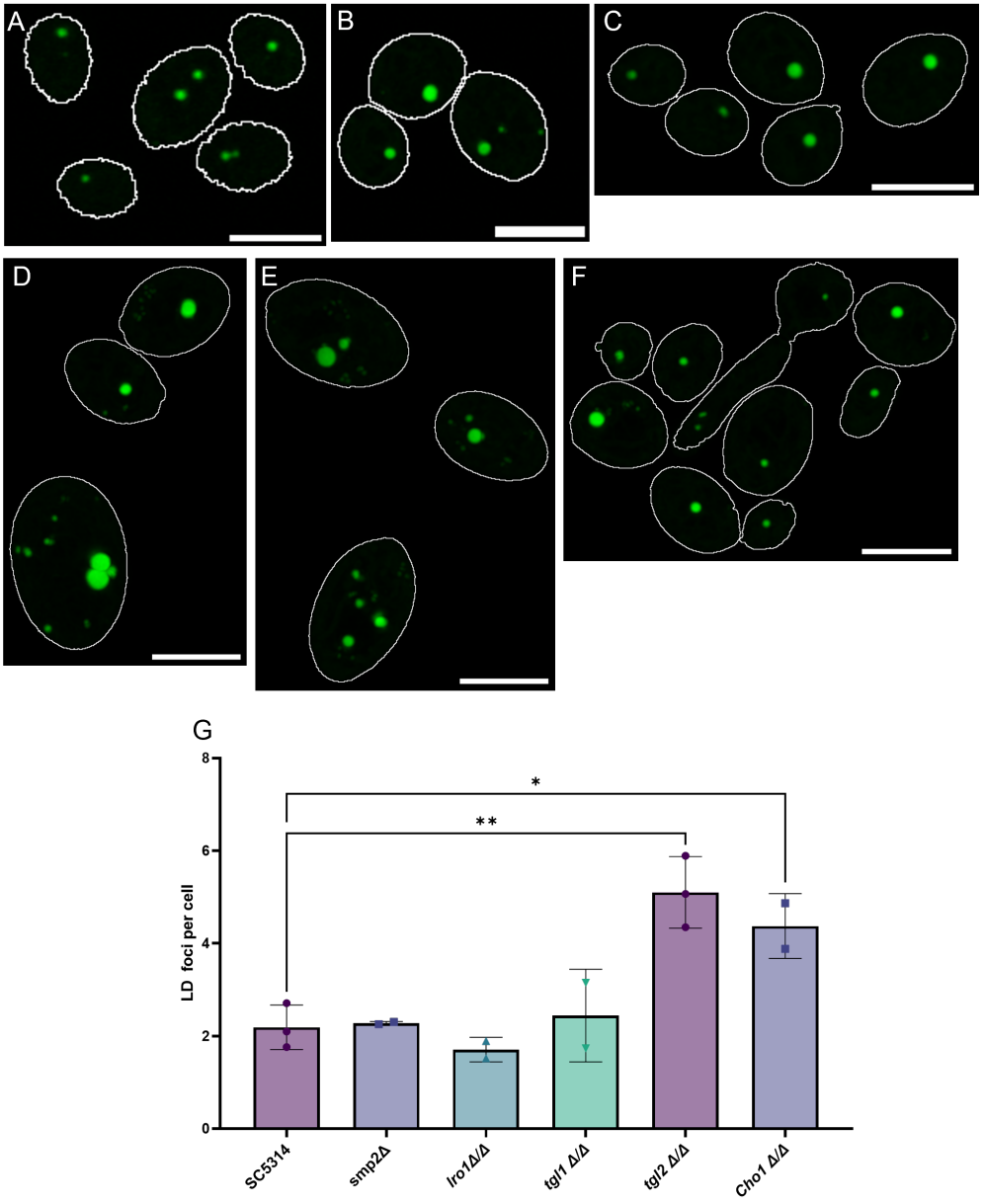

FIGURE 3.5: **Neutral lipid staining of CRISPR knockout library** **(A-F)** BODIPY staining and imaging of knockout library. Cells were grown to stationary phase, stained with 10μM BODIPY 493/503 and imaged (A, Wild type; B, *smp2* Δ; C, *lro1* Δ/Δ; D, *tgl1* Δ/Δ; E, *tgl2* Δ/Δ; F, *cho1* Δ/Δ). Scale bar denotes 5μm, and white outline masks denote cell borders. **G** quantification of neutral lipid foci. BODIPY 493/503 stained cells were scored for number of neutral lipid foci, with at least 200 cells analyzed per biological replicate; n=3 for SC5314, *tgl2* Δ/Δ; n=2 for *smp2* Δ, *lro1* Δ/Δ, *tgl1* Δ/Δ, *cho1* Δ/Δ. Significance was determined with an ordinary one-way ANOVA and Dunnet's multiple comparisons test, where where * = $P < 0.05$ and ** = $P < 0.01$

also had an increased number of lipid droplet foci; these cells also displayed pseudohyphal growth in standard growth conditions (Fig. 3.5F). Other studies have determined

CHO1 homozygous null mutations to cause severe growth defects and require choline supplementation to compensate for disrupted de novo phospholipid biosynthesis [321, 213]. In all, these data highlight the significant impact that *TGL2* and *CHO1* null mutations have on the lipid profile of *C. albicans.*

3.2.3 Aberrant glycerolipid metabolic pathways disrupt filamentation in solid and liquid media

Having established the impact of our various glycerolipid metabolism mutants on intracellular neutral lipids and phospholipids, I next investigated the role these proteins play in driving the morphological changes seen in *C. albicans* under hyphae-inducing conditions. Each strain was grown on both YPD and spider medium; spider medium and its mannitol carbon source are a known trigger of filamentous colonies (Fig. 3.6, Fig. 3.7).

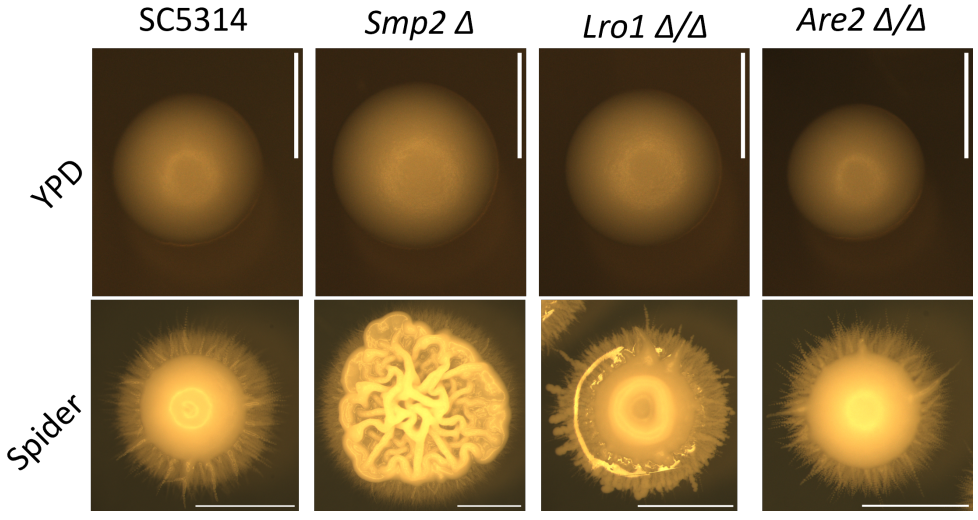

FIGURE 3.6: **Filamentation of CRISPR knockout library on solid medium**
Wild type, *smp2* Δ, *lro1* Δ/Δ and *are2* Δ/Δ were plated for single colonies and grown for 6 days on YPD and spider medium. Scale bars denote 2mm

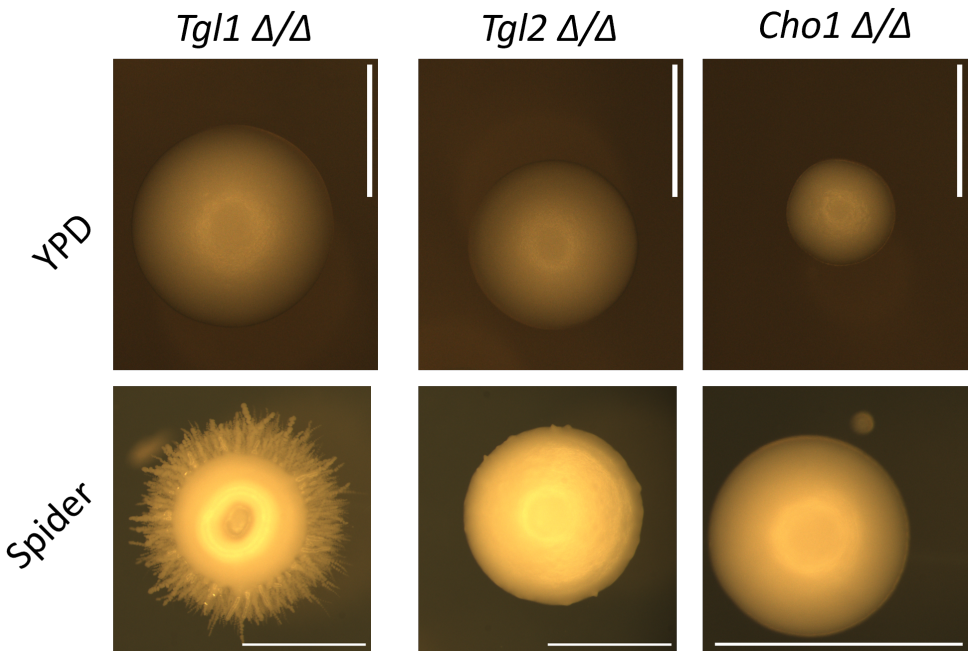

FIGURE 3.7: **Filamentation of CRISPR knockout library on solid medium**
Wild type, *tgl1* Δ/Δ, *tgl2* Δ/Δ and *cho1* Δ/Δ were plated for single colonies and grown for 6 days on YPD and spider medium. Scale bars denote 2mm

On spider medium, the wild type colonies were uniformly filamentous (Fig. 3.6). Across all assayed strains, all except *cho1* Δ/Δ grew normally on YPD. The *smp2* Δ, curiously, exhibited a wrinkled colony morphology when grown on spider medium. This was indicative of either pseudohyphal growth or a documented starvation response in *S. cerevisiae* [351]. Both *lro1* Δ/Δ (Fig. 3.6) and *tgl1* Δ/Δ (Fig. 3.7) colonies displayed filamentation on spider medium, but with an altered colony morphology; a raised ring-like colony, as opposed to the domed colony akin to the wild type. The *are2* Δ/Δ colonies were comparable to that of the wild type on spider medium (Fig. 3.6). Curiously, both the *tgl2* Δ/Δ and *cho1* Δ/Δ colonies displayed a filamentation defect on spider medium (Fig. 3.7). *cho1* Δ/Δ colonies were smaller than that of the wild type (Fig. 3.7) on both YPD and spider medium; typically *cho1* Δ/Δ proved difficult to grow for extended periods even in normal medium, likely owing to deficiencies in de novo PL synthesis. *cho1* Δ/Δ colonies remained comparably small on spider medium, and perfectly smooth

and domed. *tgl2* Δ/Δ displayed largely smooth colonies with the occasional blebbing, though showed no true filaments or agar invasion when compared to that of the wild type. I sought then to determine whether deleting *TGL2* affected filamentation in a liquid medium as well (Fig. 3.8). Wild type and *tgl2* Δ/Δ strains were grown for 90 min in DMEM containing 10% serum in both normal air and 5% CO_2, stained, and their capacity to filament observed.

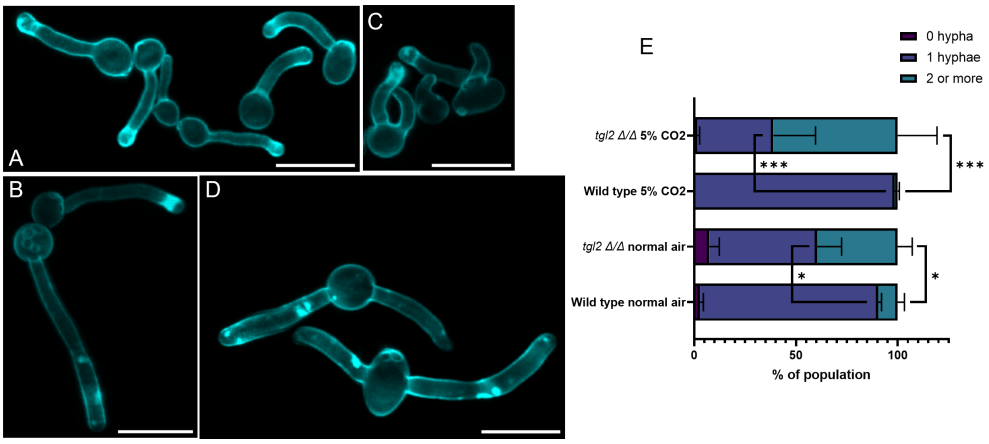

FIGURE 3.8: ***TGL2* disruption causes increased incidence of multi-hyphal cells**

(A-D Confocal imaging of hyphal-induced cells. Cells from overnight cultures were grown for 90 min in DMEM containing 10% serum in normal air **(A,C)** and 5% CO_2 **(B,D)**, before staining with CFW. Scale bars denote 10μm. **(A)** = wild type, normal air; **(B)** = wild type, 5% CO_2; **(C)**, *tgl2* Δ/Δ, normal air; **(D)**, *tgl2* Δ/Δ, 5% CO_2. **(E)** Stacked bar graph depicting proportions of cells displaying no filamentation, one hyphae, or two or more hyphae. At least 200 cells were scored per condition per biological replicate, in a biological duplicate. Statistical significance was determined using an ordinary 2-way ANOVA with Tukey's multiple comparisons, where * = $P < 0.05$, ** = $P < 0.01$, and *** = $P < 0.001$

cho1 Δ/Δ was omitted from further analysis in this study owing to the unreliable growth during assays, likely owing to a choline auxotrophy I had not accounted for [213, 321]. When grown in DMEM containing serum, in both normal air and 5% CO_2, wild type cells predominantly initiated growth of 1 germ tube (Fig. 3.8A-B), with hyphae in the CO_2 condition developing faster than the normal air condition. Growth of the *tgl2* Δ/Δ in DMEM containing serum led to some interesting hyphal and growth abnormalities

(Fig. 3.8C-D). Of those cells that could be considered to have developed true hyphae, in both normal air and 5% CO_2, the majority exhibit at least two hyphal protrusions. Quantification of the number of hyphae per cell revealed that in normal air, 40% of *tgl2* Δ/Δ cells have at least 2 developed true hyphae (Fig. 3.8E), whereas this was observed in approximately 10% of wild type cells. This difference was more pronounced in 5% CO_2, where almost 100% of analysed wild type cells had exactly 1 true hypha; in contrast, approximately 60% of the analyzed *tgl2* Δ/Δ cells had 2 or more hyphae.

The above refers to the cells exhibiting true hyphal growth. Amongst the *tgl2* Δ/Δ grown in DMEM with serum in normal air, a large portion of cells displayed aberrant and atypical growth (Fig. 3.9).

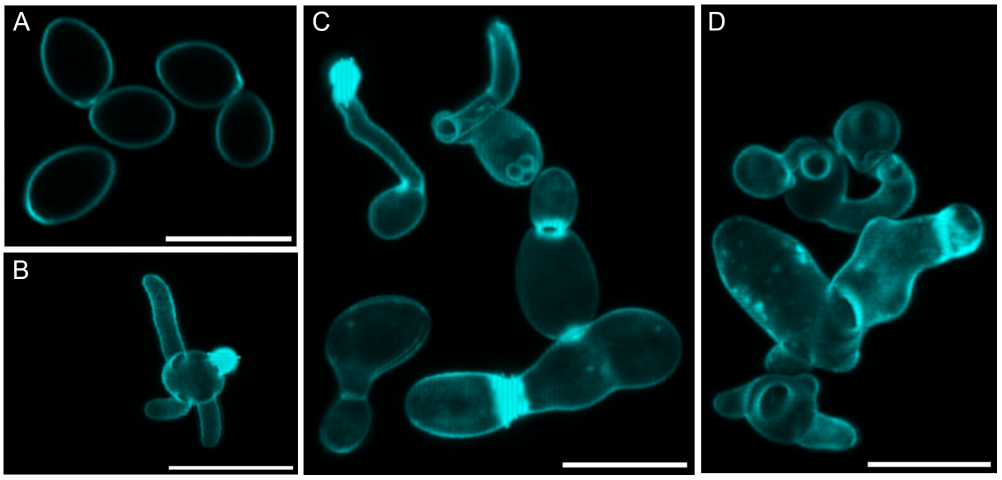

FIGURE 3.9: ***TGL2* deletion causes growth defects when grown in hyphal-inducing conditions**
(A-D) Confocal imaging of *tgl2* Δ/Δ. Cells were stained with CFW and imaged. Scale bar denote 10μm. **(A)** *tgl2* Δ/Δ at time 0, prior to hyphal induction. **(B-D)** Representative images displaying aberrant morphologies of *tgl2* Δ/Δ grown in DMEM containing 10% serum at 37°C for 90 min.

Under standard growth conditions and before induction of filamentation (Fig. 3.9A), *tgl2* Δ/Δ cells exhibited typical ovoid morphology. Growing cells in DMEM containing 10% serum, and at 37°C, however, I saw that *tgl2* Δ/Δ exhibited growth atypical of *C. albicans* under these conditions. As described previously, there was a significantly

heightened incidence of multiple developing hyphae (Fig. 3.8, 3.9B) with some mother cells initiating upward of 4 germ tubes within a 90 min span (Fig. 3.9B). There were also many cells that, as opposed to a commitment to hyphal development, displayed aberrant growth patterns, including elongated chains of cells with an apparent septation defect (Fig. 3.9C) and abnormally large and malformed cells with peculiar protrusions in place of hyphae (Fig. 3.9D). From these observations, I was able to determine that disruption of Tgl2 activity and TAG mobilization caused a filamentation defect in cells grown in serum, manifesting as cell cycle defects and over-commitment to filamentous growth at several sites at once.

3.2.4 *TGL2 disruption does not increase susceptibility to ROS, cell wall or azole stresses*

Having established the importance of *TGL2* in the mobilization of TAG, phospholipid regulation and filamentous growth in hyphal inducing conditions, I sought to determine whether disruption of TAG mobilization would affect the susceptibility of *C. albicans* to common stresses such as cell wall stress, peroxide stress and azole treatment. As such, growth analysis was conducted comparing wild type and *tgl2* Δ/Δ growth patterns in the presence of congo red, hydrogen peroxide (H_2O_2) and fluconazole (Fig. 3.10).

The SC5314 wild type was grown in the presence 2.5 and 5μg/mL the cell wall perturbing agent congo red (Fig. 3.10A). There was a mild perturbation of growth in the form of an extended lag phase following 5 μg/mL treatment. When *tgl2* Δ/Δ was subject to the same concentrations of Congo red, there was no significant change in growth compared to that of the wild type, indicating that deletion of *TGL2* does not alter susceptibility

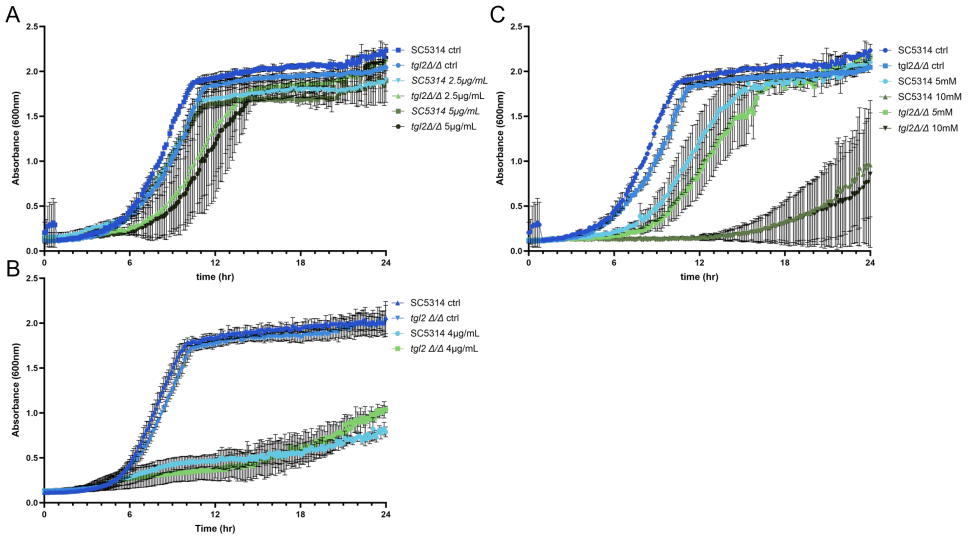

FIGURE 3.10: ***TGL2* disruption does not alter *C. albicans*' sensitivity to azole, oxidative or cell wall stresses**

Growth curves of wild-type and *tgl2* Δ/Δ, displaying 24 hr growth with and without treatment of **(A)** 2.5μg/mL and 5μg/mL congo red, **(B)** 4μg/mL fluconazole, and **(C)** 5mM and 10mM H_2O_2.

to cell wall stress.

Both SC5314 and *tgl2* Δ/Δ were treated with 4 μg/mL fluconazole (Fig. 3.10B). *tgl2* Δ/Δ displayed a growth profile comparable to that of the wild type when treated with 4 μg/mL fluconazole, suggesting no change in susceptibility to the drug in response to *TGL2* deletion (Fig. 3.10B). The same could be said for growth in 5mM and 10mM (H_2O_2) (Fig. 3.10C), where growth of the wild type and *tgl2* Δ/Δ showed no significant difference in growth. From these results, I could conclude that *TGL2* disruption, despite alterations to filamentous growth in response to serum, does not confer sensitivity to cell wall perturbing agents, reactive oxygen species (ROS) or azole stress under typical growth conditions.

3.2.5 *TGL2* deletion causes a reduction in virulence in a *G. mellonella* model

Having established a filamentation defect and abnormal growth patterns in the *TGL2* null mutant, I sought to determine the impact of our gene deletions on the virulence of *C. albicans*. 250,000 *C. albicans* cells were injected into the last left proleg of *G. mellonella* and determined rates of *Galleria* survival over the course of a week (Fig. 3.11).

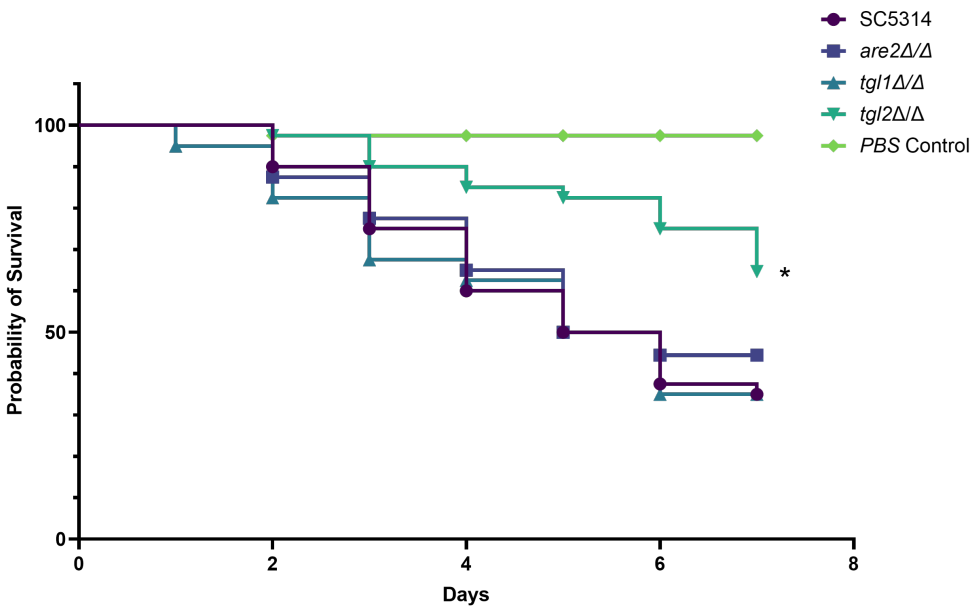

FIGURE 3.11: ***C. albicans* virulence is reduced following disruption of *TGL2***

Kaplan-Meier survival curves. *G. mellonella* larvae were infected with 2.5x10^5 cells, and the larvae scored for survival over 7 days. 20 larvae were infected per condition per biological replicate, for a total n=40. Significance was determined using a log-rank (Mantel-Cox) test, where * = $P < 0.05$, ** = $P < 0.01$

This *G. mellonella* infection assay displayed, with 250,000 cells injected, an approximate 30% population survival in wild type-infected larvae by the 7-day time point. The *tgl1* Δ/Δ and *are2* Δ/Δ survival curves were comparable to that of the wild type, with *ARE2* and *TGL1* disruption having no apparent impact on the overall virulence of *C.*

albicans. *tgl2* Δ/Δ, led to a significant reduction in virulence, with 60% of assayed larvae surviving, however, the deletion mutant was not avirulent. From this, I was able to conclude that TAG mobilization through the action of Tgl2 is important for infection and adaptation in vivo, but that *C. albicans* is still capable of infection with disrupted TAG mobilization.

3.2.6 *TGL2* deletion reduces chronological lifespan of *C. albicans*

Lipid droplets, in large part, are a cell's means for storage of excess fatty acids to fuel growth and to adapt to stresses. With *TGL2* showing triacylglycerol lipase activity and a role in lipid droplet catabolism, I sought to establish whether deletion of *TGL2* has an impact on the chronological lifespan of *C. albicans*, where chronological lifespan is the survival of yeast having reached maximum density and cell division has halted. Strains were seeded to the same cell density in YPD, and grown over a week (Fig. 3.12). Population survival was assessed with propidium iodide staining and flow cytometry analysis.

Over 1 week, having exhausted available resources in the media, the SC5314 wild type displayed almost no propidium iodide staining of the population, suggesting no necrotic cells within the population (Fig.3.12). In contrast, the *tgl2* Δ/Δ mutant showed a gradual increase in propidium iodide staining over the week, with day 7 showing a significantly higher necrotic population when compared to that of the wild type. As such, I was able to conclude that the *TGL2* null deletion, and the reduction in TAG mobilisation, caused a drop in the chronological lifespan of *C. albicans*.

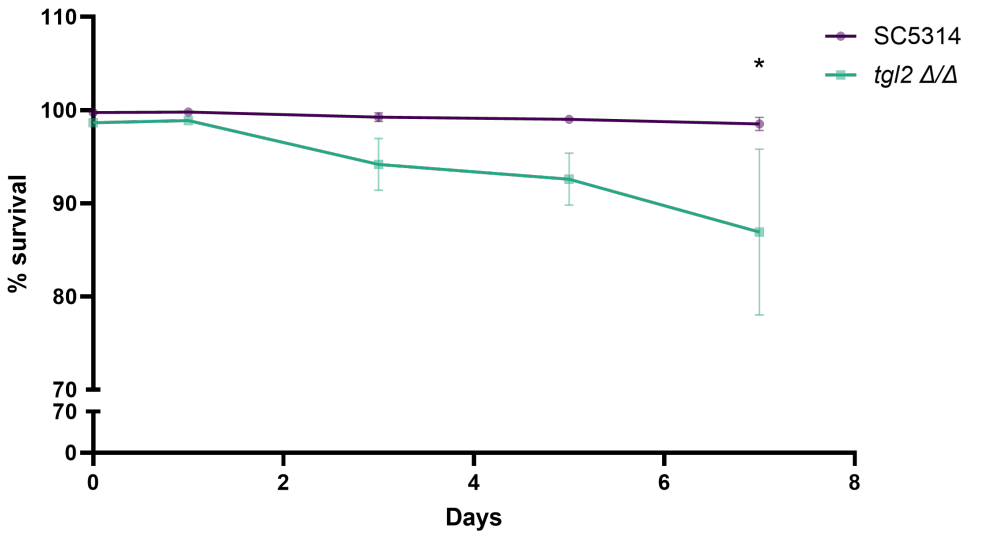

FIGURE 3.12: ***TGL2* disruption reduces chronological lifespan of *C. albicans***

Line graph displaying % survival over a week. Cells were seeded to OD_{600} 0.1 and grown at 30°C, and analyzed with flow cytometry on days 0, 1, 3, 5 and 7. At least 20,000 singlet cells were analyzed per day per condition, in biological duplicate. Unpaired multiple t-tests were used to compare statistical significance, with Holm-Šídák correction for multiple comparisons. * = $P \leq 0.05$ for indicated day.

3.3 DISCUSSION

In yeast, as well as in higher eukaryotes, lipid droplets contribute to homeostasis of phospholipids, sterols and excess fatty acids by reversible storage as the neutral lipids TAG and SE, providing cells with building blocks for membrane biosynthesis upon resumption of growth [352]. Lipid droplet biogenesis and catabolism have been well documented in *S. cerevisiae* [195, 353, 279, 280], and their direct and indirect impact on cell signalling and stress response mechanisms is an emerging area of study [296]. Thus far, however, little work has explored lipid droplet regulation, and the link between lipid droplets and virulence of *C. albicans*. This study sought to use CRISPR Cas9 gene editing to develop a library of mutants lacking genes involved in neutral lipid storage, neutral lipid catabolism, and de novo phospholipid biosynthesis (Table 3.1). Whilst the study began

as a documentation of the impact of all of these deletions on virulence traits and fitness of *C. albicans*, the study gradually focused on the putative triacylglycerol lipase Tgl2. In *S. cerevisiae*, fatty acid storage and generation of TAGs protects cells from lipotoxicity [347, 186, 187] and allows for fine-tuned metabolic and transcriptional control of de novo phospholipid biosynthesis [197]. In deleting *SMP2* and *LRO1*, I sought to disrupt the generation of DAG and TAG neutral lipid classes, respectively. In *S. cerevisiae*,*LRO1* is one of two DAG acyltransferases. Our HPTLC analysis revealed a shared functionality in *C. albicans*, with a homozygous null mutation causing a reduction in TAG concentration and elevated free fatty acids when compared to the wild type (Fig. 3.3A). The role of *LRO1* in *C. albicans* virulence is further explored in chapter 5. In *S. cerevisiae*, ScPah1p exhibits phosphatidate phosphatase activity that dephosphorylates PA into DAG classes [204]. The *C. albicans* orthologue is *SMP2*, a putative phosphatidate phosphatase. To our knowledge, there are no studies to date into *SMP2* function, save for its transcript being highlighted as under regulation by transcription factor Nrg1 [354]. A heterozygous null disruption of *SMP2* was sufficient to reduce intracellular TAG compared to the wild type (Fig. 3.3A), providing evidence to suggest that CaSmp2p fulfils a similar role to ScPah1p. *Smp2* Δ also caused wrinkly colony morphology when grown on spider medium (Fig. 3.6). Wrinkly colony morphology has been associated with growth in a carbon poor environment, a starvation response [351]; the wrinkled colony morphology in an *SMP2/smp2* heterozygote could imply a reduced capacity for utilisation of the mannitol carbon source in spider medium, or perhaps inappropriate activation of nutrient starvation responses. The inability to generate a homozygous null deletion for *SMP2* could potentially hint at it being essential for survival, though *S. cerevisae Pah1* Δ mutants are capable of survival [214, 204]. Owing to the lack of a homozygous null mutant, *Smp2* Δ was omitted from further analysis, though would prove

an interesting point of study in further works.

In *S. cerevisiae*, the *TGL* gene family controls catabolism of TAGs [279, 280] and SEs [355, 356]. ScTgl1p and ScTgl4p are partially redundant sterol ester hydrolases [280], responsible for catabolism of sterol esters into sterols. Control of this process contributes to control of plasma membrane fluidity [257]. *S. cerevisae TGL1* has a potential, uncharacterized orthologue in *C. albicans*. Our disruption of *TGL1* in this study led to a significant reduction in intracellular sterol content compared to the wild type (Fig. 3.4A), suggesting a conserved sterol ester hydrolase functionality for *TGL1* in *C. albicans*. However, there were no alterations to sterol ester concentrations as I might have expected following an inability to mobilize SEs; further study would be required to better understand control of sterol mobilization in *C. albicans*.

To date, there are only 2 described members of the *TGL* family in *C. albicans*; *TGL1* (as above), and *TGL2*, whose *S. cerevisiae* orthologue exhibits triacylglycerol lipase activity. In disrupting *TGL2*, I saw increased intracellular TAG (Fig. 3.4A) and elevated number of lipid droplets (Fig. 3.5G) synonymous with an inability to break down TAG, as well as increases in PC, PI, PE and CL phospholipids. The elevated phospholipids could be the result of an inherent increase in cell size; lipid extractions were performed on cell cultures normalised by OD_{600}, as opposed to cell number. It could be, then, that as *tgl2* Δ/Δ cells were inherently larger than the wild type, phospholipid concentration was inherently skewed. A more appropriate means of normalisation, should the experiment be repeated, would be to account for cell size whilst normalising and extract from exact, known cell numbers.

TGL2 disruption led to an array of defects within *C. albicans*. Whilst exhibiting typical growth patterns in standard growth conditions, I first noted a lack of filamentation when grown on spider medium (Fig. 3.7), for which there could be a few causes. Spider

medium mimics a more nutritionally deplete environment than YPD, with mannitol as an alternate carbon source and a neutral pH. *C. albicans* filamentation can be attributed to activation and crosstalk of several signalling pathways, including: Ras-cAMP-PKA mediated activation in response to serum, co_2, sugars and N-acetylglucosamine, activating transcription factor Efg1 [21]; nutrient scarcity triggering derepression of transcription factor Brg1 [357]; Cek1-mediated activation of transcription factor Cph1 is resultant from cell wall damage, as well as crosstalk from Ras1 [358]; Rim101 signalling, largely attributed to pH sensing [77] but with links as a lipotoxicity sensor in *S. cerevisiae*, activating Efg1 and downstream hypha-associated genes. Inability to filament on spider medium could be the result of the disruption of a combination of these processes. Deletion of the gene *UME6*, coding for a hyphal associated transcription factor, causes a similar non-filamentous colony morphology on spider medium [359], as well as a slowed hyphal elongation in response to serum and morphological defects somewhat similar to those I have seen in liquid medium (Fig. 3.9). Ume6 is activated by Efg1 and Brg1. As such, the lack of filamentation on spider medium and filamentation defect in serum could be due to aberrant Ras1 or Rim101 signalling impacting the regulation of Ume6. Ras1, alongside activation of downstream effectors leading to Efg1 control, has been linked to Cdc42 activation and control of polarized growth [69]. Indeed, the target of Cdc42 Bni1 has roles in polarisome function that drive actin assembly at sites of polarized growth. A *bni1* Δ/Δ mutant causes filamentation defects on spider medium and serum comparable to those seen in the *tgl2* Δ/Δ, as well as formation of multiple hyphae in liquid medium containing serum [360]. The mechanism through which *tgl2* Δ/Δ would cause a loss of control of polarized growth following Ras1 activation (serum, mannitol, CO_2) remains unclear. One possibility, not explored within the scope of this study, is that *tgl2* Δ/Δ and sequestration of resources of TAG impacts upon sphingolipid

biosynthetic pathways, as has been documented in *S. cerevisiae* [356]. Sphingolipid and ergosterol enrichment are important in the generation of lipid raft microdomains in cell membranes [361]. These microdomains have been associated with the maintenance of polarised growth in *S. cerevisae* [362], and there is some evidence to suggest that they play a role in appropriate signalling for lipid-anchored proteins [363].

I saw a significant attenuation of virulence in the *tgl2* Δ/Δ, as well as a reduced chronological lifespan; these could be owing to an inability to adapt as capably to shifting environments, unable to catabolize TAG for de novo phospholipid biosynthesis [321]. Attenuated virulence could also, of course, be owing to dysfunctional hyphal development necessary for *C. albicans* virulence [64]. Given that of the *TGL* genes deleted, only *TGL2* disruption caused attenuation of virulence in *G. mellonella*, this likely highlights an important role in tight control of DAG and TAG in the virulence of *C. albicans.*

Chapter 4

Triacylglycerol storage in C. albicans, and potential links to virulence

4.1 INTRODUCTION

The opportunistic fungal pathogen *C. albicans* exists, for the most part, in a state of commensalism within several niches in a human host, including oral [3], vulvovaginal [364] and gastrointestinal tracts [4], though can take advantage of changes in environment to cause superficial and widespread, systemic infections [365]. Its success as an opportunist can be attributed, in large part, to its versatility and ability to adapt to different environments. For example, *C. albicans* exhibits genomic plasticity, able to execute chromosomal rearrangements to promote drug tolerance [366, 367]. *C. albicans* can also undergo a hyphal switch in response to environmental cues including elevated CO_2, serum, and changes in pH [368, 32, 53, 369]. This versatility in morphology allows for the establishment of robust and difficult-to-treat biofilms [56] and tissue penetration during systemic infection [370].

C. albicans can avoid detection and clearing using several strategies; it is capable of nullifying opsonophagocytosis by recruiting host factors [364], and avoid detection by the host immune system through modulation of cell wall components [161, 371]. β-1,3-glucans are a pathogen-associated molecular pattern (PAMP) readily detected by dectin-1 receptors expressed by macrophages, but *C. albicans* can fine-tune exposure or shielding of this PAMP by "masking" it behind the outer cell wall, comprised of a mannan brush [141]. "Unmasked" cells are more susceptible to phagocytic uptake, and indeed, mutations that affect cell wall remodelling impact upon phagocytic uptake [372].

Successful persistence in a human host is reliant on the fine-tuned utilization of available resources, for which *C. albicans* has excellent adaptive scavenging mechanisms that allow recovery of iron from the host, and from microbes through a siderophore uptake

mechanism([365, 56], as well as zinc scavenging through the action of Pra1 [373]. *C. albicans* also expresses several secreted phospholipases to help acquire lipid building blocks for growth and invasion of host cells [374]. Storage of such lipids during times of plenty for use during times of necessity is a conserved process throughout eukaryotes, typically in lipid droplets.

Lipid droplets are a transient organelle that acts to store excess sterols and fatty acids in a non-toxic neutral lipid [347]. Lipid droplets comprise a neutral lipid core of triacylglycerides (TAG) and sterol esters (SE), encapsulated in a protein-studded phospholipid monolayer [375, 347]. Lipid droplets develop within the envelope of the endoplasmic reticulum (ER), under the control of diacylglycerol(DAG): acyltransferases for TAG generation, and acyl-CoA:sterol acyltransferases for SE generation. These processes have yet to be fully characterized in *C. albicans*, though insight can be gleaned from research into the yeast *S. cerevisiae*. In *S. cerevisiae*, terminal lipid droplet formation is controlled by 4 proteins; the DAG:acyltransferases dga1p and lro1p, and the sterol:acyltransferases are1p and are2p [376, 245, 353, 377]. The TAG precursor, DAG, itself is thought to contribute to cell wall integrity (CWI) signalling, owing to a high affinity to the protein kinase Pkc1 [225, 241]. In *C. albicans*, the heterozygous null *LRO1/lro1* displays a reduction in virulence in a *Caenorhabditis elegans* model [330]. Lipid droplets act to support lipid flux and phospholipid metabolism [356, 378]. TAG breakdown, either through autophagy of lipid droplets [186] or through the action of members of the tgl family [350], TAG lipases allow reversible conversion of TAGs into DAG and phosphatidic acid (PA) to be funnelled into de novo and Kennedy pathways for phospholipid biosynthesis. Briefly, PA supports synthesis of all important phospholipid (PL) classes; phosphatidylserine (PS) synthase generates PS, which in turn may be fed into phosphatidylethanolamine (PE) through the action of PS decarboxylases (psd1

and psd2), which can lastly be converted into phosphatidylcholine (PC) through PE methyltransferases [321, 213, 379]. A careful balance of each of these PLs contributes to cellular function; PC makes up a considerable portion of membrane phospholipids [380], PE acts as an ethanolamine donor in glycerophospholipid inositol (GPI) anchor biosynthesis [322, 381], and PS has been linked to signal transduction and several signalling processes including the mitogen-activated protein kinase (MAPK) cell wall integrity (CWI) and cell wall remodelling pathways [225, 161].

The Kennedy pathway makes up another pathway for PC biosynthesis from ATP, CTP and choline [356, 378, 328], and *C. albicans* expresses transporters for the acquisition of choline from the host. However, reliance on the Kennedy pathway has been posited to not be sufficient to sustain an adaptable and virulent *C. albicans* [321].

This work sought to build upon the understanding of TAG storage in *C. albicans*, as well as determine the impact of disruption of TAG storage on traits linked to the success of *C. albicans* as an opportunistic fungal pathogen. I observed loss of TAG storage upon deletion of the putative DAG: acyltransferase genes *DGA2* and *LRO1*. The inability to store TAG in lipid droplets led to a reduction in PS and PC content and elevated DAG and FFA levels. The reduced ability to regulate lipid homeostasis reduced filamentation and led to a marked increase in susceptibility to fluconazole that was accompanied by decreased peroxisomal function and a reduced capacity for ergosterol biosynthesis. TAG storage mutants displayed a thinner mannan layer and unmasked β-1,3-glucans, which increased detection and phagocytosis by macrophages. TAG-depleted cells were also impaired in virulence in a *G. mellonella* infection model. Overall, our data highlight the importance of TAG storage for C. albicans cells to adapt and elicit key virulence traits.

4.2 RESULTS

4.2.1 Deletion of the diacylglycerol acyltransferases *DGA2* and *LRO1* alters the lipid profile of *C. albicans*

Storage of excess FFAs in the form of triacylglycerols and sterol esters is highly conserved in eukaryotes, with the biogenesis of lipid droplets by diacylglycerol acyltransferases and sterol acyltransferases being key. Although the functionality of their *S. cerevisiae* orthologues has been well characterized, the *C. albicans* orthologues have yet to be verified. I therefore sought to determine the impact that loss of *LRO1* and *DGA2* would have in *C. albicans*; .

Homozygous null mutants of both *LRO1* and *DGA2* and a double mutant *dga2/lro1* Δ/Δ were generated in the SN250 background using CRISPR Cas9 (Fig. A.1, and the effects on lipid droplet formation and lipid profiles were determined (Fig. 4.1, Fig. B.1).

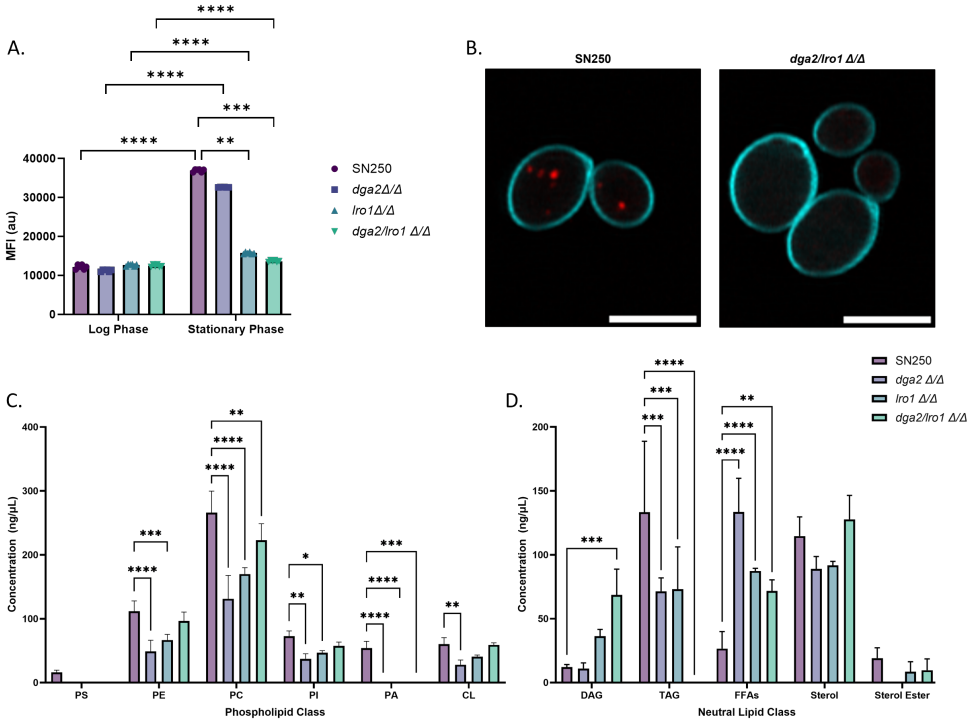

FIGURE 4.1: **Deletion of *DGA2* and *LRO1* reduces neutral lipid content and alters intracellular lipid profiles**

(A) Flow cytometry analysis of neutral lipids during log and stationary phases of growth. Neutral lipids within cells were stained with BODIPY 493/503 and the median fluorescence intensity (MFI) analysed through flow cytometry. At least 20,000 singlet cells were analysed for a total of 6 repeats; a 2-way ANOVA with Tukey's multiple comparisons test determined significance, where * = $P < 0.05$, ** = $P < 0.01$, *** = $P < 0.001$, and **** = $P < 0.0001$. **(B)** Representative images of BODIPY-stained SN250 and *dga2/lro1* Δ/Δ cells. Cells were stained with BODIPY 493/503 (in red) to observe neutral lipids, and calcofluor white (CFW) to stain the cell wall (in cyan) Scale bars denote 5μm. **(C-D)** HPTLC lipid profiling of wild type and lipid storage mutants at stationary phase. Lipids were harvested from stationary phase cells, resolved and compared to phospholipid (C) and neutral lipid (D) standards. **(C)** Resolved phosphatidylcholine (PC), phosphatidic acid (PA), phosphatidylinositol (PI) and cardiolipin (CL) were stained with primuline to allow for quantification; phosphatidylethanolamine (PE) and phosphatidylserine (PS) require additional staining detection with ninhydrin. Lipids were quantified as described in methods. Data represents 3 biological replicates, save for an omission of an outlier for *dga2/lro1* Δ/Δ. **(D)** Neutral lipids diacylglycerol (DAG), triacylglycerol (TAG), sterol esters (SE), sterols and free fatty acids (FFAs) were analysed as described above, all stained with primuline and compared to standards. For both (C-D), significance was determined with a 2-way ANOVA and Dunnett's multiple comparisons test, where * = $P < 0.05$, ** = $P < 0.01$, *** = $P < 0.001$, and **** = $P < 0.0001$.

Log and stationary phase cells were stained with the neutral lipid stain BODIPY 493/503 (Fig. 4.1A). In wild-type cells, I observed a median fluorescence intensity (MFI) of ~12,000 during log-phase, with a significantly increased MFI for staining of stationary phase cells. This pattern reflects the use of neutral lipids during growth and storage within droplets as cells enter a quiescent state. *DGA2* and *LRO1* single knockouts, as well as *dga2/lro1*Δ/Δ, had MFIs comparable to that of the wild type during log phase. During stationary phase, deletion of *LRO1* alone was sufficient to yield a median fluorescence intensity (MFI) of ~43% of that of the wild type, indicative of a significant reduction in neutral lipid staining; *dga2/lro1* Δ/Δ showed a ~63% reduction in MFI compared to that of the wild type, with deletion of *DGA2* not significantly reducing MFI. In line with what I expected, a *dga2/lro1* Δ/Δ diacylglycerol acyltransferase mutation was sufficient to eliminate most lipid droplet foci in *C. albicans* (Fig. 4.1B).

To further corroborate BODIPY staining and gain insight into the impact of TAG storage disruption on the lipidome of *C. albicans*, I performed whole cell lipid extractions and resolved them with high performance thin-layer chromatography (HPTLC) (Fig. 4.1C). Resolving for phospholipids, There was a loss of detectable phosphatidic acid (PA) upon deletion of either *DGA2* or *LRO1* when compared to the wild type, as well as a significant reduction in phosphatidylcholine (PC) in *dga2* Δ/Δ, *lro1*Δ/Δ and *dga2/lro1* Δ/Δ. Curiously, Phosphatidylethanolamine (PE) levels were significantly decreased in the single knockouts only, and both phosphatidylinositol (PI) and the mitochondrial glycerophospholipid cardiolipin (CL), were significantly decreased in *dga2* Δ/Δ only compared to the wild type.

Resolving for neutral lipids, I was able to confirm a reduction in triacylglycerol in the *dga2*Δ/Δ and *lro1*Δ/Δ (107.2μg/mL and 73.2μg/mL respectively compared to

133.2μg/mL in the wild type), with a complete ablation in the *dga2/lro1*Δ/Δ double knockout. Alongside this, I saw elevated levels of free fatty acids (FFAs) in single and double knockouts, and significantly increased diacylglycerol (DAG), the triacylglycerol precursor, in the *dga2/lro1*Δ/Δ double knockout. The sterol and sterol ester profile of single and double knockouts remained comparable to those of the wild type in both single and double knockouts. These findings are synonymous with an inability to store excess fatty acids as TAG. The necessity for a deletion of both DAG-acyltransferases to eliminate TAG species would suggest conserved functionality of these proteins to their *Saccharomyces cerevisiae* orthologues (*dga1p* and *lro1p*).

These results, taken with the phospholipid lipid profiles *DGA2* and *LRO1* null mutants, confirm a role of Dga2 and Lro1 as DAG-acyltransferases, and highlight the necessity for neutral lipid storage for lipid homeostasis and phospholipid biosynthesis.

4.2.2 Insufficient neutral lipid storage reduces *C. albicans* capacity for filamentation

Having confirmed the role of *DGA2* and *LRO1* for TAG storage in *C. albicans*, I sought to investigate the effects on key virulence traits, starting with the yeast-to-hyphal switch. Wild type and *dga2/lro1*Δ/Δ cells were inoculated into hyphal-inducing media (DMEM containing 10% serum), and were grown statically for 90 min in both normal air and 5% CO_2 (Fig. 4.2), and subsequently stained with calcofluor white (CFW).

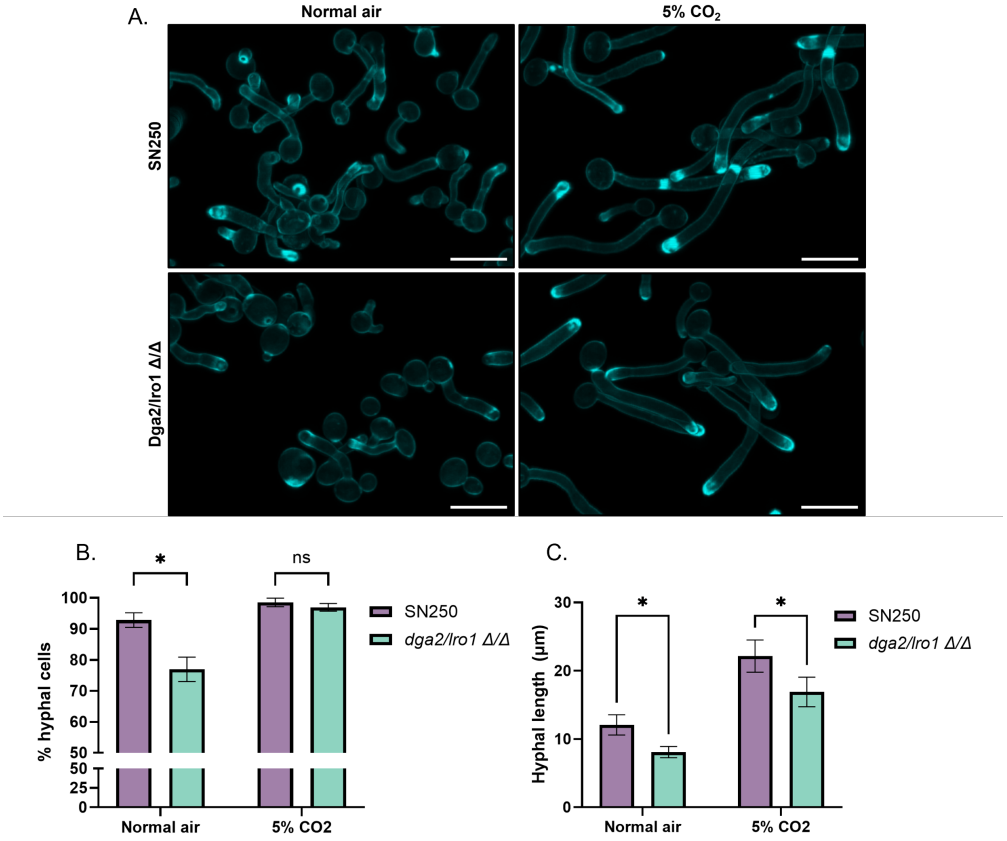

FIGURE 4.2: **Disruption of neutral lipid storage hinders *C. albicans* filamentation**

(A) Confocal imaging of filamenting cells in ambient air and 5% CO_2. Cells were grown in DMEM containing 10% serum for 90 min prior to staining with CFW and imaging. Scale bars denote 10μm. **(B)** Bar chart showing percentage of mother cells committing to hyphal induction after 90 min in DMEM containing 10% serum in either normal air or 5% CO_2. Cells imaged in (A) were scored as either having 0 discernible germ tubes or 1 or more. 250 cells were scored per condition per biological replicate, for a total of 750 cells scored per condition. **(C)** Bar chart showing average hyphal length of filamenting cells in wild type compared to *dga2/lro1* Δ/Δ. Cells with a discernible germ tube were manually measured from the base of the hyphae to the tip in ImageJ; 250 cells were measured per condition per biological replicate, for a total of 750 hyphae measured per condition. For both (B-C), multiple unpaired Holm-*Šídák* t-tests were conducted using the where * = P $\leq$ 0.05

I observed a reduction in filament length between wild type *dga2/lro1*Δ/Δ cells in both normal air and 5% CO_2 at the 90 min time-point (Fig. 4.2A). To corroborate, a total of 750 cells per condition were scored, firstly, on their commitment to filamentation (Fig. 4.2B), and secondly, the length of individual hypha (Fig. 4.2C). As shown in (Fig. 4.2B), under normal air conditions, almost 93% of wild type cells had committed to hyphal growth, whilst only 77% of *dga2/lro1*Δ/Δ cells analyzed had distinguishable hyphae. The difference in hyphal induction was absent in 5% CO_2 conditions, with almost all wild type and *dga2/lro1*Δ/Δ cells displaying hyphae. Measuring hyphal lengths revealed significantly smaller hyphae in both normal air and 5% CO_2 (Fig. 4.2C). These findings suggest a role for TAG storage in lipid droplets in both the yeast-hyphal switch and in hyphal elongation.

4.2.3 Analysis of the effects of loss of TAG storage on the *C. albicans* transcriptome

Having established a filamentation defect as a result of *DGA2* and *LRO1* deletion, I sought to investigate the impact that insufficient TAG storage would have on *C. albicans*' transcriptional profile under normal growth conditions. mRNA was extracted from wild type and *dga2/lro1*Δ/Δ cells during the log phase of growth, and subject to downstream analysis (Fig. 4.3).

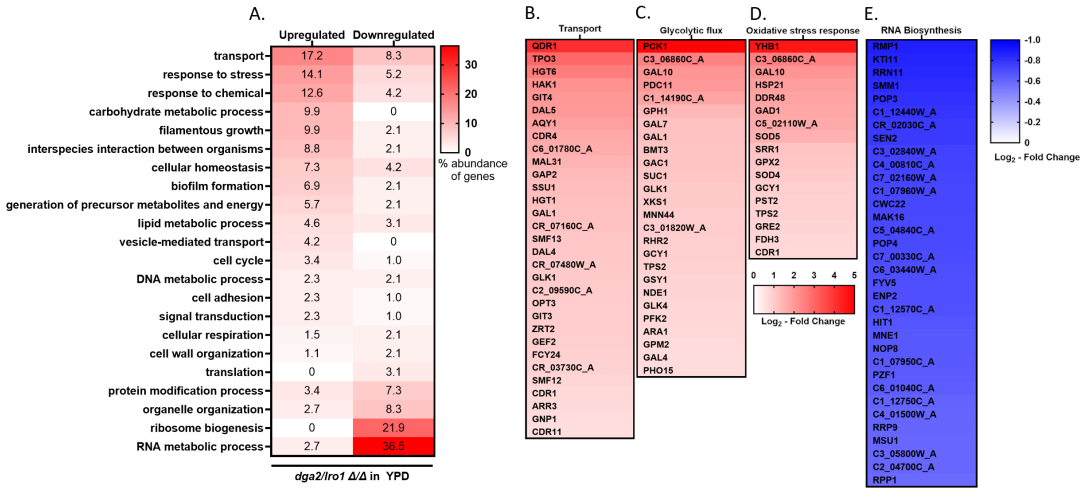

FIGURE 4.3: **Deleting *DGA2* and *LRO1* alters the transcriptional profile of C. albicans**

(A) Heat map depicting GOSlim mapping of processes up and down regulated in *dga2/lro1*Δ/Δ cells under standard growth conditions, % abundance indicating how many genes (subject to an adjusted p-value cutoff of 0.05, and a fold-change of at least 1.5x) appeared in each term relative to the total number of genes up/down regulated (up, 262 genes; down, 96 genes) **(B-D)** Genes involved in selected GO terms ((**B**), transport; **(C)**, carbon metabolism; **(D)**, oxidative stress; **(E)**, RNA Biosynthesis), where $p \leq 0.1$.

There was an enrichment of carbohydrate processing terms in *dga2/lro1*Δ/Δ cells when compared to wild type(Fig 4.3A); Genes in affiliated GO terms were linked to control of glycolysis (*GAL4*, L_2-FC 0.68; *GPM2*, L_2-FC 0.69; *PFK2*, L_2-FC 0.77;*GLK4*, L_2-FC 0.78; *GLK1*, L_2-FC 1.03), pyruvate regulation (*PCK1*, L_2-FC 4.9; *PDC11*, L_2-FC 2; *GPH1*, L_2-FC 1.39) and utilization of galactose (*GAL10*, L_2-FC 2.10; *GAL7*, L_2-FC 2; *GAL1*, L_2-FC 1.19) (Fig. 4.3C).

Also enriched in *dga2/lro1*Δ/Δ were transmembrane transport processes (Fig. 4.3A), including transporters involved in drug transport (*QDR1*, L_2-FC 4.08; *CDR4*, L_2-FC 1.67; *CDR1*, L_2-FC 0.74; *CDR11*, L_2-FC 0.65), sugar transport (*HGT6*, L_2-FC 2.55; *MAL31*, L_2-FC 1.46; *HGT1*, L_2-FC 1.25), metal ion transport (*HAK1*, L_2-FC 2.14; *C6_01780C_A*, L_2-FC 1.62; *SMF13*, L_2-FC 1.09; *C2_09590C_A*, L_2-FC 1; *ZRT2*, L_2-FC 0.96; *GEF2*, L_2-FC 0.96; *SMF12*, L_2-FC 0.81) and choline acquisition (*GIT4*, L_2-FC 2.02; *GIT3*, L_2-FC 0.97) (Fig. 4.3B). This upregulation of glycerophosphocholine uptake, alongside acetyl-CoA synthesis from glucose sources and the upregulation of *PLB1* (L_2-FC 2.92)(appendix C), led us to hypothesise an upregulation of processes necessary for phospholipid biosynthesis through the TAG-independent Kennedy pathway.

Transcripts linked to stress response mechanisms were also elevated in *dga2/lro1*Δ/Δ cells (Fig 4.3A), with a focus on oxidative stress (*SOD5*, L_2-FC 1.53; *SOD4*, L_2-FC 1.03; *PST2*, L_2-FC 0.89) (Fig. 4.3D) and the drug transporter *CDR1* (L_2-FC 0.74). Also of note was the Ras-PKA-regulated biofilm-linked transcription factor *BRG1* (L_2-FC 3.32), as well as *RAS2* (L_2-FC 2.72). Lastly, there was a downregulation of genes relating to RNA metabolism and ribosomal biosynthesis (Fig 4.3A,E). These results, taken in tandem, may indicate that a scarcity of resources for de novo phospholipid metabolism through TAG utilization has a significant impact on cells grown in nutrient-replete media in log phase.

4.2.4 Reduced neutral lipid storage increases *C. albicans*' susceptibility to fluconazole

Azoles target the synthesis of ergosterol. I therefore sought to ascertain the impact of *DGA2* and *LRO1* deletion on susceptibility and response to fluconazole exposure. Wild type, *dga2* Δ/Δ, *lro1*Δ/Δ and *dga2/lro1* Δ/Δ were grown in the presence and absence of 2μg/mL fluconazole in RPMI at 37°C (Fig. 4.2A-B).

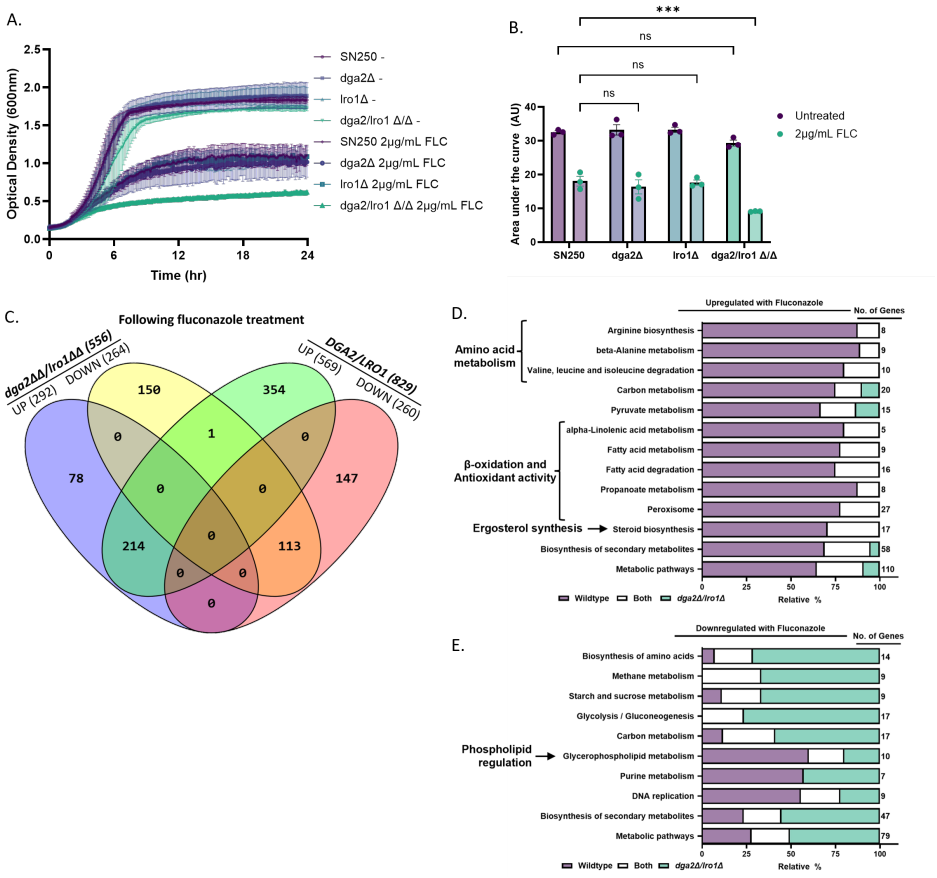

FIGURE 4.4: **Disruption of neutral lipid storage increases cell sensitivity to fluconazole**

(A) Growth curve data of wild type and lipid knockouts grown in RPMI and treated with 2μg/mL fluconazole. Cells were seeded to an OD_{600} of 0.1 in a microtitre plate and grown at 37°C for 24h. 9 technical repeats were conducted across 3 biological replicates. **(B)** area under the curve analysis of growth curves from (A). Statistical significance was determined with a 2-way ANOVA, Tukey's multiple comparisons test where **** = $P < 0.0001$. **(C-E)** Transcriptional profiling of wild type and lipid knockouts following fluconazole treatment. **(C)** Venn diagram showing genes differentially expressed by the *DGA2/LRO1* wild type (increased, green; decreased, red) and the *dga2/lro1* Δ/Δ double knockout (increased, blue; decreased, yellow) where fold change in expression was at least 1.5x higher than the untreated condition. **(D-E)** Stacked bar graph displaying KEGG pathways linked to genes upregulated (D) and downregulated (E) in response to fluconazole, including a wild-type specific response (purple bar), shared response (white bar) and *dga2/lro1* Δ/Δ specific response. Bars are indicative of relative percentage of genes affiliated with each KEGG pathway attributed to each genotype, with the total number of genes associated with the pathway displayed to the right. Not all KEGG pathway hits have been shown; KEGG enrichment over-representation analysis was conducted as described in methods, and only pathways with an adjusted p-value of ≥ 0.05 have been shown.

Area under the curve data (AUC) (Fig. 4.4B) revealed a significantly increased sensitivity to fluconazole in the *dga2/lro1* Δ/Δ double knockout. Curiously, neither a *DGA2* nor a *LRO1* single deletion led to sensitivity. The SE component of a lipid droplet's neutral lipid core helps to maintain sterol homeostasis, and thus, plays a key role in ergosterol regulation. To further elaborate upon the mechanism by which capacity for TAG storage impacts fluconazole sensitivity, mRNA was isolated from actively growing wild type and *dga2/lro1* Δ/Δ cells with and without a 90 min fluconazole treatment (Fig. 4.4-4.6 and appendices D-E) comparing genes that were at least 1.5x differentially expressed. There were shared genes that were up and downregulated upon fluconazole treatment in both wild type and *dga2/lro1* Δ/Δ cells (214, up; 113, down) (Fig. 4.4C). Amongst these was the transcription factor *UPC2*, known to contribute to regulation of ergosterol biosynthesis (wild type, Log_2 FC 1.47;*dga2/lro1* Δ/Δ, L_2-FC 0.59), and the phosphatidylserine synthase *CHO1* (wild type, L_2-FC 1.45; *dga2/lro1* Δ/Δ, L_2-FC 1.36) coupled with a wild type exclusive up-regulation of the transcription factor *INO4* (L_2-FC 0.63) (appendix D. These highlight the importance for tight phospholipid regulation in response to fluconazole stress.

Processes differentially expressed following fluconazole treatment, both shared and unique to either wild type or *dga2/lro1* Δ/Δ, were further distinguished through KEGG mapping and enrichment analysis (Fig. 4.4D-E). Comparing upregulated wild type processes to those of the *dga2/lro1* Δ/Δ (Fig. 4.4D), one standout is steroid biosynthesis; 30% of the 17 genes were significantly upregulated in both wild type and *dga2/lro1* Δ/Δ strains (*ERG6, ERG251, ERG1, ERG2* and *ERG25*), but the other 70% were significantly upregulated exclusively in the wild type (Fig. 4.4D, Fig. 4.5A). KEGG mapping these genes (Fig. 4.5B) highlighted an upregulated compensatory ergosterol biosynthesis

mechanism in the wild type when treated with fluconazole, and this response is largely absent or diminished with reduced transcripts for genes affiliated sterol biosynthesis in the *dga2/lro1* Δ/Δ strain.

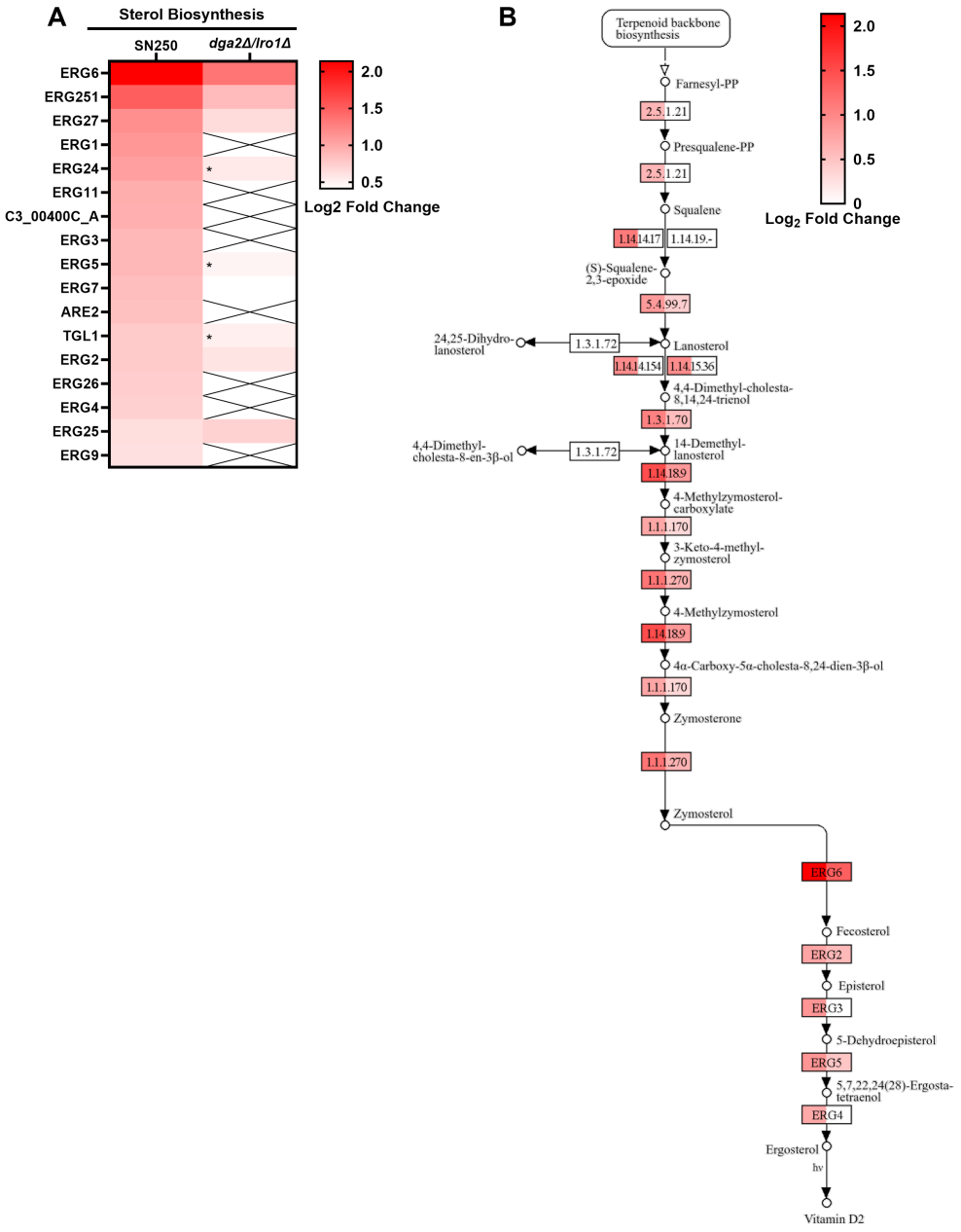

FIGURE 4.5: **Sterol biosynthesis in response to fluconazole**
(A) heat map of genes involved in sterol biosynthesis that are upregulated following fluconazole treatment, ranked by Log_2 Fold-change compared to the untreated condition. Genes below the adjusted p-value cutoff of 0.05 are depicted by a cross through the box, while a star denotes a gene below the 1.5x fold-change cutoff. **(B)** Kegg map depicting ergosterol biosynthetic process, overlaying Log_2 Fold-changes compared to the untreated condition. Left side of coloured genes are the wild type response, whilst the right side of coloured genes is the *dga2/lro1* Δ/Δ response.

Another prominent cluster of enriched KEGG pathways highlighted an upregulation of genes associated with peroxisomal assembly and β-oxidation and H_2O_2 detoxification, though for each of these processes, the majority of affiliated genes were uniquely upregulated in the wild type (peroxisome, 77.8% of genes, fatty acid degradation, 75% of genes)((Fig. 4.4D). Notably, the carnitine acetyltransferases *CTN1* and *CAT2* were strongly upregulated in both (CTN1: wild type, $\log_2$ FC 4.77 and *dga2/lro1* Δ/Δ L_2 FC 2.12; CAT2: L_2 FC 1.39 and *dga2/lro1* Δ/Δ L_2 FC 0.59) whilst CTN3 was exclusively upregulated by the wild type (L_2 FC 4.94); the catalase *CAT1*, commonly seen upregulated following fluconazole treatment and a hallmark of oxidative stress response, is upregulated in the wild type (L_2 FC 1.10), but not in *dga2/lro1* Δ/Δ (Fig. 4.6A). Mapping genes from (Fig. 4.6A) to KEGG pathways (Fig. 4.6B) revealed an emphasis on peroxisomal biogenesis, as well as trafficking of material into peroxisomes for degradation.

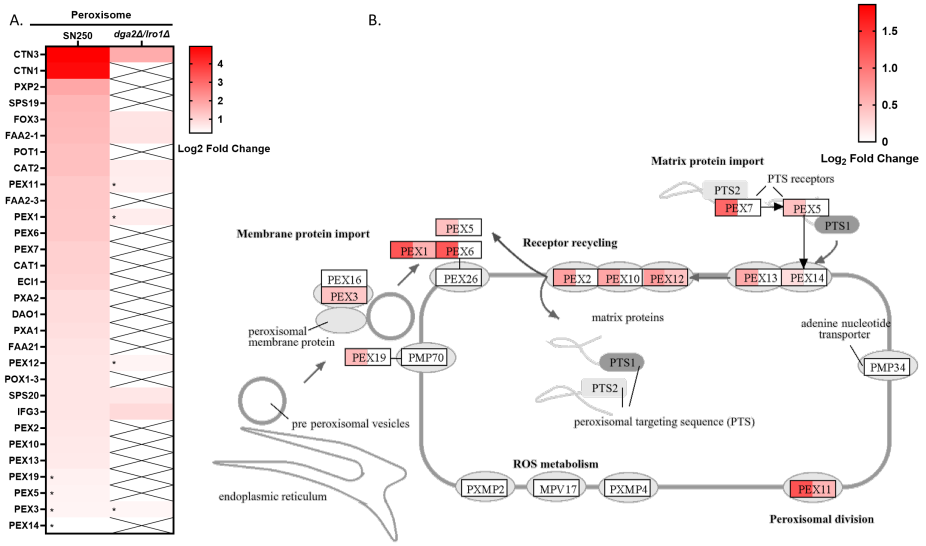

FIGURE 4.6: **Peroxisomal biogenesis in response to fluconazole**
(A) heat map of genes involved in peroxisomal that are upregulated following fluconazole treatment, ranked by Log_2 Fold-change compared to the untreated condition. Genes below the adjusted p-value cutoff of 0.05 are depicted by a cross through the box, while a star denotes a gene below the 1.5x fold-change cutoff. **(B)** Kegg map depicting peroxisomal biogenesis and function, overlaying Log_2 Fold-changes compared to the untreated condition. Left side of coloured genes are the wild type response, whilst the right side of coloured genes is the *dga2/lro1* Δ/Δ response.

I compared downregulated wild type and *dga2/lro1* Δ/Δ responses to fluconazole through similar means (Fig. 4.4E). This highlighted downregulation of genes linked to glycerophospholipid metabolism predominantly within the wild type (*OPI3*, L_2 FC -0.6; *GDE1*, -0.61; *C2_00790C_A*, L_2 FC -0.7), a repression of which suggests a repression of PC and PE, but not PS, biosynthesis. A process more prominently downregulated in fluconazole in *dga2/lro1* Δ/Δ, curiously, was glycolysis/gluconeogenesis and acetic acid production (Fig. 4.4E).

4.2.5 Deletion of *DGA2* and *LRO1* leads to cell wall defects and inappropriate phosphorylation of the cell wall integrity linked MAPK Mkc1

I sought to determine whether deletion of *DGA2* and *LRO1* impacted upon cell wall integrity. Previous studies in *S. cerevisae* established a link between ScDga1p and ScLro1p and restoration of cell wall integrity (CWI) signaling fidelity in a constitutively active model [296]; Given the aberrant stress response mechanisms apparent in the *C. albicans dga2/lro1* Δ/Δ strain, and the importance of cell wall remodelling in *C. albicans* virulence, it seemed prudent to investigate if *dga2/lro1* Δ/Δ displayed altered cell wall form and function.

I first assessed the sensitivity of wild type and TAG mutants to congo red (CR), a known cell wall intercalating agent (Fig. 4.7A-B). Cells were grown in the presence or absence of 40μg/mL CR in RPMI at 37°C for 24h. I observed an increased lag phase in the *dga2/lro1* Δ/Δ compared to that of the wild type (Fig. 4.7A), with a reduced maximum OD_{600} as growth plateaued; this was reflected in the AUC analysis (Fig. 4.7B) where the CR treated dga2/lro1 Δ/Δ displayed greatly reduced growth when compared to the CR treated wild type.

Following this, I sought to determine whether CR sensitivity could be attributed to disrupted CWI signaling. I conducted western blotting analysis, probing for phosphorylated Mkc1, *C. albicans'* CWI MAPK (Fig. 4.7C-D); I observed negligible phosphorylation of Mkc1 from log phase protein extracts. Curiously, there was a significant increase in p-Mkc1 relative density in both *lro1* Δ/Δ and *dga2/lro1* Δ/Δ, as determined by densitometry of three separate blots, while *dga2* Δ/Δ was not significantly different to the

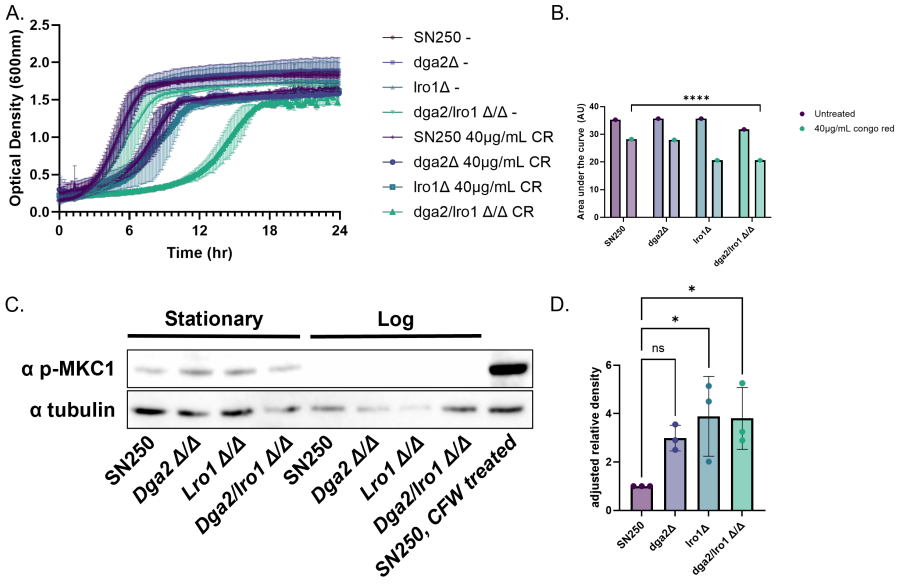

FIGURE 4.7: **Disruption of neutral lipid storage increases sensitivity to cell wall perturbing agents and increases phosphorylation of the Mkc1**

(A) Growth curve data of wild type and lipid knockouts grown in RPMI and treated with 40μg/mL fluconazole. Cells were seeded to an OD_{600} of 0.1 in a microtitre plate and grown at 37°C for 24h. 9 technical repeats were conducted across 3 biological replicates. **(B)** area under the curve analysis of growth curves from (A). Statistical significance was determined with a 2-way ANOVA, Tukey's multiple comparisons test where **** = $P < 0.0001$. **(C)** Western blot analysis of Mkc1 phosphorylation in wild type and lipid knockouts in both log and stationary phase. Cells were grown for 4h and 24h, respectively, before protein extraction. Blots were probed for p-Mkc1, with tubulin as a loading control for normalisation. Blots were completed in triplicate. **(D)** Densitometry analysis of western blots from (C). Images were analysed and readings normalised to the loading control. A one-way ANOVA was performed to determine significance, where * = $P < 0.05$

wild type. These data would suggest a role for lipid droplet homeostasis in maintaining cell wall integrity during the stationary phase of growth.

4.2.6 Insufficient TAG storage causes a thinning of the outer cell wall and a spike in exposed β-1,3-glucan

One of the factors that gives *C. albicans* an advantage within a given environment and during infection is its capacity for masking PAMPs that would otherwise be recognizable by the immune system. β-1,3-glucan, one of the primary components that make up the inner cell wall, is a common PAMP that *C. albicans* masks behind a mannan layer. Tight regulation of fungal cell wall structure sits at the centre of *C. albicans'* adaptable nature that makes it such a successful opportunist. As such, and given previous findings outlining cell wall sensitivities, I sought to determine what impact, if any, TAG depletion had on cell wall structure (Fig. 4.8).

TEM imaging of the wild type and TAG mutants revealed an almost 50$\tilde{\%}$ reduction in thickness of the mannan brush layer in the *dga2/lro1* Δ/Δ double knockout compared to the wild type (Fig. 4.8A-B). There was no discernible change in outer cell wall in either single knockout, which would indicate thinning resulting from complete TAG ablation. Curiously, both *dga2* Δ/Δ and *lro1* Δ/Δ also displayed significantly thicker inner cell walls when compared to the wild type((Fig. 4.8C), though the *dga2/lro1* Δ/Δ revealed an inner cell wall comparable to the wild type.

Corroborating the thinner brush layer, cells stained for mannan, chitin and β-1,3-glucan content were analyzed with flow cytometry (Fig. 4.8D); in this, I saw a significant decrease in mannan in the *dga2/lro1* Δ/Δ mutant, with mannan and chitin content across the single knockouts being comparable to the wild type. Most striking was a corresponding increase in β-1,3-glucan staining in dga2/lro1 Δ/Δ. A thinner mannan layer, confirmed by TEM and flow cytometry, coupled with increased β-1,3-glucan staining, in

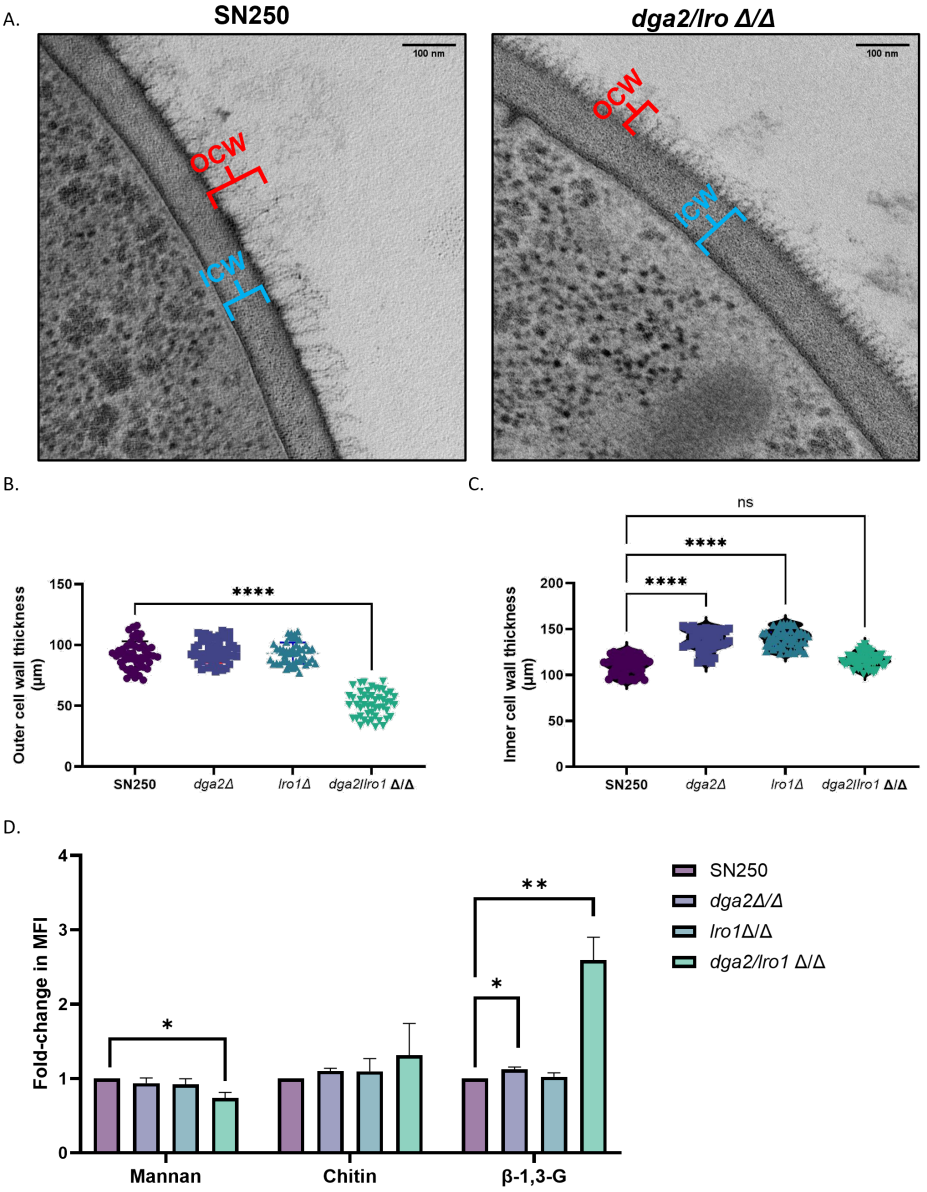

FIGURE 4.8: ***dga2/lro1* Δ/Δ cells have a thinner mannan layer and exposed *β*-1,3-glucan**

(A) Transmission electron microscopy of SN250 and *dga2/lro1* Δ/Δ, with inner cell wall (ICW; blue) and outer cell wall (OCW; red) labelled. Scale bars denote 100nm. TEM sample preparation and imaging kindly conducted by Dr Louise Walker of the Aberdeen Fungal Group **(B-C)** quantification of inner and outer cell wall thicknesses from **(A)** 50 thickness measurements were made across 10 cells. **D** Flow cytometric analysis of cell wall composition. Log phase cells were fixed and stained (Mannans, concanavalin A; Chitin, wheat germ agglutinin. *β*-1,3-glucan was probed for with a dectin-1 antibody. Median fluorescence intensity (MFI) was determined through flow cytometry, analysing at least 20,000 singlets (n=3). The graph represents fold-change compared to the wild type. Statistical significance of raw data was determined through ratio-paired t-tests, where * = $P < 0.05$, ** = $P < 0.01$.

tandem suggest an unmasking effect in the dga2/lro1 Δ/Δ; a thinning of the outer cell wall to expose the β-1,3-glucans of the inner cell wall.

4.2.7 *dga2/lro1* Δ/Δ increases cell susceptibility to phagocytic uptake

C. albicans's success as an opportunistic fungal pathogen can, in large part, be attributed to its adaptability. Control of the fungal cell wall, masking itself from immune recognition through shielding β-1,3-glucans from macrophages expressing dectin-1. Having seen a thinning of the brush layer in our *dga2*Δ/Δ *lro1*Δ/Δ, then, accompanied by greatly increased β-1,3-glucan staining, I next sought to confirm whether these would be attributed to an increased susceptibility for cells to be phagocytosed (Fig. 4.10).

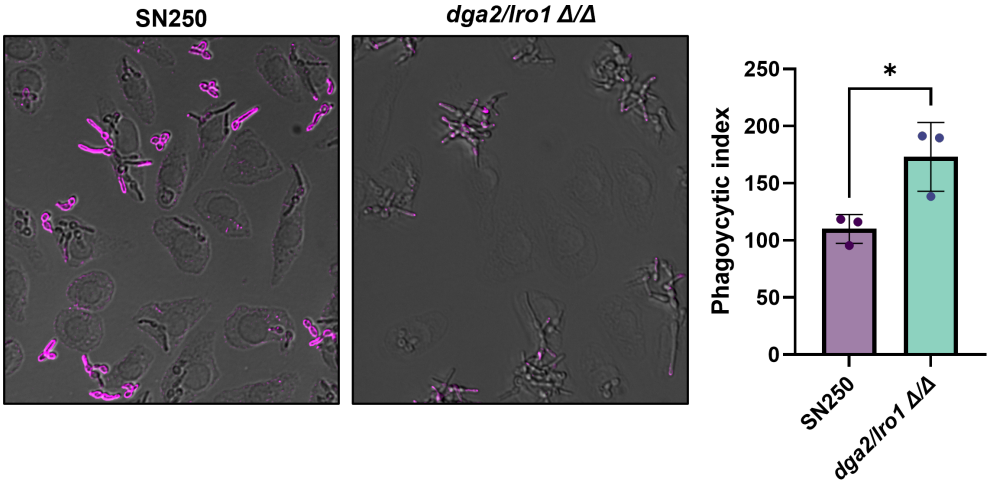

FIGURE 4.9: ***dga2/lro1* Δ/Δ cells are more readily engulfed by macrophages**
log-phase wild type and *dga2/lro1* Δ/Δ were co-incubated with J774 macrophages for 60 min. **(A)** Widefield imaging of macrophage assay, overlaying brightfield imaging with deconvolved fluorescent images. Cells were fixed and stained (ConA, magenta) to determine engulfment; unstained fungal cells are counted as phagocytosed, and a stained mother cell is counted as outside. **(B)** Bar chart depicting phagocytic index; n=6 across 3 biological repeats, where ~500 macrophages were scored per technical repeat. An unpaired t-test was run to determine significance, where * = $P < 0.05$.

Wild type and *dga2*Δ/Δ *lro1*Δ/Δ were assessed for propensity toward being phagocytosed after 60 min co-cultured with J774 macrophages. Fixation and staining with concanavalin A allowed for identification of cells that remained outside of macrophages, or were associated with macrophages, but not engulfed. *dga2*Δ/Δ *lro1*Δ/Δ displayed a significantly higher phagocytic index than that of the wild type. With this, I was able to conclude a correlation between neutral lipid homeostasis and *C. albicans*' immune evasion mechanisms.

4.2.8 *dga2/lro1* Δ/Δ *C. albicans* display a reduction in virulence in a *G. mellonella* model

Having established a hindrance of commitment to filamentation, as well as cell wall defects, sensitivity to various compounds and generally aberrant stress response mechanisms, I sought to determine whether deletion of *DGA1*, *LRO1* or a combination of the two would exhibit an overall reduction in virulence (Fig. 4.10). *G. mellonella* was used as an infection model; the wax moth larvae have an innate immunity, and their use as an early infection model in bacterial and fungal research has become more prevalent in recent years. Infection with 250,000 CFUs was selected to allow gradual death of the wild-type over a week. In both single knockouts, infected larvae were scored as dead at a similar rate to that of the wild type. I saw very little death over the first few days of the assay when infected with *dga2*Δ/Δ *lro1*Δ/Δ *cells*, and an overall significant reduction in virulence compared to the wild type. The reduction in virulence observed in *dga2/lro1*Δ/Δ cells, taken with a reduced capacity for immune evasion (Fig. 4.9), azole and cell wall sensitivity (Fig. 4.4,4.7 highlight a role for maintenance of neutral lipid storage for environmental adaptation and *C. albicans*' virulence.

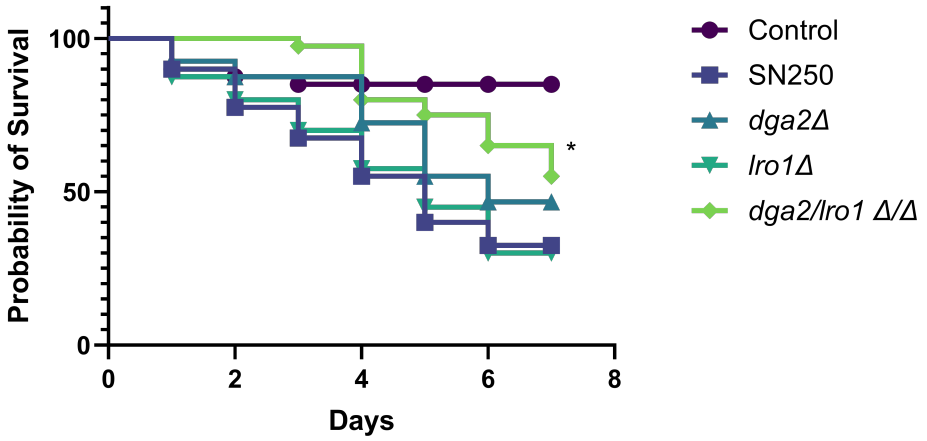

FIGURE 4.10: ***dga2/lro1* Δ/Δ is less virulent in a *G. mellonella* infection model**

Kaplan-Meier survival curves displaying likelihood of *Galleria mellonnella* survival when infected with *C. albicans*. Larvae were injected with 2.5x10^5 cells and stored daily to assess virulence of *DGA2* and *LRO1* deletion strains compared to wild type. n=40 *larvae* were infected per condition across 2 biological repeats. Statistical significance was determined using a Gehan-Breslow-Wilcoxon test, and * = $P \leq 0.05$.

4.3 DISCUSSION

In *S. cerevisiae*, terminal steps of neutral lipid biosynthesis are controlled by 4 proteins: Dga1p, Lro1p, Are1p and Are2 [347], with control of TAG biosynthesis being controlled predominantly by Dga1p and Lro1p. This reversible process allows for storage of excess fatty acids, for subsequent use in phospholipid metabolism. Previous works have established a conserved functionality in the DAG: acyltransferase Lro1 between *S. cerevisiae* and *C. albicans* in TAG metabolism [330], though to our knowledge the partnering DAG:acyltransferase has yet to be verified. In previous works, heterozygous *LRO1* deletion displayed an overall reduction in virulence in a *C. elegans* model [330]. I sought to elaborate further, testing the import for both Lro1 and the putative DAG :acyltransferase Dga2 in *C. albicans*' virulence.

In support of a tandem conserved role for *DGA2* and *LRO1*, HPTLC showed a drop in intracellular TAG in both of the single mutants, as well as elevated free fatty acids. Deletion of both genes was sufficient to prevent TAG production entirely, with a corresponding elevated DAG and FFAs. There were also sweeping alterations to phospholipid profiles, in line with observed effects in *S. cerevisiae* [382]. Lipid droplets, and TAG, act to regulate phospholipid biosynthesis via CDP-DAG-dependent phospholipid biosynthesis. Perturbation of this process would likely render cells more reliant on the Kennedy pathway for phospholipid generation, a dependence upon which has been shown to limit virulence within the host owing to an inability to scavenge enough ethanolamine [321]. In support of this, *dga2/lro1* Δ/Δ cells upregulated genes for funnelling additional sugars into acetyl-CoA metabolism (Fig. 4.3C), choline transport (Fig. 4.3B) and lipid scavenging (*PLB1)*. It is possible that diminished or slowed phospholipid metabolism owing to a scarcity of TAG resulted in the hyphal development that I identified, though whether this is also the cause for reduced commitment to filamentation in normal air remains unclear. Increased CO_2 overcame this phenotype, possibly through Ras-mediated upregulation of filamentation and biofilm-linked transcription factors Brg1 and Rob1 [53, 36, 83].

In *dga2/lro1* Δ/Δ, I identified an upregulation of stress response mechanisms, including oxidative stress response genes (*SOD4*, *SOD5*), members of the ras-cAMP-PKA pathway including *RAS2* and downstream biofilm-linked transcription factors *BRG1* and *ROB1* [36]. This in itself raises questions, as current understanding of the small GTPase ras2 in *C. albicans*, which suggests it works in opposition to the more prominently expressed ras1, to reduce intracellular cAMP and repress complex transcriptional network that includes *BRG1* and *ROB1*[36, 383, 83]. *RAS2* upregulation may be a compensatory mechanism to switch off inappropriately elevated transcription of *BRG1* and *ROB1*. I

observed an upregulation in glucose uptake mechanisms in *dga2/lro1* Δ/Δ, and with D-glucose, a known activator of ras1 [384, 358], it is conceivable that this causes activation of ras-cAMP-PKA signalling. There is also some evidence to suggest that PS depletion mislocalizes K-ras in tumour cell lines and locks it to the plasma membrane [385], so perhaps a similar mislocalisation of ras2 in *C. albicans* leads to unchecked ras-cAMP-pka upregulation of *BRG1* and *ROB1*.

Having noted a sensitivity of *dga2/lro1* Δ/Δ to fluconazole, I compared the transcriptional responses of wild type and *dga2/lro1* Δ/Δ cells to fluconazole treatment. The transcription factor Upc2, linked to ergosterol regulation, was upregulated more prominently in wild-type cells (wild-type, L_2FC 1.47; *dga2/lro1* Δ/Δ, L_2FC 0.59). This, coupled with comparably lower transcript levels for all elements of the ergosterol biosynthesis pathway, with core genes such as *ERG1* and *ERG11* not significantly upregulated in the *dga2/lro1* Δ/Δ strain, suggested a weaker response to fluconazole and a reduced capacity for adaptation to the stress. In the presence of fluconazole, in the wild-type I also observed an upregulation in genes associated with peroxisomal biogenesis, function and organisation and β-oxidation, a stress response mechanism using available fatty acid sources (such as those stored in lipid droplets) to fuel a high energy demand [386]. Peroxisomes have been observed forming within close proximity to, and actively invading, LDs for the purposes of β-oxidation [292, 289], so it is likely that following fluconazole stress, wild-type upregulation of peroxisomal biogenesis was to allow for ready catabolism of stored fatty acids as a part of the stress response. In *dga2/lro1* Δ/Δ, where TAG-containing LDs were largely non-existent, I do not see a similar upregulation of peroxisomal biogenesis. This may contribute to the *dga2/lro1* Δ/Δ strains' sensitivity to fluconazole, and indeed to other observed stresses. Peroxisomal biogenesis

also requires a steady source of phosphatidylcholine for membrane biogenesis [380], so in cells lacking stored TAGs, PC availability for peroxisomal biogenesis may be limited.

I noted a sensitivity to cell wall stresses in the *dga2/lro1* Δ/Δ double knockout, and an increased basal activation of the cell wall integrity pathway. There are a number of possible causes for this. There was no evidence in our transcriptomic data to suggest altered regulation of CWI signalling, though it should be noted that these data were taken during log phase growth, whereas cell wall integrity signalling was increased at stationary phase. Whilst this is something worth considering, CWI activation in this instance is likely post-translational. Disruption of TAG biosynthesis led to elevated intracellular DAG, a known Pkc1 agonist [241, 225]; it is possible, therefore, that elevated intracellular DAG causes inappropriate Pkc1 phosphorylation and CWI activation. There is also the deletion's impact on phospholipid profiles to consider; whilst our data did not show a significant difference between wild type and *dga2/lro1* Δ/Δ PE levels, there were significant reductions of PE in the single knockouts, and reduced PC in all three genotypes compared to wild type. PE is thought to play a role in GPI anchor biosynthesis, acting as an ethanolamine donor [381, 322]; it is possible, therefore, that in reducing *C. albicans*' capacity for TAG synthesis, there may be an effect on GPI-anchoring of membrane to cell wall, as well as an impact on GPI-anchored protein fidelity, though the exact mechanism can only be speculated upon in this study.

There was no evidence in our data to suggest that unmasking of the fungal cell wall apparent with a *dga2/lro1* Δ/Δ was a transcriptional response, as the Cek1 MAPK pathway showed no signs of upregulation. Instead, the answer could lie again with changes to the cell's lipidome. Previous studies have also highlighted a potential link between PS

and unmasking [161], displaying similar unmasking to what we've observed in a phosphatidylserine synthase mutant. Given the phospholipid changes imparted by *DGA2* and *LRO1* deletion, I may be seeing a similar effect. The exact means by which PS depletion would cause unmasking has yet to be determined; PS is known to be involved as a signalling molecule in multiple pathways and, like DAG, is a known activator of Pkc1 [161, 225]. In *S. cerevisiae*, PS, as well as anionic phospholipid PI4,5BP, have been implicated in the mediation of activating the CWI pathway [387]; aberrant lipid homeostasis may impact upon this mechanism. There are also several post-transcriptional mechanisms for tight control of fungal cell wall biosynthesis, including families of RNA-binding proteins [388], though I have no evidence to suggest these processes are being impacted.

This phenotype, however, led to increased binding of the Fc-Dectin-1 antibody as determined through flow cytometry, and as such increased exposure of β-1,3-glucan, a PAMP in the inner cell wall. Increased β-1,3-glucan exposure is associated with increased innate immune recognition by macrophages and other immune cells expressing the C-type lectin receptor Dectin-1. In line with this, *dga2/lro1* Δ/Δ cells, displaying increased β-1,3-glucan exposure, were also more susceptible to phagocytic uptake by murine macrophages. In a *G. mellonella* infection model, infection with *dga2/lro1* Δ/Δ cells led to killing significantly slower than that of the wild type, which is in line with our previous findings. Deletion of *DGA2* and *LRO1* ultimately led to cells exhibiting slower filamentation, diminished stress responses and a reduced capacity for immune evasion that culminated in reduced virulence in *G. mellonella*.

One of the more highly upregulated genes in *dga2/lro1* Δ/Δ was *PLB1*, which codes for a secreted phospholipase B protein that is thought to be linked to adherence to, and penetration of host cells [389, 374]. It stands to reason that cells unable to rely on stored

fatty acids for de novo biosynthesis of PS, PE and PC would upregulate scavenging mechanisms to compensate. Not conducted within this study, though worth considering, is the impact that supplementation of choline and ethanolamine would have on observed phenotypes, and whether these would be sufficient for restoration of virulence. Overall, I have determined conserved function between the *S. cerevisiae* DAG: acyltransferases ScDga1p and ScLro1p and the *C. albicans* CaDga2p and CaLro1p. In exploring TAG storage in *C. albicans*, I determined a hitherto unexplored role of TAG regulation in hyphal formation, *C. albicans*' adaptability and stress response mechanisms, cell wall organisation and capacity for immune evasion. All of this culminated in a reduction in virulence of *C. albicans*.

Chapter 5

Lipotoxicity as a novel approach to enhance the management of *C. albicans* biofilms

5.1 INTRODUCTION

C. albicans is a budding yeast that, for the most part, exists in a state of commensalism within human hosts [3, 4],. However, *C. albicans* is also an opportunistic pathogen and has been listed as a critical priority by the World Health Organisation [390].

C. albicans' pathogenicity can be attributed to several factors. For example, the yeast is highly adaptive to changes in environment, capable of genomic rearrangements in response to stress [391], and can exist within several human niches including the oral cavity [3], gastrointestinal tract [4, 392] and vulvovaginal tracts [393]. *C. albicans* is adept at avoiding detection by the host immune system, masking the pathogen-associated molecular pattern (PAMP) β-1,3-glucan behind a mannan layer [161].

Next, and perhaps best known, is *C. albicans'* morphological plasticity [394]. *C. albicans* typically grows in yeast form, but environmental triggers such as elevated CO_2 [53], presence of serum and physiological temperatures [395], and shift to a more basic pH [396], can cause a yeast-to-hyphal switch that promotes polarised, filamentous and invasive growth [397].

C. albicans' success as a pathogen can also be attributed to the biofilms it can create. Biofilms are a mass colonisation of either biotic surfaces, such as mucosa [392], or abiotic surfaces such as on indwelling medical devices [55]. *C. albicans* biofilm formation comprises an attachment period, in which cell adhesins Hwp1[383], Als1 [398] and Als3 [370] among others bind yeast cells to a surface. Cells then proliferate and begin to differentiate, forming dense and complex meshes of both hyphal and yeast cells [399], whilst building an extracellular matrix to act both as mortar to hold the structure together, and shield from environmental stress[400, 399] and the immune system[399, 92]. The result of this is a multi-drug resistant reservoir of protected *C. albicans*, capable of shedding "persister" cells capable of causing infection. In resource scarce environments,

C. albicans is capable of scavenging trace metals[56, 373], proteins and lipids [365], and invading host tissue through release of phospholipases, aspartyl proteases and the toxin candidalysin [401, 402].

In at-risk patients, such as the immunocompromised, elderly, and those in intensive care, *C. albicans* biofilms, and the potential for candidaemia and systemic candidiasis, poses a clinical threat associated with high mortality [403, 392, 404]. The presence of medical devices such as catheters, cannulas and tracheostomy tubes provide an abiotic surface upon which *C. albicans* biofilms can form and present an infection risk that is poorly addressed within current medical practice. Evidence also suggests that several bacterial pathogens can use *C. albicans* biofilms as a scaffold upon which to gain their own foothold, increasing risk of bacterial infection [55, 405], For example, *Staphylococcus aureus* can bind to *C. albicans* and this has been shown to increase their ability to invade the host [406].

We require better approaches to be able to limit *C. albicans* biofilms growth and considerable efforts are being made to develop new anti-biofilm strategies that can be applied to medical devices [407], An emerging area of interest is in the use of organic coatings that provide an effective anti-biofilm medical device surface, with lipophilic coatings proving efficacious [408]. Several studies have shown the potential of certain monounsaturated fatty acids (MUFAs), such as the dietary fatty acid palmitoleic acid (POA) [236, 409], as antifungal agents. Typically, higher eukaryotes stave off lipotoxicity by storing excess free fatty acids within ER-associated lipid droplets (LDs)[347](Fig. 5.1), comprising a neutral lipid core surrounded by a protein-studded phospholipid monolayer. A relatively conserved process that has been well characterised in *S. cerevisiae*, lipid droplet formation involves conversion of free fatty acids into triacylglycerols (TAG) and excess sterols into sterol esters (SE). Important for lipid homeostasis within cells,

LDs also act as a buffer against lipotoxicity in the presence of excess exogenous fatty acids, though POA exposure reportedly leads to lipotoxicity and necrosis in yeast as it is poorly metabolised within fungal cells.

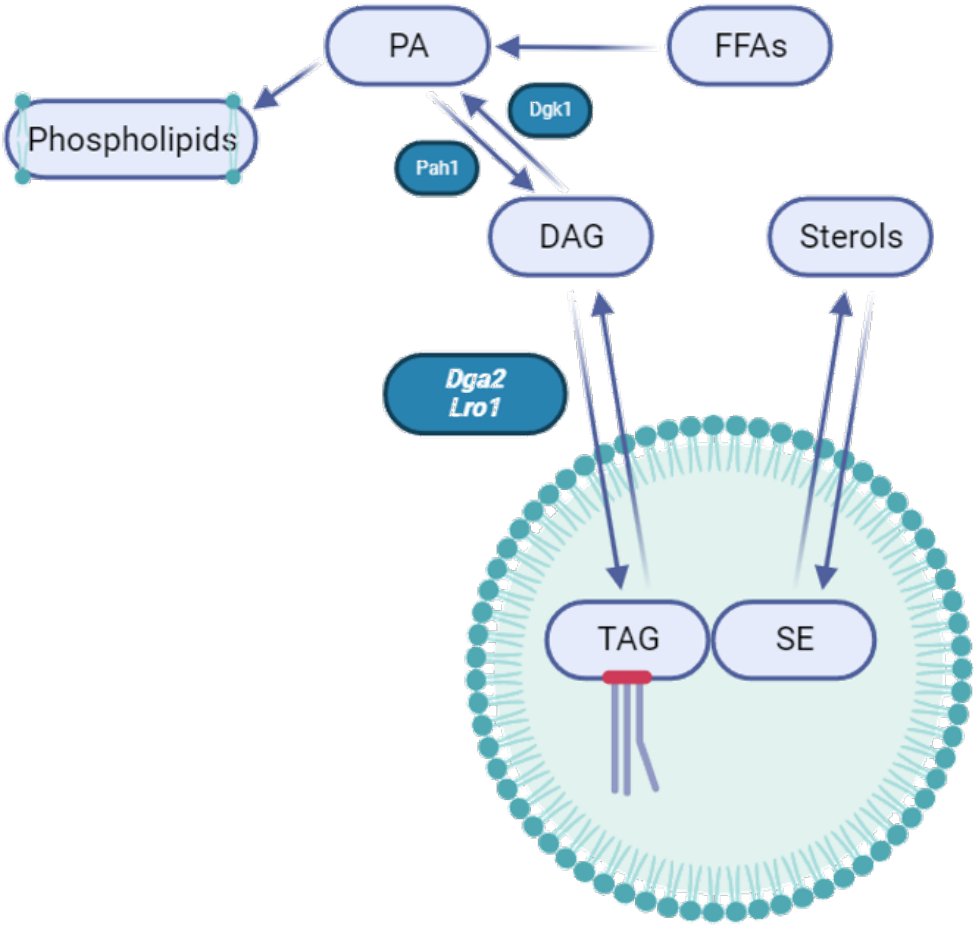

FIGURE 5.1: **Excess lipid storage in yeast**
Excess free fatty acids (FFAs) are funnelled into lipid droplet formation. Conversion of diacylglycerols (DAG) to triacylglycerols involve the action of diacylglycerol acyltransferases Dga2 (orthologue of the *S. cerevisiae dga1p*) and Lro1. The process may be reversed, allowing for remobilisation of stored lipids for CDP-DAG phospholipid biosynthesis.

I sought to determine the potential of POA application in the management of *C. albicans'* biofilms. Our findings demonstrate that POA is effective at introducing a lipotoxic challenge that renders cells vulnerable to additional stress. A failure to store excess POA promotes necrosis and prevents the formation of a biofilm. The impregnation of silicone

with POA was sufficient to prevent biofilm formation and POA acted synergistically with fluconazole to limit cell growth. Overall our findings suggest that lipotoxicity generated by a dietary fatty acid that is poorly metabolised by *C. albicans* represents an effective approach to augment the management of biofilm formation on medical devices.

5.2 RESULTS

5.2.1 Lipid storage defects impact on the development of biofilms in a high CO_2 environment

Given the clinical importance of *C. albicans* biofilms, and their difficult to treat nature, I sought to determine the role that lipid droplet formation played in biofilm establishment and tested whether lipotixicity could be employed as an anti-fouling strategy.

To determine the role that lipid droplet formation played in biofilm establishment and growth I conducted assays using C. albicans cells lacking genes required for droplet formation, namely *dga2*Δ, *lro1*Δ and *dga2*Δ/*lro1*Δ. Biofilms were initially assessed over a 24h period and quantified through crystal violet staining (Fig. 5.2A). *C. albicans* biofilms were also grown for 24 and 48 hours and stained with calcofluor white before confocal imaging to examine the role of lipid droplet storage on maturation.

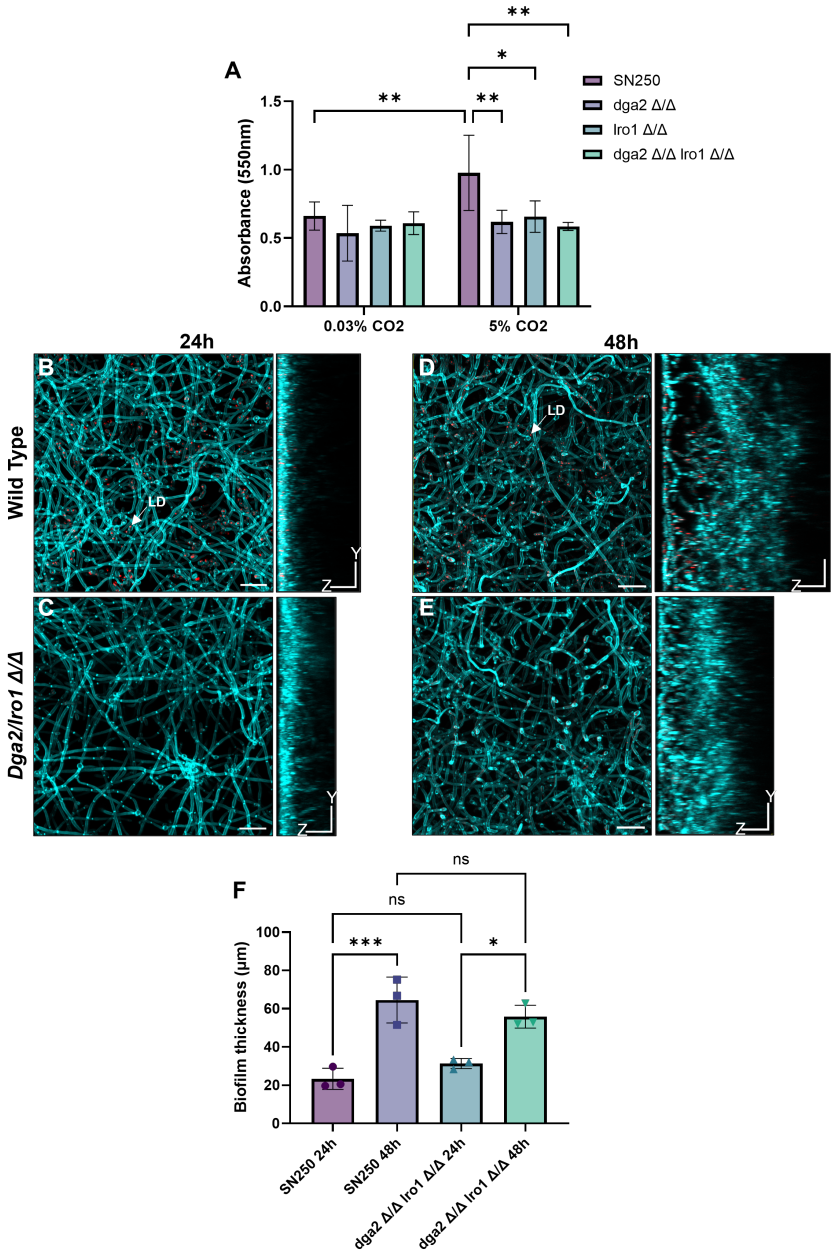

FIGURE 5.2: **Biofilm development is impacted by manipulation of lipid metabolism**

(A) Biofilms were grown on the bottom of 96 well plates in both normal air and 5% CO_2, crystal violet stained, destained and analysed in a plate reader. (B-E) Biofilms grown in 5% CO_2 were calcofluor and BODIPY 493/503 stained and imaged with airyfast confocal imaging; images depict maximum intensity projections and orthogonal views, where (B) is the wild-type at 24h growth, (C) a 24h *dga2*Δ/*lro1*Δbiofilm, (D) a 48h wild-type biofilm and (E) a 48h *dga2*Δ/*lro1*Δ biofilm. (F) Biofilm thickness was measured in the XZ and YZ planes of confocal images, 150 measurements across 3 biological replicates. Scale bars on confocal images represent 25μm. Error bars denote SEM, and asterisks denote p-values where * = $P < 0.05$, ** = $P < 0.01$, *** = $P < 0.001$, and **** = $P < 0.0001$.

No difference was observed between the *dga2*Δ/*lro1*Δ mutant or wild type biofilms grown in 0.03% Co2 (Fig. 5.2A). As has previously been reported, the elevation of CO_2 to 5% led to an increase in biofilm growth for the wild type, [56] which was not observed in the *dga2*Δ/*lro1*Δ mutant (Fig. 5.2A).

Confocal microscopy was employed to examine biofilms grown in elevated CO_2 at 24h and 48h timepoints (Fig. 5.2B-E). Biofilms were calcofluor-stained, as well as stained with BODIPY 493/503 to highlight lipid droplet deposits throughout the biofilms. Notably, in both the 24h and 48h *dga2*Δ/*lro1*Δ mutant biofilms (Fig. 5.2C and E, respectively) there was a distinct lack of lipid droplet foci throughout the biofilm, highlighting the impact of these mutations on lipid storage. In the wild-type biofilms, at 24h lipid droplet foci can be seen predominantly within the cell bodies, but at 48h, lipid deposits appear present throughout hyphae within the biofilm.

Taking thickness measurements from the orthogonal views of biofilms, surprisingly there was no significant difference in biofilm thickness between wild type and the *dga2*Δ/*lro1*Δ mutant at either a 24 or a 48h timepoint, though I could determine a significant increase in biofilm thickness in both wild type and *dga2*Δ/*lro1*Δ with the longer incubation time of 48h. These results, taken in tandem, suggest that whilst dga2Δ/lro1Δ may impact upon overall biofilm biomass as evidenced by the crystal violet staining, biofilm thickness may not be impacted.

5.2.2 Exogenous palmitoleic acid exposure inhibited *C. albicans*' growth when lipid storage was disrupted

The storage of excess free fatty acids as neutral lipid to stave off lipotoxicity is one of the primary functions of the lipid droplet. As reduced lipid storage capability had a marked

impact on biofilm formation, I sought to determine whether overwhelming lipid storage mechanisms, or lipotoxicity, would also have a negative impact on *C. albicans* biofilm formation. The monounsaturated fatty acid, palmitoleic acid (POA), has previously been reported to induce lipotoxicity in the yeast *Saccharomyces cerevisiae* [236, 409], with toxic effects linked to overwhelming lipid storage mechanisms, leading to lipotoxicity and necrosis. POA can be found in relatively high concentrations in macadamia nuts, sea buckthorn and sardine oil, is safe for human consumption and as an omega-7 fatty acid, has some associated health benefits [410, 411]. Its reported effectiveness against *S. cerevisiae*, coupled with it being safe to use in humans, made it an ideal candidate for investigation.

I determined the impact of POA on the growth of *C. albicans*, ranging from 125μM-2mM (Fig. 5.3). Cells were grown in the presence of palmitoleic acid at 37°C in RPMI-1640 for 24h.

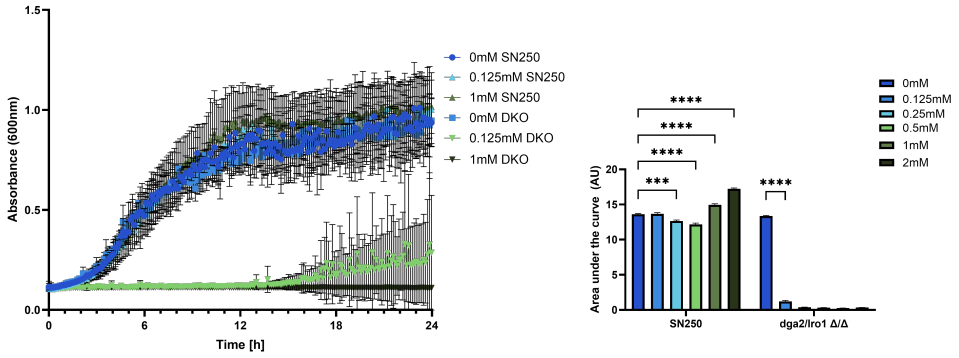

FIGURE 5.3: **The effect of palmitoleic acid on the growth of wild-type and lipid storage defective *C. albicans* strains**
Wild-type and *dga2*Δ/*lro1*Δ cells were grown overnight and seeded to OD_{600} 0.1 in RPMI, and grown for 24h with varying concentrations of exogenous POA. (A) Growth curves over 24h. Curves represent 9 pooled replicates over biological triplicate, and error bars denote Standard deviation from the mean. (B) Area under the curve analysis of growth curves from (A). A two-way ANOVA was conducted, and error bars denote standard error of the mean, and asterisks depict statistical differences of p-values where * = $P < 0.05$, ** = $P < 0.01$, *** = $P < 0.001$, and **** = $P < 0.0001$.

The *dga2*Δ*/lro1*Δ mutant was more sensitive to the presence of exogenous palmotoleic acid compared to the wild type, anything above 0.125mM displaying full growth inhibition at 24h, and 0.125mM showing a severely increased lag time with some growth apparent by the 15h mark. The wild-type, however. displayed an interesting response to POA. At 0.25mM and 0.5mM, SN250 displays a small but significant slowing of growth (Fig. 5.3B). However, at higher concentrations of 1mM and above, SN250 appears to overcome and even thrive, with 1mM and 2mM SN250 reaching a higher maximum OD_600 than that of the untreated wild type.

The severe impact on growth of *dga2*Δ*/lro1*Δ in the presence of low concentrations of POA highlights the necessity for triacylglycerol (TAG) synthesis in the presence of excess fatty acids. Seeing as 0.25mM and 0.5mM POA seem to reduce the carrying capacity of the wild-type, whilst 1mM and 2mM seem to bolster growth, is an interesting result that bears further investigation, but early evidence suggests wild type *C. albicans* using exogenous palmitoleic acid to bolster growth.

5.2.3 Palmitoleic acid exposure promotes necrosis in *C. albicans*

Having seen that palmitoleic acid has a strong impact on the growth of *dga2*Δ*/lro1*Δ cells and a more minor impact on wild-type *C. albicans*, I addressed the mechanism of action. PBS suspended cells were subjected to a 90' POA treatment at 1mM or 100μM, stained with propidium iodide to assess necrotic cell death, and then analysed with flow cytometry (Fig. 5.2.3). Propidium iodideis a cell impermeant DNA intercalator which enters cell upon membrane destabilisation and fluoresces when bound to nucleic acids,

it therefore acts as a marker of necrosis.

Flow cytometry analysis revealed a minimal necrotic population in both wild type and *dga2*Δ/*lro1*Δ cells when treated with 100μM POA (Fig. 5.2.3). A 1mM POA treatment, however, delivered a much more pronounced effect. In 90 min, approximately half of the wild-type cells analysed were PI-positive, suggesting a strong lipotoxicity-induced cell death. The effect was considerably stronger in the *dga2*Δ/*lro1*Δ, with these cells displaying an almost 90% PI-positive population. As palmitoleic is reported to be incorporated into lipid droplets to offset lipotoxic effects [409], it would appear an ability to generate TAG is crucial for survival of uptake of the monounsaturated fatty acid, hence such a pronounced effect on the *dga2*Δ/*lro1*Δ mutant. 50% necrosis in the wild-type at 90 min is not inkeeping with the observation that POA did not affect the growth of the wild-type particularly strongly, and proved an intriguing result.

5.2.4 Palmitoleic acid increases *C. albicans'* sensitivity to fluconazole

The proposed mechanism of POA-induced lipotoxicity suggests that POA not incorporated into protective LDs generates POA-containing PL species that cause an increase in cell membrane permeability. This may occur by skewing phosphatidylethanolamine ratios in the plasma membrane. With that in mind, I sought to determine whether POA increases *C. albicans*' susceptibility to antifungals that target sterol production, which is essential for cell growth and maintenance of membrane permeability.

Wild type *C. albicans* was grown for 24h in dilution series comprising 0-1600 μM POA and 0-8 μg/mL fluconazole, and their growth patterns were analysed (Fig. 5.5). Area

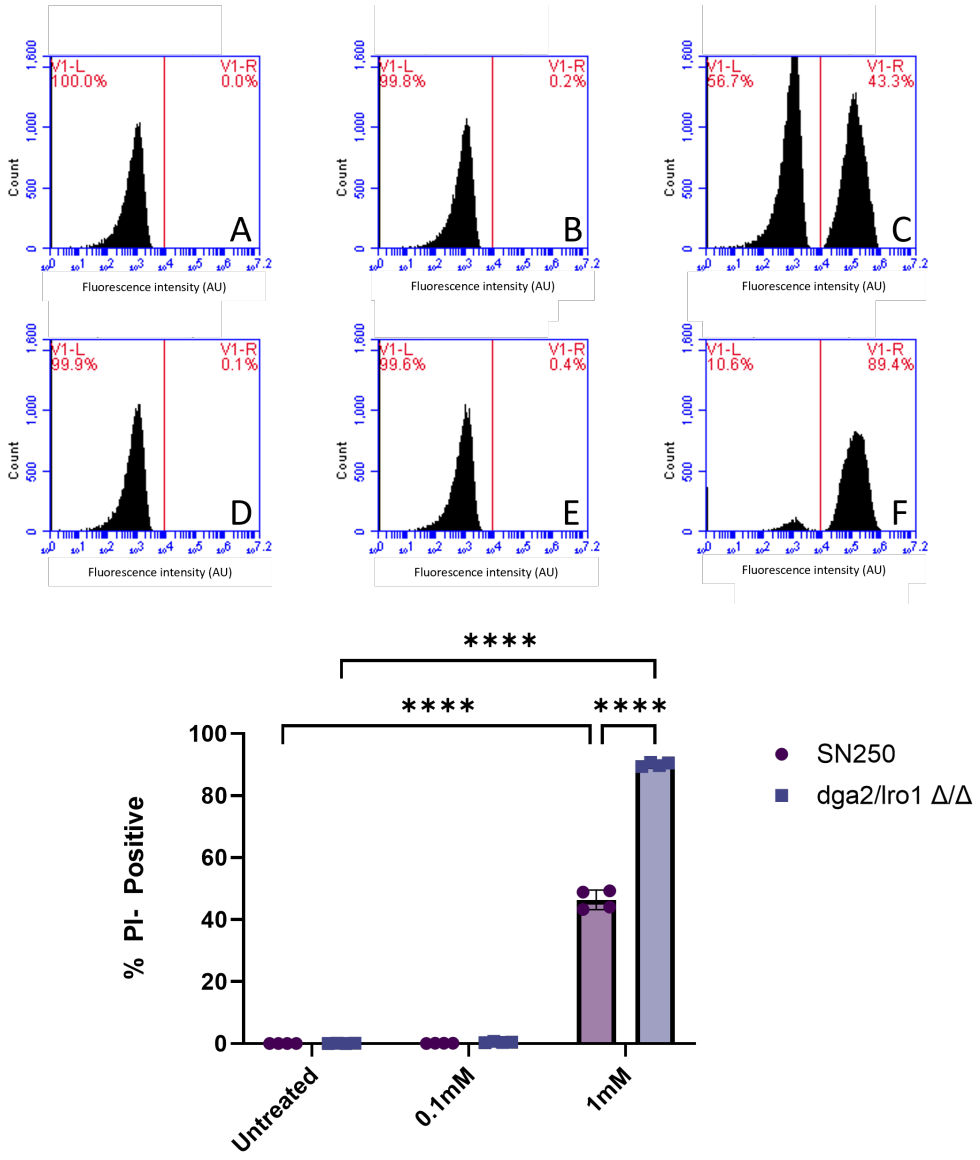

FIGURE 5.4: **Palmitoleic acid causes lipotoxicity and necrosis in *C. albicans***

Cells were treated with 100μM or 1mM POA at 37°C, 5% CO_2 for 90 min. Cells were then stained with propidium iodide and analysed using flow cytometry. Representative histograms of one replicate analysing 20,000 cells are presented (A-F) . (A), (B) and (C) represent wild-type cells treated with 0mM, 100μM and 1mM POA, respectively. (D), (E) and (F) represent *dga2*Δ*/lro1*Δ treated with 0mM, 100μM and 1mM POA, respectively. (G) 80,000 cells were analysed over 4 independent experiments, following treatment with either 100μM and 1mM POA. Error bars denote standard error of the mean, and asterisks depict statistical differences of p-values where * = $P < 0.05$, ** = $P < 0.01$, *** = $P < 0.001$, and **** = $P < 0.0001$..

under the curve analysis was conducted as a means of better assessing impact on overall growth.

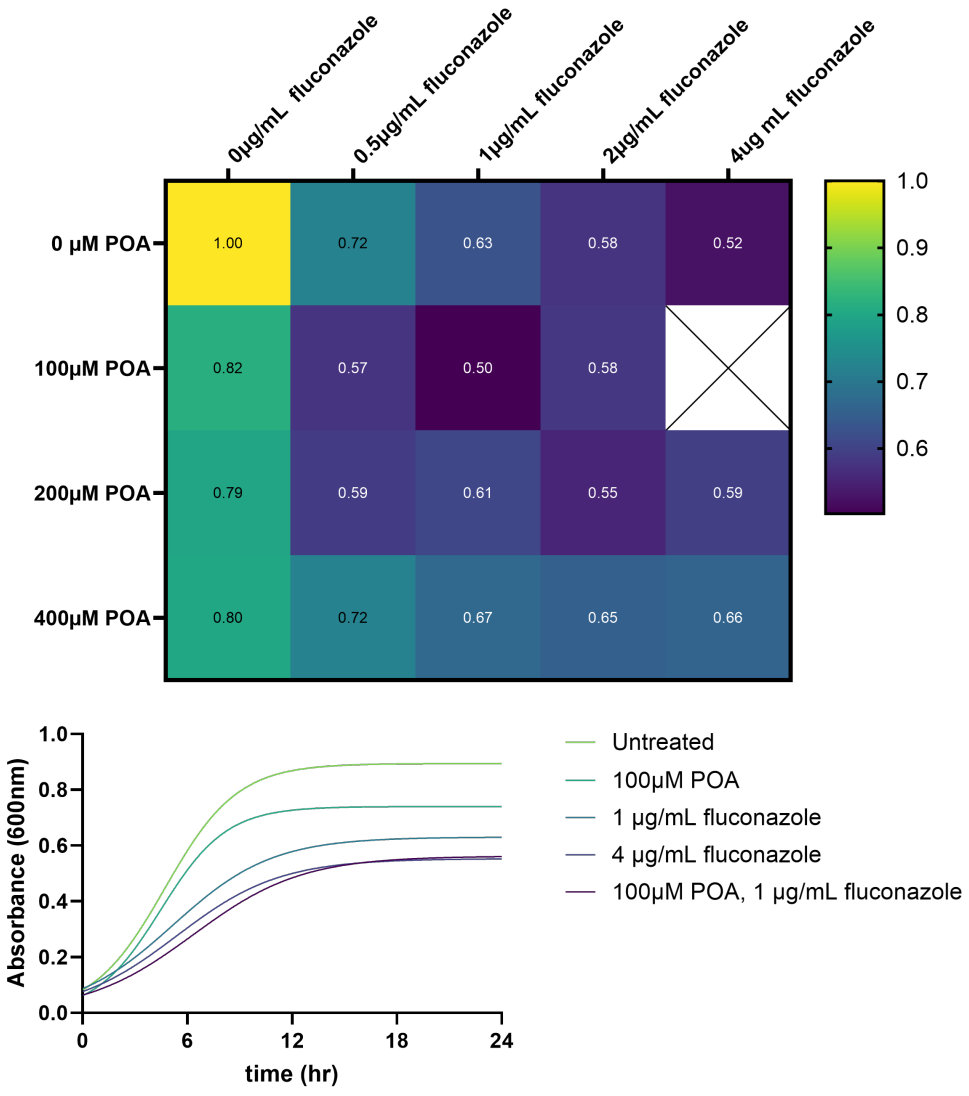

FIGURE 5.5: **Combination treatment of *C. albicans* with fluconazole palmitoleic acid**

C. albicans Wild type *C. albicans* was subjected to a combination of fluconazole and palmitoleic acid treatments at concentrations ranging from 0-16μM Palmitoleic acid and 0-8μg/mL fluconazole for 24h at 37°C in RPMI. (A) A heat map depicting fold-change in growth compared to the untreated condition, seen in the top left. Concentrations trending toward purple depict greater levels of inhibition. White squares containing a cross represent absent concentration combinations absent in the assay. Data represents n $\geq$ 7 replicates across 3 independent experiments. (B) Growth curves of untreated *C. albicans*, as well as cells treated with 100μM POA, 1μg/mL and 4μg/mL fluconazole, and a combination treatment of 1μg/mL fluconazole and 100μM POA, as seen in (A). Curves represent an average of n $\geq$ 7 curves, fit to a logistic growth model.

Cells were grown in RPMI at 37°C. Under these conditions, the MIC_{50} of fluconazole was 4μg/mL (Fig. 5.5A), with an MIC_{50} for POA unable to be determined (0-400μM shown). When grown in combination, an MIC_{50} was reached at 100μM POA with 1μg/mL fluconazole. Calculating fractional inhibitory concentration (FIC) for these data, with an FIC index of 0.3125 (where FIC $\ll$ 0.5 s considered synergistic), it can be concluded that the presence of 100μM POA is greatly synergistic with fluconazole, increasing *C. albicans*' susceptibility to the drug.

5.2.5 Palmitoleic acid inhibits cell attachment to silicone, but does not impact maturing biofilm development

Given the ability for palmitoleic acid to cause necrotic effects in *C. albicans*, impact upon typical growth patterns and increase susceptibility of commonly used antifungals, I sought to establish the impact that palmitoleic acid would have on the stages of biofilm formation on PDMS (silicone), as this is commonly used in the manufacture of medical implants [55].

Biofilms, once mature, are notoriously difficult to permeate and treat, usually displaying a greatly elevated drug tolerance, and given the cells' shift toward filamentation and building dense biofilm at this stage, I sought to delineate both whether POA could prevent biofilm formation on medical devices and whether the timing of administration was important.

Silicone leaflets were incubated in a *C. albicans* cell suspension (OD_{600} 1, in PBS) for 90 min at 37°C, before non-adhered cells were washed off and early biofilms were incubated in RPMI for 24h. Biofilms were treated with varying concentrations of POA either in

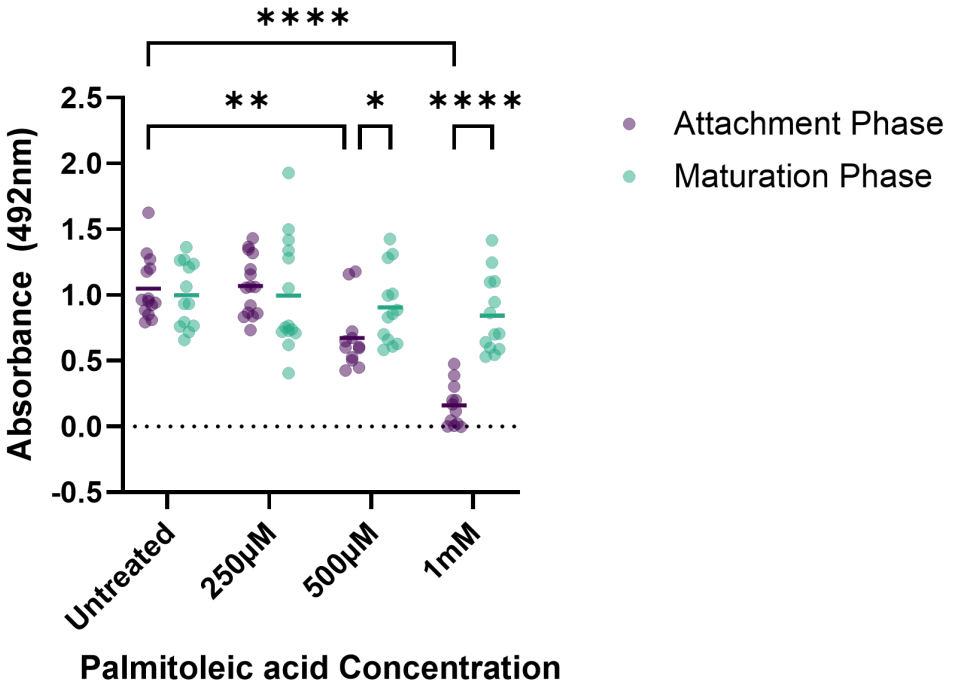

FIGURE 5.6: **Palmitoleic acid inhibits biofilm formation on silicone** Biofilms were grown in the presence of varying concentrations in either the (A) 90 min attachment phase of biofilm development or (B) after 24h maturation phase of biofilm development. Biofilm size and viability was analysed with using an XTT assay and reading absorbance at 492nm. Bars represent at least 12 technical replicates conducted over biological triplicate. Error bars denote standard error of the mean, and asterisks depict statistical differences of p-values where * = $P < 0.05$, ** = $P < 0.01$, *** = $P < 0.001$, and **** = $P < 0.0001$.

the attachment phase (the first 90 min in PBS) or during the maturation phase (24 hr incubation in RPMI). XTT assaying of the attachment phase revealed 0.5mM and 1mM POA had a significant impact on biofilm development on silicone (Fig. 5.6), with 1mM causing a 90% reduction in quantifiable biofilm. Curiously, there was no discernible impact on biofilm initiation if biofilm growth medium was supplemented with POA during the maturation phase. From these data I could conclude that POA was effective at inhibiting cell attachment, but adhered cells were less susceptible to the effects.

5.2.6 Palmitoleic acid infused silicone inhibits *C. albicans* biofilm formation

Having determined the efficacy of POA at inhibiting biofilm formation on silicone, it was clear that treatment was more efficacious during the attachment phase, or as a prophylactic, to prevent *C. albicans* establishment. I sought to determine whether infusing silicone with palmitoleic acid would be sufficient to inhibit *C. albicans* biofilm formation. Biofilms were grown on PDMS (Polydimethylsiloxane), a silicone polymer, which had been impregnated with a range of concentrations of POA up to 5% w/w (Fig. 5.7).

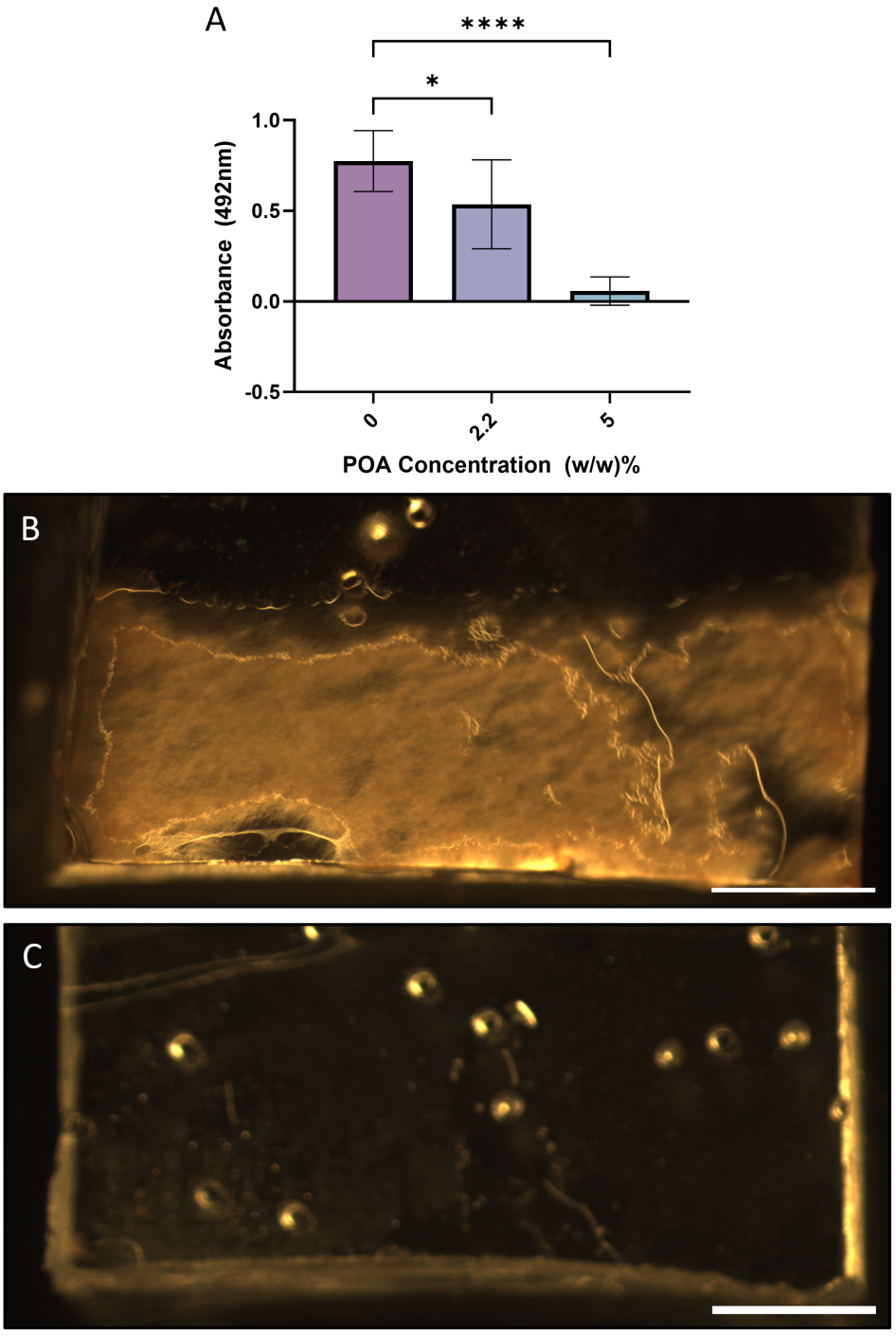

FIGURE 5.7: **Biofilm development on POA treated PDMS**
Biofilms were grown on POA-treated PDMS for 24h. (A) XTT readings of biofilms. Data represents at least 7 biofilms over 2 biological replicates. Error bars denote standard error of the mean, and asterisks depict statistical differences of p-values where * = $P < 0.05$, ** = $P < 0.01$, *** = $P < 0.001$, and **** = $P < 0.0001$. (B-C) Imaging of biofilms grown on POA-treated PDMS, where B is 0% w/w POA-treated and C is 5% w/w POA-treated. Scale bar represents 0.2mm.

I was able to determine that 2.2% w/w POA was effective in reducing biofilm formation

by 30% and a 5% w/w POA-treated PDMS able to inhibit *C. albicans* biofilm formation by 92.5% (Fig. 5.7A).

Images captured of C. albicans biofilms grown on silicone squares (Fig. 5.7B-C), showed clearly that while untreated PDMS became covered in a dense *C. albicans* biofilm, the presence of POA prevented colonisation (Fig. 5.7B-C). These data suggest that palmitoleic acid can be embedded into silicone and released to prevent biofilm formation.

5.3 DISCUSSION

The threat posed by the opportunistic human fungal pathogen *C. albicans* is one that continues to grow [390]. For example, during the COVID-19 pandemic, the increased burden in ICUs and reliance on mechanical ventilators brought with it an increase in incidences of candidaemia [98]. There is also strong evidence to suggest that *C. albicans* colonisation of airway management devices in those reliant on a ventilator can lead to an increase in bacterial respiratory infection and ventilator-associated pneumonia [412, 413]. The use of medical devices in the airway is, of course, vital, but the propensity for biofilm formation in an already at risk patient cohort presents a significant clinical problem [414]. Biofilm formation on medical devices can cause device failures [55] but also act as reservoirs for difficult to treat infections, and it may be the case that *C. albicans* presence can act as a scaffold for bacterial pathogens such as *Staphylococcus aureus* [406] and *Pseudomonas aeruginosa* [405, 412], which allow them to thrive.

One approach to limit medical device-associated infection may be to reduce *C. albicans* establishment and hence its role as scaffold for more complex poly-microbial assemblies. This study sought to determine whether this could be achieved using a natural fatty

acid, POA, that is readily metabolised by humans but that can induce lipotoxic effects in yeast. I observed that an inability to store excess fatty acids in lipid droplets led to significant effects on biofilm formation and a sensitivity to the lipotoxic effects of POA. One possibility to account for the effects on biofilm growth could be the result of resource scarcity. An inability to store TAG in lipid droplets, achieved through deletion of the diacylglerol acyltransferases *DGA2* and *LRO1*, may lead to a bottleneck at CDP-DAG, a precursor molecule for generation of vital phospholipid classes necessary for membrane development [303]. This may also lead to an over-reliance on de novo PL synthesis [321, 328] via the Kennedy pathway. The, inability to store excess free fatty acids (FFAs) and diacylglycerol (DAG) could also account for the observed lipotoxic effects of POA treatment[236] whereby intermediates accumulate within membrane compartments and induce a loss of stability.

Treating wild type and LD defective cells with the monounsaturated fatty acid POA in RPMI highlighted the importance of proper TAG storage mechanisms in *C. albicans*, as LD storage mutants displayed an MIC_{90} as low as 125μM POA. Conversely, wild-type cells were able to grow to 85-90% their typical capacity at 500μM, with higher concentrations of 1mM and 2mM even bolstering growth. This is in contradiction to propidium iodide staining of POA-treated cells, where the wild type displayed a 50% PI-positive population; it should be noted that these cells were stationary and treated in PBS, as opposed to actively growing and in medium. This may suggest that the lipotoxic effects are contingent upon growth conditions and this will require further investigation. One possibility is that POA uptake and metabolism is altered by growth media conditions. It is also entirely possible that, as cells were already stationary and accumulating LDs, 1mM POA was sufficient in these circumstances to overwhelm lipid storage mechanisms

in the wild type.

PI-staining sought to highlight the lipotoxic effects of the monounsaturated fatty acid, with a 90% necrotic population in cells incapable of incorporating POA into lipid droplets. A 100μM treatment, a sub-MIC_{90} concentration of POA for the *dga2*Δ*/lro1*Δ mutant, showed no necrotic population, suggesting a fungistatic effect in lower concentrations Typically, endocytosed POA could find one of many fates: conversion into TAGs for storage in LDs; β-oxidation in peroxisomes; incorporation into mitochondrial membranes, leading to a drop in membrane potential and either mitophagy (a pro-survival mechanism) or generation of ROS, widespread oxidative damage and eventual liponecrosis; and incorporation into the plasma membrane, impacting membrane curvature, increasing permeability and thus passage of small molecules (another mechanism by which cells commit to liponecrosis) ([236, 409]). In the *dga2*Δ*/lro1*Δ mutant, where storage as TAG is not possible, the cell is far more likely to succumb to these lipotoxic effects.

I observed POA concentrations of 100μM increasing cell susceptibility to fluconazole. One possibility for this lies in the aforementioned increase in membrane permeability associated with skewed PE ratios caused by POA integration [409]- this could increase cell uptake of fluconazole. Another possibility lies in fluconazole's mechanism of action. In targeting *ERG11*, fluconazole limits ergosterol production, itself contributing to an increase in membrane permeability [415]. These two compounds may work in synergy, delivering a two-pronged assault on yeast cell lipid metabolism.

The biofilm prevention mechanisms of POA seemed to rely on POA being present whilst cells were planktonic and not yet adhered to the material, as the inclusion of POA in the maturation phase of the biofilm growth had no effect. This speaks to a potential

shift in metabolic requirements; perhaps adhered cells already devoted to biofilm growth and maturation are less likely to internalise exogenous palmitoleic acid. Not explored within this study is the impact of treating an already mature biofilm with POA; given a biofilm's propensity for scavenging of exogenous resources, this might prove a fruitful avenue of investigation.

Given the potent anti-biofilm potential of POA when embedded within the silicone, early data would suggest POA is a strong candidate for a prophylactic coating to prevent cell attachment and biofilm maturation on medical devices. In addition, the synergism that POA displayed with fluconazole in vitro increases its potential, as such an agent could be useful in supplementing preexisting therapeutic regimens like lock therapy (whereby high concentrations of drugs are "locked" within a medical device for a prolonged treatment by shutting off valves before being removed) and typical antifungal treatment strategies. It would be worthwhile to explore further synergies with other antifungals targeting different elements, including echinocandins, to see if POA synergises well with β-glucan disruption. Lastly, it would be interesting to explore the potential application and delivery of antifungal drugs in liposomes generated largely of POA-based lipids to see if this increases the efficacy of pre-existing drugs.

Chapter 6

Discussion

6.1 CaDga2 and CaLro1p have a conserved diacylglycerol acetyltransferase functionality necessary for TAG biosynthesis

This body of work was largely associated with bettering understanding of glycerolipid metabolism in the pathogenic yeast *C. albicans*, and how lipid droplet regulation influences adaptability and virulence. I investigated the putative diacylglycerol acyltransferases Dga2p and Lro1, whose *S. cerevisiae* homologs are instrumental in the generation of the neutral lipid triacylglycerol from diacylglycerol. I identified a conserved functionality in the *C. albicans* homologs, with *dga2* and *lro1* Δ/Δ exhibiting reduced intracellular TAG and a double knockout halting TAG production entirely (4.1D). In *S. cerevisiae*, the sterol esterases ScAre1p and ScAre2p also exhibit acetyl-CoA:DAG acyltransferase activity [272]. My HPTLC analysis on the generated CaAre2p did not display reduced TAG production, suggesting that TAG acetyl-CoA:DAG acyltransferase activity is not conserved in CaAre2p (3.3). Disruption of TAG biosynthesis led to changes in phospholipid content during stationary phase, with comparably less of the major PC and PA in the *dga2/lro1*Δ/Δ (4.1D). The reduced intracellular PA content raised the notion that PL alterations could be due to a repression of UAS_{INO} controlled phospholipid biosynthetic genes [197]. However our transcriptomic data did not necessarily support this hypothesis, with no differential expression of UAS_{INO} controlled genes such as *CHO1*, *INO1*. *OPI3* observed (C). It should be taken into consideration that the transcriptomic profile of the wild type and *dga2/lro1*Δ/Δ strains were compared during the exponential growth phase, whereas differences in PL composition were identified at the stationary phase. To reconcile whether PL alterations were owing to transcriptional dysregulation

due to PA dysbiosis or otherwise, further work would need to be done.

Comparing transcript profiles of wild type and *dga2/lro1*Δ/Δ cells highlighted increased glucose transport, as well as upregulation of gluconeogenesis and funnelling of stored sugars toward DHAP and G3P production (C, 4.3). It is possible that, as *dga2/lro1*Δ/Δ lack stored TAGs typically utilized for de novo PL biosynthesis, there is a compensatory upregulation of glycolytic flux in an effort to assimilate FFAs and synthesise PA for PL biosynthesis during growth resumption. A simple way to investigate the effects of this may be to control glucose availability in the medium to determine whether *dga2/lro1*Δ/Δ cells are inherently slower growing or are slower to resume growth in glucose-deplete medium. Our HPTLC data suggested an elevated intracellular DAG during the stationary phase (3.1), which could presumably still be metabolised into PA and CDP-DAG for de novo phospholipid biosynthesis which poses the question as to why *dga2/lro1*Δ/Δ cells show hallmarks of a shift toward Kennedy biosynthesis of PE and PC, including increased expression of Git3 and Git4 choline transporters.

6.2 The putative TGL family members in *C. albicans* display conserved sterol ester hydrolase and Triacylglycerol lipase activity

In *S. cerevisiae*, TAG lipolysis is predominantly coordinated by ScTgl3p, ScTgl4p and ScTgl5p [279, 280]. Tgl homologs in *C. albicans* remain uncharacterized; in this work I generated knockouts of *TGL1* and *TGL2* A.3,A.4), two of the only *C. albicans* genes

with direct *S. cerevisiae* orthologs. The generated *tgl1* Δ/Δ strain displayed a significant reduction in sterol content synonymous with reduced sterol esterase activity (3.4A); this could suggest a conserved role for CaTgl1p in sterol ester mobilization, although I saw no correlating spike in SE concentration in the *tgl1* Δ/Δ cells.

In *S. cerevisiae*, Tgl2 has been described as having TAG lipase activity but is predominantly associated with mitochondrial lipid metabolism [416]. A *tgl2* Δ/Δ knockdown in *C. albicans* led to elevated intracellular TAG as well as an increased number of neutral lipid foci per cell (3.4,3.5). Although I did not conduct experiments to determine neutral lipid deposition, it can be surmised that in *C. albicans* Tgl2 exhibits TAG lipase activity similar to the *S. cerevisiae* homolog. *tgl2* Δ /Δ cells also showed almost double the concentration of PC, PI, PE, and CL species (3.4). Here I must consider the the impact that cell size might have on HPTLC data interpretation. During experimental design, cell culture for lipid extraction was normalised using OD_{600}. The *tgl2* Δ/Δ mutant cells are considerably larger than wild type cells, which might account for increased PL content; a more accurate method would have been to adjust cell pellets based on precise cell counts to ensure concentrations could be adjusted to reflect more precisely the amount of different phospholipids per cell.

6.3 Defective neutral lipid storage and mobilization alters *C. albicans* adaptability and virulence

6.3.1 TAG catabolism and virulence

Of the mutants assessed, only *tgl2* Δ/Δ cells displayed a reduction in virulence in the *Galleria mellonella* model (3.11). This may be a result in a defect in hyphal transition observed upon *TGL2* deletion. I observed that tgl2 Δ/Δ cells displayed a filamentation defect when grown in hyphal inducing conditions (spider agar and 10% serum supplementation + 5% CO2) 3.7,3.8). Whilst *tgl2* Δ/Δ cells were capable of filamenting, a large proportion of cells had developed at least 2 germ tubes by the 90 min timepoint, whilst wild type cells committed to 1 germ tube (3.8). This effect was far more pronounced in 5% CO_2, with over 50% of the *tgl2* Δ/Δ population displaying 2 or more germ tubes, shorter than the single germ tubes observed in wild type. There was also a very prominent morphological aberration apparent in a subpopulation of *tgl2* Δ/Δ cells, where they were found to have either multiple hyphae at once, or exhibited abnormal morphologies (3.9). A lack of filamentation on spider medium, alongside other filamentation defects upon exposure to serum and 5% CO_2, may be due to a polarity defect and dysregulated polarisome assembly. This could be the result of dysregulation of Ras1 activation, known to trigger Cdc42- mediated polarisome assembly [417], and as such the induction of, and subsequent abandonment of, germ tubes at several sites. CO_2 circumvents Ras1 for driving filamentation, instead activating Cyr1 cAMP production directly [53], so this may be why the more aberrant morphologies are absent in a combination

of serum and 5% CO_2; it would be prudent to investigate the cell morphology in media without serum where 5% CO_2 is the trigger to determine if the polarity defect is specific to Ras1-mediated filamentation. This filamentation defect is likely a contributing factor to the reduction in virulence in *G. mellonella*, however.

Another potential contributing factor lies in the sequestration of resources in *tgl2* Δ/Δ cells. An inability to mobilise TAGs to DAG and PA likely causes an over-reliance on generation of PL precursors from other sources (assimilation of exogenous fatty acids, for instance). *cho1* Δ/Δ cells are unable to generate PS, PE and PC through de novo PL biosynthesis and so depend on the Kennedy pathway biosynthesis of PE and PC, and this renders cells avirulent due to an inability to scavenge sufficient choline and ethanolamine to support itself [321]. I observed a reduction in chronological lifespan of *tgl2* Δ/Δ, which could be due to an inability to acquire sufficient resources from the media to support prolonged survival; this could translate to the *G. mellonella* assay where cells were less capable of adapting to the host environment to establish a foothold and kill the larvae.

6.3.2 TAG storage and virulence

The *dga2/lro1* Δ/Δ strain displayed a few characteristics that may impact virulence and pathogenicity. Firstly, I observed a reduction in hyphal growth rate and reduced commitment to filamentation, with approximately 25% of mother cells failing to show emerging germ tubes after 90 min of exposure to serum (4.2). Some studies have highlighted the necessity for appropriately localised pools of DAG and its relocalisation to a forming bud to ensure timely bud development in *S. cerevisiae* [231]. With elevated intracellular DAG and disrupted storage, a similar mechanism may lead to perturbation

of early germ tube emergence here. Our HPTLC data revealed reduced PA at stationary phase in the dga2/lro1 Δ/Δ mutant compared to wild type (4.1); it may be the case that, upon growth resumption there is a considerably slower resumption of PL biosynthesis owing to depleted PA leading to an Opi1 repression of UAS_{INO} PL synthesis genes. Another possibility is a generally slower shift to filamentous growth owing to the importance of TAG for rapid generation of PLs to support new membrane development. Further study would be required to appropriately determine the means by which hyphal growth and commitment to filamentation. I also observed a reduction in biofilm development in the *dga2/lro1* Δ/Δ mutant, although the differences in biofilm growth were only discernible when grown in 5% CO_2 (5.2). This raises the question as to whether this filamentation and biofilm defect is at all linked with Ras/cAMP/PKA signalling; comparing wild type to dga2/lro1 Δ/Δ transcript profiles during growth, I highlighted an upregulation of biofilm regulators *BRG1* and *ROB1* in dga2/lro1 Δ/Δ, as well as putative negative regulator of the adenylate cyclase Cyr1, *RAS2* (C). I highlighted a depletion in PS in dga2/lro1 Δ/Δ cells (4.1, so there is also a possibility that depletion of PS results in mislocalisation of Ras and inappropriate signalling in the *dga2/lro1* Δ/Δ as has been seen in mammalian tumour cell lines [385]. The impact that TAG and LD depletion has on Ras-mediated filamentation would require further investigation.

I also observed chemical sensitivities in the *dga2/lro1* Δ/Δ mutant, mainly to azole treatment, cell wall stresses such as Congo red and calcofluor white (4.4, 4.7), and an increased susceptibility to lipotoxicity induced by treatment with monounsaturated fatty acid POA (5.3). Combating the lipotoxic effects of FFAs is one of a lipid droplet's primary functions[347, 236]. Elevated free fatty acids and DAGs are associated with changes to the asymmetry of mitochondrial, ER and plasma membrane PL bilayers,

dysfunction and, if unable to adapt, necrosis [236, 418, 409]. Given *dga2/lro1* Δ/Δ already exhibit elevated FFAs (4.1), an increased susceptibility to POA is in line with our understanding of the importance of neutral lipid storage; inability to store exogenous POA in lipid droplets, coupled with increased FFA concentrations, ultimately triggers liponecrosis.

The loss of *DGA2/LRO1* function led to the upregulation of stress response pathways under typical growth conditions, including an upregulation of GPI-anchored superoxide dismutases Sod4 and Sod5 (C, 4.3), both of which have been linked to detoxification of the extracellular environment following exposure to oxidative stress [30]. It is possible that an inability to store TAG, and the corresponding elevation of free fatty acids and DAGs, reduces the cell's capacity for adaptation to stress. In line with this, when conducting transcriptomic analysis of wild-type and *dga2/lro1* Δ/Δ cell's responses to azole stress I observed an upregulation of the ergosterol biosynthesis pathway, in compensation of Erg11 inhibition by the drug in our wild type cells, including an upregulation of ergosterol transcriptional regulator *UPC2* ($\log_2$FC 1.47) (4.4,4.5). The upregulation of ergosterol biosynthesis upon fluconazole treatment was not observed in *dga2/lro1* Δ/Δ, with no significant upregulation of *ERG1* for the commitment of squalene to sterol production, no upregulation of *ERG11* to combat inhibition and whilst *UPC2* was upregulated, it was a considerably reduced response to the presence of the drug ($\log_2$FC 0.59). These findings, coupled with an upregulation of drug efflux pump coding gene *MDR1* in wild-type ($\log_2$FC 1.26), and no such upregulation in *dga2/lro1* Δ/Δ, suggest a reduced capacity for adaptation to fluconazole-induced stress. Under fluconazole stress, I also identified that wild type cells upregulate genes required for peroxisome biogenesis and to support its role in fatty acid β-oxidation. This response was largely absent in *dga2/lro1* Δ/Δ cells (4.6). β-oxidation of fatty acids supplements a high energy demand

and peroxisomes have been seen to actively develop on, and penetrate LDs [292, 289]. With the absence of LDs, it stands to reason that this source of fats for peroxisomal degradation may not be as readily available. Rapid biogenesis of peroxisomes is also contingent on a readily available source of PC [380], so peroxisomal biogenesis and fatty acid catabolism to support stress response may be slowed in a similar way that hyphal development is slowed in *dga2/lro1* Δ/Δ.

The loss of both DGA2 and LRO1 led to cell wall alterations and sensitivity to cell wall stress (4.7,4.8). One explanation for this may be that changes in lipid composition of the plasma membrane lead to changes in signalling that support cell wall construction. I observed an increase in phosphorylation of Mkc1 (4.7), the *C. albicans* MAPK responsible for coordination of cell wall integrity signalling; this could be the result of elevated DAG, a known Pkc1 agonist [419]. Phospholipid composition has also been linked to the tethering of MAPK activators and Rho-like GTPases in *S. cerevisae*, such as Rho1 and Cdc42 [387]. Given the observed unmasking in *dga2/lro1* Δ/Δ and polarity defects in *tgl2* Δ/Δ, the impact of glycerolipid storage and mobilisation on PL content, and the potential impact of that on mislocalisation of proteins involved in MAPK signalling and polarity should be considered and warrants further investigation.

PE is also an important precursor for GPI-anchor biosynthesis, and our *dga2* and *lro1* single knockouts showed significantly less PE than the wild-type (4.1). In the *dga2/lro1* Δ/Δ, PE levels were not significantly different to the wild type, though it should still be considered that total TAG disruption may impact upon PE availability. In this circumstance, there may be a scarcity of PE available for GPI-anchor biosynthesis; disrupted GPI-anchor biosynthesis could contribute to aberrant localisations of core cell wall biosynthesis and remodelling proteins and this in turn may underlie the observed cell wall changes. I also noted a comparably thinner mannan brush layer in the *dga2/lro1*

Δ/Δ mutant compared to the wild type, and a greater exposure of the PAMP β-1,3-glucan in the inner cell wall as a result (4.8). This had the added effect of increasing *C. albicans* susceptibility to recognition and phagocytic uptake by murine macrophages (4.9), alluding to a role for lipid droplet regulation in maintenance of masking PAMPs and *C. albicans* innate immune evasion mechanisms. These reductions in resistance to chemical stress, reduced capacity for filamentation and avoidance of innate immunity culminated in an overall decrease in virulence in a *G. mellonella* model (4.10). These findings suggest a significant role for glycerolipid metabolism in host-cell and cell-cell interactions that may prove important in environments where lipid levels fluctuate, such as the gut.

6.4 Lipotoxicity as an anti-fouling measure

This work also studied whether *C. albicans*' propensity to scavenge exogenous fatty acids could be manipulated as a means of bolstering pre-existing antifungal strategies and mitigating biofilm formation on medical devices. Following on from literature describing the dietary monounsaturated LCFA POA as inducing lipotoxicity in *S. cerevisiae* [409], I studied its impact on *C. albicans* biofilm formation. Combinatorial treatment of planktonic *C. albicans* with POA and fluconazole unveiled a synergistic anti-fungal action (5.5). The described mechanism of lipotoxicity-induced necrosis is a gradual increase in membrane permeability allowing for passage of small molecules [409], so POA treatment may allow for increased dose delivery of fluconazole. It is also possible, given that fluconazole targets ergosterol biosynthesis and as such likely alters membrane permeability, that fluconazole and POA synergise in disrupting *C. albicans* membrane. This finding supports the notion that POA, or potentially other LCFAs, could be used in conjunction

with azole class antifungals to support current treatment regimens. Inclusion of POA during lock therapy could lead to better fungal clearance in medical devices such as PEG tubes. I can also envisage the application of an ambisome-like delivery system with an encapsulation of fluconazole in a lipid nanoparticle comprised largely of POA, that following uptake into the cell is capable of impacting ergosterol biosynthesis coupled with lipotoxicity.

I highlighted an inhibition of biofilm formation if palmitoleic acid was included during the attachment phase of biofilm development (5.6). However, POA exposure did not affect biofilm formation if added to cells post-attachment. This suggests that any anti-biofilm effects of POA need to occur as a measure to prevent *C. albicans* biofilm establishment and not to limit its growth once established. There could also be a transcriptional shift following adhesion that focusses less on nutrient scavenging from the environment and more on rapid proliferation meaning the POA is not taken up as readily [88]. The effectiveness of POA in preventing adhesion may occur as a result of changes in hydrophobicity at the surface of the silicone tested, or a reduction in the efficacy of *C. albicans* adhesin-mediated adhesion. It is also entirely possible, given that the attachment phase is conducted in PBS and the maturation phase is in RPMI, that the observed anti-biofilm effect is an artefact of the assay; to discount this, biofilm work should be recreated with cell attachment being conducted in RPMI medium. However, in this work, I were also able to show that impregnation of silicone with dietary POA was able to inhibit biofilm formation (5.7). Anti-fouling coatings are an emerging topic of study, and our work supports the notion that dietary fatty acids could be used to coat certain medical devices to mitigate the risk of *C. albicans* colonisation.

Appendix A

Confirmation of CRISPR Cas9 generated mutations

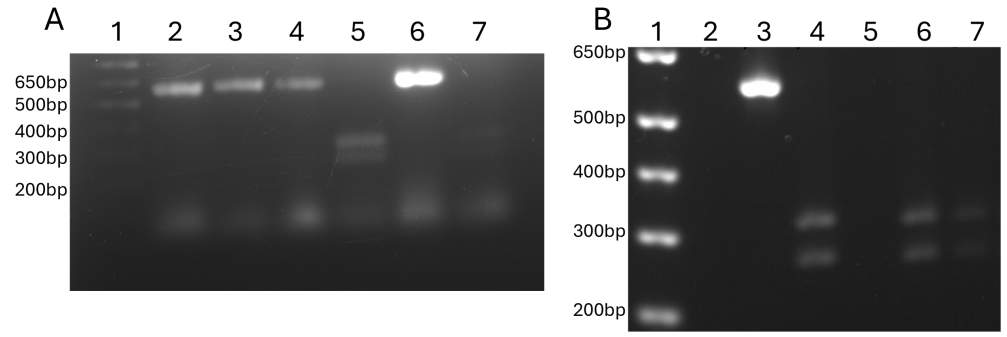

FIGURE A.1: **Colony PCR and digest confirmation of stop codon insertion to silence DGA2 in SN250 and SN250 *lro1***

(A). Colony PCR and digest screen for *DGA2* deletion in SN250. Gel layout- 1, 100bp ladder; 2-5, colonies 1-4; 6, Fragment digest from untransformed colony; 7, colony 5. Control and unsuccessful transformants have a 564bp amplified fragment; Colonies 4 and 5 display expected fragment sizes of 234 and 330bp following Esp3I digest, indicating successful replacement of PAM site with stop codon and Esp3I restriction site. (B). Colony PCR and digest for *DGA2* disruption in SN250 *lro1 δ/δ. Gel layout- 1, 100bp ladder; 2, empty; 3, fragment digest from untransformed colony; 4-7, colonies 1-4. Fragment sizes as in* ***(A)***

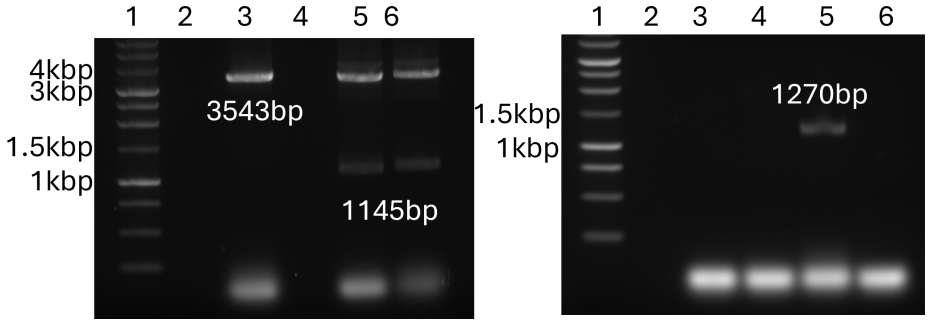

FIGURE A.2: **Colony PCR confirmation of HERNDAY Cas9 deletion of *SMP2* and *CHO1***

(A). Colony PCR confirmation of *smp2 δ heterozygote.* Gel layout- 1, 1kb ladder (promega); 2, empty; 3, negative control; 4, empty; 5-6, *SMP2 δ heterozygotes* with expected fragment size 1145bp. (B). Colony PCR confirmation of *cho1 δ/*Δ. Gel layout- 1, 1kb ladder (promega); 2, empty; 3-6, colonies 1-4. Lane 5 contains a successful colony with an expected fragment size 1270bp.

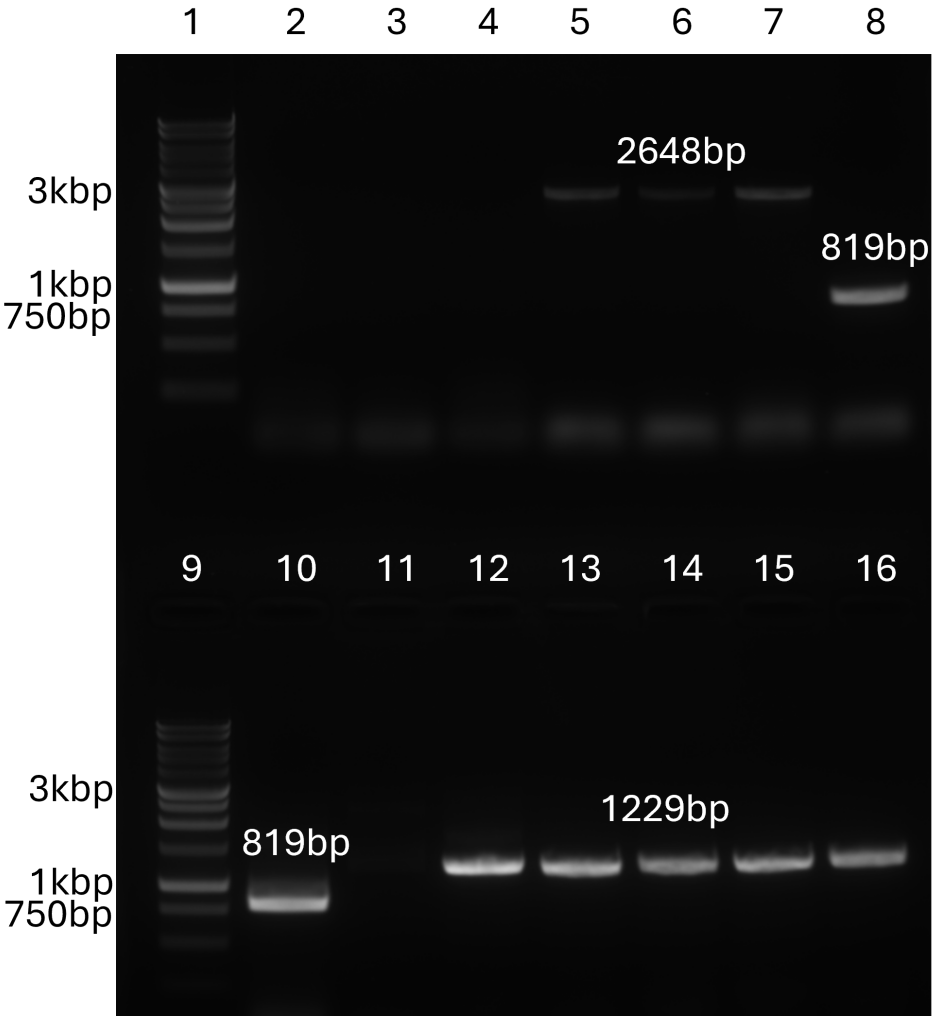

FIGURE A.3: **Colony PCR confirmation of HERNDAY Cas9 deletion of *ARE2* and *TGL1***

Gel layout- 1 and 9, 1kb ladder (promega); 2, empty; 3-8 and 10, Are2 transformant colonies; 11, empty; 12-16, Tgl1 transformant colonies. 8 and 10 show successful *are2* Δ/Δ transformants with expected band size 819bp. 12-16 show successful *tgl1* Δ/Δ with expected band size 1229bp

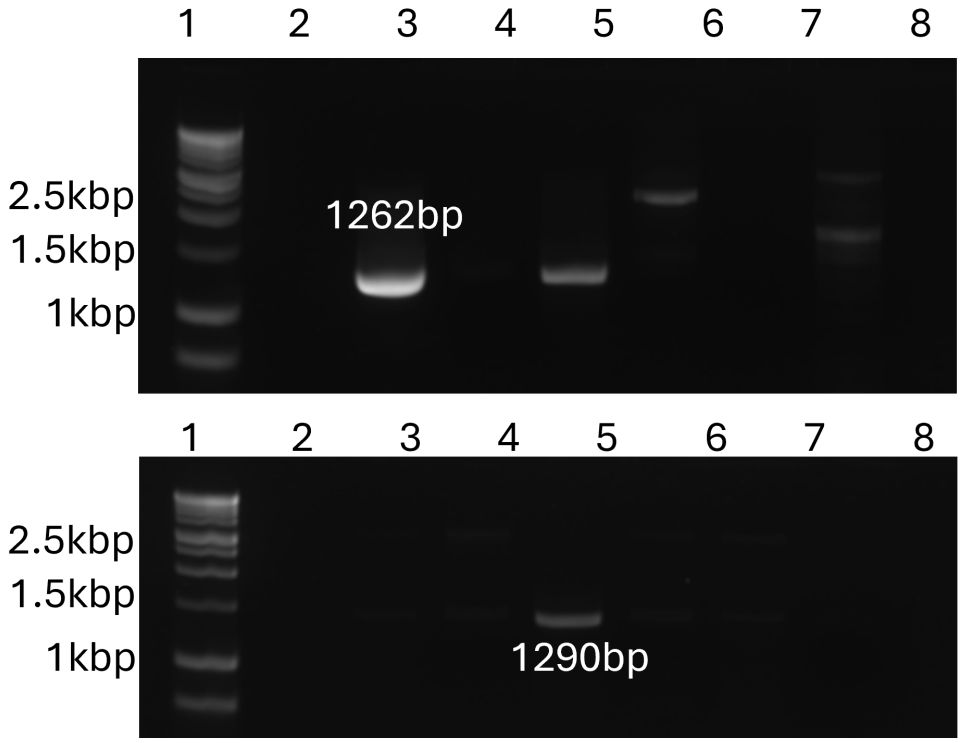

FIGURE A.4: **Colony PCR confirmation of HERNDAY Cas9 deletion of *TGL2* and *PSD1***

(A). Colony PCR confirmation of *tgl2* δ/Δ. Gel layout- 1, 1kb ladder (promega); 2, empty; 3-8, Tgl2 transformant colonies. Lanes 3 and 5 contain successful transformants with expected band size 1262 (B). Colony PCR confirmation of *psd1* δ/Δ. Gel layout- 1, 1kb ladder (promega); 2, empty; 3-8, Psd1 transformant colonies. Lane 5 contains a successful colony with an expected fragment size 1290bp.

Appendix B

HPTLC resolution of neutral lipids and phospholipids

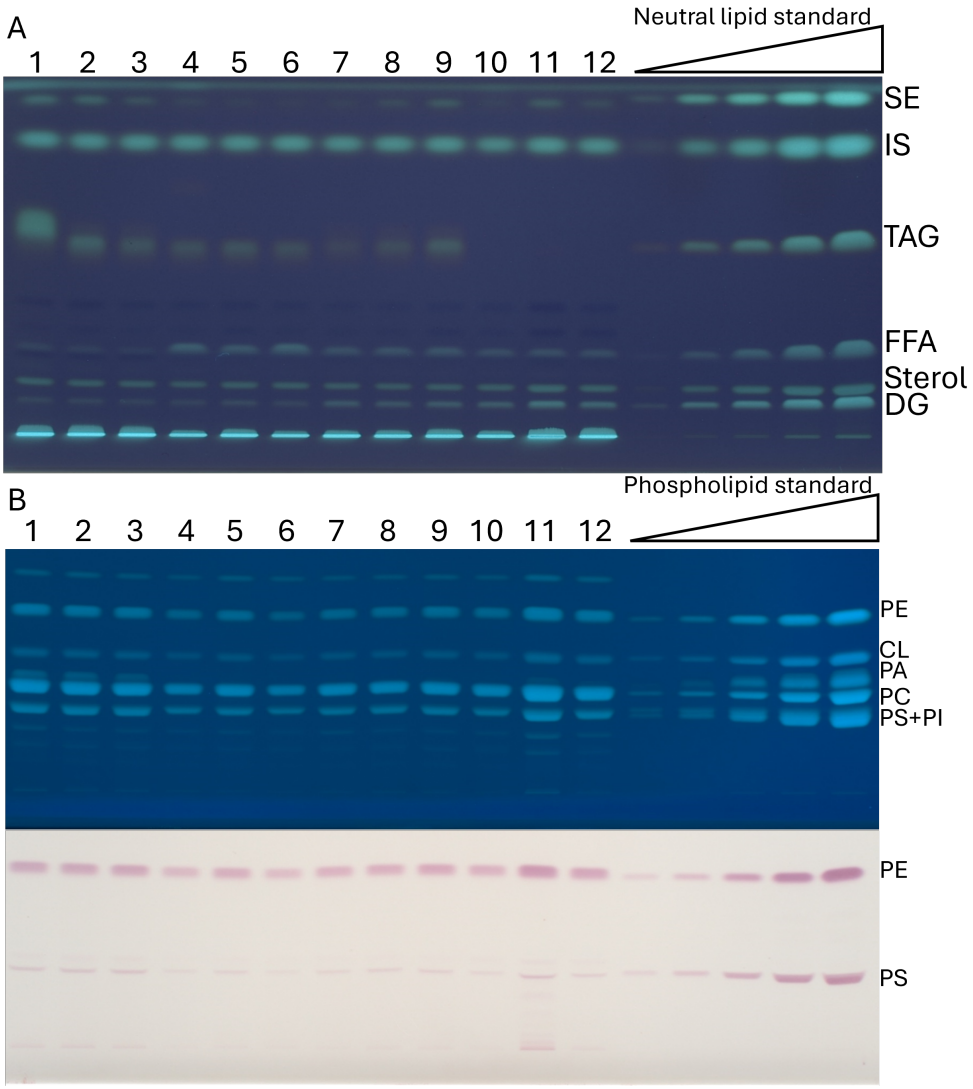

FIGURE B.1: **HPTLC resolution of neutral lipids and phospholipids-SN250, *dga2* Δ/Δ, *lro1* Δ/Δ and *dga2/lro1* Δ/Δ**

(A). Neutral lipid resolution, staining with primuline and imaging. Neutral lipid standard denotes bands for SE, IS (included internal standard), TAG, FFAs, sterols and DAG **(B)**. Phospholipid resolution, staining with primuline and ninhydrin prior to imaging. On the primuline plate, phospholipid internal standard bands denote PE, CL, PA, PC, and a combined PS/PI band. On the ninhydrin plate, phospholipid internal standard bands denote PE and PS. For both **(A)** and **(B)**, samples 1-3 are SN250 biological replicates, samples 4-6 are *dga2* Δ/Δ biological replicates, 7-9 are *lro1* Δ/Δ biological replicates and 10-12 are *dga2/lro1* Δ/Δ biological replicates.

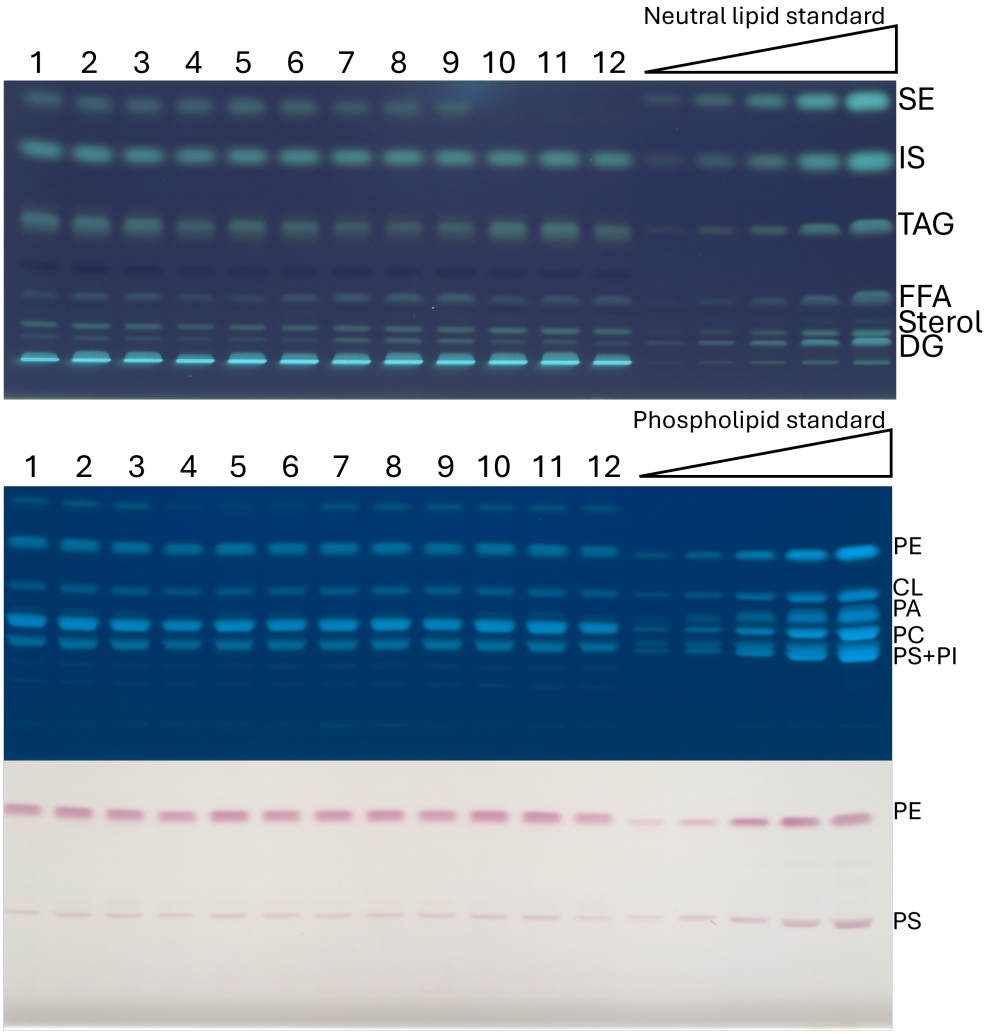

FIGURE B.2: **HPTLC resolution of neutral lipids and phospholipids- SC5314, *smp2* Δ, *lro1* Δ/Δ and *are2* Δ/Δ**

(A). Neutral lipid resolution, staining with primuline and imaging. Neutral lipid standard denotes bands for SE, IS (included internal standard), TAG, FFAs, sterols and DAG **(B)**. Phospholipid resolution, staining with primuline and ninhydrin before imaging. On the primuline plate, phospholipid internal standard bands denote PE, CL, PA, PC, and a combined PS/PI band. On the ninhydrin plate, phospholipid internal standard bands denote PE and PS. For both **(A)** and **(B)**, samples 1-3 are SC5314 biological replicates, samples 4-6 are *smp2* Δ biological replicates, 7-9 are *lro1* Δ/Δ biological replicates and 10-12 are *are2* Δ/Δ biological replicates

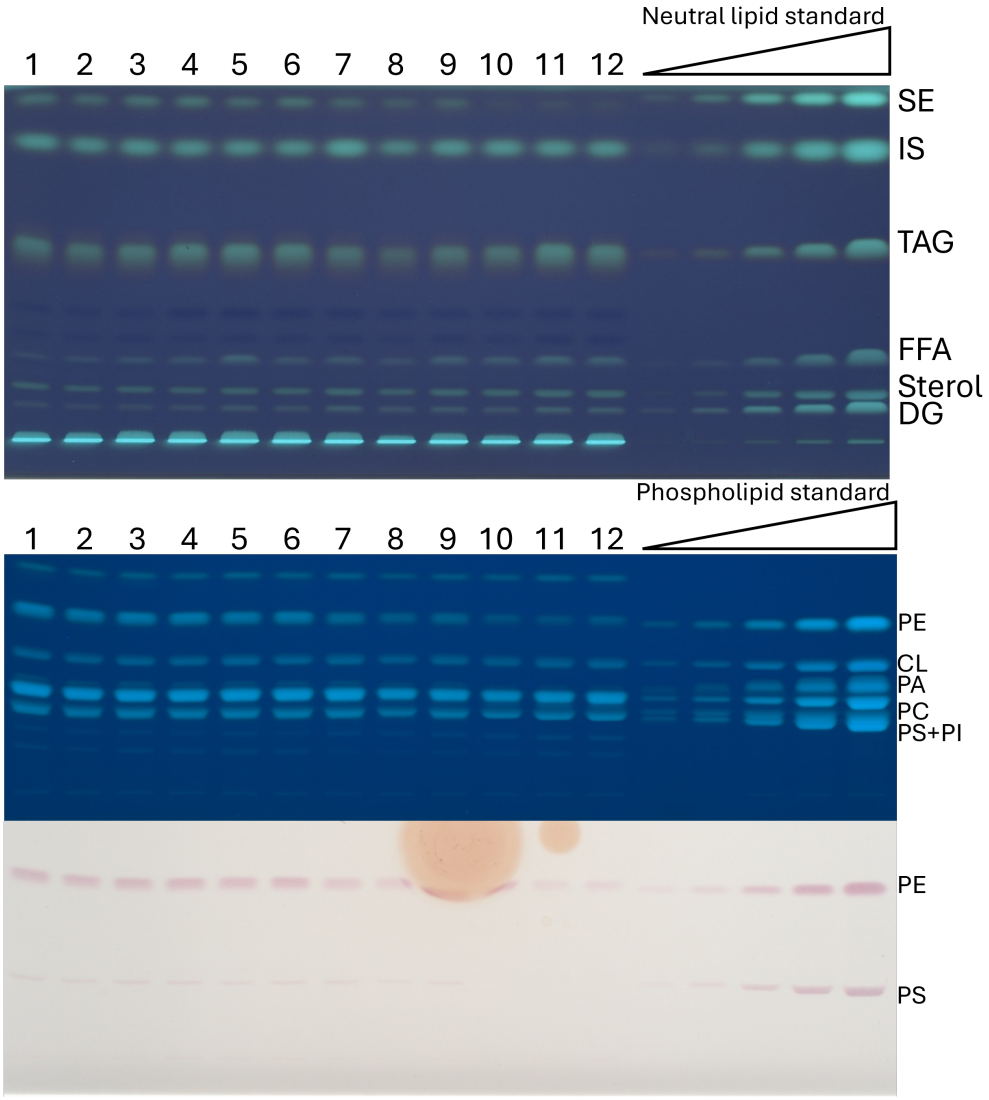

FIGURE B.3: **HPTLC resolution of neutral lipids and phospholipids-SN250, *dga2* Δ/Δ, *lro1* Δ/Δ and *dga2/lro1* Δ/Δ**

(A). Neutral lipid resolution, staining with primuline and imaging. Neutral lipid standard denotes bands for SE, IS (included internal standard), TAG, FFAs, sterols and DAG **(B)**. Phospholipid resolution, staining with primuline and ninhydrin prior to imaging. On the primuline plate, phospholipid internal standard bands denote PE, CL, PA, PC, and a combined PS/PI band. On the ninhydrin plate, phospholipid internal standard bands denote PE and PS. For both **(A)** and **(B)**, samples 1-3 are *tgl1* Δ/Δ biological replicates, samples 4-6 are *tgl2* Δ/Δ biological replicates, 7-9 are *psd1* Δ/Δ biological replicates and 10-12 are *cho1* Δ/Δ biological replicates

Appendix C

Genes differentially expressed following *DGA2* and *LRO1* deletion

Upregulated genes		Downregulated genes	
Gene name	L_2FC	Gene name	L_2FC
C2_10070W_A	7.870523023	PGA44	-3.804395449
AOX2	6.918686158	LRO1	-3.027517444
UCF1	6.495507367	SAP8	-2.849470779
C2_08300C_A	5.597156454	ATO1	-1.568733884
C1_11320C_A	5.576434099	C3_03760W_A	-1.0585471
C5_03770C_A	4.998238763	C5_04030W_A	-1.055008043
PCK1	4.899307565	C1_11410C_A	-1.029181652
YHB1	4.534032926	ANP1	-1.006842506
FDH1	4.451763042	C4_00490W_A	-0.999622963
STF2	4.28355684	FRP5	-0.883300684
QDR1	4.075027224	RMP1	-0.881006928
C6_03370W_A	3.986193323	PGA26	-0.86882434
C2_00760C_A	3.81023566	KTI11	-0.860458365
BLP1	3.322212992	RRN11	-0.850085051
BRG1	3.321271843	SMM1	-0.828915984
C5_03510C_A	3.17803801	POP3	-0.81209293
TPO3	2.941570007	C4_07170C_A	-0.798694763
PLB1	2.920146431	C1_12440W_A	-0.793204824
SUT1	2.882094383	C3_07650C_A	-0.791745082
C1_05160C_A	2.832036568	C6_03110C_A	-0.788483178
AOX1	2.773287191	C5_03150W_A	-0.781476409
RAS2	2.71786796	CR_02030C_A	-0.774613883
HPD1	2.583007906	SEN2	-0.772718478
C7_00310C_A	2.575277729	C2_09100C_A	-0.764807572
ADH5	2.547193329	CR_00810W_A	-0.761521283
HGT6	2.545654881	C3_02840W_A	-0.74891411
C6_01360W_A	2.528062306	C4_00810C_A	-0.740377781
C1_07160C_A	2.495482744	C7_02160W_A	-0.730436619
C3_06860C_A	2.453108942	C2_09920W_A	-0.729975875
MAE1	2.384176915	C1_07960W_A	-0.722818525
PHO112	2.365095621	CWC22	-0.722242249
FCR1	2.349603869	MAK16	-0.719306595
C4_00530C_A	2.266285761	C5_04840C_A	-0.718138222
ALS1	2.261963047	CR_03840C_A	-0.717810013
CR_07840C_A	2.238404779	POP4	-0.715295706
C7_00350C_A	2.214320685	C7_00330C_A	-0.706517646
C1_00270W_A	2.172370069	C4_07150W_A	-0.699808763
C4_05900C_A	2.15645158	C6_03440W_A	-0.697573948
PHO100	2.152645683	FYV5	-0.69323485
HAK1	2.139047738	ENP2	-0.691003589
C1_11270W_A	2.100673264	C6_03220W_A	-0.688949297
GAL10	2.095493515	C1_12570C_A	-0.688326276
WH11	2.081246107	C2_01050W_A	-0.688171697
C1_11850W_A	2.063288805	C2_05830C_A	-0.687835232
GIT4	2.023333953	C4_07160W_A	-0.687594772
POL93	2.007107911	C5_01710C_A	-0.686519899
CR_09350C_A	1.999874817	CR_01710W_A	-0.672805528

PDC11	1.999390772
C1_01510W_A	1.98925021
DAL5	1.985680812
HSP21	1.896281028
AQY1	1.868757081
ADH1	1.866227361
C1_08610C_A	1.82699525
DDR48	1.786321839
C1_14190C_A	1.770307534
STP4	1.743386597
GAD1	1.736438183
C7_01430C_A	1.733618212
MSN4	1.700889336
CDR4	1.67427772
C5_02110W_A	1.663533036
C2_07630C_A	1.643527606
C3_00360W_A	1.640212107
ALD6	1.637214424
C6_01780C_A	1.621807818
CR_09530C_A	1.598996014
TRY6	1.581764205
RBT5	1.57138956
HSP12	1.554506525
SOD5	1.531878007
GDH2	1.506390189
CR_07830C_A	1.487141791
MAL31	1.463672466
OSM1	1.462556753
CR_04820W_A	1.452792854
C6_02790C_A	1.439463797
INO1	1.438784787
ADAEC	1.432771711
GPH1	1.38658002
PTC8	1.368100763
RTA4	1.359307166
CR_10200W_A	1.352878642
MAF1	1.352756045
CR_00310C_A	1.343411023
GAP2	1.341751667
IFD6	1.333535255
CSP37	1.311992079
BMT9	1.298462834
SSU1	1.289691703
ECM21	1.285169923
HGT1	1.247899861
CYB2	1.236638254
IFE1	1.224251875
PXP2	1.21132289
MUM2	1.201859287
GAL7	1.199751336
HIT1	-0.669135309
C6_04240W_A	-0.665791263
C3_05380W_A	-0.665731821
C1_04510W_A	-0.662186764
CR_08470W_A	-0.661983595
C2_01060C_A	-0.660985015
C4_02260C_A	-0.66067574
MNE1	-0.657822704
NOP8	-0.655233685
C5_00250C_A	-0.654679337
SET6	-0.654203168
C1_07950C_A	-0.652381588
C2_08530C_A	-0.648858208
PZF1	-0.648780131
MUP1	-0.647220297
RSM22	-0.645180071
NOG2	-0.642500845
C6_01040C_A	-0.642212364
PPR7	-0.640611592
C7_03590C_A	-0.639258343
C2_02080W_A	-0.638183528
CR_01600C_A	-0.637048067
QDR2	-0.634371676
RLM1	-0.631826597
C1_13820C_A	-0.629084401
AEP3	-0.628614542
C7_01680C_A	-0.626427848
CR_06230W_A	-0.625368386
C3_01440C_A	-0.614438346
FGR39	-0.61275052
C1_12750C_A	-0.612404589
CCC2	-0.611909426
C1_10250C_A	-0.610446893
FTR1	-0.609951433
C3_01430W_A	-0.60666631
C4_01500W_A	-0.60604029
CR_07310W_A	-0.605225639
RRP9	-0.602919215
CR_04750W_A	-0.601879473
RAD4	-0.601478569
MSU1	-0.599409929
C1_09540W_A	-0.598379764
C3_05800W_A	-0.597647334
C2_04700C_A	-0.59745462
C3_04510W_A	-0.593412415
C5_02590C_A	-0.592319589
C3_02670W_A	-0.59034078
C1_05220C_A	-0.588062194
RPP1	-0.587327044

C1_07220W_A	1.194503197
CR_02880W_A	1.193751038
STB3	1.188390638
GAL1	1.186995459
CR_07160C_A	1.179692965
CRG1	1.176500093
C2_05770W_A	1.172100834
PRM9	1.163030329
SRR1	1.159041819
C4_00950C_A	1.156021422
BMT3	1.146069295
GAC1	1.139426077
C2_08950W_A	1.120345743
CR_09460C_A	1.120172766
BUB3	1.115956599
C7_02920W_A	1.109397509
C2_09710C_A	1.107109539
SUC1	1.105950329
GPX2	1.102917477
SMF13	1.093075222
CR_00600C_A	1.092727643
SDS24	1.090404787
DAL4	1.090381964
C7_03780C_A	1.085344627
C3_07280C_A	1.075548833
CDG1	1.057485562
CR_07480W_A	1.05065759
CR_04680C_A	1.046774049
IFF4	1.041140997
C2_00770W_A	1.029809106
GLK1	1.02826318
C1_03270W_A	1.027578214
C1_01710W_A	1.027223036
XKS1	1.02669068
SOD4	1.025274123
AMO1	1.015149633
CBF1	1.014116707
CR_03250C_A	1.012516412
C2_09590C_A	1.009567751
AGT1	1.001499738
C1_07450W_A	1.001128457
C2_06930C_A	1.000888371
CR_02570C_A	0.99840553
ASR2	0.988866456
ECM331	0.971803894
MNN44	0.971672543
OPT3	0.9671487
GIT3	0.966680967
C5_04470C_A	0.965680214
ZRT2	0.964553757

C3_01820W_A	0.962578121
C7_03580C_A	0.962260504
ASR1	0.960702288
RHR2	0.959781922
GEF2	0.957526702
GCY1	0.954486698
OSM2	0.952193515
PSA2	0.945798345
C5_04870W_A	0.932725844
CR_03260W_A	0.93146348
C3_06490W_A	0.925560534
C2_00740C_A	0.921649861
MSO1	0.91563744
FCY24	0.908882415
C6_02200C_A	0.902293921
IML2	0.895721072
PST2	0.891235168
TPS2	0.882411117
CR_03730C_A	0.875099724
WOR3	0.865934081
AIF1	0.863565178
ROB1	0.854708977
C6_02420W_A	0.853759883
UBP13	0.840570142
GSY1	0.839785741
LIP4	0.837717455
C4_03370C_A	0.833762711
MSN5	0.825547358
GRE2	0.825480587
NDE1	0.824263973
GAT1	0.81460311
C4_03190W_A	0.813724081
SMF12	0.805206963
APG7	0.796180123
SKN2	0.793668448
C5_05440C_A	0.787845285
C1_01340C_A	0.784506049
MHP1	0.784411585
GLK4	0.780506319
FDH3	0.777151884
IFF6	0.776669629
C1_10360C_A	0.774397182
PFK2	0.771678935
CR_02510W_A	0.77064423
CR_04490C_A	0.766310914
LEU1	0.763968906
C4_07210W_A	0.761156954
ZCF1	0.760074339
BNA31	0.757373944
XYL2	0.752214746

C7_03260C_A	0.75121281
C1_00630W_A	0.75037366
YAK1	0.749750374
PMP5	0.747681151
CR_03000C_A	0.747460748
C6_04420W_A	0.745553478
EVP1	0.744044504
CDR1	0.743514496
C2_09110C_A	0.741468479
C3_02630C_A	0.732999227
ARA1	0.731852331
C3_01950C_A	0.723449589
C2_03290W_A	0.72248589
CSO99	0.720234541
CUP1	0.718904745
C4_03600C_A	0.71601994
C2_02920W_A	0.714766842
ARR3	0.713473926
C4_03200C_A	0.711924048
DUG3	0.706143654
CR_05750W_A	0.705912127
C5_02690W_A	0.70543468
C1_11670W_A	0.694318927
CR_05460W_A	0.693162674
C1_01930W_A	0.688266347
GPM2	0.686483209
RIB3	0.686461154
C1_06970C_A	0.684312491
GAL4	0.683137513
C4_02690W_A	0.680360433
C1_10510W_A	0.672622044
AKR1	0.670520894
PHO15	0.668291407
C5_04540C_A	0.657739936
MNN15	0.651545213
CR_00090C_A	0.650653242
GNP1	0.648045398
YTH1	0.647221286
CDR11	0.64577898
C2_09680W_A	0.645369782
C2_09810C_A	0.643292321
C7_03240W_A	0.638799958
C1_10310W_A	0.638185654
C1_09000W_A	0.638154964
GYP7	0.636998313
OYE32	0.62970689
ZFU2	0.628043346
MODF	0.625346289
HMO1	0.622691912
C5_00100C_A	0.621261891

MCT1	0.620429019
RIM20	0.619923513
ASR3	0.617499142
DLD2	0.613310323
C2_00940W_A	0.612070129
CR_09050C_A	0.610948501
CR_09140C_A	0.608751395
C1_14030W_A	0.607158756
CR_00220W_A	0.606992042
C2_00490W_A	0.605113546
REG1	0.598488882
C3_03160C_A	0.596947443
C3_03430C_A	0.596052621
C2_08770C_A	0.59255564
C2_03170W_A	0.590160482

Appendix D

Genes differentially expressed by Wild-type cells following fluconazole treatment

Upregulated genes		Downregulated genes	
Gene name	L_2FC	Gene name	L_2FC
SAP4	6.527863132	C1_00310W_A	-0.817359936
RBR1	5.89438627	C1_00520W_A	-0.659003639
CTN3	4.938907872	ASM3	-1.195656331
CTN1	4.772229763	IHD2	-1.124040479
TRY4	4.620465594	C1_02470W_A	-0.784955006
ICL1	4.572762703	PMM1	-0.645577861
PGA31	4.513015901	tR(UCU)4	-1.635482602
HGT12	4.326271931	MNN44	-0.704561188
HGT19	4.16125851	TPS2	-0.609542217
LDG3	3.901484312	PDR16	-0.830675396
GAP2	3.868380554	C1_03960C_A	-0.618147631
C7_02260W_A	3.840865109	C1_04220C_A	-0.651885972
PGA23	3.743243933	SSA2	-1.260340722
JEN2	3.568288792	SYG1	-0.927511224
C4_03310C_A	3.565457692	C1_04930C_A	-0.864326351
CR_01220W_A	3.540791352	C1_05540C_A	-0.979555086
C3_06660C_A	3.519112908	PGA26	-0.938603904
HGT10	3.508389797	POL32	-0.639777208
SOU2	3.429247429	PRN2	-0.698278164
HGT2	3.357029847	PRN3	-0.615372146
ASR1	3.332008128	PRN4	-0.910276212
SAP6	3.288633334	C1_05950C_A	-0.884632121
C1_00190C_A	3.236557274	C1_06270W_A	-0.907302944
CR_08830W_A	3.06309028	GAP4	-1.098494791
CR_06550C_A	3.049661128	C1_07160C_A	-1.249806772
C7_02280W_A	3.029626105	YMC1	-0.868196952
CMI1	3.026505141	PHO15	-0.655063918
ADR1	2.937829704	GPX3	-0.757893462
C2_10020C_A	2.925595101	C1_07490C_A	-0.67889589
CR_03580C_A	2.918698161	C1_07810C_A	-0.633411969
HXT5	2.874186402	C1_08240C_A	-0.780255909
C1_11260C_A	2.75567959	C1_08350C_A	-0.666312283
C3_05820W_A	2.730044821	SAM4	-0.79366833
C2_10160W_A	2.702764623	CAF16	-0.621580504
PHR2	2.672075034	C1_08440C_A	-0.701885302
CR_04820W_A	2.650447704	EAF6	-0.642394092
HAK1	2.638545822	YMC2	-0.663343709
C7_02010C_A	2.634975261	TPO3	-1.139300069
ZCF25	2.54581357	C1_08900W_A	-0.86792116
C2_02220C_A	2.505755158	DAK2	-0.95862341
C4_05200C_A	2.416601621	CRP1	-1.450966202
PBR1	2.402229312	HCM1	-1.265892151
MLS1	2.369443234	PHO8	-2.084561064
SOU1	2.362336237	ALP1	-0.667789534
CR_07170W_A	2.358182053	C1_11100W_A	-0.587440974
C5_04380C_A	2.293414345	TOS4	-0.995118642
XOG1	2.290169041	PHO84	-0.63120658

IFF11	2.283745927	BTA1	-2.991546281
PIR1	2.277260978	ZCF3	-0.656411537
C1_04460C_A	2.268540894	KIP4	-0.628516667
C2_03020C_A	2.26673594	C1_12110C_A	-0.782578228
HGT17	2.255341018	MCD4	-0.870487324
C3_01540W_A	2.205161338	CDC6	-0.861213432
SFC1	2.177907902	RIB3	-1.182554919
C5_00530W_A	2.160846522	C1_12370W_A	-0.744407497
C2_06630C_A	2.147794387	MSH6	-0.762866215
ERG6	2.138872863	HSP70	-0.83371696
C4_04540C_A	2.100476564	C1_13820C_A	-0.811654177
C3_03460C_A	2.091327578	MET3	-1.257860996
WH11	2.072678538	C1_13950C_A	-0.836508656
HGT13	2.067138217	C1_14180W_A	-0.814213423
FOX2	2.04756153	C1_14190C_A	-0.626523091
DAG7	2.042139532	FTR2	-0.710726219
ZCF4	2.041092706	SAS2	-0.718671078
DDR48	2.035557309	PHHB	-0.654618179
C4_02930W_A	2.031346084	C2_00760C_A	-0.805861364
TEF4	2.023577455	C2_00790C_A	-0.697648566
C2_02910W_A	2.011569	HGT6	-0.889045933
CAN1	2.001792712	SRD1	-1.361812773
ZCF16	1.979140689	SAM37	-0.72712165
C6_04420W_A	1.978830341	ZRT2	-1.011045066
C2_08170W_A	1.952498478	C2_02660W_A	-1.198977324
GNP2	1.949865847	PDR17	-1.134633926
FTH1	1.932533736	MET1	-0.807229285
C3_01230C_A	1.927253959	SMP3	-0.634836424
TNA1	1.911570965	RIM2	-0.646137733
CRZ2	1.899961356	ARH2	-0.721495982
C6_00890W_A	1.880281465	tD(GUC)5	-1.260489792
PXP2	1.858521418	ABP2	-0.777798717
C3_01060W_A	1.837698661	SGO1	-0.870841375
C3_02570W_A	1.832753927	DAD2	-0.748883607
ATO6	1.82880283	CDC7	-0.615231134
PMC1	1.822309132	C2_05570C_A	-0.664648642
HGT1	1.809981278	CDC46	-0.67424308
C1_10240C_A	1.798550788	C2_06440C_A	-0.965995808
RTA2	1.789849579	C2_06520C_A	-0.766562617
PGA7	1.788198246	C2_06570C_A	-0.631225929
C6_00730W_A	1.785555803	GIT1	-2.160143056
ATO9	1.778858683	C2_06920C_A	-0.687668087
AGP2	1.776662413	HSH49	-0.622889114
C1_11200W_A	1.767607804	C2_07420W_A	-0.603114711
C7_01170C_A	1.750426027	RNR22	-0.793946399
AAP1	1.726221986	PHO86	-0.894596992
TES15	1.724912663	ORF298	-0.623691089
C4_06470W_A	1.713584143	C2_08300C_A	-0.653899403
ATO5	1.701863092	MET10	-0.874976443
SAP9	1.701231353	C2_09630C_A	-0.790549728

C1_01510W_A	1.691352552	PMI1	-0.739122488
CR_06650C_A	1.689754413	C2_10130W_A	-0.834042234
PDK2	1.66869133	GPD1	-0.645306935
AQY1	1.664990526	ZSF1	-1.31320682
C7_03280C_A	1.63962271	C2_10790C_A	-0.658001152
C1_02040C_A	1.636313903	TLO7	-0.683362846
SET3	1.633770884	C3_00170C_A	-1.013625661
MRV8	1.629052612	C3_00360W_A	-1.216490308
PGA37	1.617880226	C3_01620W_A	-0.725713008
C3_00210C_A	1.614369472	C3_01820W_A	-0.659813399
FGR22	1.610493121	C3_02270W_A	-0.654820888
RPN4	1.607387322	C3_02330C_A	-1.297300538
C1_02270C_A	1.584775377	C3_02360C_A	-0.628626737
ADH2	1.582721865	CCP1	-0.819004146
DIP5	1.577432949	SLC1	-0.72058297
PLC2	1.573411939	DAL5	-1.036900616
CR_07250C_A	1.562598848	C3_03210W_A	-0.647305883
STP4	1.561514109	tE(UUC)1	-1.571110153
FRP1	1.557822602	NDE1	-0.601607955
C1_00880W_A	1.547845961	POL1	-0.738601756
OPT4	1.546802865	MEA1	-0.597819817
C4_00860C_A	1.545571213	C3_05280C_A	-0.638764696
FOX3	1.537306856	C3_05450C_A	-0.65079631
LIG4	1.534327539	TRM12	-0.608712241
GTT13	1.53219025	C3_06140W_A	-0.767264917
C1_11850W_A	1.525485535	OPI3	-0.596582706
C1_11270W_A	1.520206703	TRY6	-1.332076148
C1_07990C_A	1.51553775	PGA32	-0.790149977
SPO11	1.514581226	BMT1	-0.671159151
C5_00600C_A	1.508481107	C3_07590W_A	-0.661229636
PGA10	1.507722442	C4_00530C_A	-3.737774993
C1_04470C_A	1.505825101	CSP2	-1.098217351
ERG251	1.503101219	PTC8	-0.959567636
HAP41	1.498755973	ASK1	-0.589044692
FMO1	1.495928345	AAT22	-1.251716806
FAA2-1	1.492375662	C4_01240C_A	-0.850660905
C7_01430C_A	1.490665168	NAT4	-0.931825811
HGT8	1.483164182	PGA53	-0.687948758
CRZ1	1.472373541	ZCF27	-0.947790495
UPC2	1.467210725	TIM12	-0.651393215
CR_00290W_A	1.465930897	C4_01760W_A	-0.90804866
BMT7	1.464655676	POL30	-0.747313369
C1_03150C_A	1.450528392	PHO89	-1.119529294
CHO1	1.447388539	SUL2	-1.687507368
C3_02140C_A	1.44078673	SEN2	-0.873066691
SLP3	1.437360699	RBT7	-1.574145615
C3_01130C_A	1.430976794	VTC4	-0.859357184
SIP5	1.42968603	C4_03370C_A	-0.820700793
C2_07630C_A	1.428046526	C4_03960W_A	-0.765283997
C4_05250W_A	1.418760662	C4_04160W_A	-0.979418775

POT1	1.404861343	C4_04230W_A	-0.667267167
ECS1	1.401720313	MRP8	-0.79880657
IPK2	1.394947123	XKS1	-0.898085109
CAT2	1.394087912	CFL1	-0.631532942
MRV2	1.39329385	PRI2	-0.780904064
C7_01700W_A	1.388532246	PDC11	-1.32008605
CAT8	1.385240259	CBF1	-2.011986771
C7_03310W_A	1.384126233	CCJ1	-0.835745432
MIT1	1.37624249	ZRT101	-0.934806779
SGA1	1.374221444	PRA1	-0.853751891
C4_04140W_A	1.372685127	C4_07080C_A	-0.950536795
C6_00810C_A	1.351706528	C5_00400C_A	-0.587071812
TRY5	1.349158593	MET14	-1.175897951
BLP1	1.341308755	THR1	-0.870276204
C4_02620C_A	1.336616493	CTF8	-0.926046771
C4_02740W_A	1.336331251	GIT4	-2.592189794
C3_07100C_A	1.33124641	GIT2	-0.691625415
CR_07700W_A	1.329431553	TRY3	-0.84359884
ARG1	1.32916058	C5_01590W_A	-0.913446997
C2_08620W_A	1.325200052	C5_02330W_A	-0.736259401
HOL4	1.312104112	MNN1	-0.983204748
C5_01260W_A	1.311679657	C5_02640W_A	-0.644392655
HYR1	1.300320565	C5_02850W_A	-0.585346749
C2_02390W_A	1.297677466	SUT1	-0.729565301
C2_09880C_A	1.297492312	C5_03170C_A	-0.616480816
RTA3	1.292146593	C5_03440W_A	-0.835641508
HPD1	1.285443573	C5_03740W_A	-0.87012174
RBR2	1.283780584	C5_03780C_A	-0.802048972
RBT5	1.27682429	GUK1	-0.866473765
CRG1	1.271089904	CHT2	-0.603292672
C4_02720C_A	1.266111874	GDE1	-0.605210067
PGA58	1.262665016	CUP1	-0.953273053
MDR1	1.262388023	CRH12	-0.805809361
C6_00930C_A	1.261866743	PFK1	-0.717709674
C6_02650C_A	1.260480868	PGA4	-0.631935717
ALK8	1.259036803	C6_00080C_A	-0.645273614
PEX11	1.257831856	C6_00090W_A	-0.601598538
IML2	1.256555829	PGA48	-0.76741025
IFR1	1.24911968	FET31	-0.674041348
C3_05750C_A	1.248912683	CAN3	-0.967598332
IRF1	1.24678307	GPX2	-0.980877825
FAA2-3	1.244468512	GPX1	-0.719120115
PEX1	1.242677066	C6_00980C_A	-0.874888038
PEX6	1.226735981	RIM9	-0.975833118
SRG1	1.214538558	C6_01360W_A	-2.082781608
ALD6	1.21166548	OYE23	-1.828418798
C2_08510W_A	1.209905697	MAE1	-1.419634724
SLD1	1.205972504	C6_01780C_A	-1.383949592
ZMS1	1.190480196	C6_01960W_A	-0.687695587
OYE22	1.188002663	CTF5	-0.829900568

ERG27	1.173740222	C6_02200C_A	-1.067374679
IFD1	1.172318703	C6_02330W_A	-1.258694219
CPA1	1.170045468	C6_03090W_A	-0.893254746
C1_12910W_A	1.164456589	AYR2	-1.093844459
SEF2	1.160709112	C6_03300C_A	-0.669656992
C3_02870C_A	1.155091141	C6_03310W_A	-1.227467591
CR_02300C_A	1.154150969	IHD1	-0.95945589
HAP3	1.152064983	C6_04230W_A	-0.876093126
ARG8	1.146744286	NAG3	-1.43048456
RBT4	1.135937627	C7_00240W_A	-0.596147069
C1_10140C_A	1.134157344	FGR2	-2.564063377
IFU5	1.132892914	C7_00630C_A	-0.779516586
HRQ2	1.130161153	C7_00770W_A	-0.599912432
C6_03260W_A	1.125714391	MCM1	-0.678113885
C2_09280C_A	1.1240426	C7_00910C_A	-0.786890294
C3_06680C_A	1.123256907	C7_01500W_A	-0.674499799
GCA2	1.122675154	KCH1	-0.603438676
HSP12	1.120854177	RNH35	-0.679531345
SPO1	1.120834331	C7_01650W_A	-0.808983287
IFF4	1.119188794	PFK2	-0.909743908
HGT4	1.118686044	HSP90	-0.707698855
PEX7	1.113835189	DPP3	-0.810060596
ERG1	1.112345249	C7_02610C_A	-0.68276117
C4_00080C_A	1.112133458	PRX1	-0.811270736
C2_06890C_A	1.10649942	DBF4	-0.60530498
C1_06000W_A	1.103604079	C7_03040W_A	-0.730204448
C6_01490C_A	1.09974888	C7_03200C_A	-0.962256641
ZCF21	1.09919266	SNG3	-0.813336135
CAT1	1.098727427	C7_03610C_A	-0.765989033
CR_07140C_A	1.096881153	ATP9	-3.879697643
C2_10000C_A	1.096255426	NAD2	-4.955806346
C5_05360C_A	1.091895804	CR_00310C_A	-0.745194827
CRH11	1.087849144	CR_00380W_A	-0.853641145
CR_05750W_A	1.07935332	PHO81	-1.09276578
C1_07220W_A	1.077726742	CR_01440C_A	-1.032125322
ATO10	1.075280494	RSR1	-0.60639281
AGC1	1.071091623	PHO113	-1.796265843
ECM38	1.070915174	ALG5	-0.671635039
RCT1	1.069141313	VTC3	-0.824576681
OSH2	1.06858184	SCR1	-1.063990052
SFP1	1.062767646	FUM11	-0.624379568
ECI1	1.058594709	DIT2	-0.832725106
ERG24	1.057606826	DIT1	-0.859361771
CR_08670C_A	1.057348226	CR_05760C_A	-0.804264839
SVF1	1.05373356	CR_05770W_A	-0.801963076
RSN1	1.052890965	PGI1	-0.63718511
PST3	1.052675385	CR_06570C_A	-0.950932903
C1_12830C_A	1.050574433	CFL11	-0.636238215
COQ4	1.047748786	CR_06790C_A	-0.671637749
C5_02220C_A	1.03807078	CR_07740W_A	-1.194477589

C3_05680W_A	1.034096093
C5_02110W_A	1.033545214
C2_03110W_A	1.031016767
C5_04940W_A	1.0300371
CSP37	1.027988919
CIT1	1.026382272
MNN42	1.024252376
EHD3	1.023373065
GCY1	1.020644356
UGA6	1.017251525
CYB2	1.016990732
ZCF13	1.013880054
KRE1	1.013068984
CAN2	1.010601024
RHD1	1.008213714
C1_11950W_A	1.007084994
PRC2	1.006509751
RIM8	1.005408878
PNG2	1.002234027
ANT1	1.001074848
C1_13100W_A	1.000610819
C2_00940W_A	0.986753757
BUL1	0.986418476
CR_04870C_A	0.9861598
CR_03510W_A	0.985128941
C1_12140W_A	0.984031243
C4_04250W_A	0.982104133
C3_04210W_A	0.979900327
OMA1	0.978064691
C4_01300W_A	0.970357847
C7_01940C_A	0.969642742
MIG1	0.967260653
MDM34	0.966654508
SFL1	0.966512511
PTP2	0.96647908
C7_01390W_A	0.966312169
PGA62	0.963639449
MUC1	0.961107379
CR_09100C_A	0.960069514
ASR2	0.959122077
ERG11	0.958075258
NRG1	0.955264857
C3_00400C_A	0.953929049
C3_05760W_A	0.949140872
ZCF6	0.948227633
C1_07530W_A	0.946154588
KRE6	0.945259347
AGT1	0.94293063
C2_05820W_A	0.940969549
BIO2	0.938297445
YHB1	-0.947793959
ASF1	-0.893779538
MPS1	-0.626679144
CR_09060W_A	-0.980597029
CR_09070C_A	-1.358648973
FCY24	-0.764010714
CR_09530C_A	-1.104735574
YKE2	-0.617703746
ALO1	-0.740950129
DEF1	-0.620328313
CR_10200W_A	-1.49915492
CR_10460W_A	-0.59123342
MCD1	-0.676302639

GAP6	0.937617092
ARG5,6	0.936025541
PCL5	0.93594255
C1_05480C_A	0.934498061
GUT1	0.927079547
SHE9	0.922627787
C3_04330C_A	0.922290251
C4_03300C_A	0.9158182
GDH2	0.91526695
IRS4	0.912829933
ECM331	0.912469551
ZCF15	0.912456162
C6_02020C_A	0.908552882
CWH8	0.906223574
CR_03780C_A	0.903507255
C3_07760C_A	0.903214456
NCP1	0.897727143
C4_04660C_A	0.897314784
CR_06040W_A	0.896783637
C3_02790W_A	0.895646594
CR_04220C_A	0.893467416
ERG3	0.893368223
CR_08920W_A	0.893358614
SCW11	0.891352436
ERG5	0.890645084
PEX4	0.887798001
C1_07980C_A	0.887306254
PXA2	0.886670387
C5_01300C_A	0.884083964
CR_09610C_A	0.883508832
DAO1	0.879483147
MSC7	0.874321704
FMA1	0.869458953
SOD6	0.867902214
INN1	0.86716034
PHO87	0.863958224
C4_02920W_A	0.86264617
MNN4	0.861225107
C2_07220W_A	0.861178781
LEU42	0.860841499
SSU1	0.858617891
ARD	0.856657454
C3_07330W_A	0.856570552
HAP31	0.854572935
C3_04800C_A	0.853439144
ERG7	0.853258071
MOH1	0.85045795
OSM2	0.847993833
CR_06010W_A	0.84740516
ZCF11	0.84529136

PEX8	0.843223384
C1_04580C_A	0.841451711
SAC6	0.839996885
CAS5	0.838999312
PXA1	0.835796
RGS2	0.834767424
ARE2	0.833687767
ECM22	0.82987935
CPA2	0.829151455
CR_04120C_A	0.829090552
C6_00290W_A	0.827931793
DOT5	0.824726306
RHD3	0.824399555
C6_02210W_A	0.820299697
C3_06490W_A	0.818952146
CR_04280C_A	0.818182626
PIS1	0.814687711
OXR1	0.812086936
C3_04920C_A	0.811756795
EFH1	0.811604831
C2_04110W_A	0.810705598
C2_07270W_A	0.809818522
C5_05200C_A	0.809045215
C1_14060W_A	0.806602069
WOR1	0.805413768
HOS3	0.80520679
C5_03490C_A	0.804532055
KNS1	0.801133466
C3_06860C_A	0.798701797
ALS1	0.79856412
SAC7	0.797382087
PMP5	0.797125601
LYS144	0.791532897
C3_05330C_A	0.790584477
ORM1	0.789033773
C7_03780C_A	0.788675663
MNN46	0.788447603
TCA17	0.787724993
ADAEC	0.787420188
C7_01690W_A	0.78388595
C2_05990C_A	0.782749531
HGT3	0.782434025
FBP1	0.781664646
C4_05440C_A	0.78058226
DSE1	0.777282384
CTA4	0.775571327
C7_01670W_A	0.774646729
FRP3	0.774480957
C1_00860W_A	0.773895949
C3_05360C_A	0.773643568

C1_13430C_A	0.773420325
C5_04350C_A	0.772499913
C3_03370C_A	0.771903253
C2_00740C_A	0.771640593
FAV1	0.771321862
ERG2	0.767859147
FUM12	0.767399927
C1_05160C_A	0.764720134
FAA21	0.763719222
C1_11010C_A	0.759667887
LEU1	0.756413874
YDC1	0.75633741
C1_10410W_A	0.755906097
C1_08770W_A	0.753394894
C2_08330W_A	0.752954799
NTG1	0.751766454
GUT2	0.751435958
PGA13	0.750639373
ERG26	0.75047735
ACF2	0.749843361
C1_11280W_A	0.749513177
C6_03590C_A	0.748769936
C6_03050C_A	0.746851872
UGA2	0.741115797
CRC1	0.737623383
VPS21	0.735484757
LEU5	0.732024728
GLK1	0.731364853
C2_00510W_A	0.728258995
LRO1	0.727941508
PUT2	0.72750026
C1_11690W_A	0.726875975
ERG4	0.725972706
PEX12	0.725452748
POX1-3	0.725197332
C3_07380W_A	0.725057973
CHA1	0.723090006
C6_02030C_A	0.719420192
ASR3	0.715873047
RAS2	0.715786733
SPS20	0.71441906
BTS1	0.714198118
IFG3	0.713877988
GPD2	0.713480636
C2_05860C_A	0.711365517
MDH1	0.711058141
SOK1	0.706867444
C1_04700C_A	0.706687102
C3_07070C_A	0.705588018
C5_02520W_A	0.705523059

C7_02160W_A	0.705455273
C1_13250W_A	0.701347057
ECM42	0.69918876
HAP42	0.698992728
SLY41	0.698296871
C4_00750C_A	0.697329418
C1_11930W_A	0.695502711
MODF	0.695345907
SKO1	0.693740222
HGT5	0.693561306
NSG2	0.692760401
C1_01490W_A	0.691730714
CHS2	0.69123007
PTC6	0.690839364
C6_03470W_A	0.69010575
IFF5	0.689956614
C3_06940W_A	0.689952
C1_09060C_A	0.689695456
C6_02450W_A	0.687842
PEX2	0.687720241
C2_09030W_A	0.687138246
WOR4	0.685296727
ECM7	0.68222563
DLD1	0.681655771
C2_09980W_A	0.680243092
RGT1	0.679517038
HIP1	0.679251117
PGA52	0.678528663
FAD1	0.675193122
VPS51	0.67338065
CBR1	0.671653314
DFG5	0.670918251
PLB3	0.67006685
C2_06710W_A	0.669022156
C7_03860W_A	0.668461601
ALK2	0.667597264
C1_11890W_A	0.666084905
C7_02290W_A	0.665598807
CR_05450C_A	0.664893005
RIM101	0.664026662
ATC1	0.663084034
CSU57	0.662929751
CR_07160C_A	0.662445403
C1_04640W_A	0.662405871
ARL3	0.661008052
FAV2	0.658345411
BPH1	0.657689307
RIM111	0.65755231
ORC3	0.655604062
C2_07790C_A	0.654116695

C1_02210W_A	0.651176276
C4_00320C_A	0.650948542
RIM15	0.649658232
C2_01870C_A	0.649151475
C6_00800C_A	0.648970829
VRP1	0.647133822
C3_06670C_A	0.646223106
C6_03180C_A	0.644144271
GLK4	0.643108856
C7_02170C_A	0.642924574
RAD14	0.642791565
ALT1	0.64209559
PRB1	0.639563961
C7_01320W_A	0.639080847
ZNC1	0.63689474
INO4	0.636030986
RGA2	0.634384641
TPK1	0.63399911
CR_05880W_A	0.633497175
ERG25	0.633482437
C6_03040C_A	0.631000716
CDC21	0.630588222
ALD5	0.63038136
C3_04260W_A	0.629293107
C1_06920C_A	0.627736843
CHT3	0.627679433
C5_04260W_A	0.62572407
HSE1	0.624676655
C6_02560W_A	0.624056192
ERG10	0.623798763
CR_01260W_A	0.621203403
YBH3	0.620966972
AKR1	0.620396786
CR_02270C_A	0.619963857
PEX13	0.619712043
C2_10600W_A	0.618800227
ERG9	0.61763563
ADH5	0.616517035
C4_02770C_A	0.61502969
BCR1	0.615021609
C5_01440C_A	0.613960196
MYO5	0.613902239
C4_00070C_A	0.613251718
SCP1	0.61308905
C3_01570W_A	0.610095092
FAV3	0.609708168
MDM12	0.605677822
ABP1	0.604885296
C3_07370W_A	0.604874319
C4_00500W_A	0.603483989

C2_03290W_A	0.602962689
C2_08910C_A	0.600739161
GUP1	0.599899723
PTR22	0.598522833
C2_03500W_A	0.59640595
SDS24	0.596281129
CR_04860C_A	0.595315894
HGT16	0.594472471
ZTA1	0.594425289
C1_02060W_A	0.594231346
ZCF23	0.592880531
C1_00810W_A	0.591376922
CR_05900W_A	0.589514229
C2_09960W_A	0.58818704
C3_05510W_A	0.587868517
HEM14	0.587543277
MSO1	0.587394893
C2_09930W_A	0.586798508
COQ6	0.586125146
ATG11	0.586094112
CR_05980W_A	0.585977749
FLC2	0.585350032

Appendix E

Genes differentially expressed by *dga2/lro1* $\triangle/\triangle$ cells following fluconazole treatment

Upregulated genes		Downregulated genes	
Gene name	L_2FC	Gene name	L_2FC
tR(CCU)1	7.20976677	C1_00310W_A	-0.672828762
RBR1	4.21894343	UGA32	-0.648003992
PBR1	3.554394412	IHD2	-0.745020653
HAK1	3.4837051	C1_01360C_A	-0.950668577
PGA13	2.833790495	C1_01930W_A	-0.729200126
OP4	2.728955275	C1_02470W_A	-0.702974455
SAP4	2.714330678	PUT4	-0.669677124
CR_06550C_A	2.657769549	TPS2	-0.703872734
PGA39	2.640335383	C1_03510C_A	-1.187950139
C1_11270W_A	2.413233543	C1_03750W_A	-1.299392255
C6_04420W_A	2.363335708	PDR16	-0.733268199
C3_06660C_A	2.352280566	C1_03960C_A	-0.715684453
PGA23	2.34544728	ACS2	-0.651742909
HGT2	2.282904684	GPM2	-0.701291934
C1_11260C_A	2.248280184	DUR1,2	-0.632912792
C7_04080C_A	2.241517907	PRD1	-0.658406261
MRV2	2.219733279	C1_05540C_A	-1.127715031
DAG7	2.213463431	PGA26	-1.3428887
SOD5	2.156540154	PRN2	-0.947481396
C1_01310W_A	2.119079655	PRN4	-0.766494886
PIR1	2.116198776	C1_05950C_A	-0.993452317
C4_04540C_A	2.079536375	C1_06250W_A	-0.61820846
C1_11320C_A	2.070275052	C1_06270W_A	-0.659200873
C4_06910W_A	2.038279032	C1_06320W_A	-0.948651645
RTA2	1.968792406	GLT1	-0.610908318
C4_05200C_A	1.957725953	C1_06870C_A	-1.208367494
C2_02220C_A	1.931101495	C1_07040C_A	-1.195937272
C2_10160W_A	1.92193902	GAP4	-1.242269571
SAP9	1.917190343	YMC1	-0.599796657
ASR1	1.885274705	C1_07480C_A	-1.244660758
WH11	1.87147882	C1_07650W_A	-0.730410468
C2_10020C_A	1.836702452	MED15	-0.605072997
C1_06620C_A	1.832128934	SAM4	-0.722258769
C3_04450C_A	1.821713491	CAF16	-0.916751807
PMP5	1.7716014	ENO1	-0.814003734
CTN3	1.769725924	C1_08780W_A	-0.690569907
PGA37	1.742733265	TPO3	-1.030959191
C2_02910W_A	1.701210274	C1_08900W_A	-1.143568623
FTH1	1.676625168	DAK2	-1.192878035
C2_08620W_A	1.664808674	CRP1	-1.085002787
PMC1	1.65239976	URA1	-1.014020116
C1_02690C_A	1.631823462	HCM1	-0.684726128
C2_00940W_A	1.623890174	LIP3	-1.656309952
C2_03020C_A	1.615616461	C1_09930W_A	-0.740364864
IFD1	1.613351107	PHO8	-1.343366057
ICL1	1.600977019	ALP1	-0.821835046
C1_00190C_A	1.600619812	C1_10820C_A	-0.759358141

RHD1	1.586888488	TOS4	-0.644032794
C3_02710W_A	1.561683742	GIN1	-0.753516936
C2_00670C_A	1.549740042	PHO84	-0.800582247
C4_00860C_A	1.530943157	C1_12000C_A	-1.10650045
C6_00810C_A	1.520078234	KIP4	-0.618411067
C5_04470C_A	1.516497316	LCB4	-0.639908436
C1_04470C_A	1.516047856	RIB3	-1.62322957
CR_04820W_A	1.503471161	C1_12370W_A	-0.747232273
XOG1	1.487379266	C1_12720C_A	-1.160909781
C7_02010C_A	1.473643047	MSH6	-0.615389006
C5_04480C_A	1.464929502	KIS2	-0.74372373
C1_07990C_A	1.464549939	FTR2	-1.092919099
CRZ1	1.445729503	C1_14630C_A	-1.343227937
C6_03670C_A	1.441652986	C2_01250W_A	-0.666372832
HGT8	1.432743469	C2_01420C_A	-0.614933279
C1_06000W_A	1.43093036	C2_01540W_A	-1.013580221
AAP1	1.421628111	C2_01800W_A	-0.616000462
AGP2	1.416459452	SRD1	-1.036545838
PST3	1.404380808	C2_02050C_A	-0.821320503
SLP3	1.385112634	SAM37	-0.888821626
C7_01700W_A	1.383722588	C2_02660W_A	-0.791572022
CR_06040W_A	1.378794262	C2_02930C_A	-0.690988502
ADH2	1.369818035	RNR21	-0.813279497
C3_02570W_A	1.368744056	C2_03260W_A	-0.585747687
CHO1	1.36291545	GPM1	-1.242252344
ERG6	1.344632292	C2_04360W_A	-0.81052615
C3_02140C_A	1.339733573	IFA4	-0.736279376
RPN4	1.334536711	CDC19	-1.350691473
IFU5	1.314218862	MKK2	-0.617706323
C2_06630C_A	1.300369522	ECM17	-0.743893787
C4_06470W_A	1.292887196	CIS302	-0.589005017
C1_05160C_A	1.28936313	C2_06570C_A	-0.916473273
PHR2	1.27241418	GIT1	-1.028037012
C4_02720C_A	1.267400589	PHO86	-0.714083255
MRV8	1.267359293	ORF298	-0.701028545
PLC2	1.266682089	C2_08260W_A	-1.829540302
IML2	1.24320601	PST2	-1.135352151
INN1	1.240473643	C2_09070C_A	-0.637350893
CR_00290W_A	1.231555918	C2_09100C_A	-0.658617252
DDR48	1.230049476	C2_09420W_A	-0.977914647
CRZ2	1.229407248	C2_09820W_A	-0.852247756
NRG1	1.227590985	C2_10130W_A	-0.759245385
C1_04460C_A	1.225450764	ACS1	-0.873423446
IPK2	1.222877065	FGR6-4	-0.623511751
CWH8	1.201895123	TPS3	-0.791478831
TES15	1.201810268	C2_10790C_A	-0.677063865
MNN46	1.197815533	C3_00170C_A	-0.708322002
TEF4	1.188186183	DAL1	-0.897083968
CHS2	1.165735951	HRK1	-0.76505841
C2_09880C_A	1.165152962	C3_00790W_A	-0.66229207

ITS1	1.162919391	ATO2	-0.849932392
CSH1	1.162523677	ARF3	-0.839227151
HAP41	1.160012471	C3_01620W_A	-0.768488479
HGT1	1.158724656	C3_02330C_A	-0.733001682
FRP1	1.157404837	CCP1	-0.999004927
CAN1	1.153646746	SLC1	-0.673798389
PGA7	1.137351232	DAL5	-1.185002029
C1_10240C_A	1.125686265	tE(UUC)1	-1.789673017
PGA58	1.124191919	FCY2	-1.017923956
CR_07170W_A	1.112463808	POL1	-0.775186095
C1_03150C_A	1.109899072	TEC1	-0.69412541
CR_06650C_A	1.099970169	MEA1	-0.698525402
SAC6	1.095290276	C3_05290C_A	-0.93254135
RCT1	1.090942135	GPI1	-0.612923865
ECS1	1.088925636	C3_05450C_A	-1.118702529
C2_08170W_A	1.083056563	C3_05880C_A	-0.653086798
SIP5	1.066590778	C3_06270C_A	-0.709785235
C1_01510W_A	1.064961722	TRY6	-1.288103377
C1_14060W_A	1.061589033	TDH3	-0.78584182
HOS3	1.048190765	PGA32	-0.606533903
C2_04670W_A	1.042983711	BMT1	-0.734475457
C7_01170C_A	1.040092183	C3_07240W_A	-0.985462812
STP4	1.039680866	TPI1	-1.009539752
RTA3	1.034754617	EVP1	-0.828628106
PLB3	1.027690073	C3_07590W_A	-0.729674647
MDM34	1.017947745	RCH1	-0.867276907
RBT5	1.011261992	PCT1	-0.596994358
PUT1	1.01067211	CSP2	-1.367332897
TPK1	1.002327903	C4_00730C_A	-0.861560506
CR_02300C_A	0.997492347	AAT22	-0.949284029
RBT1	0.99662054	C4_01240C_A	-0.901430924
C1_10140C_A	0.994526283	NAT4	-1.259287618
C4_04140W_A	0.994214222	PGA53	-0.775776645
C1_11850W_A	0.990966442	ZCF27	-1.276233039
C4_04660C_A	0.984427864	HRT2	-0.781772619
C6_03260W_A	0.980854933	C4_01730C_A	-0.68321935
C1_10580C_A	0.980701079	TIM12	-0.777705875
SHA3	0.978182955	FBA1	-1.260452141
C3_06680C_A	0.975753591	C4_01760W_A	-1.24988765
HAP3	0.963632992	POL30	-0.758121165
C1_12140W_A	0.954882277	PDC12	-0.858932535
C6_00930C_A	0.954154357	C4_01860C_A	-0.749883177
FUM12	0.951501154	RFX2	-0.64856955
CCH1	0.946215924	GPI14	-0.992856815
CSP37	0.943840375	AHP1	-0.783720439
CAS5	0.93786324	SUL2	-1.543729174
C3_02790W_A	0.932692983	GST2	-1.044341289
IFG3	0.931069993	VTC4	-0.651722197
C1_10590W_A	0.93019387	C4_03370C_A	-0.704570323
PGA62	0.927620393	ECE1	-0.605964662

ADR1	0.927514434	C4_03960W_A	-1.197438121
C5_02110W_A	0.907388402	C4_03990C_A	-0.805450638
CR_07480W_A	0.902805464	C4_04160W_A	-0.592699203
SCW11	0.901046139	AXL2	-0.603335079
C1_02040C_A	0.893701195	C4_04230W_A	-1.075514777
C4_05810W_A	0.892022424	C4_04620C_A	-0.934336085
MNN47	0.885851433	C4_04950W_A	-0.819008143
GUT1	0.882962434	XKS1	-1.024948701
C2_02390W_A	0.874539281	C4_05350W_A	-0.869518629
ERG251	0.86774386	C4_05390W_A	-0.662315754
GUT2	0.862979058	ARO9	-0.749491607
SDS24	0.862167131	GAT1	-1.0138568
ECM22	0.861295991	AGO1	-0.778065396
HRQ2	0.856851272	PDC11	-1.27899218
IFD6	0.85271613	C4_06660W_A	-0.863340904
CR_02880W_A	0.84234231	C5_00100C_A	-0.64804029
FRE9	0.840035234	IFF8	-0.639680273
CR_09100C_A	0.839702288	GIT2	-0.601166366
RAS2	0.83840391	TRY3	-0.605289344
C7_01360C_A	0.836099794	C5_01220W_A	-0.69014527
SCP1	0.832384901	C5_01590W_A	-1.040422654
PGA52	0.828470503	C5_02690W_A	-0.925099293
MIT1	0.82231415	GRE3	-0.750966052
C1_07980C_A	0.81974918	RUT1	-0.669676263
C7_01390W_A	0.819045645	C5_03210C_A	-0.885729908
C2_10730W_A	0.816976496	C5_03740W_A	-0.842448247
C4_02330C_A	0.815964565	C5_03780C_A	-1.071865904
MUC1	0.814316687	C5_03810C_A	-0.698799875
PGA57	0.811583072	C5_03970W_A	-0.677060644
C7_02370W_A	0.805663616	C5_03980W_A	-0.601661358
YCP4	0.805342018	CRH12	-0.920859807
RBE1	0.802771706	PFK1	-1.197708413
C1_04580C_A	0.802458968	ADH1	-0.778921432
C3_03460C_A	0.802256359	PGA4	-0.639016868
PUT2	0.798587881	FET34	-0.592363913
HSP12	0.79504312	FET31	-1.402423883
QCE1	0.79399793	COX15	-0.995886766
SAP6	0.789029559	PGK1	-1.354203221
C1_06480C_A	0.786620649	SUN41	-0.586980043
GTT11	0.786168318	GPX1	-0.703083194
CR_09040W_A	0.781731464	RIM9	-0.6103728
SFL1	0.781090761	EBP1	-1.257251461
PYC2	0.779272638	C6_01360W_A	-1.383331513
C7_03310W_A	0.777503226	C6_01400W_A	-1.020565319
HAP31	0.77556153	C6_01470W_A	-0.771240313
C5_00850C_A	0.770929548	OYE23	-2.204373947
IRS4	0.770309915	FMP27	-0.767373247
ALS1	0.769155725	C6_01780C_A	-0.663813058
HOL4	0.758920842	C6_01870C_A	-0.93045827
RCN1	0.757988011	CTF5	-0.934811895

BIO2	0.75550838	C6_02200C_A	-0.75617042
SAP10	0.751878967	C6_02330W_A	-0.896058055
AKR1	0.750379599	SAP5	-0.985725719
MIG1	0.749249199	C6_03090W_A	-1.226811829
FAA2-1	0.749130348	AYR2	-1.66706335
C3_04330C_A	0.743442065	C6_03320W_A	-0.818385634
SGA1	0.74335665	IHD1	-1.147606939
CHT4	0.74216556	C6_03990C_A	-0.630833457
FOX3	0.741765315	ALS2	-0.589244567
C4_02740W_A	0.740826068	NAG3	-1.31884836
C2_08330W_A	0.739526355	C7_00240W_A	-0.59562182
C7_01690W_A	0.734948817	C7_00270W_A	-0.595579425
C6_00890W_A	0.734882668	FGR2	-1.684887095
ALK2	0.733623899	C7_00630C_A	-0.867118787
C2_05040C_A	0.731768579	C7_00910C_A	-0.710493096
MOH1	0.731292433	GPH1	-0.868863261
BPL1	0.728397219	C7_01150W_A	-0.774271369
GDH2	0.727117257	NUP	-0.861832604
PTP2	0.724459121	C7_01650W_A	-0.910421841
MDH1-1	0.722173084	PFK2	-0.865871946
CRH11	0.715612656	C7_02540W_A	-0.616788362
C2_08510W_A	0.714060164	C7_02600C_A	-1.173200915
CWP419	0.713336048	C7_02610C_A	-1.969364692
C2_07270W_A	0.713276018	C7_02920W_A	-0.942223918
ERG25	0.712438155	C7_03040W_A	-0.79142182
FLC2	0.709767298	C7_03200C_A	-0.896729537
C5_05440C_A	0.708909736	RBR3	-0.601603602
C6_02210W_A	0.707210998	SNG3	-0.902833816
LIG4	0.703236912	C7_03480W_A	-0.725657242
PCL5	0.701302034	C7_03610C_A	-0.841982188
PGA1	0.700931826	C7_03830C_A	-0.603738079
ZCF16	0.698303138	C7_04160W_A	-0.677345076
C1_01490W_A	0.696819556	PHO81	-0.792159981
SFP1	0.694530576	ACC1	-0.744657114
C2_00920W_A	0.694318939	GSY1	-0.965761742
C2_04750W_A	0.693884983	TEN1	-0.665008277
ZMS1	0.693033862	CWH43	-0.5932889
SFC1	0.692030622	LYS12	-1.014284608
CR_05450C_A	0.691434275	MCM6	-0.647720221
C1_11200W_A	0.689957547	PHO113	-1.194885696
SPS20	0.683771126	OPT4	-1.86584375
C4_01300W_A	0.683345465	RFG1	-0.741403521
C2_05960C_A	0.681042018	PGA34	-0.816358788
SSU1	0.680715357	CR_02780W_A	-0.798250104
SIM1	0.676764772	PGM2	-1.043067625
CIT1	0.67638219	CR_02960W_A	-0.683429978
PDE2	0.675307132	VTC3	-0.794643485
C1_13100W_A	0.666496777	IFF3	-0.730325488
ACF2	0.663077662	MCM2	-0.708564948
C7_01670W_A	0.661282913	DAP1	-0.689708374

CHT1	0.66104647
C4_02620C_A	0.659621869
PNG2	0.655037002
C1_08610C_A	0.652200177
C5_01560C_A	0.651054398
VPS1	0.649886652
C5_01200W_A	0.649282954
C6_03370W_A	0.648535335
MNN4	0.645364745
ERG27	0.64456189
C3_07760C_A	0.643001008
CRD2	0.642324622
ATO5	0.64223992
PDK2	0.640379419
C4_00080C_A	0.639669672
CHS7	0.635175115
GFA1	0.634466647
EBP7	0.634230759
BMT4	0.634176278
FAV3	0.633477304
C1_10410W_A	0.632214063
CR_07160C_A	0.630708511
C1_04340C_A	0.624866194
AGC1	0.623328419
RIM8	0.622363463
RGA2	0.617618809
VPS24	0.615105842
C5_03510C_A	0.611918376
OMA1	0.611646176
TEA1	0.608369772
MYO5	0.607510636
CR_02940C_A	0.607284961
ENA21	0.605022417
C2_08830W_A	0.604412927
COQ4	0.603139401
PAM16	0.602160885
C5_05360C_A	0.602116202
RRN3	0.598854199
VPS51	0.595829714
SLD1	0.594033384
C4_02770C_A	0.593796527
UPC2	0.592413156
ERG2	0.590764178
CAT2	0.587594765
C6_00800C_A	0.585034843
DIT2	-0.927261766
DIT1	-0.912546553
INO80	-0.58663554
CR_04940W_A	-0.780041524
TPS1	-0.758984368
CR_05760C_A	-0.835395642
CR_05770W_A	-1.039048538
PGI1	-1.020936176
CR_06380C_A	-0.606695648
CR_06500C_A	-0.698747526
CR_07220C_A	-1.303748215
CR_08300C_A	-0.587517384
CR_09060W_A	-0.627137253
CR_09070C_A	-1.37636486
CBP1	-0.975475559
CR_09930W_A	-0.651497594
CR_10200W_A	-1.384354972

[1] Neil A.R. Gow and Bhawna Yadav. "Microbe profile: Candida albicans: A shape-changing, opportunistic pathogenic fungus of humans". In: *Microbiology (United Kingdom)* 163 (Aug. 2017), pp. 1145–1147. ISSN: 14652080. DOI: 10.1099/mic.0.000499.

[2] Betty Hebecker et al. "Pathogenicity mechanisms and host response during oral Candida albicans infections". In: 12 (2014), pp. 867–879. ISSN: 17448336. DOI: 10.1586/14787210.2014.916210.

[3] Christina Lemberg et al. "Candida albicans commensalism in the oral mucosa is favoured by limited virulence and metabolic adaptation". In: *PLOS Pathogens* 18 (4 Apr. 2022), e1010012. ISSN: 1553-7374. DOI: 10.1371/JOURNAL.PPAT.1010012.

[4] B. Anne Neville, Christophe d'Enfert, and Marie Elisabeth Bougnoux. "Candida albicans commensalism in the gastrointestinal tract". In: *FEMS yeast research* 15 (7 Nov. 2015). ISSN: 1567-1364. DOI: 10.1093/FEMSYR/FOV081.

[5] Pizga Kumwenda et al. "Estrogen promotes innate immune evasion of Candida albicans through inactivation of the alternative complement system". In: *Cell Reports* 38 (Jan. 2022). ISSN: 22111247. DOI: 10.1016/j.celrep.2021.110183.

[6] Kalyan Pande et al. "Passage through the mammalian gut triggers a phenotypic switch that promotes Candida albicans commensalism". In: *Nat Genet* 45.9 (2013), pp. 1088–1091. DOI: 10.1038/ng.2710.

[7] Rebecca A. Hall and Mairi C. Noverr. "Fungal interactions with the human host: exploring the spectrum of symbiosis". In: *Current Opinion in Microbiology* 40 (Dec. 2017), pp. 58–64. ISSN: 18790364. DOI: 10.1016/j.mib.2017.10.020.

[8] Betsy Foxman. "Urinary tract infection syndromes. Occurrence, recurrence, bacteriology, risk factors, and disease burden". In: *Infectious Disease Clinics of North America* 28 (Mar. 2014), pp. 1–13. ISSN: 08915520. DOI: 10.1016/j.idc.2013.09.003.

[9] Cecelia Tibaldi et al. "Vaginal and endocervical microorganisms in symptomatic and asymptomatic non-pregnant females: Risk factors and rates of occurrence". In: *Clinical Microbiology and Infection* 15 (2009), pp. 670–679. ISSN: 14690691. DOI: 10.1111/j.1469-0691.2009.02842.x.

[10] Nelson L. Rhodus. "Treatment of oral candidiasis." In: *Northwest dentistry* 91 (2012), pp. 32–33. ISSN: 00292915.

[11] Massimo Petruzzi and Fedora Della Vella. "Treatment of oropharyngeal candidiasis in immunocompetent and immunocompromised patients". In: *Frontiers in Physiology* 10 (2019). DOI: 10.3389/conf.fphys.2019.27.00085.

[12] M. Bacon. "Oral thrush due to antibiotic therapy: report of four cases". In: *The Journal of the Maine Medical Association* 44 (Oct. 1953), pp. 284–286. ISSN: 00250694.

[13] Manoela Domingues Martins et al. "Oral Candidiasis". In: *Clinical Decision-Making in Oral Medicine: A Concise Guide to Diagnosis and Treatment.*

Springer International Publishing, Jan. 2023, pp. 73–80. DOI: 10.1007/978-3-031-14945-0{_}11.

[14] Julie Toubiana et al. "Heterozygous STAT1 gain-of-function mutations underlie an unexpectedly broad clinical phenotype". In: *Blood* 127 (June 2016), pp. 3154–3164. ISSN: 15280020. DOI: 10.1182/blood-2015-11-679902.

[15] Jari Intra et al. "Prevalence and species distribution of microorganisms isolated among non-pregnant women affected by vulvovaginal candidiasis: A retrospective study over a 20 year-period". In: *Journal of Medical Mycology* 32 (Aug. 2022). ISSN: 17730449. DOI: 10.1016/j.mycmed.2022.101278.

[16] Kaitlin Benedict et al. "Survey of incidence, lifetime prevalence, and treatment of self-reported vulvovaginal candidiasis, United States, 2020". In: *BMC Women's Health* 22 (Dec. 2022). ISSN: 14726874. DOI: 10.1186/s12905-022-01741-x.

[17] Bojan Nedovic et al. "Mannose-binding lectin codon 54 gene polymorphism and vulvovaginal candidiasis: A systematic review and meta-analysis". In: *BioMed Research International* 2014 (2014). ISSN: 23146133. DOI: 10.1155/2014/738298.

[18] Maria Dulce Kaoro Horie Wojitani et al. "Association between mannose-binding lectin and interleukin-1 receptor antagonist gene polymorphisms and recurrent vulvovaginal candidiasis". In: *Archives of Gynecology and Obstetrics* 285 (Jan. 2012), pp. 149–153. ISSN: 09320067. DOI: 10.1007/s00404-011-1920-z.

[19] David W Williams et al. "Interactions of Candida albicans with host epithelial surfaces." In: *Journal of oral microbiology* 5 (Oct. 2013). ISSN: 2000-2297. DOI: 10.3402/jom.v5i0.22434.

[20] C. Logan, I. Martin-Loeches, and T. Bicanic. "Invasive candidiasis in critical care: challenges and future directions". In: *Intensive Care Medicine* 46 (Nov. 2020), pp. 2001–2014. ISSN: 14321238. DOI: 10.1007/s00134-020-06240-x.

[21] Hui Chen et al. "The regulation of hyphae growth in Candida albicans". In: *Virulence* 11 (1 Jan. 2020), p. 337. ISSN: 21505608. DOI: 10.1080/21505594.2020.1748930.

[22] Felix Bongomin et al. "Global and multi-national prevalence of fungal diseases—estimate precision". In: *Journal of Fungi* 3 (Dec. 2017). ISSN: 2309608X. DOI: 10.3390/jof3040057.

[23] Bart Jan Kullberg and Maiken C. Arendrup. "Invasive Candidiasis". In: *New England Journal of Medicine* 373 (Oct. 2015), pp. 1445–1456. ISSN: 0028-4793. DOI: 10.1056/NEJMra1315399.

[24] Shelley S. Magill et al. "Changes in Prevalence of Health Care–Associated Infections in U.S. Hospitals". In: *New England Journal of Medicine* 379 (Nov. 2018), pp. 1732–1744. ISSN: 0028-4793. DOI: 10.1056/nejmoa1801550.

[25] Sharon V. Tsay et al. "Burden of Candidemia in the United States, 2017". In: *Clinical Infectious Diseases* 71 (Nov. 2020), E449–E453. ISSN: 15376591. DOI: 10.1093/cid/ciaa193.

[26] George S. Baillie and L. Julia Douglas. "Role of dimorphism in the development of Candida albicans biofilms". In: *Journal of Medical Microbiology* 48 (1999), pp. 671–679. ISSN: 00222615. DOI: 10.1099/00222615-48-7-671.

[27] Judith Berman and Damian J. Krysan. "Drug resistance and tolerance in fungi". In: *Nature Reviews Microbiology* 18 (June 2020), pp. 319–331. ISSN: 17401534. DOI: 10.1038/s41579-019-0322-2.

[28] Feng Yang et al. "Antifungal Tolerance and Resistance Emerge at Distinct Drug Concentrations and Rely upon Different Aneuploid Chromosomes". In: *mBio* 14 (Mar. 2023). ISSN: 21507511. DOI: 10.1128/mbio.00227-23.

[29] Chandrasekaran Komalapriya et al. "Integrative model of oxidative stress adaptation in the fungal pathogen Candida albicans". In: *PLoS ONE* 10 (Sept. 2015). ISSN: 19326203. DOI: 10.1371/journal.pone.0137750.

[30] Ingrid E. Frohner et al. "Candida albicans cell surface superoxide dismutases degrade host-derived reactive oxygen species to escape innate immune surveillance". In: *Molecular Microbiology* 71 (Jan. 2009), pp. 240–252. ISSN: 0950382X. DOI: 10.1111/j.1365-2958.2008.06528.x.

[31] Fabien Cottier and Fritz A. Mühlschlegel. "Sensing the environment: Response of Candida albicans to the X factor". In: *FEMS Microbiology Letters* 295 (June 2009), pp. 1–9. ISSN: 03781097. DOI: 10.1111/j.1574-6968.2009.01564.x.

[32] Dana Davis. "Adaptation to environmental pH in Candida albicans and its relation to pathogenesis". In: *Current Genetics* 44.1 (Oct. 2003), pp. 1–7. ISSN: 01728083. DOI: 10.1007/S00294-003-0415-2/FIGURES/2.

[33] Neil A.R. Gow et al. "Immune recognition of Candida albicans β-glucan by dectin-1". In: *Journal of Infectious Diseases* 196 (Nov. 2007), pp. 1565–1571. ISSN: 00221899. DOI: 10.1086/523110.

[34] Robert T. Wheeler et al. "Dynamic, morphotype-specific Candida albicans β-glucan exposure during infection and drug treatment". In: *PLoS Pathogens* 4 (Dec. 2008). ISSN: 15537366. DOI: 10.1371/journal.ppat.1000227.

[35] C. G.J. McKenzie et al. "Contribution of Candida albicans cell wall components to recognition by and escape from murine macrophages". In: *Infection and Immunity* 78 (4 Apr. 2010), pp. 1650–1658. ISSN: 00199567. DOI: 10.1128/IAI.00001-10.

[36] Diane O. Inglis and Gavin Sherlock. "Ras signaling gets fine-tuned: Regulation of multiple pathogenic traits of Candida albicans". In: *Eukaryotic Cell* 12 (10 Oct. 2013), pp. 1316–1325. ISSN: 15359778. DOI: 10.1128/EC.00094-13.

[37] Guanghua Huang et al. "Multiple roles and diverse regulation of the Ras/-cAMP/protein kinase A pathway in Candida albicans". In: *Molecular Microbiology* 111 (1 Jan. 2019), pp. 6–16. ISSN: 1365-2958. DOI: 10.1111/MMI.14148.

[38] Yong Zhu et al. "Ras1 and Ras2 play antagonistic roles in regulating cellular cAMP level, stationary-phase entry and stress response in Candida albicans". In: *Molecular Microbiology* 74 (4 Nov. 2009), pp. 862–875. ISSN: 1365-2958. DOI: 10.1111/J.1365-2958.2009.06898.X.

[39] Qinghua Feng et al. "Ras Signaling Is Required for Serum-Induced Hyphal Differentiation in Candida albicans". In: *Journal of Bacteriology* 181 (20 1999), p. 6339. ISSN: 00219193. DOI: 10.1128/JB.181.20.6339-6346.1999.

[40] Johannes L. Bos et al. "GEFs and GAPs: Critical Elements in the Control of Small G Proteins". In: *Cell* (2007). DOI: 10.1016/j.cell.2007.05.018.

[41] Daniel R. Pentland et al. "Ras signalling in pathogenic yeasts". In: *Microbial Cell* 5 (2 Feb. 2017), p. 63. ISSN: 23112638. DOI: 10.15698/MIC2018.02.612.

[42] Yue Wang. "Fungal Adenylyl Cyclase Acts As a Signal Sensor and Integrator and Plays a Central Role in Interaction with Bacteria". In: *PLoS Pathogens* 9 (10 Oct. 2013), e1003612. ISSN: 15537366. DOI: 10.1371/JOURNAL.PPAT.1003612.

[43] Peter E. Sudbery. "Growth of Candida albicans hyphae". In: *Nature Reviews Microbiology* 9 (10 Oct. 2011), pp. 737–748. ISSN: 1740-1526. DOI: 10.1038/nrmicro2636.

[44] Takuya Miwa et al. "Gpr1, a Putative G-Protein-Coupled Receptor, Regulates Morphogenesis and Hypha Formation in the Pathogenic Fungus Candida albicans". In: *Eukaryotic Cell* 3 (4 Aug. 2004), p. 919. ISSN: 15359778. DOI: 10.1128/EC.3.4.919-931.2004.

[45] Mykola M. Maidan et al. "The G Protein-coupled Receptor Gpr1 and the G Protein Gpa2 Act through the cAMP-Protein Kinase A Pathway to Induce

Morphogenesis in Candida albicans". In: *Molecular Biology of the Cell* 16 (4 Apr. 2005), p. 1971. ISSN: 10591524. DOI: 10.1091/MBC.E04-09-0780.

[46] M. M. Maidan, J. M. Thevelein, and P. Van Dijck. "Carbon source induced yeast-to-hypha transition in Candida albicans is dependent on the presence of amino acids and on the G-protein-coupled receptor Gpr1". In: *Biochemical Society transactions* 33 (Pt 1 Feb. 2005), pp. 291–293. ISSN: 0300-5127. DOI: 10.1042/BST0330291.

[47] Mieke Van Ende, Stefanie Wijnants, and Patrick Van Dijck. "Sugar sensing and signaling in Candida albicans and Candida glabrata". In: *Frontiers in Microbiology* 10 (JAN 2019), p. 99. ISSN: 1664302X. DOI: 10.3389/FMICB.2019.00099/FULL.

[48] Rebecca S. Shapiro et al. "Hsp90 Orchestrates Temperature-Dependent Candida albicans Morphogenesis Via Ras1-PKA Signaling". In: *Current biology : CB* 19 (8 Apr. 2009), p. 621. ISSN: 09609822. DOI: 10.1016/J.CUB.2009.03.017.

[49] Rebecca S. Shapiro et al. "The Hsp90 Co-Chaperone Sgt1 Governs Candida albicans Morphogenesis and Drug Resistance". In: *PLoS ONE* 7 (9 Sept. 2012). ISSN: 19326203. DOI: 10.1371/JOURNAL.PONE.0044734.

[50] Xiao Li Xu et al. "Bacterial Peptidoglycan Triggers Candida albicans Hyphal Growth by Directly Activating the Adenylyl Cyclase Cyr1p". In: *Cell Host Microbe* 4 (1 July 2008), pp. 28–39. ISSN: 1931-3128. DOI: 10.1016/J.CHOM.2008.05.014.

[51] Jason M. Burch et al. "Bacterial Derived Carbohydrates Bind Cyr1 and Trigger Hyphal Growth in Candida albicans". In: *ACS Infectious Diseases* 4 (1 Jan. 2018), pp. 53–58. ISSN: 23738227. DOI: 10.1021/ACSINFECDIS.7B00154/SUPPL_FILE/ID7B00154_SI_001.PDF.

[52] Debbie A. Hudson et al. "Identification of the dialysable serum inducer of germ-tube formation in Candida albicans". In: *Microbiology* 150 (9 Sept. 2004), pp. 3041–3049. ISSN: 13500872. DOI: 10.1099/MIC.0.27121-0/CITE/REFWORKS.

[53] Torsten Klengel et al. "Fungal Adenylyl Cyclase Integrates CO2 Sensing with cAMP Signaling and Virulence". In: *Current biology : CB* 15 (22 Nov. 2005), p. 2021. ISSN: 09609822. DOI: 10.1016/J.CUB.2005.10.040.

[54] Rebecca A. Hall et al. "CO2 Acts as a Signalling Molecule in Populations of the Fungal Pathogen Candida albicans". In: *PLOS Pathogens* 6 (11 Nov. 2010), e1001193. ISSN: 1553-7374. DOI: 10.1371/JOURNAL.PPAT.1001193.

[55] Daniel R. Pentland et al. "Precision Antifungal Treatment Significantly Extends Voice Prosthesis Lifespan in Patients Following Total Laryngectomy". In: *Frontiers in Microbiology* 11 (May 2020). ISSN: 1664302X. DOI: 10.3389/FMICB.2020.00975/FULL.

[56] Daniel R. Pentland et al. "CO2 enhances the formation, nutrient scavenging and drug resistance properties of C. albicans biofilms". In: *npj Biofilms and Microbiomes* 7 (1 Dec. 2021). ISSN: 20555008. DOI: 10.1038/s41522-021-00238-z.

[57] Jeffrey M. Hollomon et al. "Global Role of Cyclic AMP Signaling in pH-Dependent Responses in Candida albicans". In: *mSphere* 1 (6 Dec. 2016). ISSN: 23795042. DOI: 10.1128/MSPHERE.00283-16.

[58] Xuefen Ding et al. "The regulatory subunit of protein kinase A (Bcy1) in candida albicans plays critical roles in filamentation and white-opaque switching but is not essential for cell growth". In: *Frontiers in Microbiology* 7 (JAN Jan. 2017), p. 2127. ISSN: 1664302X. DOI: 10.3389/FMICB.2016.02127/FULL.

[59] Dirk P. Bockmühl et al. "Distinct and redundant roles of the two protein kinase A isoforms Tpk1p and Tpk2p in morphogenesis and growth of Candida albicans". In: *Molecular microbiology* 42 (5 2001), pp. 1243–1257. ISSN: 0950-382X. DOI: 10.1046/J.1365-2958.2001.02688.X.

[60] Romina Giacometti et al. "Catalytic isoforms Tpk1 and Tpk2 of Candida albicans PKA have non-redundant roles in stress response and glycogen storage". In: *Yeast (Chichester, England)* 26 (5 2009), pp. 273–285. ISSN: 1097-0061. DOI: 10.1002/YEA.1665.

[61] Hyunsook Park et al. "Role of the fungal Ras-protein kinase A pathway in governing epithelial cell interactions during oropharyngeal candidiasis". In: *Cellular Microbiology* 7 (4 Apr. 2005), pp. 499–510. ISSN: 1462-5822. DOI: 10.1111/J.1462-5822.2004.00476.X.

[62] D. P. Bockmüh and J. F. Ernst. "A Potential Phosphorylation Site for an A-Type Kinase in the Efg1 Regulator Protein Contributes to Hyphal Morphogenesis of Candida albicans". In: *Genetics* 157 (4 Apr. 2001), pp. 1523–1530. ISSN: 00166731. DOI: 10.1093/GENETICS/157.4.1523.

[63] Theresia Lassak et al. "Target specificity of the Candida albicans Efg1 regulator". In: *Molecular Microbiology* 82 (3 Nov. 2011), pp. 602–618. ISSN: 1365-2958. DOI: 10.1111/J.1365-2958.2011.07837.X.

[64] Hsiu Jung Lo et al. "Nonfilamentous C. albicans mutants are avirulent". In: *Cell* 90 (1997), pp. 939–949. ISSN: 00928674. DOI: 10.1016/S0092-8674(00)80358-X.

[65] Duncan Wilson et al. "Deletion of the high-affinity cAMP phosphodiesterase encoded by PDE2 affects stress responses and virulence in Candida albicans". In: *Molecular Microbiology* 65 (4 Aug. 2007), pp. 841–856. ISSN: 1365-2958. DOI: 10.1111/J.1365-2958.2007.05788.X.

[66] Duncan Wilson et al. "Candida albicans Pde1p and Gpa2p comprise a regulatory module mediating agonist-induced cAMP signalling and environmental adaptation". In: *Fungal Genetics and Biology* 47 (9 Sept. 2010), pp. 742–752. ISSN: 1087-1845. DOI: 10.1016/J.FGB.2010.06.006.

[67] Ekkehard Leberer et al. "Ras links cellular morphogenesis to virulence by regulation of the MAP kinase and cAMP signalling pathways in the pathogenic fungus Candida albicans". In: *Molecular microbiology* 42 (3 2001), pp. 673–687. ISSN: 0950-382X. DOI: 10.1046/J.1365-2958.2001.02672.X.

[68] Martine Bassilana, James Blyth, and Robert A. Arkowitz. "Cdc24, the GDP-GTP Exchange Factor for Cdc42, Is Required for Invasive Hyphal Growth of Candida albicans". In: *Eukaryotic Cell* 2 (1 Feb. 2003), p. 9. ISSN: 15359778. DOI: 10.1128/EC.2.1.9-18.2003.

[69] Martine Bassilana, Julie Hopkins, and Robert A. Arkowitz. "Regulation of the Cdc42/Cdc24 GTPase Module during Candida albicans Hyphal Growth". In: *Eukaryotic Cell* 4 (3 Mar. 2005), p. 588. ISSN: 15359778. DOI: 10.1128/EC.4.3.588-603.2005.

[70] Ekkehard Leberer et al. "Signal transduction through homologs of the Ste20p and Ste7p protein kinases can trigger hyphal formation in the pathogenic fungus Candidaalbicans". In: *Proceedings of the National Academy of Sciences of the United States of America* 93 (23 Nov. 1996), p. 13217. ISSN: 00278424. DOI: 10.1073/PNAS.93.23.13217.

[71] Julia R. Köhler and Gerald R. Fink. "Candida albicans strains heterozygous and homozygous for mutations in mitogen-activated protein kinase signaling components have defects in hyphal development". In: *Proceedings of the National Academy of Sciences of the United States of America* 93 (23 Nov. 1996), p. 13223. ISSN: 00278424. DOI: 10.1073/PNAS.93.23.13223.

[72] Haoping Liu, Julia Köhler, and Gerald R. Fink. "Suppression of hyphal formation in Candida albicans by mutation of a STE12 homolog". In: *Science (New York, N.Y.)* 266 (5191 Dec. 1994), pp. 1723–1726. ISSN: 0036-8075. DOI: 10.1126/SCIENCE.7992058.

[73] Muriel Cornet, Mathias L. Richard, and Claude Gaillardin. "The homologue of the Saccharomyces cerevisiae RIM9 gene is required for ambient pH signalling in Candida albicans". In: *Research in Microbiology* 160 (Apr. 2009), pp. 219–223. ISSN: 09232508. DOI: 10.1016/j.resmic.2009.02.002.

[74] Jonathan Gomez-Raja and Dana A. Davis. "The β-arrestin-like protein Rim8 is hyperphosphorylated and complexes with Rim21 and Rim101 to promote adaptation to neutral-alkaline pH". In: *Eukaryotic Cell* 11 (May 2012), pp. 683–693. ISSN: 15359778. DOI: 10.1128/EC.05211-11.

[75] Mingchun Li et al. "Candida albicans Rim13p, a protease required for Rim101p processing at acidic and alkaline pHs". In: *Eukaryotic Cell* 3 (June 2004), pp. 741–751. ISSN: 15359778. DOI: 10.1128/EC.3.3.741-751.2004.

[76] D. Davis et al. "Candida albicans RIM101 pH response pathway is required for host-pathogen interactions". In: *Infection and immunity* 68.10 (2000), pp. 5953–5959. ISSN: 0019-9567. DOI: 10.1128/IAI.68.10.5953-5959.2000.

[77] Eric S. Bensen et al. "Transcriptional profiling in Candida albicans reveals new adaptive responses to extracellular pH and functions for Rim101p". In: *Molecular Microbiology* 54 (Dec. 2004), pp. 1335–1351. ISSN: 0950382X. DOI: 10.1111/j.1365-2958.2004.04350.x.

[78] Burkhard R. Braun and Alexander D. Johnson. "Control of filament formation in Candida albicans by the transcriptional repressor TUP1". In: *Science* 277 (July 1997), pp. 105–109. ISSN: 00368075. DOI: 10.1126/science.277.5322.105.

[79] A. Munir A. Murad et al. "NRG1 represses yeast-hypha morphogenesis and hypha-specific gene expression in Candida albicans". In: *EMBO Journal* 20 (Sept. 2001), pp. 4742–4752. ISSN: 02614189. DOI: 10.1093/emboj/20.17.4742.

[80] R. A. Khalaf and R. S. Zitomer. "The DNA binding protein Rfg1 is a repressor of filamentation in Candida albicans". In: *Genetics* 157 (2001), pp. 1503–1512. ISSN: 00166731. DOI: 10.1093/genetics/157.4.1503.

[81] B. R. Braun, D. Kadosh, and A. D. Johnson. "NRG1, a repressor of filamentous growth in C.albicans, is down-regulated during filament induction". In: *EMBO Journal* 20 (Sept. 2001), pp. 4753–4761. ISSN: 02614189. DOI: 10.1093/emboj/20.17.4753.

[82] Chang Su et al. "Hyphal induction under the condition without inoculation in Candida albicans is triggered by Brg1-mediated removal of NRG1 inhibition". In: *Molecular Microbiology* 108 (May 2018), pp. 410–423. ISSN: 13652958. DOI: 10.1111/mmi.13944.

[83] Ian A. Cleary et al. "BRG1 and NRG1 Form a Novel Feedback Circuit Regulating C. albicans Hypha Formation and Virulence". In: *Molecular Microbiology* 85.3 (Aug. 2012), p. 557. ISSN: 0950382X. DOI: 10.1111/J.1365-2958.2012.08127.X.

[84] Carla Renata Arciola, Davide Campoccia, and Lucio Montanaro. "Implant infections: Adhesion, biofilm formation and immune evasion". In: *Nature Reviews Microbiology* 16 (July 2018), pp. 397–409. ISSN: 17401534. DOI: 10.1038/s41579-018-0019-y.

[85] Gordon Ramage et al. "Denture stomatitis: A role for Candida biofilms". In: *Oral Surgery, Oral Medicine, Oral Pathology, Oral Radiology and Endodontology* 98 (July 2004), pp. 53–59. ISSN: 10792104. DOI: 10.1016/j.tripleo.2003.04.002.

[86] John E. McGinniss et al. "Molecular analysis of the endobronchial stent microbial biofilm reveals bacterial communities that associate with stent material and frequent fungal constituents". In: *PLoS ONE* 14 (May 2019). ISSN: 19326203. DOI: 10.1371/journal.pone.0217306.

[87] Mario Tumbarello et al. "Biofilm production by Candida species and inadequate antifungal therapy as predictors of mortality for patients with candidemia". In: *Journal of Clinical Microbiology* 45 (June 2007), pp. 1843–1850. ISSN: 00951137. DOI: 10.1128/JCM.00131-07.

[88] Gordon Ramage et al. "Fungal biofilms in human health and disease." In: *Nature reviews. Microbiology* (Feb. 2025). ISSN: 1740-1534. DOI: 10.1038/s41579-025-01147-0.

[89] Miguel Cámara et al. "Economic significance of biofilms: a multidisciplinary and cross-sectoral challenge". In: *npj Biofilms and Microbiomes* 8 (Dec. 2022). ISSN: 20555008. DOI: 10.1038/s41522-022-00306-y.

[90] G. S. Baillie and L. J. Douglas. "Matrix polymers of Candida biofilms and their possible role in biofilm resistance to antifungal agents". In: *Journal of Antimicrobial Chemotherapy* 46 (2000), pp. 397–403. ISSN: 03057453. DOI: 10.1093/jac/46.3.397.

[91] Jeniel E. Nett et al. "Genetic basis of Candida Biofilm resistance due to drug-sequestering matrix glucan". In: *Journal of Infectious Diseases* 202 (July 2010), pp. 171–175. ISSN: 00221899. DOI: 10.1086/651200.

[92] Jeniel E. Nett and David R. Andes. "Contributions of the biofilm matrix to candida pathogenesis". In: *Journal of Fungi* 6 (1 Mar. 2020). ISSN: 2309608X. DOI: 10.3390/jof6010021.

[93] Eric F. Kong et al. "Commensal protection of Staphylococcus aureus against antimicrobials by Candida albicans biofilm matrix". In: *mBio* 7 (Sept. 2016). ISSN: 21507511. DOI: 10.1128/mBio.01365-16.

[94] Priya Uppuluri et al. "Dispersion as an important step in the Candida albicans biofilm developmental cycle". In: *PLoS Pathogens* 6 (Mar. 2010). ISSN: 15537366. DOI: 10.1371/journal.ppat.1000828.

[95] R. Rajendran et al. "Biofilm formation is a risk factor for mortality in patients with Candida albicans bloodstream infection-Scotland, 2012-2013". In: *Clinical Microbiology and Infection* 22 (Jan. 2016), pp. 87–93. ISSN: 14690691. DOI: 10.1016/j.cmi.2015.09.018.

[96] Sujata Baidya et al. "Biofilm Formation by Pathogens Causing Ventilator-Associated Pneumonia at Intensive Care Units in a Tertiary Care Hospital: An Armor for Refuge". In: *BioMed Research International* 2021 (2021). ISSN: 23146141. DOI: 10.1155/2021/8817700.

[97] Frits van Charante et al. "Microbial diversity and antimicrobial susceptibility in endotracheal tube biofilms recovered from mechanically ventilated

COVID-19 patients." In: *Biofilm* 4 (Dec. 2022), p. 100079. ISSN: 2590-2075. DOI: 10.1016/j.bioflm.2022.100079.

[98] Bircan Kayaaslan et al. "Characteristics of candidemia in COVID-19 patients; increased incidence, earlier occurrence and higher mortality rates compared to non-COVID-19 patients". In: *Mycoses* 64 (9 Sept. 2021), p. 1083. ISSN: 14390507. DOI: 10.1111/MYC.13332.

[99] Mahzad Erami et al. "Clinical impact of Candida respiratory tract colonization and acute lung infections in critically ill patients with COVID-19 pneumonia". In: *Microbial Pathogenesis* 166 (May 2022). ISSN: 10961208. DOI: 10.1016/j.micpath.2022.105520.

[100] Darakshan Alim, Shabnam Sircaik, and Sneh Lata Panwar. "The significance of lipids to biofilm formation in Candida albicans: An emerging perspective". In: *Journal of Fungi* 4 (Dec. 2018). ISSN: 2309608X. DOI: 10.3390/jof4040140.

[101] Emily P. Fox and Clarissa J. Nobile. "A sticky situation: Untangling the transcriptional network controlling biofilm development in Candida albicans". In: *Transcription* 3.6 (2012). ISSN: 21541272. DOI: 10.4161/trans.22281.

[102] Paula Sundstrom. "Adhesion in Candida spp". In: *Cellular Microbiology* 4 (Aug. 2002), pp. 461–469. ISSN: 14625814. DOI: 10.1046/j.1462-5822.2002.00206.x.

[103] Ernesto Cota and Lois L. Hoyer. "The Candida albicans agglutinin-like sequence family of adhesins: Functional insights gained from structural analysis". In: *Future Microbiology* 10 (Oct. 2015), pp. 1635–1648. ISSN: 17460921. DOI: 10.2217/fmb.15.79.

[104] Emily P. Fox et al. "An expanded regulatory network temporally controls Candida albicans biofilm formation". In: *Molecular Microbiology* 96 (June 2015), pp. 1226–1239. ISSN: 13652958. DOI: 10.1111/mmi.13002.

[105] Clarissa J. Nobile et al. "Critical role of Bcr1-dependent adhesins in C. albicans biofilm formation in vitro and in vivo". In: *PLoS Pathogens* 2 (2006), pp. 0636–0649. ISSN: 15537366. DOI: 10.1371/journal.ppat.0020063.

[106] Audrey Beaussart et al. "Single-molecule imaging and functional analysis of Als adhesins and mannans during candida albicans morphogenesis". In: *ACS Nano* 6 (Dec. 2012), pp. 10950–10964. ISSN: 19360851. DOI: 10.1021/nn304505s.

[107] Robert Zarnowski et al. "Novel entries in a fungal biofilm matrix encyclopedia". In: *mBio* 5 (2014), pp. 1–13. ISSN: 21507511. DOI: 10.1128/mBio.01333-14.

[108] Margarida Martins et al. "Presence of extracellular DNA in the candida albicans biofilm matrix and its contribution to biofilms". In: *Mycopathologia* 169 (May 2010), pp. 323–331. ISSN: 0301486X. DOI: 10.1007/s11046-009-9264-y.

[109] Emily P. Fox and Clarissa J. Nobile. "A sticky situation: Untangling the transcriptional network controlling biofilm development in Candida albicans". In: *Transcription* 3 (6 2012). ISSN: 21541272. DOI: 10.4161/trans.22281.

[110] Clarissa J. Nobile et al. "A recently evolved transcriptional network controls biofilm development in Candida albicans". In: *Cell* 148 (Jan. 2012), pp. 126–138. ISSN: 10974172. DOI: 10.1016/j.cell.2011.10.048.

[111] Clarissa J. Nobile and Aaron P. Mitchell. "Regulation of cell-surface genes and biofilm formation by the C. albicans transcription factor Bcr1p". In: *Current Biology* 15 (June 2005), pp. 1150–1155. ISSN: 09609822. DOI: 10.1016/j.cub.2005.05.047.

[112] Clarissa J. Nobile et al. "Function of ¡i¿Candida albicans¡/i¿ Adhesin Hwp1 in Biofilm Formation". In: *Eukaryotic Cell* 5.10 (Oct. 2006), pp. 1604–1610. ISSN: 1535-9778. DOI: 10.1128/EC.00194-06.

[113] Megan D. Lenardon et al. "Scalar nanostructure of the Candida albicans cell wall; a molecular, cellular and ultrastructural analysis and interpretation". In: *The Cell Surface* 6 (Dec. 2020). ISSN: 24682330. DOI: 10.1016/j.tcsw.2020.100047.

[114] J L.-P. Chen-Wu et al. "Expression of chitin synthase genes during yeast and hyphal growth phases of Candida albicans". In: *Molecular Microbiology* (1992). DOI: 10.1111/j.1365-2958.1992.tb01494.x.

[115] Romana Gaderer, Verena Seidl-Seiboth, and Lisa Kappel. "Chitin and N-acetylglucosamine Metabolism in Fungi - A Complex Machinery Harnessed

for the Design of Chitin-Based High Value Products". In: *Current Biotechnology* 6 (3 June 2016). ISSN: 22115501. DOI: 10.2174/2211550105666160330205801.

[116] Jean-Paul Latgé. "The cell wall: a carbohydrate armour for the fungal cell." In: *Molecular Microbiology* (2007). DOI: 10.1111/j.1365-2958.2007.05872.x.

[117] Carol A Munro et al. "The PKC, HOG and Ca2+ signalling pathways co-ordinately regulate chitin synthesis in Candida albicans". In: *Molecular Microbiology* (2007). DOI: 10.1111/j.1365-2958.2007.05588.x.

[118] Carol A Munro et al. "Regulation of chitin synthesis during dimorphic growth of Candida albicans". In: *Microbiology* (1998). DOI: 10.1099/00221287-144-2-391.

[119] Louise A Walker et al. "Cell wall stress induces alternative fungal cytokinesis and septation strategies." In: *Journal of Cell Science* (2013). DOI: 10.1242/jcs.118885.

[120] Louise A Walker et al. "Stimulation of chitin synthesis rescues Candida albicans from echinocandins." In: *PLOS Pathogens* (2008). DOI: 10.1371/journal.ppat.1000040.

[121] Keunsook K Lee et al. "Elevated Cell Wall Chitin in Candida albicans Confers Echinocandin Resistance In Vivo". In: *Antimicrobial Agents and Chemotherapy* (2012). DOI: 10.1128/aac.00683-11.

[122] José Ruiz-Herrera and Lucila Ortiz-Castellanos. "Cell wall glucans of fungi. A review". In: *Cell Surface* 5 (Dec. 2019). ISSN: 24682330. DOI: 10.1016/j.tcsw.2019.100022.

[123] Rocio Garcia-Rubio et al. "The Fungal Cell Wall: Candida, Cryptococcus, and Aspergillus Species". In: *Frontiers in Microbiology* 10 (Jan. 2020). ISSN: 1664302X. DOI: 10.3389/fmicb.2019.02993.

[124] C. M. Douglas et al. "Identification of the FKS1 gene of Candida albicans as the essential target of 1,3-β-D-glucan synthase inhibitors". In: *Antimicrobial Agents and Chemotherapy* 41 (1997), pp. 2471–2479. ISSN: 00664804. DOI: 10.1128/aac.41.11.2471.

[125] C. M. Douglas. "Fungal β(1,3)-D-glucan synthesis". In: 39 (2001), pp. 55–66. ISSN: 09668454. DOI: 10.1080/mmy.39.1.55.66.

[126] Sergey V. Balashov, Steven Park, and David S. Perlin. "Assessing resistance to the echinocandin antifungal drug caspofungin in Candida albicans by profiling mutations in FKS1". In: *Antimicrobial Agents and Chemotherapy* 50 (June 2006), pp. 2058–2063. ISSN: 00664804. DOI: 10.1128/AAC.01653-05.

[127] Yasuhiro Hori and Kazutoshi Shibuya. "Role of FKS gene in the susceptibility of pathogenic fungi to echinocandins". In: *Medical Mycology Journal* 59 (2018), pp. 31–40. ISSN: 2186165X. DOI: 10.3314/mmj.18.004.

[128] Toshiyuki Mio et al. "Cloning of the Candida albicans homolog of Saccharomyces cerevisiae GSC1/FKS1 and its involvement in β-1,3-glucan synthesis". In: *Journal of Bacteriology* 179 (1997), pp. 4096–4105. ISSN: 00219193. DOI: 10.1128/jb.179.13.4096-4105.1997.

[129] Sumanun Suwunnakorn et al. "FKS2 and FKS3 genes of opportunistic human pathogen Candida albicans influence echinocandin susceptibility". In:

Antimicrobial Agents and Chemotherapy 62 (Apr. 2018). ISSN: 10986596. DOI: 10.1128/AAC.02299-17.

[130] Feng Yang et al. "Tolerance to caspofungin in Candida albicans is associated with at least three distinctive mechanisms that govern expression of FKS genes and cell wall remodeling". In: *Antimicrobial Agents and Chemotherapy* 61 (May 2017). ISSN: 10986596. DOI: 10.1128/AAC.00071-17.

[131] Rebecca A Hall and Neil A R Gow. "Mannosylation in Candida albicans: role in cell wall function and immune recognition". In: *Molecular Microbiology* (2013). DOI: 10.1111/mmi.12426.

[132] Iván Martínez-Duncker et al. "Comparative Analysis of Protein Glycosylation Pathways in Humans and the Fungal Pathogen Candida albicans." In: *International Journal of Microbiology* (2014). DOI: 10.1155/2014/267497.

[133] Carol A Munro et al. "Mnt1p and Mnt2p of Candida albicans Are Partially Redundant -1,2-Mannosyltransferases That Participate in O-Linked Mannosylation and Are Required for Adhesion and Virulence". In: *Journal of Biological Chemistry* (2005). DOI: 10.1074/jbc.m411413200.

[134] Stephan K.-H. Prill et al. "PMT family of Candida albicans: five protein mannosyltransferase isoforms affect growth, morphogenesis and antifungal resistance." In: *Molecular Microbiology* (2004). DOI: 10.1111/j.1365-2958.2004.04401.x.

[135] Claudia Timpel et al. "Multiple Functions of Pmt1p-mediated ProteinO-Mannosylation in the Fungal Pathogen Candida albicans". In: *Journal of Biological Chemistry* (1998). DOI: 10.1074/jbc.273.33.20837.

[136] Lynn M. Thomson et al. "Functional characterization of the Candida albicans MNT1 mannosyltransferase expressed heterologously in Pichia pastoris". In: *Journal of Biological Chemistry* 275 (25 June 2000), pp. 18933–18938. ISSN: 00219258. DOI: 10.1074/jbc.M909699199.

[137] Diana F Díaz-Jiménez et al. "Biochemical characterization of recombinant Candida albicans mannosyltransferases Mnt1, Mnt2 and Mnt5 reveals new functions in O- and N-mannan biosynthesis". In: *Biochemical and Biophysical Research Communications* (2012). DOI: 10.1016/j.bbrc.2012.01.131.

[138] Héctor M Mora-Montes et al. "A multifunctional mannosyltransferase family in Candida albicans determines cell wall mannan structure and host-fungus interactions." In: *Journal of Biological Chemistry* (2010). DOI: 10.1074/jbc.m109.081513.

[139] Ed T Buurman et al. "Molecular analysis of CaMnt1p, a mannosyl transferase important for adhesion and virulence of Candida albicans". In: *PNAS* 95 (1998), pp. 7670–7675.

[140] Heidrun Peltroche-Llacsahuanga et al. "Protein O-Mannosyltransferase Isoforms Regulate Biofilm Formation in Candida albicans". In: *Antimicrobial Agents and Chemotherapy* 50 (10 Oct. 2006), p. 3488. ISSN: 00664804. DOI: 10.1128/AAC.00606-06.

[141] Rebecca A. Hall et al. "The Mnn2 Mannosyltransferase Family Modulates Mannoprotein Fibril Length, Immune Recognition and Virulence of Candida albicans". In: *PLoS Pathogens* 9 (4 Apr. 2013). ISSN: 15537366. DOI: 10.1371/journal.ppat.1003276.

[142] Héctor M Mora-Montes et al. "Endoplasmic Reticulum -Glycosidases of Candida albicans Are Required for N Glycosylation, Cell Wall Integrity, and Normal Host-Fungus Interaction". In: *Eukaryotic Cell* (2007). DOI: 10.1128/ec.00350-07.

[143] Daniel J. Kelleher and Reid Gilmore. "An evolving view of the eukaryotic oligosaccharyltransferase". In: *Glycobiology* 16 (4 Apr. 2006). ISSN: 0959-6658. DOI: 10.1093/GLYCOB/CWJ066.

[144] Steven Bates et al. "Outer Chain N-Glycans Are Required for Cell Wall Integrity and Virulence of Candida albicans". In: *Journal of Biological Chemistry* (2006). DOI: 10.1074/jbc.m510360200.

[145] Susan B. Southard et al. "Molecular Analysis of the Candida albicans Homolog of Saccharomyces cerevisiae MNN9, Required for Glycosylation of Cell Wall Mannoproteins". In: *Journal of Bacteriology* 181 (24 1999), p. 7439. ISSN: 00219193. DOI: 10.1128/JB.181.24.7439-7448.1999.

[146] Pedro A. Romero et al. "Mnt2p and Mnt3p of Saccharomyces cerevisiae are members of the Mnn1p family of -1,3-mannosyltransferases responsible for adding the terminal mannose residues of O-linked oligosaccharides". In: *Glycobiology* 9 (10 Oct. 1999), pp. 1045–1051. ISSN: 0959-6658. DOI: 10.1093/GLYCOB/9.10.1045.

[147] Céline Mille et al. "Identification of a New Family of Genes Involved in β-1,2-Mannosylation of Glycans in Pichia pastoris and Candida albicans". In: *Journal of Biological Chemistry* (2008). DOI: 10.1074/jbc.m708825200.

[148] Richard P Hobson et al. "Loss of Cell Wall Mannosylphosphate in Candida albicans Does Not Influence Macrophage Recognition". In: *Journal of Biological Chemistry* (2004). DOI: 10.1074/jbc.m405003200.

[149] Sarah Höfs, Selene Mogavero, and Bernhard Hube. "Interaction of Candida albicans with host cells: virulence factors, host defense, escape strategies, and the microbiota". In: *Journal of Microbiology* 54 (Mar. 2016), pp. 149–169. ISSN: 19763794. DOI: 10.1007/s12275-016-5514-0.

[150] Mihai G. Netea et al. "An integrated model of the recognition of Candida albicans by the innate immune system". In: *Nature Reviews Microbiology* 6 (Jan. 2008), pp. 67–78. ISSN: 17401526. DOI: 10.1038/nrmicro1815.

[151] Neil A.R. Gow et al. "Candida albicans morphogenesis and host defence: Discriminating invasion from colonization". In: *Nature Reviews Microbiology* 10 (Feb. 2012), pp. 112–122. ISSN: 17401526. DOI: 10.1038/nrmicro2711.

[152] Jurgen Herre et al. "Dectin-1 uses novel mechanisms for yeast phagocytosis in macrophages". In: *Blood* 104 (Dec. 2004), pp. 4038–4045. ISSN: 00064971. DOI: 10.1182/blood-2004-03-1140.

[153] Eamon P. McGreal et al. "The carbohydrate-recognition domain of Dectin-2 is a C-type lectin with specificity for high mannose". In: *Glycobiology* 16 (May 2006), pp. 422–430. ISSN: 09596658. DOI: 10.1093/glycob/cwj077.

[154] Remi Hatinguais, Janet A. Willment, and Gordon D. Brown. "C-type lectin receptors in antifungal immunity: Current knowledge and future developments". In: *Parasite Immunology* 45 (Feb. 2023). ISSN: 13653024. DOI: 10.1111/pim.12951.

[155] Erik-Oliver Glocker et al. "A Homozygous CARD9 Mutation in a Family with Susceptibility to Fungal Infections". In: *New England Journal of Medicine* 361 (Oct. 2009), pp. 1727–1735. ISSN: 0028-4793. DOI: 10.1056/nejmoa0810719.

[156] Shinobu Saijo et al. "Dectin-2 recognition of -mannans and induction of Th17 cell differentiation is essential for host defense against candida albicans". In: *Immunity* 32 (May 2010), pp. 681–691. ISSN: 10747613. DOI: 10.1016/j.immuni.2010.05.001.

[157] S. Tyler Hollmig, Kiyoshi Ariizumi, and Ponciano D. Cruz. "Recognition of non-self-polysaccharides by C-type lectin receptors dectin-1 and dectin-2". In: *Glycobiology* 19 (2009), pp. 568–575. ISSN: 09596658. DOI: 10.1093/glycob/cwp032.

[158] Gordon D. Brown. "Dectin-1 : A signalling non-TLR pattern-recognition receptor". In: *Nature Reviews Immunology* 6 (Jan. 2006), pp. 33–43. ISSN: 14741733. DOI: 10.1038/nri1745.

[159] Chad Steele et al. "The beta-glucan receptor dectin-1 recognizes specific morphologies of aspergillus fumigatus". In: *PLoS Pathogens* 1 (2005), pp. 0323–0334. ISSN: 15537366. DOI: 10.1371/journal.ppat.0010042.

[160] Olaf Gross et al. "Card9 controls a non-TLR signalling pathway for innate anti-fungal immunity". In: *Nature* 442 (Aug. 2006), pp. 651–656. ISSN: 14764687. DOI: 10.1038/nature04926.

[161] Sarah E. Davis et al. "Masking of β(1-3)-glucan in the cell wall of Candida albicans from detection by innate immune cells depends on phosphatidylserine". In: *Infection and Immunity* 82 (10 2014), pp. 4405–4413. ISSN: 10985522. DOI: 10.1128/IAI.01612-14.

[162] Alessandra Da Silva Dantas et al. "Oxidative stress responses in the human fungal pathogen, Candida albicans". In: *Biomolecules* 5 (Feb. 2015), pp. 142–165. ISSN: 2218273X. DOI: 10.3390/biom5010142.

[163] Mikhail Martchenko et al. "Superoxide Dismutases in Candida albicans: Transcriptional Regulation and Functional Characterization of the Hyphal-induced SOD5 Gene". In: *Molecular Biology of the Cell* 15 (Feb. 2004), pp. 456–467. ISSN: 10591524. DOI: 10.1091/mbc.E03-03-0179.

[164] Thomas R. Kozel, Leanne C. Weinhold, and David M. Lupan. "Distinct characteristics of initiation of the classical and alternative complement pathways by Candida albicans". In: *Infection and Immunity* 64 (1996), pp. 3360–3368. ISSN: 00199567. DOI: 10.1128/iai.64.8.3360-3368.1996.

[165] J. Vidya Sarma and Peter A. Ward. "The complement system". In: *Cell and Tissue Research* 343 (Jan. 2011), pp. 227–235. ISSN: 0302766X. DOI: 10.1007/s00441-010-1034-0.

[166] Andreas Klos et al. "The role of the anaphylatoxins in health and disease". In: *Molecular Immunology* 46 (Sept. 2009), pp. 2753–2766. ISSN: 01615890. DOI: 10.1016/j.molimm.2009.04.027.

[167] C. J. Baker et al. "The role of complement and antibody in opsonophagocytosis of type II Group B streptococci". In: *Journal of Infectious Diseases* 154 (1986), pp. 47–54. ISSN: 00221899. DOI: 10.1093/infdis/154.1.47.

[168] Marina Serna et al. "Structural basis of complement membrane attack complex formation". In: *Nature Communications* 7 (Feb. 2016). ISSN: 20411723. DOI: 10.1038/ncomms10587.

[169] Nisha Valand et al. "Inactivation of the Complement Lectin Pathway by Candida tropicalis Secreted Aspartyl Protease-1". In: *Immunobiology* 227 (Nov. 2022). ISSN: 18783279. DOI: 10.1016/j.imbio.2022.152263.

[170] Donatella Pietrella et al. "Secreted aspartic proteases of Candida albicans activate the NLRP3 inflammasome". In: *European Journal of Immunology* 43 (Mar. 2013), pp. 679–692. ISSN: 00142980. DOI: 10.1002/eji.201242691.

[171] Grazyna Bras et al. "Secreted Aspartic Proteinases: Key Factors in Candida Infections and Host-Pathogen Interactions". In: *International Journal of Molecular Sciences* 25 (May 2024). ISSN: 14220067. DOI: 10.3390/ijms25094775.

[172] Dhirendra Kumar Singh et al. "Functional Characterization of Secreted Aspartyl Proteases in Candida parapsilosis". In: *mSphere* 4 (Aug. 2019). ISSN: 2379-5042. DOI: 10.1128/msphere.00484-19.

[173] Francesco Citiulo et al. "Candida albicans scavenges host zinc via Pra1 during endothelial invasion". In: *PLoS Pathogens* 8 (June 2012). ISSN: 15537366. DOI: 10.1371/journal.ppat.1002777.

[174] Shanshan Luo et al. "Immune evasion of the human pathogenic yeast Candida albicans: Pra1 is a Factor H, FHL-1 and plasminogen binding surface protein". In: *Molecular Immunology* 47 (Dec. 2009), pp. 541–550. ISSN: 01615890. DOI: 10.1016/j.molimm.2009.07.017.

[175] Shanshan Luo et al. " Secreted pH-Regulated Antigen 1 of Candida albicans Blocks Activation and Conversion of Complement C3 ". In: *The Journal of Immunology* 185 (Aug. 2010), pp. 2164–2173. ISSN: 0022-1767. DOI: 10.4049/jimmunol.1001011.

[176] Shanshan Luo et al. "The pH-regulated antigen 1 of Candida albicans binds the human complement inhibitor C4b-binding protein and mediates fungal complement evasion". In: *Journal of Biological Chemistry* 286 (Mar. 2011), pp. 8021–8029. ISSN: 00219258. DOI: 10.1074/jbc.M110.130138.

[177] Slavena Vylkova et al. "The fungal pathogen candida albicans autoinduces hyphal morphogenesis by raising extracellular pH". In: *mBio* 2 (2011). ISSN: 21507511. DOI: 10.1128/mBio.00055-11.

[178] Suman Ghosh et al. "Arginine-Induced germ tube formation in Candida albicans is essential for escape from murine macrophage line RAW 264.7". In: *Infection and Immunity* 77 (Apr. 2009), pp. 1596–1605. ISSN: 00199567. DOI: 10.1128/IAI.01452-08.

[179] Françios A.B. Olivier et al. "The escape of Candida albicans from macrophages is enabled by the fungal toxin candidalysin and two host cell death pathways". In: *Cell Reports* 40 (Sept. 2022). ISSN: 22111247. DOI: 10.1016/j.celrep.2022.111374.

[180] Chao Wen Wang. "Lipid droplet dynamics in budding yeast". In: *Cellular and Molecular Life Sciences: CMLS* 72.14 (July 2015), p. 2677. ISSN: 14209071. DOI: 10.1007/S00018-015-1903-5.

[181] Daniel Sorger et al. "A yeast strain lacking lipid particles bears a defect in ergosterol formation". In: *Journal of Biological Chemistry* 279.30 (July 2004), pp. 31190–31196. ISSN: 00219258. DOI: 10.1074/jbc.M403251200.

[182] Claudia Schmidt et al. "Analysis of Yeast Lipid Droplet Proteome and Lipidome". In: *Methods in Cell Biology* 116 (Jan. 2013), pp. 15–37. ISSN: 0091-679X. DOI: 10.1016/B978-0-12-408051-5.00002-4.

[183] Vineet Choudhary and Roger Schneiter. "Lipid droplet biogenesis from specialized ER subdomains". In: *Microbial cell (Graz, Austria)* 7.8 (June 2020), pp. 218–221. ISSN: 2311-2638. DOI: 10.15698/MIC2020.08.727.

[184] Tibor Czabany, Karin Athenstaedt, and Günther Daum. "Synthesis, storage and degradation of neutral lipids in yeast". In: *Biochimica et Biophysica Acta (BBA) - Molecular and Cell Biology of Lipids* 1771.3 (Mar. 2007), pp. 299–309. ISSN: 1388-1981. DOI: 10.1016/J.BBALIP.2006.07.001.

[185] Tibor Czabany et al. "Structural and biochemical properties of lipid particles from the yeast Saccharomyces cerevisiae". In: *Journal of Biological*

Chemistry 283 (June 2008), pp. 17065–17074. ISSN: 00219258. DOI: 10.1074/jbc.M800401200.

[186] Ariadna P. Velázquez et al. "Lipid droplet-mediated ER homeostasis regulates autophagy and cell survival during starvation". In: *Journal of Cell Biology* 212 (6 Mar. 2016), pp. 621–631. ISSN: 15408140. DOI: 10.1083/jcb.201508102.

[187] Sona Rajakumari, Karlheinz Grillitsch, and Günther Daum. "Synthesis and turnover of non-polar lipids in yeast". In: *Progress in Lipid Research* 47 (May 2008), pp. 157–171. ISSN: 01637827. DOI: 10.1016/j.plipres.2008.01.001.

[188] Denis J. Murphy and Jean Vance. "Mechanisms of lipid-body formation". In: *Trends in Biochemical Sciences* 24 (Mar. 1999), pp. 109–115. ISSN: 09680004. DOI: 10.1016/S0968-0004(98)01349-8.

[189] Stephen L. Sturley and M. Mahmood Hussain. "Lipid droplet formation on opposing sides of the endoplasmic reticulum". In: *Journal of lipid research* 53.9 (Sept. 2012), pp. 1800–1810. ISSN: 1539-7262. DOI: 10.1194/JLR.R028290.

[190] Nicolas Jacquier et al. "Lipid droplets are functionally connected to the endoplasmic reticulum in Saccharomyces cerevisiae". In: *Journal of Cell Science* 124.14 (July 2011), pp. 2424–2437. ISSN: 00219533. DOI: 10.1242/jcs.076836.

[191] J. Zanghellini, F. Wodlei, and H. H. von Grünberg. "Phospholipid demixing and the birth of a lipid droplet". In: *Journal of Theoretical Biology* 264

(June 2010), pp. 952–961. ISSN: 00225193. DOI: 10.1016/j.jtbi.2010.02.025.

[192] Florian Wilfling et al. "Triacylglycerol synthesis enzymes mediate lipid droplet growth by relocalizing from the ER to lipid droplets". In: *Developmental Cell* 24 (Feb. 2013), pp. 384–399. ISSN: 15345807. DOI: 10.1016/j.devcel.2013.01.013.

[193] D. Sorger and G. Daum. "Triacylglycerol biosynthesis in yeast". In: *Applied Microbiology and Biotechnology* 61 (2003), pp. 289–299. ISSN: 01757598. DOI: 10.1007/s00253-002-1212-4.

[194] Nathan E. Wolins, Dawn L. Brasaemle, and Perry E. Bickel. "A proposed model of fat packaging by exchangeable lipid droplet proteins". In: *FEBS Letters* 580 (Oct. 2006), pp. 5484–5491. ISSN: 00145793. DOI: 10.1016/j.febslet.2006.08.040.

[195] Aaron Turkish and Stephen L. Sturley. "Regulation of Triglyceride Metabolism. I. Eukaryotic neutral lipid synthesis: "Many ways to skin ACAT or a DGAT"". In: *American Journal of Physiology - Gastrointestinal and Liver Physiology* 292 (Apr. 2007). ISSN: 01931857. DOI: 10.1152/ajpgi.00509.2006.

[196] Stylianos Fakas et al. "Phosphatidate Phosphatase Activity Plays Key Role in Protection against Fatty Acid-induced Toxicity in Yeast". In: *Journal of Biological Chemistry* 286 (33 Aug. 2011), pp. 29074–29085. ISSN: 0021-9258. DOI: 10.1074/JBC.M111.258798.

[197] Susan A. Henry, Sepp D. Kohlwein, and George M. Carman. "Metabolism and regulation of glycerolipids in the yeast Saccharomyces cerevisiae". In: *Genetics* 190 (Feb. 2012), pp. 317–349. ISSN: 00166731. DOI: 10.1534/genetics.111.130286.

[198] Karin Athenstaedt et al. "Redundant systems of phosphatidic acid biosynthesis via acylation of glycerol-3-phosphate or dihydroxyacetone phosphate in the yeast Saccharomyces cerevisiae". In: *Journal of Bacteriology* 181 (1999), pp. 1458–1463. ISSN: 00219193. DOI: 10.1128/jb.181.5.1458-1463.1999.

[199] Zhifu Zheng and Jitao Zou. "The initial step of the glycerolipid pathway: Identification of glycerol 3-phosphate/dihydroxyacetone phosphate dual substrate acyltransferases in Saccharomyces cerevisiae". In: *Journal of Biological Chemistry* 276 (Nov. 2001), pp. 41710–41716. ISSN: 00219258. DOI: 10.1074/jbc.M104749200.

[200] Karin M. Overkamp et al. "Metabolic engineering of glycerol production in Saccharomyces cerevisiae". In: *Applied and Environmental Microbiology* 68 (2002), pp. 2814–2821. ISSN: 00992240. DOI: 10.1128/AEM.68.6.2814-2821.2002.

[201] Nirpinder Singh and James K. Stoops. "Yeast Fatty Acid Synthase: Structure to Function Relationship". In: *Biochemistry* 24 (Nov. 1985), pp. 6598–6602. ISSN: 15204995. DOI: 10.1021/bi00344a044.

[202] Oksana Tehlivets, Kim Scheuringer, and Sepp D. Kohlwein. "Fatty acid synthesis and elongation in yeast". In: *Biochimica et Biophysica Acta* -

Molecular and Cell Biology of Lipids 1771 (Mar. 2007), pp. 255–270. ISSN: 13881981. DOI: 10.1016/j.bbalip.2006.07.004.

[203] Mohammed Benghezal et al. "SLC1 and SLC4 encode partially redundant acyl-coenzyme A 1-acylglycerol-3-phosphate O-acyltransferases of budding yeast". In: *Journal of Biological Chemistry* 282 (Oct. 2007), pp. 30845–30855. ISSN: 1083351X. DOI: 10.1074/jbc.M702719200.

[204] Shoily Khondker, Gil Soo Han, and George M. Carman. "Phosphorylation-mediated regulation of the Nem1-Spo7/Pah1 phosphatase cascade in yeast lipid synthesis". In: *Advances in biological regulation* 84 (May 2022), p. 100889. ISSN: 22124926. DOI: 10.1016/J.JBIOR.2022.100889.

[205] George M. Carman and Susan A. Henry. "Phosphatidic acid plays a central role in the transcriptional regulation of glycerophospholipid synthesis in Saccharomyces cerevisiae". In: *Journal of Biological Chemistry* 282 (52 Dec. 2007), pp. 37293–37297. ISSN: 00219258. DOI: 10.1074/jbc.R700038200.

[206] Maria Laura Gaspar et al. "Phosphatidic acid species 34:1 mediates expression of the myo-inositol 3-phosphate synthase gene INO1 for lipid synthesis in yeast". In: *Journal of Biological Chemistry* 298 (7 July 2022), p. 102148. ISSN: 0021-9258. DOI: 10.1016/J.JBC.2022.102148.

[207] David A. Eiznhamer et al. "Expression of the INO2 regulatory gene of Saccharomyces cerevisiae is controlled by positive and negative promoter elements and an upstream open reading frame". In: *Molecular Microbiology* 39 (Mar. 2001), pp. 1395–1405. ISSN: 0950-382X. DOI: 10.1111/j.1365-2958.2001.02330.x.

[208] Roshini Wimalarathna, Chen Han Tsai, and Chang Hui Shen. "Transcriptional control of genes involved in yeast phospholipid biosynthesis". In: *Journal of Microbiology* 49 (Apr. 2011), pp. 265–273. ISSN: 12258873. DOI: 10.1007/s12275-011-1130-1.

[209] Michael J. White, Jeanne P. Hirsch, and Susan A. Henry. "The OPI1 gene of Saccharomyces cerevisiae, a negative regulator of phospholipid biosynthesis, encodes a protein containing polyglutamine tracts and a leucine zipper". In: *Journal of Biological Chemistry* 266 (Jan. 1991), pp. 863–872. ISSN: 00219258. DOI: 10.1016/s0021-9258(17)35253-5.

[210] Felix Kliewe et al. "Opi1 mediates repression of phospholipid biosynthesis by phosphate limitation in the yeast Saccharomyces cerevisiae". In: *Yeast* 34 (Feb. 2017), pp. 67–81. ISSN: 10970061. DOI: 10.1002/yea.3215.

[211] Maria L. Gaspar et al. "Interaction between repressor Opi1p and ER membrane protein Scs2p facilitates transit of phosphatidic acid from the ER to mitochondria and is essential for INO1 gene expression in the presence of choline". In: *Journal of Biological Chemistry* 292 (Nov. 2017), pp. 1813–18728. ISSN: 1083351X. DOI: 10.1074/jbc.M117.809970.

[212] Harald F. Hofbauer et al. "The molecular recognition of phosphatidic acid by an amphipathic helix in Opi1". In: *Journal of Cell Biology* 217 (Sept. 2018), pp. 3109–3126. ISSN: 15408140. DOI: 10.1083/jcb.201802027.

[213] Chelsi D. Cassilly et al. "Role of phosphatidylserine synthase in shaping the phospholipidome of Candida albicans". In: *FEMS Yeast Research* 17 (2 Mar. 2017), fox007. ISSN: 15671364. DOI: 10.1093/FEMSYR/FOX007.

[214] Gil Soo Han, Symeon Siniossoglou, and George M. Carman. "The cellular functions of the yeast lipin homolog PAH1p are dependent on its phosphatidate phosphatase activity". In: *The Journal of biological chemistry* 282 (51 Dec. 2007), pp. 37026–37035. ISSN: 0021-9258. DOI: 10.1074/JBC.M705777200.

[215] Jack Phan and Karen Reue. "Lipin, a lipodystrophy and obesity gene". In: *Cell metabolism* 1 (1 Jan. 2005), pp. 73–83. ISSN: 1550-4131. DOI: 10.1016/J.CMET.2004.12.002.

[216] George M. Carman and Gil Soo Han. "Fat-regulating phosphatidic acid phosphatase: a review of its roles and regulation in lipid homeostasis". In: *Journal of lipid research* 60 (1 2019), pp. 2–6. ISSN: 1539-7262. DOI: 10.1194/JLR.S087452.

[217] Florencia Pascual and George M. Carman. "Phosphatidate phosphatase, a key regulator of lipid homeostasis". In: *Biochimica et biophysica acta* 1831 (3 Mar. 2013), pp. 514–522. ISSN: 0006-3002. DOI: 10.1016/J.BBALIP.2012.08.006.

[218] Wen Min Su et al. "Protein kinase A-mediated phosphorylation of Pah1p phosphatidate phosphatase functions in conjunction with the Pho85p-Pho80p and Cdc28p-Cyclin B kinases to regulate lipid synthesis in yeast". In: *Journal of Biological Chemistry* 287 (Sept. 2012), pp. 33364–33376. ISSN: 00219258. DOI: 10.1074/jbc.M112.402339.

[219] Wen Min Su, Gil Soo Han, and George M. Carman. "Cross-talk Phosphorylations by Protein Kinase C and Pho85p-Pho80p Protein Kinase Regulate Pah1p Phosphatidate Phosphatase Abundance in Saccharomyces cerevisiae". In: *The Journal of Biological Chemistry* 289 (27 July 2014), p. 18818. ISSN: 1083351X. DOI: 10.1074/JBC.M114.581462.

[220] Hyeon Son Choi et al. "Pho85p-Pho80p phosphorylation of yeast pah1p phosphatidate phosphatase regulates its activity, location, abundance, and function in lipid metabolism". In: *Journal of Biological Chemistry* 287 (Mar. 2012), pp. 11290–11301. ISSN: 00219258. DOI: 10.1074/jbc.M112.346023.

[221] Azam Hassaninasab et al. "Yck1 casein kinase I regulates the activity and phosphorylation of Pah1 phosphatidate phosphatase from Saccharomyces cerevisiae". In: *The Journal of biological chemistry* 294 (48 Nov. 2019), pp. 18256–18268. ISSN: 1083-351X. DOI: 10.1074/JBC.RA119.011314.

[222] Eleftherios Karanasios et al. "A phosphorylation-regulated amphipathic helix controls the membrane translocation and function of the yeast phosphatidate phosphatase". In: *Proceedings of the National Academy of Sciences of the United States of America* 107 (41 Oct. 2010), pp. 17539–17544. ISSN: 1091-6490. DOI: 10.1073/PNAS.1007974107.

[223] Symeon Siniossoglou et al. "A novel complex of membrane proteins required for formation of a spherical nucleus". In: *EMBO Journal* 17 (Nov. 1998), pp. 6449–6464. ISSN: 02614189. DOI: 10.1093/emboj/17.22.6449.

[224] Wen Min Su et al. "Protein kinase A phosphorylates the Nem1-Spo7 protein phosphatase complex that regulates the phosphorylation state of the phosphatidate phosphatase Pah1 in yeast". In: *The Journal of biological chemistry* 293 (41 Oct. 2018), pp. 15801–15814. ISSN: 1083-351X. DOI: 10.1074/JBC.RA118.005348.

[225] Prabuddha Dey et al. "Phosphorylation of lipid metabolic enzymes by yeast protein kinase C requires phosphatidylserine and diacylglycerol". In: *Journal of Lipid Research* 58 (4 2017), p. 742. ISSN: 15397262. DOI: 10.1194/JLR.M075036.

[226] Prabuddha Dey et al. "Protein kinase C mediates the phosphorylation of the Nem1-Spo7 protein phosphatase complex in yeast". In: *The Journal of biological chemistry* 294 (44 Nov. 2019), pp. 15997–16009. ISSN: 1083-351X. DOI: 10.1074/JBC.RA119.010592.

[227] Mona Mirheydari et al. "The Spo7 sequence LLI is required for Nem1-Spo7/Pah1 phosphatase cascade function in yeast lipid metabolism". In: *The Journal of biological chemistry* 295 (33 Aug. 2020), pp. 11473–11485. ISSN: 1083-351X. DOI: 10.1074/JBC.RA120.014129.

[228] Ruta Jog, Gil Soo Han, and George M. Carman. "The Saccharomyces cerevisiae Spo7 basic tail is required for Nem1–Spo7/Pah1 phosphatase cascade function in lipid synthesis". In: *Journal of Biological Chemistry* 300 (Jan. 2024). ISSN: 1083351X. DOI: 10.1016/j.jbc.2023.105587.

[229] Joanna M. Kwiatek et al. "Phosphatidic Acid Mediates the Nem1-Spo7/Pah1 Phosphatase Cascade in Yeast Lipid Synthesis". In: *Journal of Lipid Research* 63 (11 Nov. 2022), p. 100282. ISSN: 15397262. DOI: 10.1016/J.JLR.2022.100282.

[230] Sudipta Mondal, Biswajit Pal, and Rajan Sankaranarayanan. "Diacylglycerol metabolism and homeostasis in fungal physiology". In: *FEMS Yeast Research* 24 (Jan. 2024), p. 36. ISSN: 1567-1356. DOI: 10.1093/FEMSYR/FOAE036.

[231] Suriakarthiga Ganesan et al. "Metabolic control of cytosolic-facing pools of diacylglycerol in budding yeast". In: *Traffic (Copenhagen, Denmark)* 20 (3 Mar. 2019), pp. 226–245. ISSN: 1600-0854. DOI: 10.1111/TRA.12632.

[232] James A Hamilton et al. "The Interfacial Conformation and Transbilayer Movement of Diacylglycerols in Phospholipid Bilayers*". In: *The Journal of Biological Chemistry* 266.2 (1991), pp. 1177–1186. DOI: 10.1016/S0021-9258(17)35299-7.

[233] Matthew L. Starr and Rutilio A. Fratti. "The Participation of Regulatory Lipids in Vacuole Homotypic Fusion". In: *Trends in biochemical sciences* 44.6 (June 2018), p. 546. ISSN: 13624326. DOI: 10.1016/J.TIBS.2018.12.003.

[234] Terry Sasser et al. "Yeast Lipin 1 Orthologue Pah1p Regulates Vacuole Homeostasis and Membrane Fusion". In: *The Journal of Biological Chemistry* 287.3 (Jan. 2011), p. 2221. ISSN: 00219258. DOI: 10.1074/JBC.M111.317420.

[235] Yi Guo et al. "Functional genomic screen reveals genes involved in lipid-droplet formation and utilization". In: *Nature* 453.7195 (May 2008), pp. 657–661. ISSN: 14764687. DOI: 10.1038/nature06928.

[236] Patrick Rockenfeller et al. "Diacylglycerol triggers Rim101 pathway–dependent necrosis in yeast: a model for lipotoxicity". In: *Cell Death and Differentiation* 25 (4 Mar. 2018), p. 765. ISSN: 14765403. DOI: 10.1038/S41418-017-0014-2.

[237] Yasutomi Nishizuka and Yasutomi Nishizuka. "Protein kinase C and lipid signaling for sustained cellular responses." In: *The FASEB Journal* (1995). DOI: 10.1096/fasebj.9.7.7737456.

[238] Jeroen P. Roose et al. "A diacylglycerol-protein kinase C-rasGRP1 pathway directs ras activation upon antigen receptor stimulation of T cells". In: *Molecular and Cellular Biology* (2005). DOI: 10.1128/mcb.25.11.4426-4441.2005.

[239] Benjamin A. Olenchock et al. "Disruption of diacylglycerol metabolism impairs the induction of T cell anergy". In: *Nature Immunology* (2006). DOI: 10.1038/ni1400.

[240] Yuanyuan Zha et al. "T cell anergy is reversed by active Ras and regulated by diacylglycerol kinase". In: *Nature Immunology* (2006). DOI: 10.1038/ni1394.

[241] Sachin S. Katti et al. "Structural anatomy of Protein Kinase C C1 domain interactions with diacylglycerol and other agonists". In: *Nature Communications 2022 13:1* 13.1 (May 2022), pp. 1–11. ISSN: 2041-1723. DOI: 10.1038/s41467-022-30389-2.

[242] Isabel Mérida et al. "Diacylglycerol kinases : at the hub of cell signalling". In: *Biochemical Journal* (2008). DOI: 10.1042/bj20071040.

[243] Rachel McMullan et al. "Rho is a presynaptic activator of neurotransmitter release at pre-existing synapses in C. elegans". In: *Genes and Development* 20 (1 Jan. 2006), pp. 65–76. ISSN: 08909369. DOI: 10.1101/gad.359706.

[244] Keimpe D.B. Wierda et al. "Interdependence of PKC-Dependent and PKC-Independent Pathways for Presynaptic Plasticity". In: *Neuron* 54 (Apr. 2007), pp. 275–290. ISSN: 08966273. DOI: 10.1016/j.neuron.2007.04.001.

[245] D. Sorger and G. Daum. "Synthesis of triacylglycerols by the acyl-coenzyme A:diacyl-glycerol acyltransferase Dga1p in lipid particles of the yeast Saccharomyces cerevisiae". In: *Journal of bacteriology* 184.2 (2002), pp. 519–524. ISSN: 0021-9193. DOI: 10.1128/JB.184.2.519-524.2002.

[246] Daniel F. Markgraf et al. "An ER protein functionally couples neutral lipid metabolism on lipid droplets to membrane lipid synthesis in the ER". In: *Cell reports* 6.1 (2013), p. 44. ISSN: 22111247. DOI: 10.1016/J.CELREP.2013.11.046.

[247] Shingo Iwasa et al. "The Phospholipid:Diacylglycerol Acyltransferase Lro1 Is Responsible for Hepatitis C Virus Core-Induced Lipid Droplet Formation

in a Yeast Model System". In: *PLoS ONE* 11.7 (July 2016). ISSN: 19326203. DOI: 10.1371/JOURNAL.PONE.0159324.

[248] Vineet Choudhary, Nicolas Jacquier, and Roger Schneiter. "The topology of the triacylglycerol synthesizing enzyme Lro1 indicates that neutral lipids can be produced within the luminal compartment of the endoplasmatic reticulum: Implications for the biogenesis of lipid droplets". In: *Communicative & integrative biology* 4.6 (Nov. 2011), pp. 781–784. ISSN: 1942-0889. DOI: 10.4161/CIB.17830.

[249] Anders Dahlqvist et al. "Phospholipid:diacylglycerol acyltransferase: An enzyme that catalyzes the acyl-CoA-independent formation of triacylglycerol in yeast and plants". In: *Proceedings of the National Academy of Sciences of the United States of America* 97 (June 2000), pp. 6487–6492. ISSN: 00278424. DOI: 10.1073/pnas.120067297.

[250] Peter Oelkers et al. "The DGA1 gene determines a second triglyceride synthetic pathway in yeast". In: *The Journal of biological chemistry* 277.11 (Mar. 2002), pp. 8877–8881. ISSN: 0021-9258. DOI: 10.1074/JBC.M111646200.

[251] Erick J Dufourc. "Sterols and membrane dynamics." In: *Journal of chemical biology* 1 (Nov. 2008), pp. 63–77. ISSN: 1864-6158. DOI: 10.1007/s12154-008-0010-6.

[252] W. Dowhan. "Molecular basis for membrane phospholipid diversity: Why are there so many lipids?" In: *Annual Review of Biochemistry* 66 (1997), pp. 199–232. ISSN: 00664154. DOI: 10.1146/annurev.biochem.66.1.199.

[253] Tania Jordá and Sergi Puig. "Regulation of ergosterol biosynthesis in saccharomyces cerevisiae". In: *Genes* 11 (July 2020), pp. 1–18. ISSN: 20734425. DOI: 10.3390/genes11070795.

[254] Angela Cirigliano et al. "Ergosterol reduction impairs mitochondrial DNA maintenance in S. cerevisiae". In: *Biochimica et Biophysica Acta - Molecular and Cell Biology of Lipids* 1864 (Mar. 2019), pp. 290–303. ISSN: 18792618. DOI: 10.1016/j.bbalip.2018.12.002.

[255] Zhihong Hu et al. "Recent Advances in Ergosterol Biosynthesis and Regulation Mechanisms in Saccharomyces cerevisiae." In: *Indian journal of microbiology* 57 (Sept. 2017), pp. 270–277. ISSN: 0046-8991. DOI: 10.1007/s12088-017-0657-1.

[256] Fernando Martínez Montañés, Amparo Pascual-Ahuir, and Markus Proft. "Repression of ergosterol biosynthesis is essential for stress resistance and is mediated by the Hog1 MAP kinase and the Mot3 and Rox1 transcription factors". In: *Molecular Microbiology* 79 (Feb. 2011), pp. 1008–1023. ISSN: 0950382X. DOI: 10.1111/j.1365-2958.2010.07502.x.

[257] Hau Lam Choy, Elizabeth A. Gaylord, and Tamara L. Doering. "Ergosterol distribution controls surface structure formation and fungal pathogenicity". In: *mBio* 14 (Aug. 2023), e0135323. ISSN: 21507511. DOI: 10.1128/mbio.01353-23.

[258] M. Bard et al. "Sterol synthesis and viability of erg11 (cytochrome P450 lanosterol demethylase) mutations in Saccharomyces cerevisiae and Candida albicans". In: *Lipids* 28 (Nov. 1993), pp. 963–967. ISSN: 00244201. DOI: 10.1007/BF02537115.

[259] M. Bard et al. "Cloning and characterization of ERG25, the Saccharomyces cerevisiae gene encoding C-4 sterol methyl oxidase". In: *Proceedings of the National Academy of Sciences of the United States of America* 93 (Jan. 1996), pp. 186–190. ISSN: 00278424. DOI: 10.1073/pnas.93.1.186.

[260] D. Gachotte et al. "Characterization of the Saccharomyces cerevisiae ERG26 gene encoding the C-3 sterol dehydrogenase (C-4 decarboxylase) involved in sterol biosynthesis". In: *Proceedings of the National Academy of Sciences of the United States of America* 95 (Nov. 1998), pp. 13794–13799. ISSN: 00278424. DOI: 10.1073/pnas.95.23.13794.

[261] C. Mo et al. "Protein-protein interactions among C-4 demethylation enzymes involved in yeast sterol biosynthesis". In: *Proceedings of the National Academy of Sciences of the United States of America* 99 (July 2002), pp. 9739–9744. ISSN: 00278424. DOI: 10.1073/pnas.112202799.

[262] Jia L. Song et al. "The Candida albicans Lanosterol 14-α-Demethylase (ERG11) Gene Promoter Is Maximally Induced after Prolonged Growth with Antifungal Drugs". In: *Antimicrobial Agents and Chemotherapy* 48 (Apr. 2004), pp. 1136–1144. ISSN: 00664804. DOI: 10.1128/AAC.48.4.1136-1144.2004.

[263] Josimary Morais Vasconcelos Oliveira et al. "Detection of ERG11 Overexpression in Candida albicans isolates from environmental sources and clinical isolates treated with inhibitory and subinhibitory concentrations of fluconazole". In: *Mycoses* 64 (Feb. 2021), pp. 220–227. ISSN: 14390507. DOI: 10.1111/myc.13208.

[264] Yonghao Xu et al. "ERG11 mutations and expression of resistance genes in fluconazole-resistant Candida albicans isolates". In: *Archives of Microbiology* 197 (Nov. 2015), pp. 1087–1093. ISSN: 1432072X. DOI: 10.1007/s00203-015-1146-8.

[265] Volmir Pitt Benedetti et al. "ERG11 gene polymorphisms and susceptibility to fluconazole in Candida isolates from diabetic and kidney transplant patients". In: *Revista da Sociedade Brasileira de Medicina Tropical* 52 (2019). ISSN: 00378682. DOI: 10.1590/0037-8682-0473-2018.

[266] Suzanne Paley et al. "Pathway collages: Personalized multi-pathway diagrams". In: *BMC Bioinformatics* 17 (Dec. 2016). ISSN: 14712105. DOI: 10.1186/s12859-016-1382-1.

[267] Åshild Vik and Jasper Rine. " Upc2p and Ecm22p, Dual Regulators of Sterol Biosynthesis in Saccharomyces cerevisiae ". In: *Molecular and Cellular Biology* 21 (Oct. 2001), pp. 6395–6405. ISSN: 02707306. DOI: 10.1128/mcb.21.19.6395-6405.2001.

[268] Samantha J. Hoot et al. "An A643V amino acid substitution in Upc2p contributes to azole resistance in well-characterized clinical isolates of Candida albicans". In: *Antimicrobial Agents and Chemotherapy* 55 (Feb. 2011), pp. 940–942. ISSN: 00664804. DOI: 10.1128/AAC.00995-10.

[269] Clemens J. Heilmann et al. "An A643T mutation in the transcription factor Upc2p causes constitutive ERG11 upregulation and increased fluconazole resistance in Candida albicans". In: *Antimicrobial Agents and Chemotherapy* 54 (Jan. 2010), pp. 353–359. ISSN: 00664804. DOI: 10.1128/AAC.01102-09.

[270] Huiseon Yang et al. "Structural mechanism of ergosterol regulation by fungal sterol transcription factor Upc2". In: *Nature Communications* 6 (2015). ISSN: 20411723. DOI: 10.1038/ncomms7129.

[271] Lingchen Tan et al. "Structural basis for activation of fungal sterol receptor Upc2 and azole resistance". In: *Nature Chemical Biology* 18 (Nov. 2022), pp. 1253–1262. ISSN: 15524469. DOI: 10.1038/s41589-022-01117-0.

[272] Hongyuan Yang et al. "Sterol esterification in yeast: A two-gene process". In: *Science* 272 (May 1996), pp. 1353–1356. ISSN: 00368075. DOI: 10.1126/science.272.5266.1353.

[273] E. Zinser, F. Paltauf, and G. Daum. "Sterol composition of yeast organelle membranes and subcellular distribution of enzymes involved in sterol metabolism". In: *Journal of Bacteriology* 175 (1993), pp. 2853–2858. ISSN: 00219193. DOI: 10.1128/jb.175.10.2853-2858.1993.

[274] Yu Chunjiang et al. "Molecular cloning and characterization of two isoforms of Saccharomyces cerevisiae Acyl-CoA:sterol acyltransferase". In: *Journal of Biological Chemistry* 271 (1996), pp. 24157–24163. ISSN: 00219258. DOI: 10.1074/jbc.271.39.24157.

[275] Dagmar Zweytick et al. "Contribution of Are1p and Are2p to steryl ester synthesis in the yeast Saccharomyces cerevisiae". In: *European Journal of Biochemistry* 267 (2000), pp. 1075–1082. ISSN: 00142956. DOI: 10.1046/j.1432-1327.2000.01103.x.

[276] K. Jensen-Pergakes et al. "Transcriptional regulation of the two sterol esterification genes in the yeast Saccharomyces cerevisiae". In: *Journal of bacteriology* 183.17 (2001), pp. 4950–4957. ISSN: 0021-9193. DOI: 10.1128/JB.183.17.4950-4957.2001.

[277] Ki Young Kim et al. "Molecular cloning and biochemical characterization of Candida albicans acyl-CoA:sterol acyltransferase, a potential target of antifungal agents". In: *Biochemical and Biophysical Research Communications* 319 (July 2004), pp. 911–919. ISSN: 0006291X. DOI: 10.1016/j.bbrc.2004.05.076.

[278] Line Sandager et al. "Storage lipid synthesis is non-essential in yeast". In: *The Journal of biological chemistry* 277.8 (Feb. 2002), pp. 6478–6482. ISSN: 0021-9258. DOI: 10.1074/JBC.M109109200.

[279] Karin Athenstaedt and Günther Daum. "YMR313c/TGL3 Encodes a Novel Triacylglycerol Lipase Located in Lipid Particles of Saccharomyces cerevisiae". In: *Journal of Biological Chemistry* 278.26 (June 2003), pp. 23317–23323. ISSN: 0021-9258. DOI: 10.1074/JBC.M302577200.

[280] Karin Athenstaedt and Günther Daum. "Tgl4p and Tgl5p, Two Triacylglycerol Lipases of the Yeast Saccharomyces cerevisiae Are Localized to Lipid Particles". In: *Journal of Biological Chemistry* 280.45 (Nov. 2005), pp. 37301–37309. ISSN: 0021-9258. DOI: 10.1074/JBC.M507261200.

[281] Birgit Ploier et al. "Screening for hydrolytic enzymes reveals Ayr1p as a novel triacylglycerol lipase in Saccharomyces cerevisiae". In: *Journal of Biological Chemistry* 288 (Dec. 2013), pp. 36061–36072. ISSN: 00219258. DOI: 10.1074/jbc.M113.509927.

[282] Karin Athenstaedt et al. "Identification and characterization of major lipid particle proteins of the yeast Saccharomyces cerevisiae". In: *Journal of Bacteriology* 181.20 (1999), pp. 6441–6448. ISSN: 00219193. DOI: 10.1128/JB.181.20.6441-6448.1999.

[283] Christoph F. Kurat et al. "Cdk1/Cdc28-Dependent Activation of the Major Triacylglycerol Lipase Tgl4 in Yeast Links Lipolysis to Cell-Cycle Progression". In: *Molecular Cell* 33 (Jan. 2009), pp. 53–63. ISSN: 10972765. DOI: 10.1016/j.molcel.2008.12.019.

[284] Isabella Klein et al. "Regulation of the yeast triacylglycerol lipases Tgl4p and Tgl5p by the presence/absence of nonpolar lipids". In: *Molecular Biology of the Cell* 27.13 (July 2016), p. 2014. ISSN: 19394586. DOI: 10.1091/MBC.E15-09-0633.

[285] René Köffel et al. "The Saccharomyces cerevisiae YLL012 / YEH1 , YLR020 / YEH2 , and TGL1 Genes Encode a Novel Family of Membrane-Anchored Lipases That Are Required for Steryl Ester Hydrolysis". In: *Molecular and Cellular Biology* 25 (Mar. 2005), pp. 1655–1668. ISSN: 02707306. DOI: 10.1128/mcb.25.5.1655-1668.2005.

[286] Andrea Wagner et al. "Mobilization of steryl esters from lipid particles of the yeast Saccharomyces cerevisiae". In: *Biochimica et Biophysica Acta - Molecular and Cell Biology of Lipids* 1791 (Feb. 2009), pp. 118–124. ISSN: 13881981. DOI: 10.1016/j.bbalip.2008.11.004.

[287] Birgit Ploier et al. "Regulatory link between steryl ester formation and hydrolysis in the yeast Saccharomyces cerevisiae". In: *Biochimica et Biophysica Acta - Molecular and Cell Biology of Lipids* 1851 (June 2015), pp. 977–986. ISSN: 18792618. DOI: 10.1016/j.bbalip.2015.02.011.

[288] Helena Santos-Rosa et al. "The yeast lipin Smp2 couples phospholipid biosynthesis to nuclear membrane growth". In: *EMBO Journal* 24 (June 2005), pp. 1931–1941. ISSN: 02614189. DOI: 10.1038/sj.emboj.7600672.

[289] Derk Binns et al. "An intimate collaboration between peroxisomes and lipid bodies". In: *Journal of Cell Biology* 173 (June 2006), pp. 719–731. ISSN: 00219525. DOI: 10.1083/jcb.200511125.

[290] James A. Olzmann and Pedro Carvalho. "Dynamics and functions of lipid droplets". In: *Nature Reviews Molecular Cell Biology* 20 (Mar. 2019), pp. 137–155. ISSN: 14710080. DOI: 10.1038/s41580-018-0085-z.

[291] Sepp D. Kohlwein, Marten Veenhuis, and Ida J. van der Klei. "Lipid droplets and peroxisomes: Key players in cellular lipid homeostasis or a matter of fat-store'em up or burn'em down". In: *Genetics* 193.1 (Jan. 2013), pp. 1–50. ISSN: 00166731. DOI: 10.1534/genetics.112.143362.

[292] Amit S. Joshi et al. "Lipid droplet and peroxisome biogenesis occur at the same ER subdomains". In: *Nature Communications* 9 (Dec. 2018). ISSN: 20411723. DOI: 10.1038/s41467-018-05277-3.

[293] Micah B. Schott et al. "Lipophagy at a glance". In: *Journal of Cell Science* 135 (Mar. 2022). ISSN: 14779137. DOI: 10.1242/jcs.259402.

[294] Tim Van Zutphen et al. "Lipid droplet autophagy in the yeast Saccharomyces cerevisiae". In: *Molecular Biology of the Cell* 25.2 (Jan. 2014), p. 290. ISSN: 10591524. DOI: 10.1091/MBC.E13-08-0448.

[295] Garrett Fairman and Mireille Ouimet. "Lipophagy pathways in yeast are controlled by their distinct modes of induction". In: *Yeast* 39 (Aug. 2022), pp. 429–439. ISSN: 10970061. DOI: 10.1002/yea.3705.

[296] Jack Davis et al. "A dynamic actin cytoskeleton is required to prevent constitutive VDAC-dependent MAPK signalling and aberrant lipid homeostasis". In: *iScience* 26.9 (Sept. 2023), p. 107539. ISSN: 25890042. DOI: 10.1016/J.ISCI.2023.107539.

[297] Nancy Marr et al. "Controlling lipid fluxes at glycerol-3-phosphate acyltransferase step in yeast: Unique contribution of Gat1p to oleic acid-induced lipid particle formation". In: *Journal of Biological Chemistry* 287 (Mar. 2012), pp. 10251–10264. ISSN: 00219258. DOI: 10.1074/jbc.M111.314112.

[298] Heimo Wolinski et al. "Seipin is involved in the regulation of phosphatidic acid metabolism at a subdomain of the nuclear envelope in yeast". In: *Biochimica et Biophysica Acta - Molecular and Cell Biology of Lipids* 1851 (Aug. 2015), pp. 1450–1464. ISSN: 18792618. DOI: 10.1016/j.bbalip.2015.08.003.

[299] Margherita Cortini et al. "Uncovering the protective role of lipid droplet accumulation against acid-induced oxidative stress and cell death in osteosarcoma." In: *Biochimica et biophysica acta. Molecular basis of disease* 1871 (Feb. 2025), p. 167576. ISSN: 1879-260X. DOI: 10.1016/j.bbadis.2024.167576.

[300] Tomer Shpilka et al. "Lipid droplets and their component triglycerides and steryl esters regulate autophagosome biogenesis". In: *The EMBO Journal* 34 (Aug. 2015), pp. 2117–2131. ISSN: 0261-4189. DOI: 10.15252/embj.201490315.

[301] Karlheinz Grillitsch et al. "Lipid particles/droplets of the yeast Saccharomyces cerevisiae revisited: lipidome meets proteome." In: *Biochimica et biophysica acta* 1811 (Dec. 2011), pp. 1165–76. ISSN: 0006-3002. DOI: 10.1016/j.bbalip.2011.07.015.

[302] Claudia Schmidt et al. "Analysis of Yeast Lipid Droplet Proteome and Lipidome". In: *Methods in Cell Biology* 116 (Jan. 2013), pp. 15–37. ISSN: 0091-679X. DOI: 10.1016/B978-0-12-408051-5.00002-4.

[303] Ying Lien Chen et al. "Phosphatidylserine synthase and phosphatidylserine decarboxylase are essential for cell wall integrity and virulence in Candida albicans". In: *Molecular Microbiology* 75 (5 Mar. 2010), pp. 1112–1132. ISSN: 1365-2958. DOI: 10.1111/J.1365-2958.2009.07018.X.

[304] Haizhan Jiao, Yan Yin, and Zhenfeng Liu. "Structures of the Mitochondrial CDP-DAG Synthase Tam41 Suggest a Potential Lipid Substrate Pathway from Membrane to the Active Site". In: *Structure* 27 (8 Aug. 2019), 1258–1269.e4. ISSN: 0969-2126. DOI: 10.1016/J.STR.2019.04.017.

[305] Haifa Shen et al. "The CDS1 gene encoding CDP-diacylglycerol synthase in Saccharomyces cerevisiae is essential for cell growth". In: *The Journal of biological chemistry* 271 (2 Jan. 1996), pp. 789–795. ISSN: 0021-9258. DOI: 10.1074/JBC.271.2.789.

[306] Nicholas J. Blunsom and Shamshad Cockcroft. "CDP-Diacylglycerol Synthases (CDS): Gateway to Phosphatidylinositol and Cardiolipin Synthesis". In: *Frontiers in Cell and Developmental Biology* 8 (Feb. 2020), p. 63. ISSN: 2296634X. DOI: 10.3389/FCELL.2020.00063.

[307] Yasushi Tamura et al. "Tam41 is a CDP-diacylglycerol synthase required for cardiolipin biosynthesis in mitochondria". In: *Cell metabolism* 17 (5 May 2013), pp. 709–718. ISSN: 1932-7420. DOI: 10.1016/J.CMET.2013.03.018.

[308] Gil Soo Han et al. "Characterization of the Yeast DGK1-encoded CTP-dependent Diacylglycerol Kinase". In: *The Journal of Biological Chemistry* 283 (29 July 2008), p. 20443. ISSN: 00219258. DOI: 10.1074/JBC.M802866200.

[309] Arlette Bochud and Andreas Conzelmann. "The active site of yeast phosphatidylinositol synthase Pis1 is facing the cytosol". In: *Biochimica et Biophysica Acta (BBA) - Molecular and Cell Biology of Lipids* 1851 (5 May 2015), pp. 629–640. ISSN: 1388-1981. DOI: 10.1016/J.BBALIP.2015.02.006.

[310] Yingzheng Liu et al. "Function of the phosphatidylinositol synthase Pis1 in maintenance of endoplasmic reticulum function and pathogenicity in Candida albicans". In: *Fungal Genetics and Biology* 160 (May 2022), p. 103674. ISSN: 1087-1845. DOI: 10.1016/J.FGB.2022.103674.

[311] A. Audhya, M. Foti, and S. D. Emr. "Distinct roles for the yeast phosphatidylinositol 4-Kinases, Stt4p and Pik1p, in secretion, cell growth, and organelle membrane dynamics". In: *Molecular Biology of the Cell* 11 (2000), pp. 2673–2689. ISSN: 10591524. DOI: 10.1091/mbc.11.8.2673.

[312] Hassan Badrane, M. Hong Nguyen, and Cornelius J. Clancy. "Highly dynamic and specific phosphatidylinositol 4,5-bisphosphate, septin, and cell wall integrity pathway responses correlate with caspofungin activity against Candida albicans". In: *Antimicrobial Agents and Chemotherapy* 60 (June 2016), pp. 3591–3600. ISSN: 10986596. DOI: 10.1128/AAC.02711-15.

[313] Anjon Audhya and Scott D. Emr. "Stt4 Pl 4-kinase localizes to the plasma membrane and functions in the Pkc1-mediated MAP kinase cascade". In: *Developmental Cell* 2 (2002), pp. 593–605. ISSN: 15345807. DOI: 10.1016/S1534-5807(02)00168-5.

[314] Drazen Raucher et al. "Phosphatidylinositol 4,5-bisphosphate functions as a second messenger that regulates cytoskeleton-plasma membrane adhesion". In: *Cell* 100 (Jan. 2000), pp. 221–228. ISSN: 00928674. DOI: 10.1016/S0092-8674(00)81560-3.

[315] Vladimíra Džugasová et al. "Phosphatidylglycerolphosphate synthase encoded by the PEL1/PGS1 gene in Saccharomyces cerevisiae is localized in mitochondria and its expression is regulated by phospholipid precursors". In: *Current genetics* 34 (4 Oct. 1998), pp. 297–302. ISSN: 0172-8083. DOI: 10.1007/S002940050399.

[316] Christof Osman et al. "A mitochondrial phosphatase required for cardiolipin biosynthesis: the PGP phosphatase Gep4". In: *The EMBO Journal* 29 (12 June 2010), p. 1976. ISSN: 02614189. DOI: 10.1038/EMBOJ.2010.98.

[317] Jiajia Ji and Miriam L. Greenberg. "Cardiolipin function in the yeast S. cerevisiae and the lessons learned for Barth syndrome". In: *Journal of Inherited Metabolic Disease* 45 (Jan. 2022), pp. 60–71. ISSN: 15732665. DOI: 10.1002/jimd.12447.

[318] Yue Zhou, Chelsi D. Cassilly, and Todd B. Reynolds. "Mapping the Substrate-Binding Sites in the Phosphatidylserine Synthase in Candida albicans". In:

Frontiers in Cellular and Infection Microbiology 11 (Dec. 2021), p. 765266. ISSN: 22352988. DOI: 10.3389/FCIMB.2021.765266/FULL.

[319] Sahar Hasim et al. "Influence of phosphatidylserine and phosphatidylethanolamine on farnesol tolerance in Candida albicans". In: *Yeast (Chichester, England)* 35 (4 Apr. 2018), pp. 343–351. ISSN: 1097-0061. DOI: 10.1002/YEA.3297.

[320] Robert N. Tams et al. "Pathways That Synthesize Phosphatidylethanolamine Impact Candida albicans Hyphal Length and Cell Wall Composition through Transcriptional and Posttranscriptional Mechanisms". In: *Infection and immunity* 88 (3 Mar. 2020). ISSN: 1098-5522. DOI: 10.1128/IAI.00480-19.

[321] Sarah E. Davis et al. "Candida albicans cannot acquire sufficient ethanolamine from the host to support virulence in the absence of de novo phosphatidylethanolamine synthesis". In: *Infection and Immunity* 86 (8 Aug. 2018). ISSN: 10985522. DOI: 10.1128/IAI.00815-17/ASSET/29E76DF1-E9EE-4166-9EA9-C104531B2C06/ASSETS/GRAPHIC/ZII9990925040008.JPEG.

[322] Anant K Menon and Victoria L Stevens. "Phosphatidylethanolamine Is the Donor of the Ethanolamine Residue Linking a Glycosylphosphatidylinositol Anchor to Protein*". In: *THE JOURNAL OF BIOLOGICAL CHEMISTRY* 267 (22 1992), pp. 15277–15280.

[323] Tsutomu KODAKI and Satoshi YAMASHITA. "Characterization of the methyltransferases in the yeast phosphatidylethanolamine methylation pathway by selective gene disruption". In: *European Journal of Biochemistry* 185 (2 1989), pp. 243–251. ISSN: 14321033. DOI: 10.1111/j.1432-1033.1989.tb15109.x.

[324] Paulette M. Gaynor and George M. Carman. "Phosphatidylethanolamine methyltransferase and phospholipid methyltransferase activities from Saccharomyces cerevisiae. Enzymological and kinetic properties". In: *Biochimica et Biophysica Acta (BBA) - Lipids and Lipid Metabolism* 1045 (2 July 1990), pp. 156–163. ISSN: 0005-2760. DOI: 10.1016/0005-2760(90)90145-N.

[325] Henry A. Boumann et al. "Depletion of Phosphatidylcholine in Yeast Induces Shortening and Increased Saturation of the Lipid Acyl Chains: Evidence for Regulation of Intrinsic Membrane Curvature in a Eukaryote". In: *Molecular Biology of the Cell* 17 (2 Feb. 2006), p. 1006. ISSN: 10591524. DOI: 10.1091/MBC.E05-04-0344.

[326] Christopher R. McMaster and Robert M. Bell. "CDP-choline:1,2-diacylglycerol cholinephosphotransferase". In: *Biochimica et Biophysica Acta - Lipids and Lipid Metabolism* 1348 (1-2 Sept. 1997), pp. 100–110. ISSN: 00052760. DOI: 10.1016/S0005-2760(97)00097-0.

[327] Sherry C. Morash et al. "Studies employing Saccharomyces cerevisiae cpt1 and ept1 null mutants implicate the CPT1 gene in coordinate regulation of phospholipid biosynthesis". In: *Journal of Biological Chemistry* 269 (46 Nov. 1994), pp. 28769–28776. ISSN: 00219258. DOI: 10.1016/s0021-9258(19)61972-1.

[328] Robert N. Tams et al. "Overproduction of phospholipids by the kennedy pathway leads to hypervirulence in Candida albicans". In: *Frontiers in Microbiology* 10 (FEB 2019). ISSN: 1664302X. DOI: 10.3389/fmicb.2019.00086.

[329] William R. King et al. " Glycerophosphocholine provision rescues Candida albicans growth and signaling phenotypes associated with phosphate limitation ". In: *mSphere* 8 (Dec. 2023). ISSN: 23795042. DOI: 10.1128/msphere.00231-23.

[330] Dorothy Wong et al. "Genetically Compromising Phospholipid Metabolism Limits Candida albicans' Virulence". In: *Mycopathologia* 184 (2 Apr. 2019), pp. 213–226. ISSN: 1573-0832. DOI: 10.1007/S11046-019-00320-3.

[331] Tania Jordá et al. "Modulation of yeast Erg1 expression and terbinafine susceptibility by iron bioavailability". In: *Microbial Biotechnology* 15 (Nov. 2022), pp. 2705–2716. ISSN: 17517915. DOI: 10.1111/1751-7915.14102.

[332] Hans Carolus et al. "Amphotericin B and Other Polyenes-Discovery, Clinical Use, Mode of Action and Drug Resistance." In: *Journal of fungi (Basel, Switzerland)* 6 (Nov. 2020). ISSN: 2309-608X. DOI: 10.3390/jof6040321.

[333] Neil R.H. Stone et al. "Liposomal Amphotericin B (AmBisome®): A Review of the Pharmacokinetics, Pharmacodynamics, Clinical Experience and Future Directions". In: *Drugs* 76 (Mar. 2016), pp. 485–500. ISSN: 11791950. DOI: 10.1007/s40265-016-0538-7.

[334] Yue Zhou et al. "The small molecule CBR-5884 inhibits the Candida albicans phosphatidylserine synthase". In: *mBio* 15 (May 2024). ISSN: 21507511. DOI: 10.1128/mbio.00633-24.

[335] Amanda M. Gillum, Emma Y.H. Tsay, and Donald R. Kirsch. "Isolation of the Candida albicans gene for orotidine-5-phosphate decarboxylase by complementation of S. cerevisiae ura3 and E. coli pyrF mutations". In: *MGG Molecular & General Genetics* 198 (Dec. 1984), pp. 179–182. ISSN: 00268925. DOI: 10.1007/BF00328721.

[336] Suzanne M. Noble et al. "Systematic screens of a Candida albicans homozygous deletion library decouple morphogenetic switching and pathogenicity." In: *Nature Genetics* 42.7 (July 2010), pp. 590–598. ISSN: 1061-4036. DOI: 10.1038/ng.605.

[337] Peter Ralph and Ilona Nakoinz. "Phagocytosis and cytolysis by a macrophage tumour and its cloned cell line". In: *Nature* 257 (1975), pp. 393–394. ISSN: 00280836. DOI: 10.1038/257393a0.

[338] Douglas Hanahan. "Studies on transformation of Escherichia coli with plasmids". In: *Journal of Molecular Biology* 166 (June 1983), pp. 557–580. ISSN: 00222836. DOI: 10.1016/S0022-2836(83)80284-8.

[339] Valmik K. Vyas et al. "New CRISPR Mutagenesis Strategies Reveal Variation in Repair Mechanisms among Fungi". In: *mSphere* 3 (Apr. 2018). ISSN: 23795042. DOI: 10.1128/msphere.00154-18.

[340] Namkha Nguyen, Morgan M. F. Quail, and Aaron D. Hernday. "An Efficient, Rapid, and Recyclable System for CRISPR-Mediated Genome Editing in Candida albicans". In: *mSphere* 2 (Apr. 2017). ISSN: 2379-5042. DOI: 10.1128/mspheredirect.00149-17.

[341] John G. Doench et al. "Optimized sgRNA design to maximize activity and minimize off-target effects of CRISPR-Cas9". In: *Nature Biotechnology* 34 (Feb. 2016), pp. 184–191. ISSN: 15461696. DOI: 10.1038/nbt.3437.

[342] Patrick D. Hsu et al. "DNA targeting specificity of RNA-guided Cas9 nucleases". In: *Nature Biotechnology* 31 (Sept. 2013), pp. 827–832. ISSN: 10870156. DOI: 10.1038/nbt.2647.

[343] J.C Oliveros. *Venny 2.1*. 2015. URL: https://bioinfogp.cnb.csic.es/tools/venny/index.html.

[344] Dechao Bu et al. "KOBAS-i: intelligent prioritization and exploratory visualization of biological functions for gene enrichment analysis". In: *Nucleic Acids Research* 49.W1 (June 2021), W317–W325. ISSN: 0305-1048. DOI: 10.1093/nar/gkab447. eprint: https://academic.oup.com/nar/article-pdf/49/W1/W317/38842244/gkab447.pdf.

[345] Yang Lu, Chang Su, and Haoping Liu. "Candida albicans hyphal initiation and elongation". In: *Trends in microbiology* 22 (12 Dec. 2014), p. 707. ISSN: 18784380. DOI: 10.1016/J.TIM.2014.09.001.

[346] Nicolas Jacquier et al. "Lipid droplets are functionally connected to the endoplasmic reticulum in Saccharomyces cerevisiae". In: *Journal of Cell*

Science 124 (14 July 2011), pp. 2424–2437. ISSN: 00219533. DOI: 10.1242/jcs.076836.

[347] Chao Wen Wang. "Lipid droplet dynamics in budding yeast". In: *Cellular and Molecular Life Sciences: CMLS* 72 (14 July 2015), p. 2677. ISSN: 14209071. DOI: 10.1007/S00018-015-1903-5.

[348] Ludovic Enkler et al. "Functional interplay of lipid droplets and mitochondria". In: *FEBS Letters* 598 (10 May 2024), pp. 1235–1251. ISSN: 1873-3468. DOI: 10.1002/1873-3468.14809.

[349] Susanne E. Horvath et al. "Metabolic link between phosphatidylethanolamine and triacylglycerol metabolism in the yeast Saccharomyces cerevisiae". In: *Biochimica et biophysica acta* 1811 (12 Dec. 2011), pp. 1030–1037. ISSN: 0006-3002. DOI: 10.1016/J.BBALIP.2011.08.007.

[350] Isabella Klein et al. "Regulation of the yeast triacylglycerol lipases Tgl4p and Tgl5p by the presence/absence of nonpolar lipids". In: *Molecular Biology of the Cell* 27 (13 July 2016), p. 2014. ISSN: 19394586. DOI: 10.1091/MBC.E15-09-0633.

[351] Joshua A. Granek and Paul M. Magwene. "Environmental and genetic determinants of colony morphology in yeast". In: *PLoS Genetics* 6 (Jan. 2010). ISSN: 15537390. DOI: 10.1371/journal.pgen.1000823.

[352] Sona Rajakumari, Ram Rajasekharan, and Günther Daum. "Triacylglycerol lipolysis is linked to sphingolipid and phospholipid metabolism of the yeast Saccharomyces cerevisiae". In: *Biochimica et Biophysica Acta (BBA)*

- *Molecular and Cell Biology of Lipids* 1801.12 (Dec. 2010), pp. 1314–1322. ISSN: 1388-1981. DOI: 10.1016/J.BBALIP.2010.08.004.

[353] Shingo Iwasa et al. "The Phospholipid:Diacylglycerol Acyltransferase Lro1 Is Responsible for Hepatitis C Virus Core-Induced Lipid Droplet Formation in a Yeast Model System". In: *PloS one* 11 (7 July 2016). ISSN: 1932-6203. DOI: 10.1371/JOURNAL.PONE.0159324.

[354] A. Munir A. Murad et al. "Transcript profiling in Candida albicans reveals new cellular functions for the transcriptional repressors CaTup1, CaMig1 and CaNrg1". In: *Molecular Microbiology* 42 (2001), pp. 981–993. ISSN: 0950382X. DOI: 10.1046/j.1365-2958.2001.02713.x.

[355] René Köffel et al. " The Saccharomyces cerevisiae YLL012 / YEH1 , YLR020 / YEH2 , and TGL1 Genes Encode a Novel Family of Membrane-Anchored Lipases That Are Required for Steryl Ester Hydrolysis ". In: *Molecular and Cellular Biology* 25 (Mar. 2005), pp. 1655–1668. ISSN: 02707306. DOI: 10.1128/mcb.25.5.1655-1668.2005.

[356] Sona Rajakumari, Ram Rajasekharan, and Günther Daum. "Triacylglycerol lipolysis is linked to sphingolipid and phospholipid metabolism of the yeast Saccharomyces cerevisiae". In: *Biochimica et Biophysica Acta (BBA) - Molecular and Cell Biology of Lipids* 1801 (12 Dec. 2010), pp. 1314–1322. ISSN: 1388-1981. DOI: 10.1016/J.BBALIP.2010.08.004.

[357] Ian A. Cleary et al. "BRG1 and NRG1 Form a Novel Feedback Circuit Regulating C. albicans Hypha Formation and Virulence". In: *Molecular*

Microbiology 85.3 (Aug. 2012), p. 557. ISSN: 0950382X. DOI: 10.1111/J.1365-2958.2012.08127.X.

[358] Daniel R. Pentland et al. "Ras signalling in pathogenic yeasts". In: *Microbial Cell* 5 (2 Feb. 2018), pp. 63–73. ISSN: 23112638. DOI: 10.15698/mic2018.02.612.

[359] Mohua Banerjee et al. "UME6, a novel filament-specific regulator of Candida albicans hyphal extension and virulence". In: *Molecular Biology of the Cell* 19.4 (Apr. 2008), pp. 1354–1365. ISSN: 10591524. DOI: 10.1091/MBC.E07-11-1110.

[360] Ronny Martin, Andrea Walther, and Jürgen Wendland. "Ras1-induced hyphal development in Candida albicans requires the formin Bni1". In: *Eukaryotic Cell* 4 (Oct. 2005), pp. 1712–1724. ISSN: 15359778. DOI: 10.1128/EC.4.10.1712-1724.2005.

[361] Logan R Hurst and Rutilio A Fratti. "Lipid Rafts, Sphingolipids, and Ergosterol in Yeast Vacuole Fusion and Maturation." In: *Frontiers in cell and developmental biology* 8 (2020), p. 539. ISSN: 2296-634X. DOI: 10.3389/fcell.2020.00539.

[362] Javier Valdez-Taubas and Hugh R.B. Pelham. "Slow diffusion of proteins in the yeast plasma membrane allows polarity to be maintained by endocytic cycling". In: *Current Biology* 13 (Sept. 2003), pp. 1636–1640. ISSN: 09609822. DOI: 10.1016/j.cub.2003.09.001.

[363] Faustino Mollinedo. "Lipid raft involvement in yeast cell growth and death." In: *Frontiers in oncology* 2 (2012), p. 140. ISSN: 2234-943X. DOI: 10.3389/fonc.2012.00140.

[364] Pizga Kumwenda et al. "Estrogen promotes innate immune evasion of Candida albicans through inactivation of the alternative complement system". In: *Cell reports* 38 (1 Jan. 2022). ISSN: 2211-1247. DOI: 10.1016/J.CELREP.2021.110183.

[365] François L. Mayer, Duncan Wilson, and Bernhard Hube. "Candida albicans pathogenicity mechanisms". In: *Virulence* 4 (2 Feb. 2013), p. 119. ISSN: 21505608. DOI: 10.4161/VIRU.22913.

[366] Verónica Freire-Benéitez et al. "Candida albicans repetitive elements display epigenetic diversity and plasticity". In: *Scientific Reports* 6 (Mar. 2016). ISSN: 20452322. DOI: 10.1038/srep22989.

[367] Robert T. Todd et al. "Genome plasticity in Candida albicans is driven by long repeat sequences". In: *eLife* 8 (June 2019), e45954. ISSN: 2050084X. DOI: 10.7554/ELIFE.45954.

[368] D. Davis et al. "Candida albicans RIM101 pH response pathway is required for host-pathogen interactions". In: *Infection and immunity* 68 (10 2000), pp. 5953–5959. ISSN: 0019-9567. DOI: 10.1128/IAI.68.10.5953-5959.2000.

[369] Suzanne M. Noble, Brittany A. Gianetti, and Jessica N. Witchley. "Candida albicans cell-type switching and functional plasticity in the mammalian

host". In: *Nature Reviews Microbiology* 15 (2 Feb. 2017), pp. 96–108. ISSN: 17401534. DOI: 10.1038/nrmicro.2016.157.

[370] Quynh T. Phan et al. "Als3 is a Candida albicans invasin that binds to cadherins and induces endocytosis by host cells". In: *PLoS Biology* 5 (3 Mar. 2007), pp. 0543–0557. ISSN: 15449173. DOI: 10.1371/journal.pbio.0050064.

[371] Alex Hopke et al. "Dynamic Fungal Cell Wall Architecture in Stress Adaptation and Immune Evasion". In: *Trends in Microbiology* 26 (4 Apr. 2018), pp. 284–295. ISSN: 18784380. DOI: 10.1016/j.tim.2018.01.007.

[372] E. Román et al. "The Cek1-mediated MAP kinase pathway regulates exposure of -1,2 and β-1,2-mannosides in the cell wall of Candida albicans modulating immune recognition". In: *Virulence* 7 (5 July 2016), pp. 558–577. ISSN: 21505608. DOI: 10.1080/21505594.2016.1163458.

[373] Francesco Citiulo et al. "Candida albicans Scavenges Host Zinc via Pra1 during Endothelial Invasion". In: *PLOS Pathogens* 8 (6 June 2012), e1002777. ISSN: 1553-7374. DOI: 10.1371/JOURNAL.PPAT.1002777.

[374] Mahmoud A Ghannoum. "Potential Role of Phospholipases in Virulence and Fungal Pathogenesis". In: *Clinical Microbiology Reviews* 13 (1 2000), pp. 122–143.

[375] Sepp D. Kohlwein, Marten Veenhuis, and Ida J. van der Klei. "Lipid droplets and peroxisomes: Key players in cellular lipid homeostasis or a matter of fat-store'em up or burn'em down". In: *Genetics* 193 (1 Jan. 2013), pp. 1–50. ISSN: 00166731. DOI: 10.1534/genetics.112.143362.

[376] Peter Oelkers et al. "The DGA1 gene determines a second triglyceride synthetic pathway in yeast". In: *The Journal of biological chemistry* 277 (11 Mar. 2002), pp. 8877–8881. ISSN: 0021-9258. DOI: 10.1074/JBC.M111646200.

[377] K. Jensen-Pergakes et al. "Transcriptional regulation of the two sterol esterification genes in the yeast Saccharomyces cerevisiae". In: *Journal of bacteriology* 183 (17 2001), pp. 4950–4957. ISSN: 0021-9193. DOI: 10.1128/JB.183.17.4950-4957.2001.

[378] Martin Graef. "Lipid droplet-mediated lipid and protein homeostasis in budding yeast". In: *FEBS Letters* 592 (8 Apr. 2018), pp. 1291–1303. ISSN: 1873-3468. DOI: 10.1002/1873-3468.12996.

[379] George M. Carman and Gil Soo Han. "Regulation of phospholipid synthesis in yeast". In: *Journal of Lipid Research* 50 (SUPPL. Apr. 2009). ISSN: 00222275. DOI: 10.1194/jlr.R800043-JLR200.

[380] Vid V. Flis et al. "Phosphatidylcholine Supply to Peroxisomes of the Yeast Saccharomyces cerevisiae". In: *PLoS ONE* 10 (8 Aug. 2015), e0135084. ISSN: 19326203. DOI: 10.1371/JOURNAL.PONE.0135084.

[381] Iván Martínez-Duncker, Diana F. Díaz-Jímenez, and Héctor M. Mora-Montes. "Comparative analysis of protein glycosylation pathways in humans and the fungal pathogen candida albicans". In: *International Journal of Microbiology* 2014 (2014). ISSN: 16879198. DOI: 10.1155/2014/267497.

[382] Thorsten Meyer et al. "Quantifying yeast lipidomics by high-performance thin-layer chromatography (HPTLC) and comparison to mass spectrometry-based shotgun lipidomics". In: *Microbial Cell* 11 (1 2024), pp. 57–68. ISSN: 23112638. DOI: 10.15698/mic2024.02.815.

[383] Clarissa J. Nobile et al. "Function of ¡i¿Candida albicans¡/i¿ Adhesin Hwp1 in Biofilm Formation". In: *Eukaryotic Cell* 5 (10 Oct. 2006), pp. 1604–1610. ISSN: 1535-9778. DOI: 10.1128/EC.00194-06.

[384] Hassan Dihazi, Renate Kessler, and Klaus Eschrich. "Glucose-induced stimulation of the Ras-cAMP pathway in yeast leads to multiple phosphorylations and activation of 6-phosphofructo-2-kinase". In: *Biochemistry* 42 (20 May 2003), pp. 6275–6282. ISSN: 00062960. DOI: 10.1021/BI034167R/ASSET/IMAGES/LARGE/BI034167RF00008.JPEG.

[385] Kwang jin Cho et al. "Inhibition of Acid Sphingomyelinase Depletes Cellular Phosphatidylserine and Mislocalizes K-Ras from the Plasma Membrane". In: *Molecular and Cellular Biology* 36 (2 Jan. 2016), p. 363. ISSN: 10985549. DOI: 10.1128/MCB.00719-15.

[386] Praveen Kumar Rajvanshi, Madhuri Arya, and Ram Rajasekharan. "The stress-regulatory transcription factors Msn2 and Msn4 regulate fatty acid oxidation in budding yeast". In: *Journal of Biological Chemistry* 292 (Nov. 2017), pp. 18628–18643. ISSN: 1083351X. DOI: 10.1074/jbc.M117.801704.

[387] Michael C. Gustin et al. " MAP Kinase Pathways in the Yeast Saccharomyces cerevisiae ". In: *Microbiology and Molecular Biology Reviews* 62

(Dec. 1998), pp. 1264–1300. ISSN: 1092-2172. DOI: 10.1128/mmbr.62.4.1264-1300.1998.

[388] Rebecca A. Hall and Edward W.J. Wallace. "Post-transcriptional control of fungal cell wall synthesis". In: *The Cell Surface* 8 (Dec. 2022). ISSN: 24682330. DOI: 10.1016/j.tcsw.2022.100074.

[389] Steven D Leidich et al. "Cloning and Disruption of caPLB1, a Phospholipase B Gene Involved in the Pathogenicity of Candida albicans*". In: *Journal of Biological chemistry* (1998). DOI: 10.1074/jbc.273.40.26078.

[390] WHO. "WHO Fungal Priority Pathogens List to Guide Research, Development and Public Health Action". In: *Test* (2022).

[391] Anna Selmecki, Anja Forche, and Judith Berman. "Genomic Plasticity of the Human Fungal Pathogen Candida albicans". In: *Eukaryotic Cell* 9 (7 July 2010), p. 991. ISSN: 15359778. DOI: 10.1128/EC.00060-10.

[392] M. J. Kennedy and P. A. Volz. "Ecology of Candida albicans gut colonization: inhibition of Candida adhesion, colonization, and dissemination from the gastrointestinal tract by bacterial antagonism." In: *Infection and Immunity* 49 (3 1985), p. 654. ISSN: 00199567. DOI: 10.1128/IAI.49.3.654-663.1985.

[393] Hubertine M.E. Willems et al. "Vulvovaginal Candidiasis: A Current Understanding and Burning Questions". In: *Journal of Fungi* 6 (1 Mar. 2020). ISSN: 2309608X. DOI: 10.3390/JOF6010027.

[394] Peter Sudbery, Neil Gow, and Judith Berman. "The distinct morphogenic states of Candida albicans". In: *Trends in Microbiology* 12 (7 July 2004), pp. 317–324. ISSN: 0966-842X. DOI: 10.1016/J.TIM.2004.05.008.

[395] David Kadosh and Alexander D. Johnson. "Induction of the Candida albicans filamentous growth program by relief of transcriptional repression: A genome-wide analysis". In: *Molecular Biology of the Cell* 16 (6 2005), pp. 2903–2912. ISSN: 10591524. DOI: 10.1091/mbc.E05-01-0073.

[396] Ana Barbosa et al. "Candida albicans adaptation on simulated human body fluids under different ph". In: *Microorganisms* 8 (4 Apr. 2020). ISSN: 20762607. DOI: 10.3390/microorganisms8040511.

[397] Ilse D. Jacobsen et al. "Candida albicans dimorphism as a therapeutic target". In: *Expert Review of Anti-infective Therapy* 10 (1 Jan. 2012), pp. 85–93. ISSN: 14787210. DOI: 10.1586/ERI.11.152.

[398] Alyssa Ann La Bella et al. "The catheterized bladder environment promotes Efg1- and Als1-dependent Candida albicans infection." In: *Science advances* 9 (9 Mar. 2023), eade7689. ISSN: 2375-2548. DOI: 10.1126/sciadv.ade7689.

[399] Jyotsna Chandra et al. "Biofilm Formation by the Fungal Pathogen Candida albicans: Development, Architecture, and Drug Resistance". In: *JOURNAL OF BACTERIOLOGY* 183 (18 2001), pp. 5385–5394. DOI: 10.1128/JB.183.18.5385-5394.2001.

[400] S. P. Hawser and L. J. Douglas. "Resistance of Candida albicans biofilms to antifungal agents in vitro". In: *Antimicrobial Agents and Chemotherapy* 39 (9 1995), pp. 2128–2131. ISSN: 00664804. DOI: 10.1128/AAC.39.9.2128.

[401] David L. Moyes et al. "Candidalysin is a fungal peptide toxin critical for mucosal infection". In: *Nature* 532 (7597 Apr. 2016), p. 64. ISSN: 14764687. DOI: 10.1038/NATURE17625.

[402] Jasminka Talapko et al. "Candida albicans—The Virulence Factors and Clinical Manifestations of Infection". In: *Journal of Fungi 2021, Vol. 7, Page 79* 7 (2 Jan. 2021), p. 79. ISSN: 2309-608X. DOI: 10.3390/JOF7020079.

[403] Jean Francois Timsit et al. "Impact of bronchial colonization with Candida spp. on the risk of bacterial ventilator-associated pneumonia in the ICU: the FUNGIBACT prospective cohort study". In: *Intensive Care Medicine* 45 (6 June 2019), pp. 834–843. ISSN: 14321238. DOI: 10.1007/S00134-019-05622-0/TABLES/4.

[404] M. A. Pfaller and D. J. Diekema. "Epidemiology of invasive candidiasis: a persistent public health problem". In: *Clinical microbiology reviews* 20 (1 Jan. 2007), pp. 133–163. ISSN: 0893-8512. DOI: 10.1128/CMR.00029-06.

[405] Farhana Alam et al. "Pseudomonas aeruginosa increases the susceptibility of Candida albicans to amphotericin B in dual-species biofilms". In: *Journal of Antimicrobial Chemotherapy* 78 (9 Sept. 2023), pp. 2228–2241. ISSN: 14602091. DOI: 10.1093/jac/dkad228.

[406] Lisa Marie Schlecht et al. "Systemic Staphylococcus aureus infection mediated by Candida albicans hyphal invasion of mucosal tissue". In: *Microbiology (United Kingdom)* 161 (1 Jan. 2015), pp. 168–181. ISSN: 14652080. DOI: 10.1099/mic.0.083485-0.

[407] Hossein Yazdani-Ahmadabadi et al. "Durable Surfaces from Film-Forming Silver Assemblies for Long-Term Zero Bacterial Adhesion without Toxicity". In: *ACS Central Science* 8 (5 May 2022), pp. 546–561. ISSN: 23747951. DOI: 10.1021/ACSCENTSCI.1C01556/SUPPL_FILE/OC1C01556_SI_003.MP4.

[408] B. J. van Meer et al. "Small molecule absorption by PDMS in the context of drug response bioassays". In: *Biochemical and Biophysical Research Communications* 482 (2 Jan. 2017), p. 323. ISSN: 10902104. DOI: 10.1016/J.BBRC.2016.11.062.

[409] Vincent R. Richard et al. "Mechanism of liponecrosis, a distinct mode of programmed cell death". In: *Cell cycle (Georgetown, Tex.)* 13 (23 Dec. 2014), pp. 3707–3726. ISSN: 1551-4005. DOI: 10.4161/15384101.2014.965003.

[410] Young Gue Koh et al. "Efficacy and safety of oral palmitoleic acid supplementation for skin barrier improvement: A 12-week, randomized, double-blinded, placebo-controlled study". In: *Heliyon* 9 (6 June 2023). ISSN: 24058440. DOI: 10.1016/j.heliyon.2023.e16711.

[411] Miguel A. Bermúdez et al. "Roles of Palmitoleic Acid and Its Positional Isomers, Hypogeic and Sapienic Acids, in Inflammation, Metabolic Diseases

and Cancer". In: *Cells* 11 (14 July 2022). ISSN: 20734409. DOI: 10.3390/cells11142146.

[412] Elie Azoulay et al. "Candida colonization of the respiratory tract and subsequent pseudomonas ventilator-associated pneumonia". In: *Chest* 129 (1 Jan. 2006), pp. 110–117. ISSN: 00123692. DOI: 10.1378/chest.129.1.110.

[413] Marie-Soleil Delisle BCPS et al. "Impact of Candida species on clinical outcomes in patients with suspected ventilator-associated pneumonia". In: *Canadian Respiratory Journal* 18 (3 2011). DOI: 10.1155/2011/827692.

[414] Daniel O. Thomas-Rüddel et al. "Risk Factors for Invasive Candida Infection in Critically Ill Patients: A Systematic Review and Meta-analysis". In: *Chest* 161 (2 Feb. 2022), p. 345. ISSN: 19313543. DOI: 10.1016/J.CHEST.2021.08.081.

[415] Fumiyoshi Abe, Keiko Usui, and Toshiki Hiraki. "Fluconazole modulates membrane rigidity, heterogeneity, and water penetration into the plasma membrane in Saccharomyces cerevisiae". In: *Biochemistry* 48 (36 Sept. 2009), pp. 8494–8504. ISSN: 00062960. DOI: 10.1021/BI900578Y/ASSET/IMAGES/MEDIUM/BI-2009-00578Y_0006.GIF.

[416] Vitasta Tiku et al. "Characterization of the putative yeast mitochondrial triacylglycerol lipase Tgl2". In: *Journal of Biological Chemistry* 301 (Mar. 2025). ISSN: 1083351X. DOI: 10.1016/j.jbc.2025.108217.

[417] Laura A. Jones and Peter E. Sudbery. "Spitzenkörper, Exocyst, and Polarisome Components in Candida albicans Hyphae Show Different Patterns of

Localization and Have Distinct Dynamic Properties". In: *Eukaryotic Cell* 9 (10 Oct. 2010), p. 1455. ISSN: 15359778. DOI: 10.1128/EC.00109-10.

[418] Patrick Rockenfeller and Campbell W. Gourlay. "Lipotoxicty in yeast: A focus on plasma membrane signalling and membrane contact sites". In: *FEMS Yeast Research* 18 (June 2018). ISSN: 15671364. DOI: 10.1093/femsyr/foy034.

[419] Prabuddha Dey et al. "Phosphorylation of lipid metabolic enzymes by yeast protein kinase C requires phosphatidylserine and diacylglycerol". In: *Journal of Lipid Research* 58.4 (2017), p. 742. ISSN: 15397262. DOI: 10.1194/JLR.M075036.